ANALYTICAL AND EXPERIMENTAL EVALUATION OF EXISTING FLORIDA DOT BRIDGES

CONTRACT NUMBERS: BD493 (FDOT) and 6120 594 39 (FSU)

FINAL REPORT

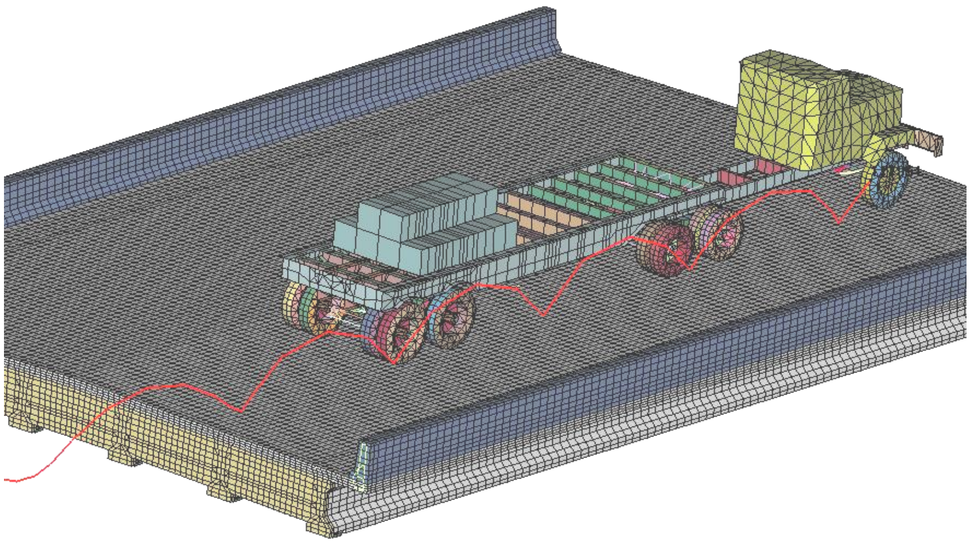

Submitted to:

Mr. Jean Ducher, State Maintenance Office, Project Manager
Florida Department of Transportation

by

Dr. Jerry Wekezer P.E., Principal Investigator
Hongyi Li
Dr. Leslaw Kwasniewski
Dr. Jerzy Malachowski

December 2004

TABLE OF CONTENTS

LIST OF FIGURES

LIST OF TABLES

ACKNOWLEDGEMENTS

This research was sponsored by the State Maintenance Office at the Florida Department of Transportation. The authors would like to express their appreciation for this generous support. The authors wish to acknowledge the assistance and support from the Project Manager Mr. Jean Ducher. The field tests were professionally performed by the Structures Lab of FDOT. Thanks are due to Mr. Marc Ansley and Mr. Garry Roufa for their excellent work and technical support. Our gratitude also goes to the research assistant Angela Wilhelm for her help with preparing the manuscript.

The finite element analysis was conducted in the Crashworthiness and Impact Analysis Laboratory (CIAL) at FAMU-FSU College of Engineering, using its computer and software resources and the FSU supercomputers IBM RS/6000 SP3 and SP4.

1. INTRODUCTION

1.1. Problem statement

The Evaluation of existing structures is critical for the efficient management of transportation facilities, especially bridges. According to 2020 Florida Transportation Plan, Safety and System Management including bridge repairs and replacements (operation and maintenance), will cost about 30 percent of all state and federal revenues between 2003 and 2020. Knowledge of the actual load effects and structure resistance can be very helpful for the determination of the load carrying capacity and condition of structures. It can help to make management decisions, such as establishing permissible weight limits, and can have important economical and safety implications. Advanced structural analysis and evaluation procedures can also be applied to structures showing difficult to explain behavior like excessive vibration, deflection, and others.

There are lot of bridges which are difficult (if not impossible) to evaluate using traditional inspection methods and simplified static analysis. In particular, the dynamic nature of live loads and vehicle-bridge interaction is not sufficiently considered in the design process. Impact factors suggested by bridge design codes usually lead to conservative solutions, especially for overloaded vehicles. Accurate and inexpensive methods are needed for diagnostics and verification of the actual dynamic effects of the bridges, as well as the impact factors.

Traditional bridge analysis is based on several simplifications of geometry, material models, boundary conditions and loading. Bridge live load is considered as one of the most questionable idealizations. The interaction between a vehicle and bridge structure is usually represented by concentrated and uniformly distributed static loads. Dynamic effects of the actual live loads are considered by scaling static loads by impact factors. The magnitude of the dynamic load allowance (impact factor) is usually determined based on the simplifications and is related only to the length of the bridge, without reference to the bridge surface roughness and dynamic characteristics of the vehicles.

The increasing computational capability of today's computers and development of commercial finite element programs allows for more advanced numerical, 3-D dynamic analysis of bridge structures. Today, it is possible to create detailed three dimensional models of bridges containing a large number of finite elements with consistent stiffness and mass distribution. Advanced material models for steel and concrete, rebar option for modeling of reinforcement, application of different types of constraints and damping options allow for more accurate descriptions of the actual bridge behavior. On the other hand there are finite element models of different vehicles, including trucks, available in the public domain. These models are ready to use, with different levels of detailed representation for suspension systems, kinematical characteristics of vehicle components and wheel models. After improvement they can be successfully used for simulation of truck passes through the bridge structure. Application of these models would allow considering complex mechanical phenomena such as contact between wheels and pavement surface, impact forces caused by surface discontinuities, and time dependence of moving live loads, caused by dynamic interaction among suspended masses representing vehicle components. Actual live loads caused by overloaded heavy vehicles can also be modeled.

A full scale bridge test should be carried out to validate computational dynamic analysis. In this project emphasis was placed on the development of experimental procedures for bridge structure evaluation. Application of the recent developments in bridge diagnostics, such as sensing techniques and wireless transfer of the signal from strain transducers to the main unit was also considered. Because extensive test programs are expensive, a considerable effort should be made to improve analytical methods, on the basis of available test data. Validated finite element models can provide extensive information about the structural behavior, which is both expensive and difficult, if not impossible, to obtain through experimental study only. This project focused on dynamic load allowance factors for short and medium span bridges, involving advanced finite element analysis and field testing.

1.2. Research objective

The main objective of the project was the validation of the dynamic response for short span (about 30-50 ft) and medium span (spans 65-100 ft) highway bridges. Emphasis was placed on the determination of actual impact factors. The study consisted of analytical work validated by a field test conducted by the Structures Lab of the Florida DOT on the selected bridge #500133 over "Mosquito Creek." Analysis included the development of finite element models for four bridges, improvement and application of available models for heavy vehicles and computer simulations of the dynamic interaction between a passing truck and bridge structure. Experimental data was used for finite model validation. The actual dynamic load allowance (impact factor) was determined numerically to account for the dynamic interaction between the bridge and moving vehicles.

The selection of existing bridges and vehicles intended for analysis was coordinated with the Florida DOT staff. Identification and evaluation of parameters having significant influence on dynamic response of the structure, such as span length, vehicle speed, suspension parameters, trucks weight, trucks position on bridge lanes, and road surface condition was also coordinated with Florida DOT.

The results are documented in Progress Reports and this Final Report submitted to FDOT. Conclusions and practical recommendations are presented in Chapter 6. The research was specially focused on Florida DOT needs. The results of the project will serve as a basis for updating the load limits for selected bridges.

1.3. Research tasks

This Section lists the research tasks which were proposed at the beginning of the project. Research activities by task are presented in Table 1.1.

PHASE I

Task 1: Literature review

The review of the available professional literature was updated covering dynamic analysis for bridges, field testing of bridges, instrumentation, and bridge diagnostics. This effort was greater at the beginning of the project in order to utilize similar research results published by others, whenever they were useful for the project. However, this task was continued with a lesser intensity throughout the entire project. The update included new publications, reports and books. This task included a survey of states on dynamic load allowance (impact factor) methods for bridge construction. The Florida DOT staff provided the State recommendations and requirements concerning load ratings, load limits and information about the heaviest trucks used in Florida.

Task 2: Selection of bridges and vehicles

One bridge was selected for field testing in collaboration with the Florida DOT Structures Lab. Experimental data included time histories of displacements, strains and accelerations of several critical points selected on the bridge. The Florida DOT staff provided design data for the bridge structure. A heavy vehicle intended for modeling was also selected in cooperation with FDOT staff. Experimental data was used to validate finite element models.

Task 3: Heavy truck model

One truck model was developed specifically for a field test (Task 2). The finite element model of the truck was based on public domain resources to reduce the cost of the project. Improvements regarding the suspension system and wheel models were applied to the existing public domain model. A computer simulation of a drop test was performed in order to validate the vehicle model developed.

Task 4: Bridge model

One finite element model of the selected bridge was developed based on data provided by FDOT staff. Preliminary computer runs were performed to validate the model. The truck model developed in Task 3 was used for computer analysis. Data concerning material characteristics of the bridge and truck was collected. Preliminary simulations of vehicle–bridge interaction were performed.

Task 5: Field testing technique

The test procedure was selected by the Structures Lab of the Florida DOT with assistance of the P.I. The field test was used for evaluation of dynamic bridge response and verification of the dynamic load factor. It was also used for validation of the computer models developed. Equipment and measurement techniques were determined to collect time histories of acceleration, strains and displacements.

Task 6: Field test of the first bridge

The test procedure developed in Task 5 of the project was used for verification of the F.E. models and dynamic load allowance. The impact factor, maximum vehicle weight and recommended speed limit were determined from field measurements of strain, accelerations and deflections of selected points on the bridge.

Task 7: Bridge model validation

Data from field testing (Task 6) was compared with results from computational mechanics analysis using F.E. models developed in Tasks 3 and 4. In particular, strain, acceleration and displacement time histories were compared from the experiment and computational analysis for selected points on the bridge.

PHASE II

Findings gained from Phase I of the project were used to create a database for bridge and truck F.E. models in the Phase II of the project.

Task 8: Additional vehicle models

Experiences gained in building the first FE model of the truck, combined with an overall experimental validation of the truck – bridge system allowed for developing the additional models of vehicle. Due to the size and load, the Project Manager selected five cranes for further FE modeling. Impact factors were determined based on test data and analytical results.

Task 9: Additional bridge models

Additional finite element models for three bridges selected by the FDOT were developed based on the model developed in Task 4. New models have different lengths, widths, number of girders, etc.

Task 10: Analysis

A database of the six F.E. truck models and three models of the bridges allowed for analysis of up to 32 different vehicle–bridge configurations. Hence, up to 32 different cases were studied resulting in recommendations regarding impact factor, speed limit and weight limit for the trucks.

Task 11: Quarterly and Final Reports

The results of tests and analytical analyses were summarized in Progress Reports submitted to the Florida DOT. All the tests were described in the Final Report submitted to the FDOT for review and comments. The measured and calculated impact factors were compared with values obtained using design code formulas. The results will serve as a basis for validation of the permissible weight limits for the tested bridges. The recommendations resulting from this project are submitted with the Final Report.

Table 1.1. Research activities by task.

No	Task description	Scheduled progress of the projects																							
		Year 1 (Phase I) quarters												Year 2 (Phase II) quarters											
		1			2			3			4			5			6			7			8		
1	Literature review	■	■	■		■			■			■			■			■			■			■	
2	Selection of bridge and vehicle		■	■	■																				
3	Heavy truck model			■	■	■	■	■	■																
4	Bridge model					■	■	■	■	■															
5	Field testing technique							■	■	■															
6	Field test of the first bridge										■	■													
7	Bridge model validation											■	■	■	■										
8	Additional crane models													■	■	■	■	■	■						
9	Additional bridge models																■	■	■	■	■	■			
10	Analysis																			■	■	■	■	■	
11	Quarterly and final reports			■			■			■			■			■			■			■	■	■	■

Completed tasks = ■

1.4. Scope of the research

The first step in the research was the field test conducted in August 2003. The description of the experiment and its results are presented in Chapters 3 and 4. The development of FE models began with the truck and the bridge examined during the field test. As it had been proposed in the Research Tasks (Section 1.3) three additional bridge models and three models of trucks were developed. Originally, 16 cases for four bridges and four trucks were considered. On the basis of the experience gained after the field test and after performing preliminary calculations, the research plan was extended. The case matrix was refined and doubled based on the discussion among the Project Manager, Principal Investigator and CIAL members, conducted in the CIAL Lab on 10.05.2004. The new matrix was developed for the previously selected three bridges described in Section 4.10 and for six trucks presented in Section 4.9. It was determined that the following six variables could have a significant influence on impact factor IM:

1. span length
2. truck speed
3. suspension parameters
4. truck weight

5. truck position on bridge lanes
6. road surface condition

The case matrix was modified in order to study the influence of some of these parameters. The original number of 16 cases was doubled. Tables 5.2, 5.3 and 5.4 present the plan for the calculations. The FE Model of the bridge #4 was excluded from further analysis. This model, already completed, can be used in future calculation, if needed. Additionally, the loading for truck #1 was modified. Based on the recorded video from the field test it was found that the dynamic effect was amplified by the loading consisting of concrete blocks jumping up and down during the passes through the bridge. This bouncing (hammering) effect was to be included in the next round of calculations.
The results of all calculations are presented in Chapter 5, summary and conclusions in Chapter 6.

1.5. Benefits to the Florida Department of Transportation

The Maintenance Office of the Florida Department of Transportation is charged with the mission of supporting and enhancing truck mobility while preserving transportation infrastructure. This mission challenges the Department to allow larger and heavier trucks on Florida highways and bridges without compromising safety. This challenge becomes even more complex if time is limited for making these decisions. FDOT issues 95,000 overweight / overdimension permits per year for heavy trucks, cranes and cargo (as heavy transformers) ranging from 80,000 lbs to over 1 million lbs. Quick decisions made by the FDOT require validated and precise information on maximum dynamic loading (impact factors) imposed by several types of moving vehicles on a wide variety of Florida bridges. Expected benefits from this research for the FDOT include:

1. Several combinations of loading cases and bridge types were selected to represent the most critical load – structure combinations.

2. Most of the over 6,300 bridges used in Florida (some of them were surveyed in this study), are short bridges with span range below 90 ft, which were shown to have a significant dynamic response due to highly concentrated live loads produced by heavy and bulky cranes. Thus, the recommendations provided to the FDOT cover 32 of the most critical cases representing a large population of vehicle and bridge types in Florida.

3. Sensitivity analysis of several parameters was conducted. These parameters include span length, vehicle weight, vehicle speed, suspension characteristics, truck position on bridge lanes, and road surface condition. The study identifies the parameters, which affect amplified dynamic response most. The importance of the parameters is discussed in Chapter 5.

4. This study considers actual parameters important for assessment of actual dynamic loading. These external factors include bridge approach depressions and thresholds before bridge approaches. These surface imperfections were surveyed by the research team for two actual bridges in Northern Florida. This study serves therefore as an important prelude to a follow-up project will include an additional 20 surveys of bridge approaches and their effect on dynamic impact factors.

5. The study also provides information on actual distribution factors, which show the percent of the total vehicle dynamic loading carried out by a given girder. This information is critical for assessment of the ultimate load bearing capacity of the girder and corresponding safety factor for quick and accurate overload permitting process.

6. The developed and validated finite element models of the bridges and the vehicles can be used for other projects of interest to the FDOT. These models are easy to modify to represent new vehicle and bridge types. They may be readily available for future projects related to health monitoring, effect of fatigue on life span of girders, effect of using high strength concrete on structural dynamics of bridges, bridge strengthening studies, and many others.

1.6. Research collaboration / subcontracting

A successful completion of research work requires careful planning of all activities and closely collaborating efforts with other groups. The actual field test is an important task for this project since it provides the most reliable information of bridge dynamic response. The experimental results were used to validate the FE model.

It had been planned to utilize filed testing experiences gained by the research team from University of Michigan directed by Professor Andrew Nowak. However, no funding budget was allocated in the budget for these efforts. Professor Nowak's team is experienced with bridge testing and he generously lent us the Noptel system, an expensive laser device for recording displacement history.

The field test was conducted mostly by the FDOT Structural Lab with the help of CIAL team. Professional suggestions and recommendations, from the reliable testing equipments to testing plan, were given by Project Manager Mr. Jean Ducher and by Mr. Garry Roufa and Mr. Marc Ansley from the Structures Lab. Instrumentation was professionally performed by the FDOT staff before the test. The testing trucks were driven through the bridge by FDOT drivers at the specified speeds. Experimental study on bridge loading was conducted in-house by the Structures Laboratory of the Florida Department of Transportation under the guidance of the Lab Chief Structures Engineer Mr. Marc Ansley.

2. Literature review

2.1. Areas of interest

The literature relevant to this project was reviewed intensively at the early stage and was continued throughout the whole project. The topics included AASHTO specifications of bridge dynamic effects, finite element modeling of bridges and vehicles, vehicle-bridge interaction, finite element applications for bridge dynamics, and bridge dynamic testing.

2.2. Consideration of dynamic effects in design codes

Highway bridges are subjected to dynamic forces imposed by moving vehicles. The corresponding dynamic effects can result in deterioration of bridges, consequently increasing the maintenance cost and decreasing the service life [18]. It is necessary to consider the dynamic effects when evaluating an existing bridge or designing a new one. In engineering practice, impact factor (now called dynamic allowance) is commonly used to account for the dynamic effects of wheel loads on bridges. The dynamic effects arise from complex vehicle-bridge interactions and are attributed to two major sources [1]:

- The hammering effect is the dynamic response of the wheel assembly to riding surface discontinuities such as deck joints, cracks, potholes and delaminations.
- The dynamic response of the bridge as a whole to passing vehicles may be due to long undulations in the roadway pavement, or to resonant excitation from the similar vibration frequencies between the vehicle and bridge.

In AASHTO (American Association of State Highway and Transportation Officials) standard specifications for highway bridges [2], the impact factor is expressed as the increment of the static response of the wheel load and is determined by the formula:

$$I = \frac{50}{L + 125} \tag{2.1}$$

L is the length in feet of the portion of the span that is loaded to produce the maximum stress in the member. The impact factor I should not exceed 30%.

In other codes, like Canada's Ontario bridge design code (1983) and NAASRA (National Association of Australian State Road Authorities), the impact factor is defined as a function of the first flexural frequency of the bridge.

The equation (2.1) is based on field tests and theoretical analysis for the specific trucks. It is not clear if the equation can be used for bridges subjected to oversized and overweight vehicles such as cranes. With the help of advanced numerical methods, research is conducted to try to accurately evaluate the wide range of bridge dynamic responses and to determine the actual impact factor.

2.3. Vehicle models

Analytical models

A large number of analytical vehicle models, with different levels of complexity, are used to study the dynamic effects of bridges. The choices concerning vehicle type and characteristics are important for realistically predicting the bridge response [38]. Analytical vehicle models are simple for mathematical convenience but consist of the most essential elements of the vehicle such as the body, wheels and suspension systems. Bodies are commonly represented by masses subjected to rigid body motions. Suspensions are assumed to be the combination of springs and dampers dissipating energy during oscillation.

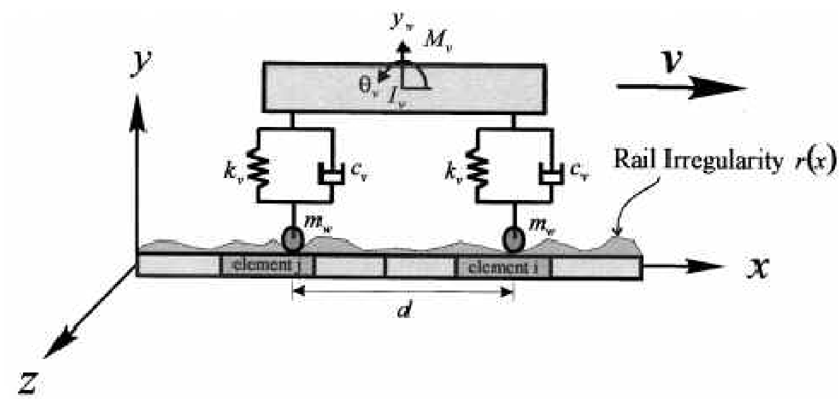

(a)

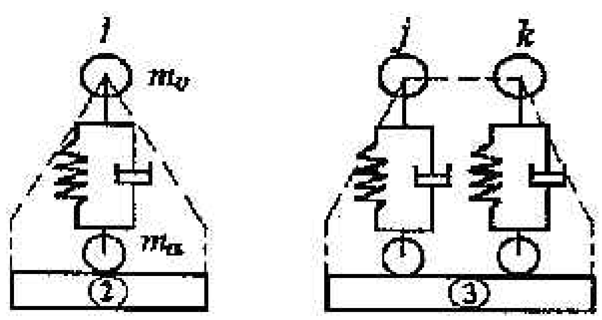

(b)

Figure 2.1. Simple vehicle models.

Figure 2.1 presents the simplest models [44], [42]. In Figure 2.1 (a), the body is modeled with a rigid bar while the suspension unit is composed of a spring and a damper. Further simplification can be achieved by using lumped masses at the ends of the bar with the rotation degrees of freedom excluded (Figure 2.1 (b)). Many similar models are discussed and used to study the dynamic interactions between vehicles and bridges in [18], [45], [15], [28], [10].

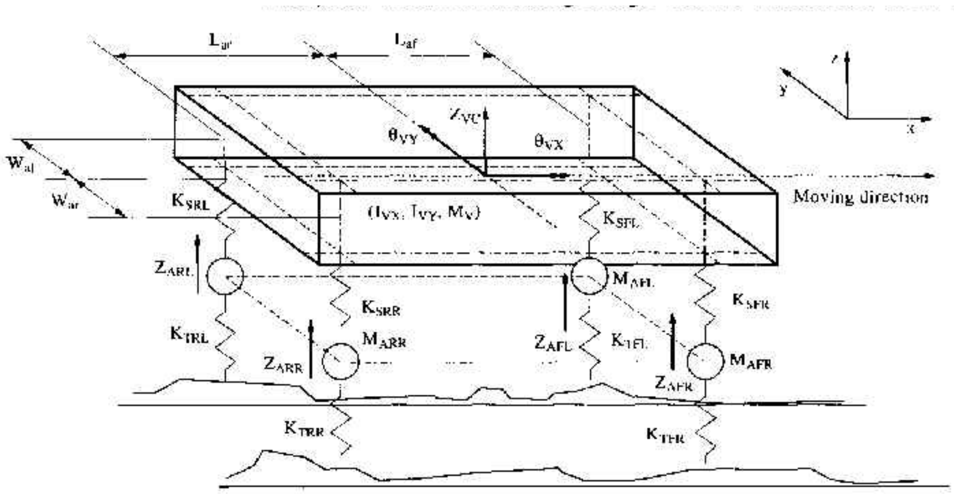

Figure 2.2. Three dimensional analytical vehicle model.

Figure 2.2 shows an example of a three-dimensional vehicle model [38]. It is modeled as a rigid chassis subjected to rigid body motions including pitching and rolling rotations. There are a total of seven degrees of freedom in this model: vertical displacement at the chassis center, pitching and rolling rotation about the two axles of the chassis, and four vertical displacements at each of its axle locations. The tires (wheels) are modeled as point followers with springs under the axles. A real multi-leaf suspension system is made up of a number of steel beams which are allowed to slide over each other. When the leaves deflect, some energy is stored in the bending of beams and rest of energy is dissipated through friction. A spring with a nonlinear relationship between load and deflection is used to represent the multi-leaf suspension. Figure 2.3 presents the configuration and load-deflection behavior of a leaf spring suspension system.

An analytical model of an AASHTO HS20-44 truck with 11 degrees of freedom was used by Florida International University and Florida Department of Transportation to evaluate the dynamic response of highway girder bridges [40]. This model is illustrated in Figure 2.4.

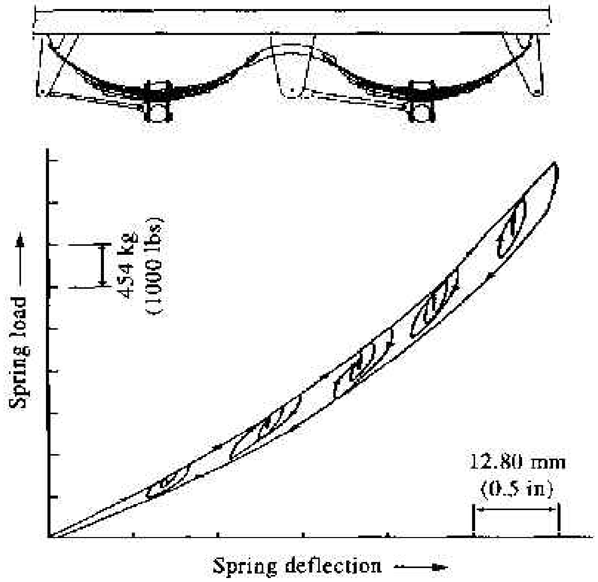

Figure 2.3. Configuration and load-deflection behavior of leaf spring suspension.

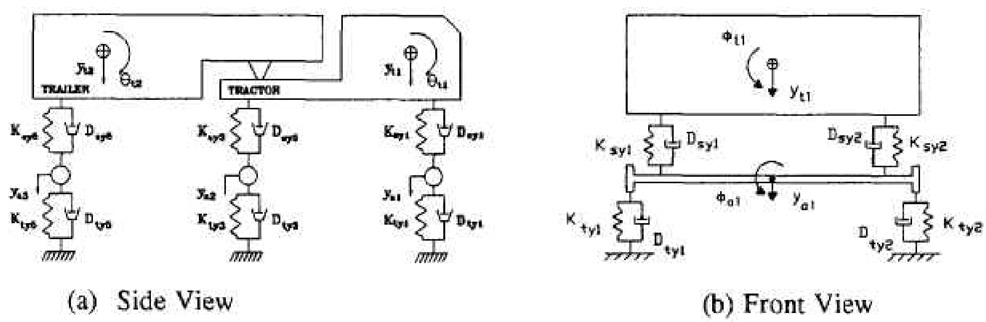

Figure 2.4. HS20-44 analytical model.

The nonlinear vehicle model comprises five rigid bodies, which represent the tractor, semi-trailer, steer-wheel-axle set, tractor-wheel-axle set and trailer-wheel-axle set. The tractor and semi-trailer are each assigned 3 degrees of freedom corresponding to vertical displacement, pitching and rolling. Two degrees of freedom in rolling and vertical displacement are assigned to each wheel-axle set. The tractor and the semi-trailer are connected at the pivot point. The suspension system is modeled with springs and dampers. Similar models were also used for interaction analysis in [25], [32], [23], [20], [11]. Even more complicated models with more degrees of freedom were used but the general structure of the models was the same [16].

Finite element models

An analytical model is treated as a multi-body system and it is convenient for studying the vehicle-bridge interaction theoretically. However, the number of degrees of freedom is limited for mathematical convenience. Current large commercial FE programs make it possible to model complex systems and to animate the results in a post processor, which is useful for the interpretation of the results [4].

Over the years, many vehicle FE models, including trucks, have been developed using reverse engineering for crashworthiness analysis. Some models are available in public domains and ready to use. Different attention is drawn to different parts of a vehicle depending on the purpose of the FE simulation. Some models consist of most structural components with different levels of detailed representation for suspension systems, kinematical characteristics of components and wheel models with airbags applied. After modification and improvement, they can be used for simulating the vehicle – bridge interaction. The vehicle response, the vibration of bridge and the interaction, including contact between wheels and pavement surface, impact forces, and moving live loads, can be modeled. Figure 2.5 presents a single unit truck model developed by NCAC and Figure 2.6 shows a heavy truck model.

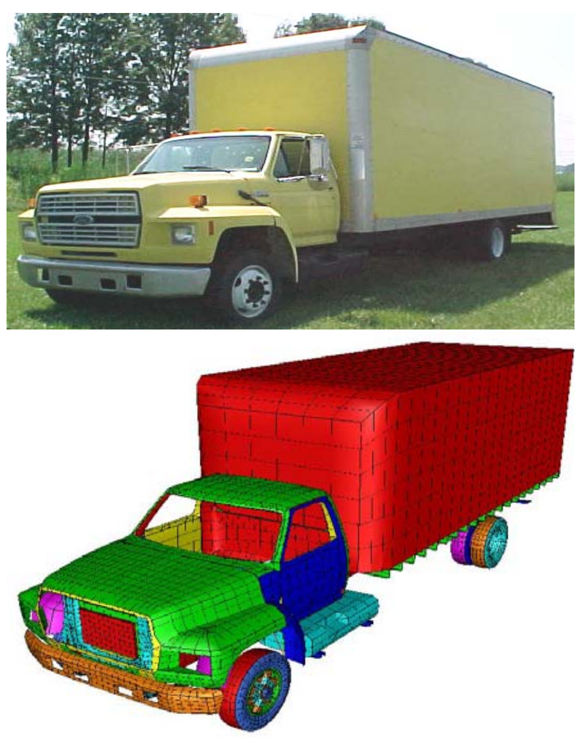

Figure 2.5. Single unite truck model developed by NCAC

.

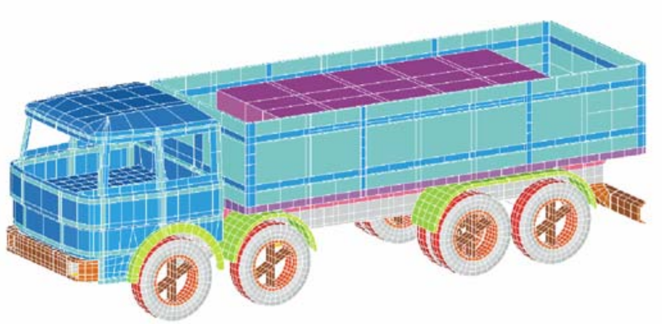

Figure 2.6. Heavy truck model.

A good example of the application is that a truck model, developed for a particular three-axle truck belonging to VTT (the technical research center of Finland), was used to study the vehicle bridge interactions by W. Baumgaertner [4]. In the model, beam elements are chosen to describe axles and body; spring and damper elements describe the suspension. The mass distributed in the beam elements is lumped at the beam nodes. Table 2.1 lists the truck modes and corresponding frequencies.

Table 2.1. Truck modes and frequencies

Eigenmode	Frequency (Hz)
frame twist	0,82
body bounce	2,01
body pitch	1,02
body roll	1,53
front axle: hop	11,08
front axle: roll	15,50
second axle: hop	9,89
second axle: roll	13,25
third axle: hop	9,97
third axle: roll	13,26

2.4 Bridge models

Analytical models

There are several levels of bridge models in use for studying dynamic response. With regard to interaction effects and changing contact points between wheels and deck, there are no close solutions when the truck is modeled as a vibrating system including mass and elasticity [4].

In some cases, bridges are modeled as simple or continuous beams. The beam analogy is relatively efficient if the bridge is straight, non-skewed and symmetric about the centerline with large length to width ratio, uniform stiffness and mass distribution, and symmetric loads. However, a beam model excludes the tortional and transverse modes, which in reality can be excited when the truck does not travel along the centerline of the bridge.

Grillage models allow for better approximation of the response of a slab since both flexural and torsional stiffness are taken into account. They have been thoroughly investigated and compared with data from full scale structures by the Cement and Concrete Association of the U.K. This model was determined to be a suitable analytical tool for bridge analysis [38]. Figure 2.7 shows a grillage element and Figure 2.8 illustrates a grillage model of a bridge.

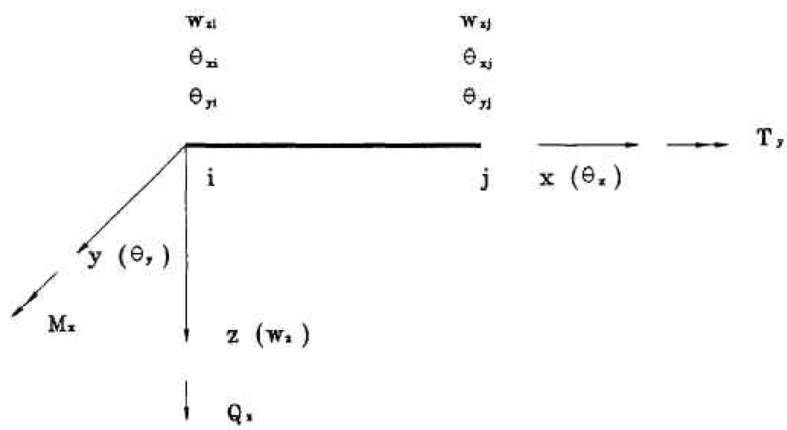

Figure 2.7. Grillage element.

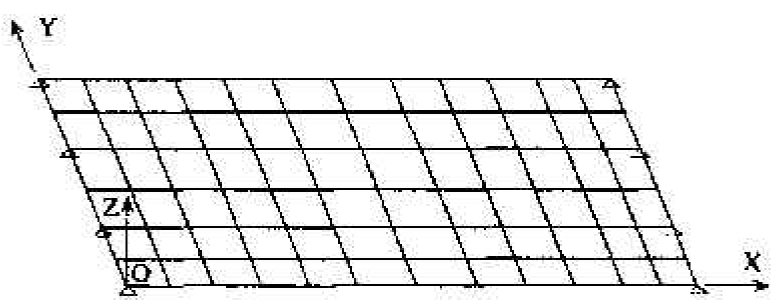

Figure 2.8. Grillage model of bridge [38].

The model is made up of a series of discrete elements, including longitudinal beams (girders) and transverse elements (diaphragms). The elements are connected at joints where loads and constraints can be applied. The stiffness and spacing of girders were determined so that the deflection of the model and the actual bridge were the same. The more girders are used, the more accurate results can be achieved. However it will increase computation time. Today with the increasing computing power, the number of elements is no longer a major limit. It is possible to develop detailed three dimensional FE models with a large number of elements.

Finite element models

As mentioned before, commercial FE programs enable the modeling of complex civil structures in detail and more accurately. The Federal Highway Administration and the National Crash Analysis Center have focused on developing highly realistic and detailed numerical models of highway bridges to conduct health monitoring. [29]. By FE method, some key features in a bridge can be accurately modeled compared with the analytical method [29]. These features include component geometry, constitutive material models, component connections, boundary conditions, and dynamic loading conditions.

In a simplified analytical model, some structural components have been ignored, which is the major reason to explain the significant discrepancy between the results of the analytical model and the real response of the bridge. The precise geometry of the concrete deck, girders and cross members has a direct impact on the overall dynamic response of a bridge [29]. Because all the components in FE models are modeled with a large number of shell and solid elements rather than beam elements, the bridge characteristics like mass, inertia, center of gravity and stiffness of structural components are more accurately represented. The detailed 3D model can also predict the buckling and torsional deformation of structural components.

When the bridge is subjected to extreme traffic loads, it is possible for the bridge to undergo nonlinear response, either locally or globally due to plastic deformation, time varying dependency of materials and aging degradation. Commercial FE codes provide many material models which can describe the nonlinear properties of materials and provide the opportunity to define a curve relating stress and strain.

Connections between components such as bolts and welds in a bridge can be correctly modeled in a FE model. LS-DYNA, a 3D explicit FE software, provides several options to model the connections with failure. In [29], over 750 rigid body constraints were used to model the bolts and connections among the different cross frame members, stiffeners and girders.

The superstructure of a bridge is connected to the piers through rollers and bearing pads. Each roller limits the relative translational motion between the girder and the pier. The bearing device allows for translation motion along the longitudinal direction of the bridge girder. In an FE model, all these supports can be modeled with their real geometry and by applying appropriate material model. Figures 2.9 - 2.11 show an example of the FE model of a highway bridge.

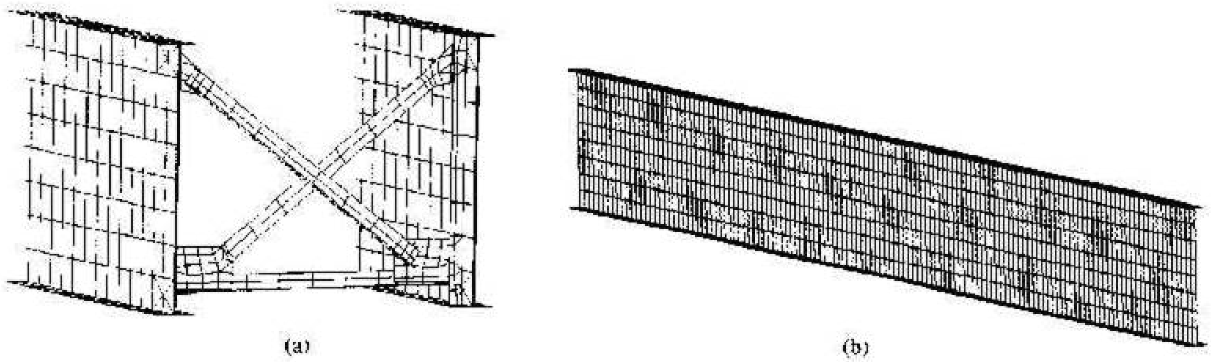

Figure 2.9. Detailed geometry described in FE model

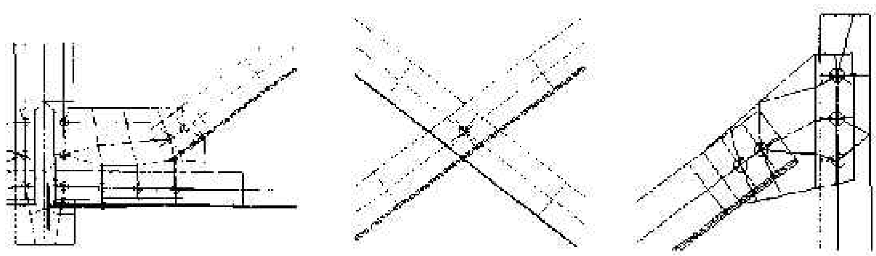

Figure 2.10. Rigid body constraints used to model bolt connection.

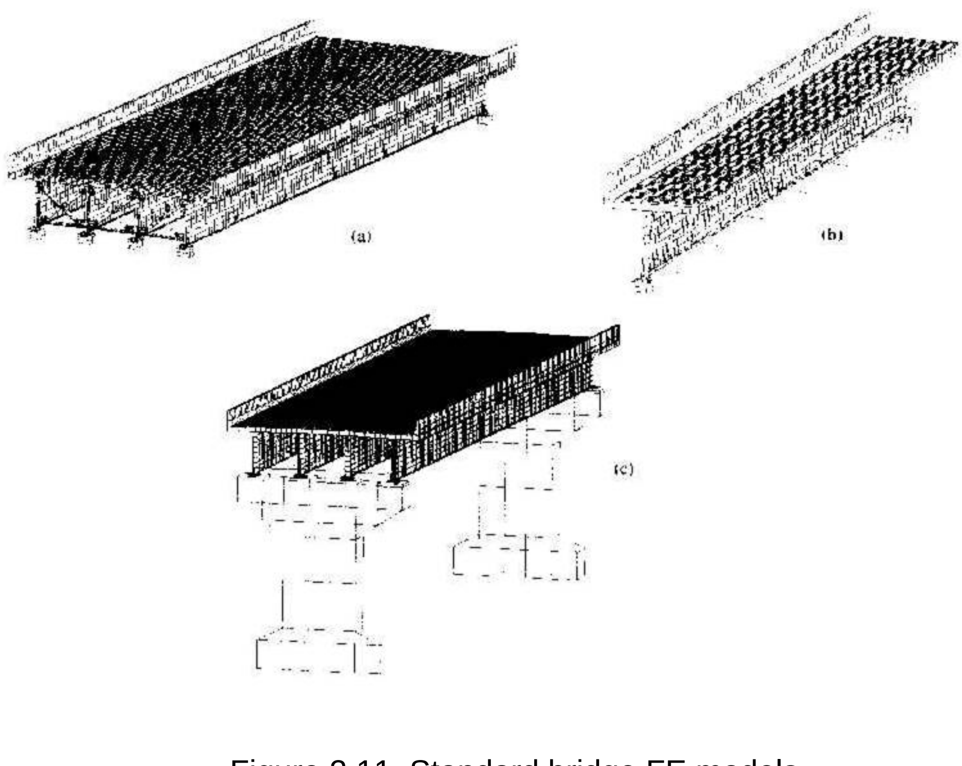

Figure 2.11. Standard bridge FE models.

Model (a) is a detailed full bridge model; (b) is a quarter bridge model and (c) is a reduced full bridge model. Summary of the models are given in Table 2.2.

Table 2.2. Summary of bridge models.

	Detailed Full Bridge Model	Quarter Bridge Model	Reduced Full Bridge Model
Number of Parts	26	19	21
Number of Nodes	26,000	7,000	13,000
Number of Shells	20.000	2,000	8,000
Number of Solids	15,000	3,000	6,000
Number of Beams	0	21	105
Simulation Time Duration	5 sec	5 sec	122 sec
CPU Time	65 hrs	4 hrs	160 hrs

Figure 2.12.shows another example of a finite element model of a bridge [39]. The deck, girders and railings are modeled with 3-D elements.

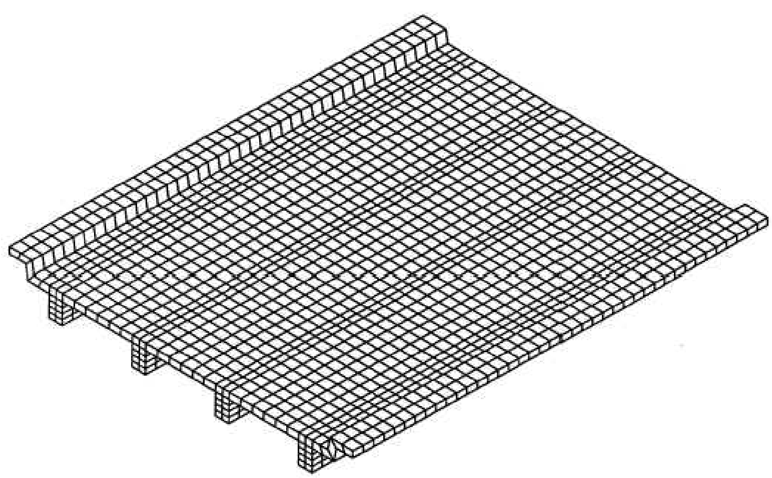

Figure 2.12 Finite element model of a bridge.

2.5. Modeling of pavement profile

The vehicle bouncing on its suspension due to roadway roughness has been recognized to be a major source of bridge dynamic effects. Sometimes road surface irregularities may cause vehicle frequencies to approach the natural frequencies of the bridge superstructure and significantly increase dynamic loads [11]. Therefore, the road profile needs to be considered in the vehicle-bridge interaction analysis. In theoretical analysis, the road profile is assumed to be a realization of a random process, which can be described by a power spectra density function (PSD) [38]. Figure 2.13 and Figure 2.14 show the road surface profile.

.

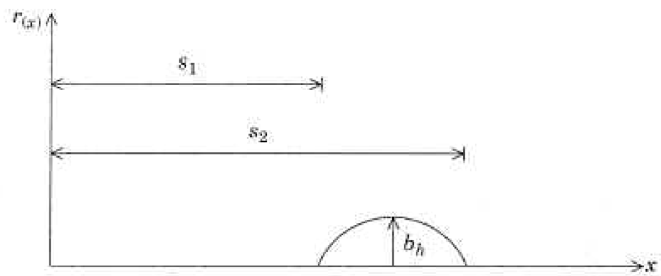

Figure 2.13 Roadway surface irregularities [11].

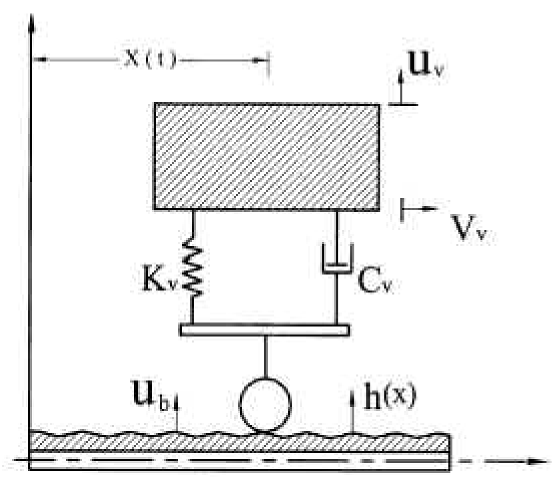

Figure 2.14. Interaction system with exaggerated surface irregularities [15].

2.6. Vehicle bridge interaction

Once the analytical models of the bridge and vehicle are developed, the direct method used to conduct interaction analysis is to formulate the governing equations of motion. The vehicle has contact points with the bridge deck and maintains that contact as it moves along the deck. For example, for a spring mass system moving along the bridge deck, two equations of motion have to be formulated. The first equation represents the dynamic equilibrium of the bridge; the second equation is for the dynamic equilibrium of the spring mass system. The interaction force between the pavement and the spring mass system depends upon the deck displacement. Hence the two equations are coupled and need to be solved simultaneously. The system governing equations are nonlinear because of the physical characteristics of the system and the components.

Reference [23] gives two ways to simulate the vehicle-bridge interaction. Figure 2.15 presents the dynamic analysis procedures of vehicle - bridge interaction.

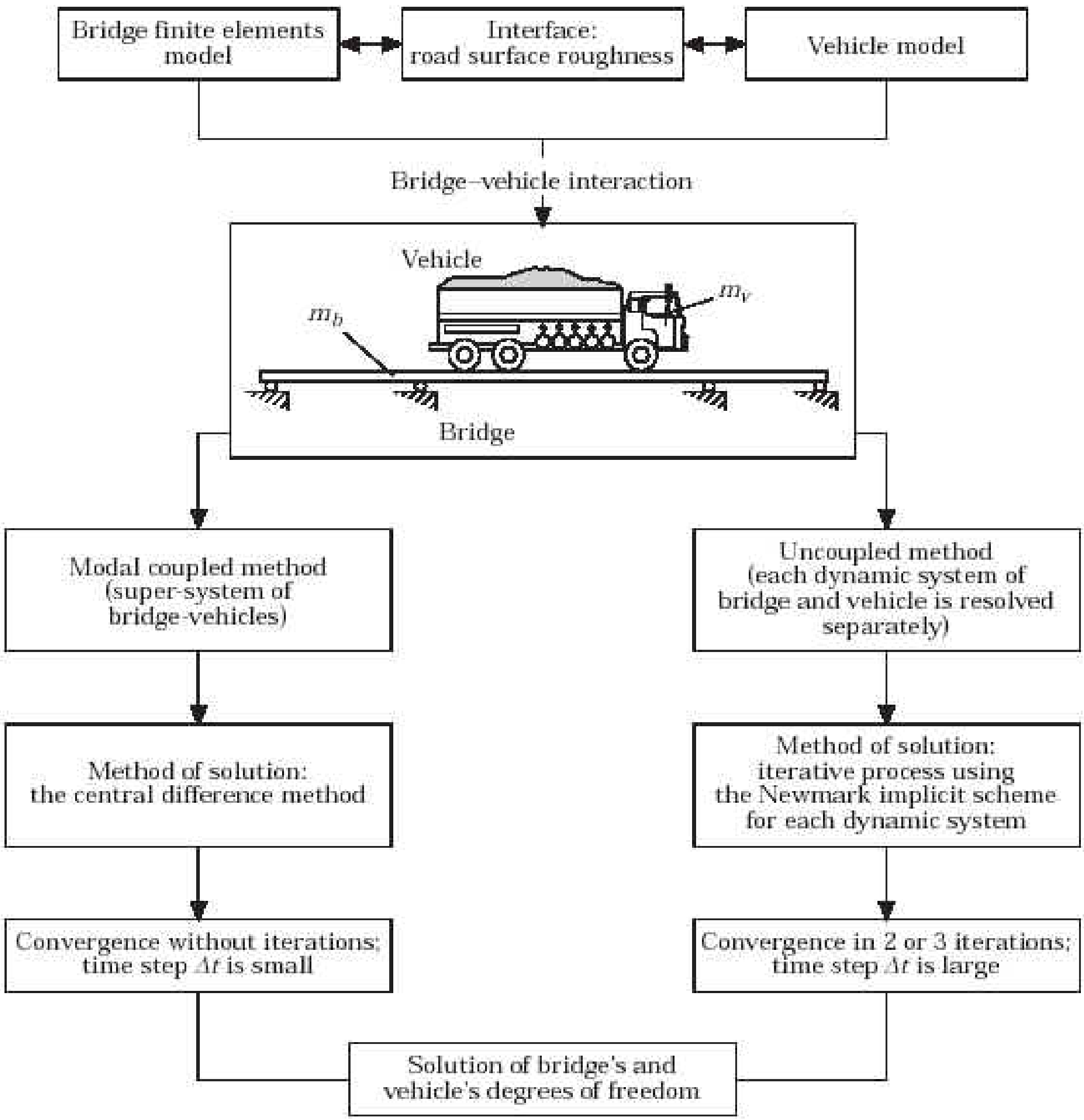

Figure 2.15. Dynamic analysis procedures of vehicle and bridge interaction.

Today's large nonlinear finite element programs allow for effective modeling of the dynamic behavior of bridge structural system.

In [4], the bridge and the truck are modeled separately to simulate three different situations. (1) the truck is running on the rough road before reaching the bridge; (2) the truck crossing the bridge with rough surface; (3) the truck has left the bridge and the bridge is in a free vibrating state.

In [29], the bridge was modeled in detail in LS-DYNA while the moving traffic flow was simplified by using concentrated nodal forces with appropriate load curves. The pressure due to tire contact with the road surface is assumed to act at the centerline of the tire and move at the same speed as the vehicle. Load curves are assigned to the nodes in the path of the vehicle motion. This simulation did not include the effects of the vehicle suspension system. The same method is also used in [39]. (see Figure 2.16).

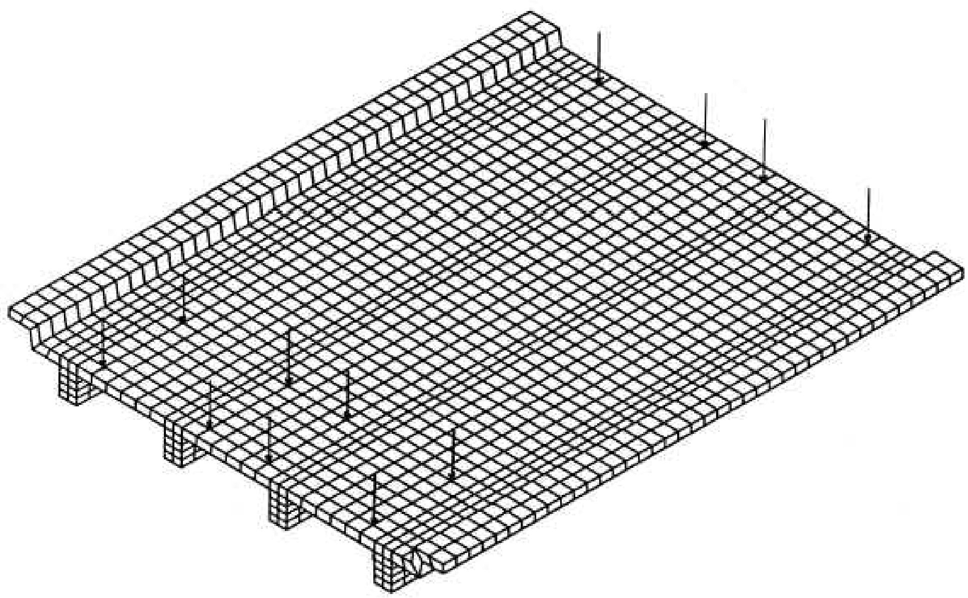

Figure 2.16. Dynamic loading configuration simulating test trucks.

2.7. Dynamic tests of bridges

Dynamic testing helps to obtain information on the dynamic behavior of a bridge, serves to increase the database on dynamic response of similar bridges and gives the opportunity to know their properties [36]. The measurements and the subsequent analysis of structural vibration allow for calculation of frequencies and the dynamic response of the bridge subjected to excitation. Subsequently, the results of dynamic testing are compared with those from the analytical model to either validate the analytical model or identify structural parameters that largely influence the dynamic bridge response [6]. Therefore, field testing is widely used by researchers in bridge engineering and monitoring.

In literature [13], the load test procedure is described and the performances of the accelerometers and strain gauges are compared. Literature [33] demonstrates the method that is used to identify the modal parameters from recorded acceleration histories. M.J.Robinson and F.M.Russo used field testing to study the relationship between structural response and damages [34]. A team from the University of Virginia tested a new deck system by using a field test. Also field testing was used by P.Paultre to determine the impact factor for existing bridges [31].

Methods of inducing bridge vibration

Different methods are used to introduce bridge vibration. They include vibrators, impactors, traffic flow and test trucks. In full scale testing of large structures, vibrators are commonly used, which are mounted on the structure and stay in contact with the structure throughout the testing period. Vibrators are usually eccentric rotating masses or electro hydraulic type. Impactors have also been successfully used in some structure tests. The simplest impactor is an instrumented hammer. The impulse delivered to a structure can vary by changing the mass [36]. In the research on the interaction between vehicles and bridges, it is natural to use the traffic flow or testing truck to induce the vibration.

In [9], up to 77 in-service vehicles, including refuse-collecting vehicles, coaches, public buses, and trucks with different weights, were recorded when conducting dynamic bridge test. Table 2.3 lists the vehicles.

Table 2.3 Different in service vehicles for dynamic testing.

No. of Axles	Description	Vehicular configuration	No. of Samples
2	Refuse collecting vehicle	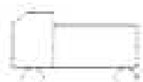	1
2	Coach		8
2	Public bus (16 seats)		5
2	Medium lorry with box body		11
2	Light goods vehicle		21
3	Platform lorry		17
3	Concrete mixer truck		7
3	Heavy lorry with box body		3
4	Articulated lorry		4
		Total	77

The disadvantage of using in-service vehicles is that no information about axle load is available.

A better way is to let a testing truck run through the bridge at different speeds and configurations. The loads on every axle of the truck can be controlled by appropriately loading the truck and using a scale or weigh station. In [3], the excitation was amplified by placing a piece of wood plank on the bridge surface. The test configuration is shown in Figure 2.17.

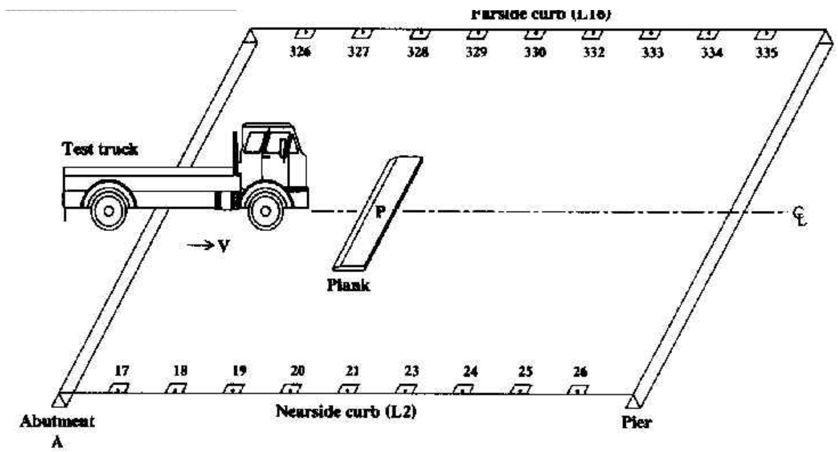

Figure 2.17. Span vibration test layout.

Data acquisition systems

In bridge tests, sensors are placed on critical load-carrying members and their responses are electronically measured and recorded as testing vehicles move on the bridge. Sensors for full-scale, large structure testing come in three general categories: displacement, velocity and acceleration transducers. Displacement transducers are extremely fragile and require a fixed datum [26]. This makes them impractical in a full scale structure test. Recently, a new displacement measurement device based on laser technology was developed for dynamic measurement of large constructions like bridges. Figure 2.18 illustrates the Noptel system which was successfully used to monitor the deflection of bridge girder in Michigan.

Figure 2.18. Noptel laser displacement measurement device.

Velocity transducers are typically used in low-frequency modal testing of structures while accelerometers are often used in a variety of strong motion applications in engineering [26]. An example of using velocity transducers is discussed in detail in [34]. Accelerometers are the most widely used transducers in bridge testing.

Strain gauges are also commonly used in structure testing to measure the strain and thus the stress in structural components to find the static and dynamic loads.

All sensors and gauges are connected by cables with a local data acquisition unit or a data logger which receives and stores the measured quantities at a constant rate and process data automatically.

Selection of appropriate sensors and data acquisition devices

The selection of appropriate transducers is based on the test purpose and quantities needed. The range of values, accuracy, sampling rate, reliability, environmental conditions, power requirement and cost should be taken into account. The output form and signal conditioning also need to be determined.

Criteria, such as accuracy, acquisition rate, number of channels, flexibility, expandability, ruggedness, and computer platform should be considered to determine the appropriate data acquisition system. The data needs to be recorded at the rate of five times the highest frequency of interest. For example, if the highest frequency is 100 Hz then the data recording should be at 500 samples per second. There also should be a filter to eliminate noise above 100 Hz.

Instrumentation

Due to a limited number of transducers, an instrument layout schematic should be designed to capture the mode shapes of structures. Measurement should be taken at points where all the modes (in the frequency range of interest) are well represented. The simplest way of achieving this is to conduct a theoretical analysis or FE analysis before testing. The best positions should be those points where the sum of magnitudes of the mode shape vectors is maximized [35].

The strain gauge layout must account for the stress-strain relationship in the instrumented components. Strain gauge rosettes are required where a biaxial stress field may be present. Figure 2.19 presents an example of instrumentation [13].

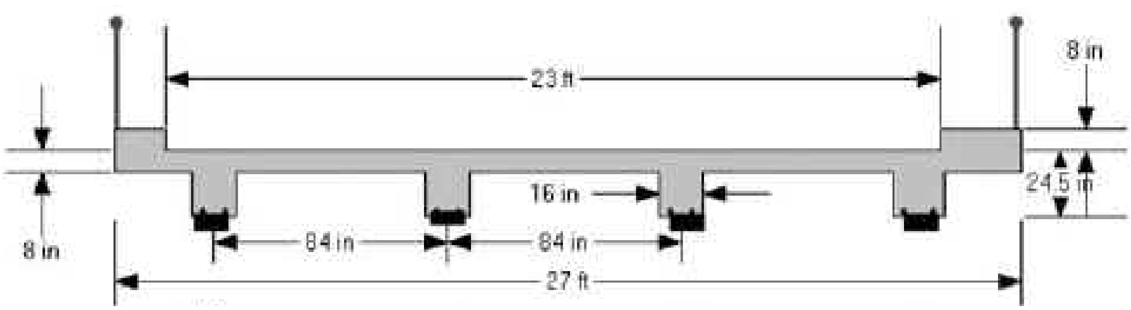

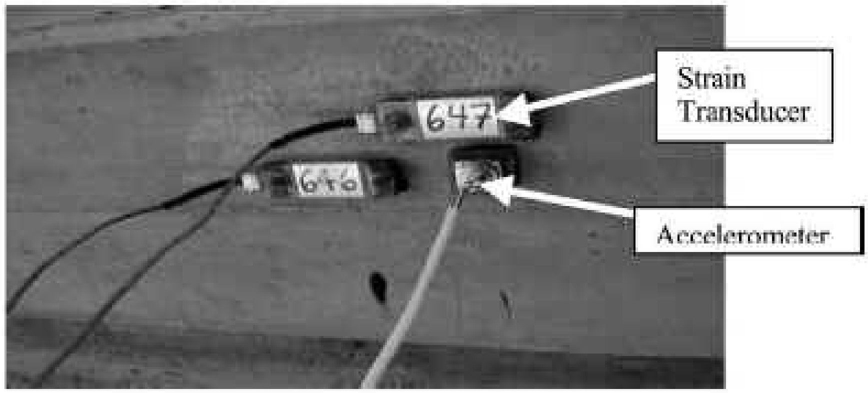

Figure 2.19. Sensor position and placement.

3. DYNAMIC BRIDGE TEST

3.1. Field test procedure

The main objective of the in situ experiment was to assess an actual dynamic load allowance (impact factor) for a selected bridge, for normal and extreme road surface conditions. The field test was also used to validate the finite element (FE) models of the truck and the bridge.

The selected bridge #500133 is a 3-span bridge, built in 1999 on US 90 over Mosquito Creek carrying 2 lanes of traffic. The total length of the bridge is 213.4 ft (65.1m), with each span 71.1 ft (21.7m) long and 46.4 ft (14.15m) wide. In each span six AASHTO type III prestressed girders are simply supported at a spacing of 7.9 ft (2.4m). The concrete deck (slab) is cast in situ as continuous. The whole structure is in good condition with no obvious deterioration such as cracks or damages. The bridge and the elevation are shown in Figure 3.1 and Figure 3.2. Figure 3.3 presents the typical cross section of the bridge. Beams are numbered from the south side (beam #1) to the north side (beam #6).

Figure 3.1. The tested bridge #500133 over Mosquito Creek.

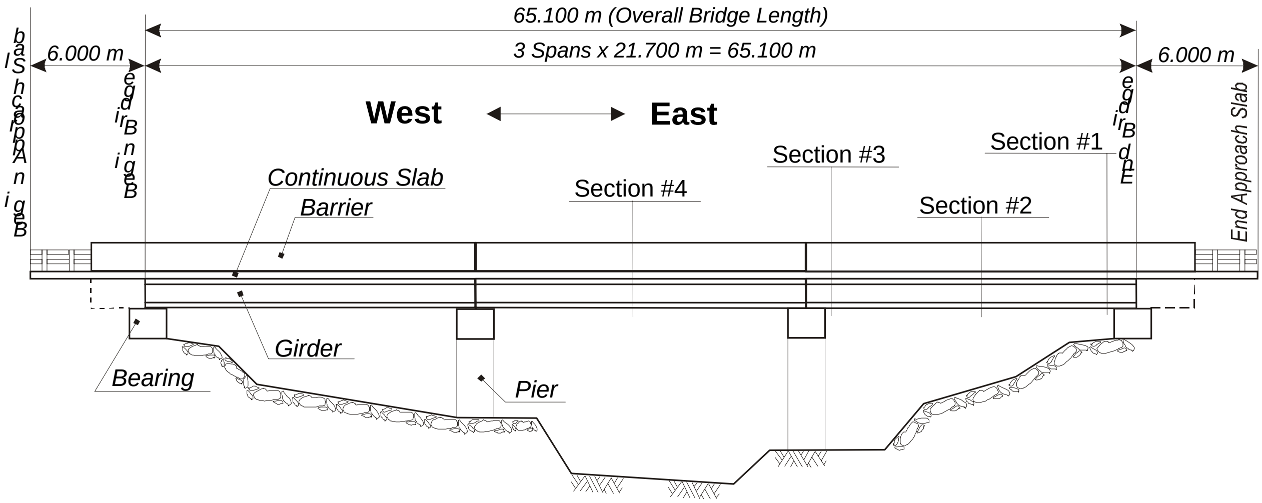

Figure 3.2. Elevation of the tested bridge.

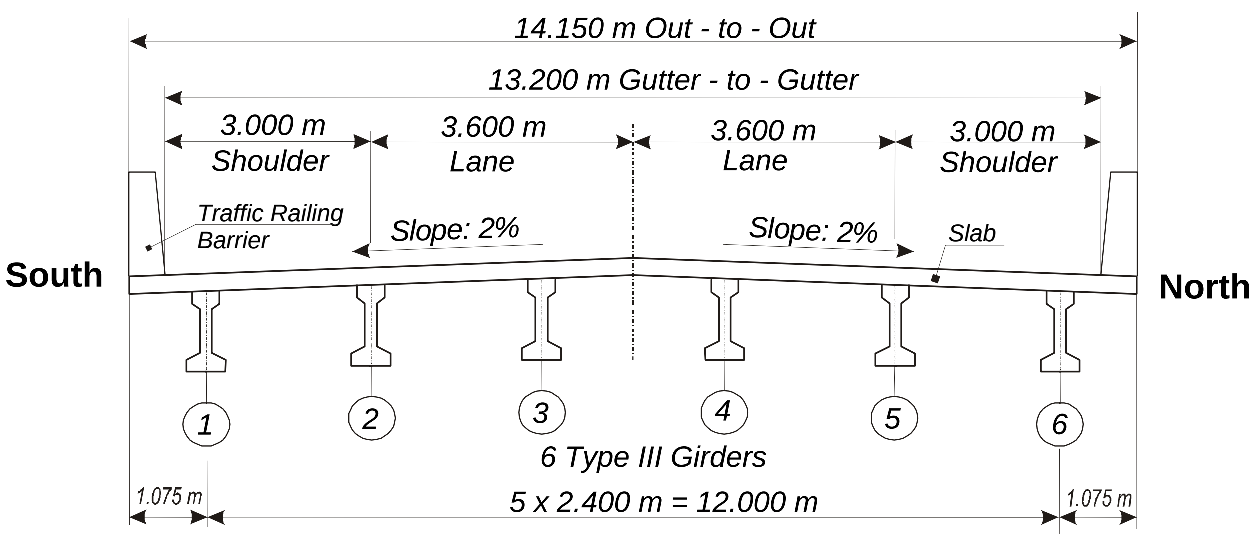

Figure 3.3. Bridge cross section.

Two identical trucks loaded with 12 concrete blocks were used in the field testing (see Figure 3.4). The reactions for each axle were measured in the DOT Structures Lab before the experiment. Section 3.2 describes the loading configuration for each of the tests.

This experiment consisted of 14 tests including 4 static and 10 dynamic tests, as well as two static and two dynamic tests with empty trucks (see Table 3.1). Most of the dynamic test runs were repeated to check the validity of the readings.

Figure 3.4 Configuration of truck used in the test.

In each test, strains and displacements in the middle of the span were measured. For the dynamic tests, accelerations were also read at the truck axle and selected points on the bridge deck. The first span (closer to the east bank) and the middle span were instrumented at four cross sections as shown in Figure 3.2. The first span was selected because of the more convenient access under the bridge. The number, type and position of the gauges are described in detail in Section 3.3.

All results are presented in the Interim Report attached in APPENDIX A - Experimental data. This attachment also includes the calculation of impact factors for all performed tests and modal analysis based on acceleration readings. In the last section of this chapter, some of the dynamic results are presented and the data reduction process is demonstrated for impact factor calculation. Some experimental data is also presented in Chapter 4, Development of FE Models.

3.2. Loading configuration

The longitudinal position of the trucks which gives the maximum strains at the middle span for static case was calculated based on the developed bridge model. Four transverse positions of the trucks were chosen as presented in Figure 3.5.

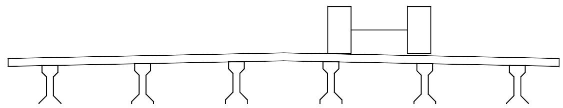

1. One truck in the center of the westbound traffic lane heading west.

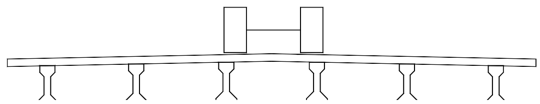

2. One truck at the center of the roadway.

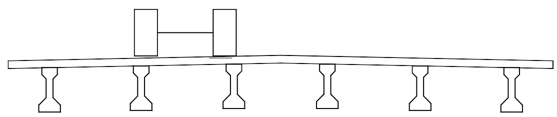

3. One truck in the center of the eastbound traffic lane heading west. This test was performed to check if the bridge structure is symmetrical (corresponding to the middle longitudinal line).

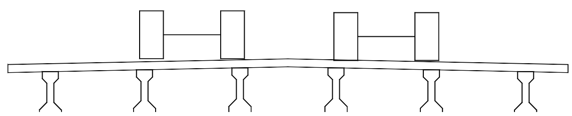

4. Two trucks side by side positioned as in 1 and 3. This test was supposed to approve validity of the superposition principle, showing the elastic response of the bridge.

Figure 3.5. Truck positions for static tests.

Dynamic tests included runs of one or two trucks side by side, with and without a plank positioned on the deck. Runs without the plank are supposed to simulate the normal traffic conditions when the surface of the deck is in good condition. During each test, the trucks entered the bridge from east, heading west.

The plank was used to simulate the extreme conditions which can happen when there is an extensive deterioration on the deck. The wooden plank, 40 mm high and 400 mm wide with a slope of about 45^0 on the entering (east) side, was nailed to the deck at the middle of the span (Figure 3.6). The longitudinal position of the plank is only one of the parameters (such as a truck type, speed, bridge structure, interaction between adjacent spans) affecting the bridge response (dominant vibration modes). Because of that, it was impossible to predict which position of the plank could cause the largest flexural vibration if the effect of the other parameters selected is unknown [3]. It was believed that for a simply supported span, impact forces applied close to the middle of the span should cause vibrations with dominant flexural modes, corresponding to low frequencies. The test confirmed this assumption.

Figure 3.6. Wooden plank used in the tests.

Two velocities of the trucks were applied: medium - 30 mph (48 km/h) and high-speed - 50 mph (80 km/h). All static and dynamic test configurations are presented in the Table 3.1. Runs #10 and #16 were excluded during the experiment. For each static test, the actual position of the truck was measured as a distance from the rear axle of the trailer to the end of the span and distance from the side of the rear wheel to the barrier.

Table 3.1. Configuration of static and dynamic tests for bridge #500133.

Configuration of static and dynamic tests for Br. No. 500133 - US 90 (SR 10) over Mosquito Creek										
Run #	**Test #**	**Pass #**	**Type**	**No. of Trucks**	**No. of Blocks**	**Position**	**Vel.**	**Plank**	**Time**	**Comments**
1	1	1	Static	1	12	Center of W.B. Lane	NA	No		
2	2	1	Static	1	12	Center of Roadway	NA	No		
3	3	1	Static	1	12	Center of E.B. Lane	NA	No		
4	4	1	Static	2	12	Centers of Both Lanes	NA	No		
5	5	1	Dynamic	1	12	Center of W.B. Lane	30 mph	No		
6	5a	2	Dynamic	1	12	Center of W.B. Lane	30 mph	No		
7	6	1	Dynamic	1	12	Center of Roadway	30 mph	No		
8	6a	2	Dynamic	1	12	Center of Roadway	30 mph	No		
9	7	1	Dynamic	2	12	Centers of Both Lanes	30 mph	No		
10	7a	2	Dynamic	2	12	Centers of Both Lanes	30 mph	No		
11	10	1	Dynamic	1	12	Center of W.B. Lane	50 mph	No		
12	10a	2	Dynamic	1	12	Center of W.B. Lane	50 mph	No		
13	11	1	Dynamic	1	12	Center of Roadway	50 mph	No		
14	11a	2	Dynamic	1	12	Center of Roadway	50 mph	No		
15	12	1	Dynamic	2	12	Centers of Both Lanes	50 mph	No		
16	12a	2	Dynamic	2	12	Centers of Both Lanes	50 mph	No		
17	8	1	Dynamic	1	12	Center of W.B. Lane	30 mph	**Yes**		
18	8a	2	Dynamic	1	12	Center of W.B. Lane	30 mph	**Yes**		
19	9	1	Dynamic	1	12	Center of Roadway	30 mph	**Yes**		
20	9a	2	Dynamic	1	12	Center of Roadway	30 mph	**Yes**		
21	13	1	Dynamic	1	12	Center of W.B. Lane	50 mph	**Yes**		
22	13a	2	Dynamic	1	12	Center of W.B. Lane	50 mph	**Yes**		
23	14	1	Dynamic	1	12	Center of Roadway	50 mph	**Yes**		
24	14a	2	Dynamic	1	12	Center of Roadway	50 mph	**Yes**		
25	17	1	Dynamic	1	Empty	Center of W.B. Lane	50 mph	**Yes**		
26	17a	2	Dynamic	1	Empty	Center of W.B. Lane	50 mph	**Yes**		
27	18	1	Dynamic	1	Empty	Center of Roadway	50 mph	**Yes**		
28	18a	2	Dynamic	1	Empty	Center of Roadway	50 mph	**Yes**		
29	15	1	Static	1	Empty	Center of W.B. Lane	NA	No		
30	16	1	Static	1	Empty	Center of Roadway	NA	No		

3.3. Instrumentation

Four sections in two spans close to the east bank were instrumented (Figure 3.7). Displacements, strains and accelerations were collected for selected points where the bridge response was well represented. The positions of transducers were also determined in accordance with the mesh of FE model of the tested bridge. Accelerometers were placed close to the location of the nearest nodes and strain gauges close to the midpoints of corresponding finite elements.

Displacement was measured for one longitudinal position using two independent devices: the Noptel Oy PSM-0 displacement measurement system and LVDT (Linear Variable Differential Transformer). The location for displacement measurements was chosen in the middle of the span, on the bottom surface of the third girder (Figure 3.9). The Noptel and LVDT were placed on both sides of the girder's bottom flange.

Strains were measured using 46 strain gauges glued to the surface of the deck and beams. The gauges were located in four cross-sections: the middle section of the first span, the one close to the abutment, the one close to the first pier and the middle section of the second span (Figure 3.7). The first cross-section near the abutment is located 945 mm from the side of the diaphragm. The third cross-section is located 847 mm from the side of the diaphragm in the first support. The sections close to the abutment and the pier were selected to determine the constraint moments at the ends of the span. These additional constraints are due to interaction between the span and supports and are different in the abutment and in the pier where there is continuous reinforcement in the deck. It was believed that at the middle section (section 2 and 4), the maximum strains are achieved and the bridge response is well represented.

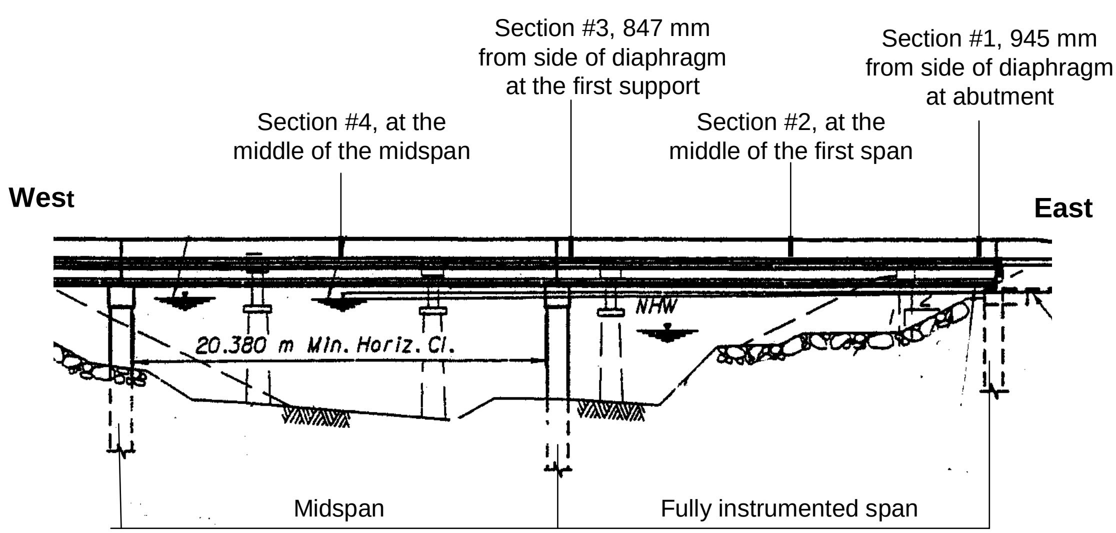

Figure 3.7. Positions of the instrumented cross-sections #1 to #4.

Cross-section #1 was located close to the abutment (Figure 3.7). A total of twelve gauges were attached in this section with one gauge at the bottom of each girder (6 gauges) and one at the side of each girder close to the deck (Figure 3.8).

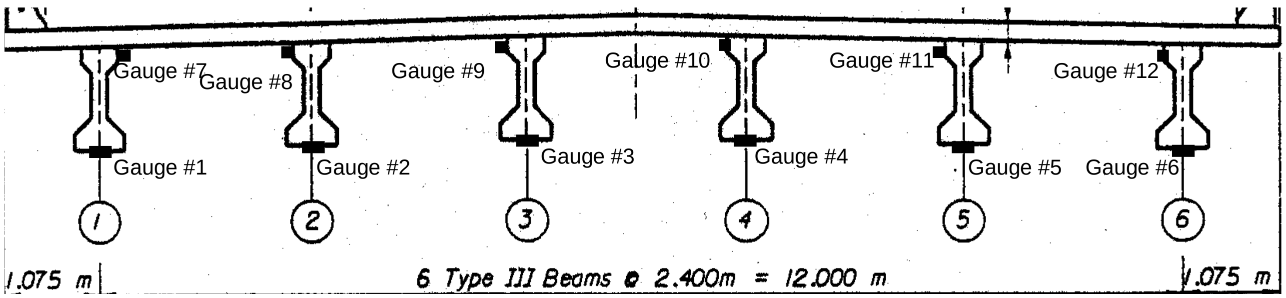

Cross section #1

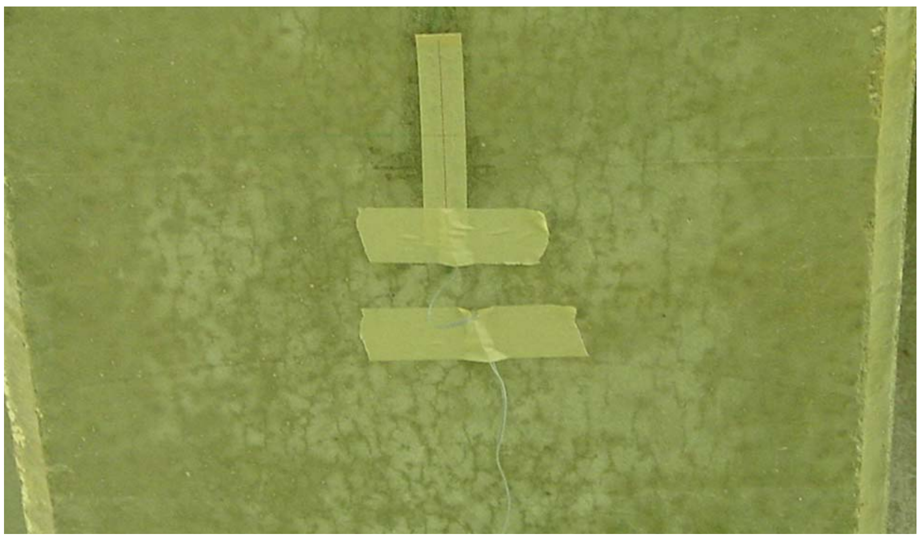

Figure 3.8. Instrumentation of strain gauges in section #1.

Cross-section #2 was located in the middle of the first span. A total of 16 gauges was attached in this section (Figure 3.9). Eight gauges were attached to the bottom surface of the beams. On beams 4 and 6 there were 2 gauges placed side by side at the bottom, symmetrically ¼ aside the middle. These parallel gauges were used to verify the accuracy of readings. Six additional gauges were glued to the sides of the girders close to the deck bottom in the same way as in the section #1. Another two gauges were attached on the deck bottom surface near girder 1 and girder 6 as shown in Figure 3.9 and 3.10. These gauges were used to assess the interaction between the deck and beams.

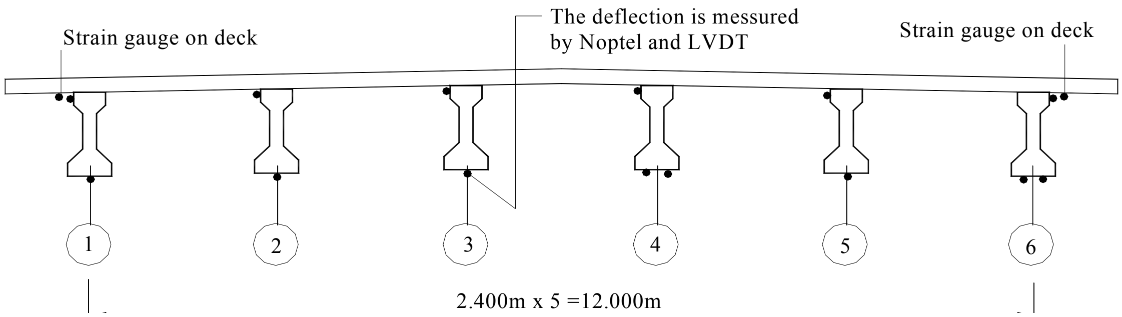

Figure 3.9. Instrumentation for strain and displacement readings in section #2.

The section #3 was located close to the first pier with a total number of 12 gauges. The position of gauges in the section is analogous to that in section #1 (Figure 3.11).

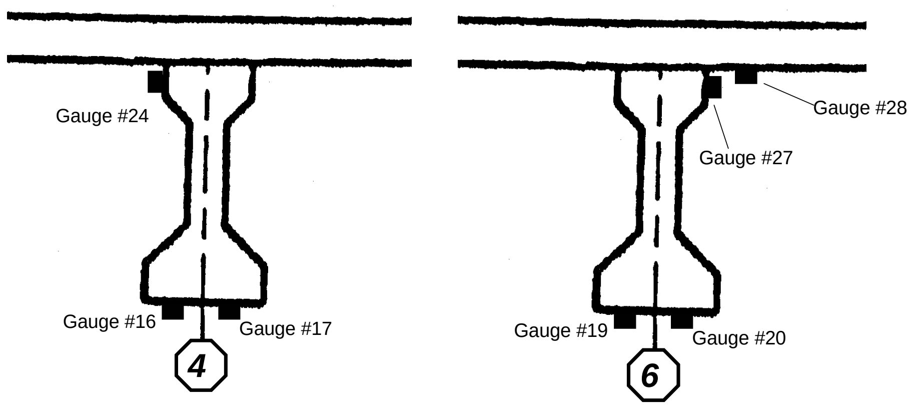

Figure 3.10. Instrumentation at beams #4 and #6.

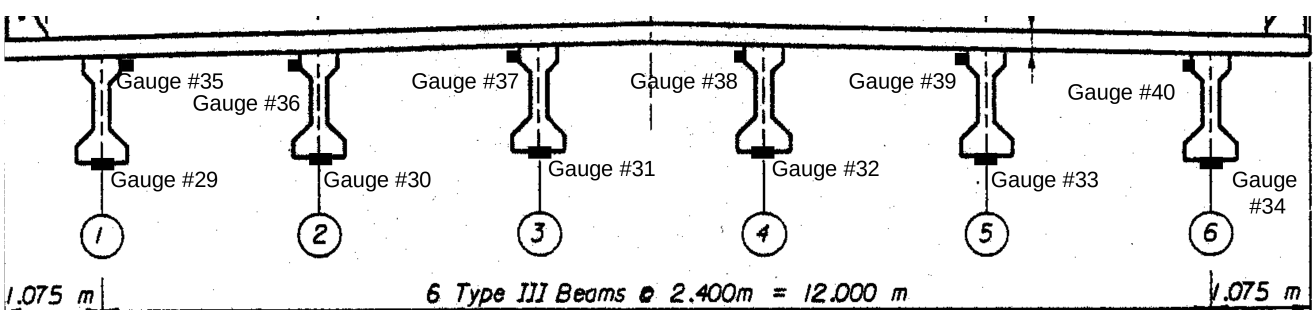

Cross section #3

Figure 3.11. Instrumentation of strain gauges in section #3.

Figure 3.12 shows the position of six gauges placed at the bottom of the beams in the middle cross-section of the second (middle) span.

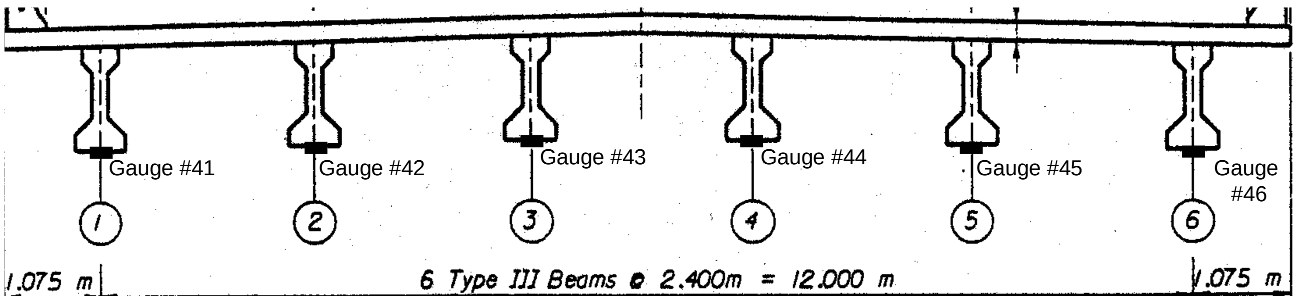

Cross section #4

Figure 3.12. Instrumentation of strain gauges in section #4.

Positions of all strain gauges are summarized in Table 3.2. Strain histories recorded for all the dynamic tests (Table 3.1) were filtered by a frequency of 60 Hz.

Table 3.2. Position of strain gauges.

Gauge #	Section	Attached to	Transverse position	Presented in Figure
1	1	Beam #1	Bottom surface	Figure 3.8
2	1	Beam #2	Bottom surface	Figure 3.8
3	1	Beam #3	Bottom surface	Figure 3.8
4	1	Beam #4	Bottom surface	Figure 3.8
5	1	Beam #5	Bottom surface	Figure 3.8
6	1	Beam #6	Bottom surface	Figure 3.8
7	1	Beam #1	Top side of girder	Figure 3.8
8	1	Beam #2	Top side of girder	Figure 3.8
9	1	Beam #3	Top side of girder	Figure 3.8
10	1	Beam #4	Top side of girder	Figure 3.8
11	1	Beam #5	Top side of girder	Figure 3.8
12	1	Beam #6	Top side of girder	Figure 3.8
13	2	Beam #1	Bottom surface	Figure 3.9
14	2	Beam #2	Bottom surface	Figure 3.9
15	2	Beam #3	Bottom surface	Figure 3.9
16	2	Beam #4	Bottom surface (left)	Figure 3.9, 3.10
17	2	Beam #4	Bottom surface(right)	Figure 3.9, 3.10
18	2	Beam #5	Bottom surface	Figure 3.9
19	2	Beam #6	Bottom surface (left)	Figure 3.9, 3.10
20	2	Beam #6	Bottom surface(right)	Figure 3.9, 3.10
21	2	Beam #1	Top side of girder	Figure 3.9
22	2	Beam #2	Top side of girder	Figure 3.9
23	2	Beam #3	Top side of girder	Figure 3.9
24	2	Beam #4	Top side of girder	Figure 3.9, 3.10
25	2	Deck	Close to girder #1	Figure 3.9, 3.10
26	2	Beam #5	Top side of girder	Figure 3.9
27	2	Beam #6	Top side of girder	Figure 3.9, 3.10
28	2	Deck	Close to girder #6	Figure 3.9, 3.10
29	3	Beam #1	Bottom surface	Figure 3.11
30	3	Beam #2	Bottom surface	Figure 3.11
31	3	Beam #3	Bottom surface	Figure 3.11
32	3	Beam #4	Bottom surface	Figure 3.11
33	3	Beam #5	Bottom surface	Figure 3.11
34	3	Beam #6	Bottom surface	Figure 3.11
35	3	Beam #1	Top side of girder	Figure 3.11
36	3	Beam #2	Top side of girder	Figure 3.11
37	3	Beam #3	Top side of girder	Figure 3.11
38	3	Beam #4	Top side of girder	Figure 3.11
39	3	Beam #5	Top side of girder	Figure 3.11
40	3	Beam #6	Top side of girder	Figure 3.11
41	4	Beam #1	Bottom surface	Figure 3.12
42	4	Beam #2	Bottom surface	Figure 3.12
43	4	Beam #3	Bottom surface	Figure 3.12
44	4	Beam #4	Bottom surface	Figure 3.12
45	4	Beam #5	Bottom surface	Figure 3.12
46	4	Beam #6	Bottom surface	Figure 3.12

Acceleration histories were collected for the bridge and one of the trucks at selected positions. Fourteen Endevco Model 7596A-10 accelerometers (Table 3.3) were attached to the bridge deck and four ADXL210 models were applied to the truck.

Table 3.3. Characteristics of the Endevco Model 7596A-10accelerometer.

	Unit	Value
Range	g (peak)	± 10
Sensitivity (at 100 Hz)	mV/g	200 ± 20
Frequency response	Hz	0 to 500
Mounted resonance frequency	Hz	3000
Damping ratio		0.7
Resolution	g	0.0025

Two accelerometers were attached on the tractor with one at the middle of rear axle and the other on the transverse beam as shown in Figure 3.13. The next two accelerometers were fastened to the trailer, one to the rear axle and one to the cross member on the frame. The information about the suspension system can be found by comparing the readings from accelerometers placed on an axle and frame.

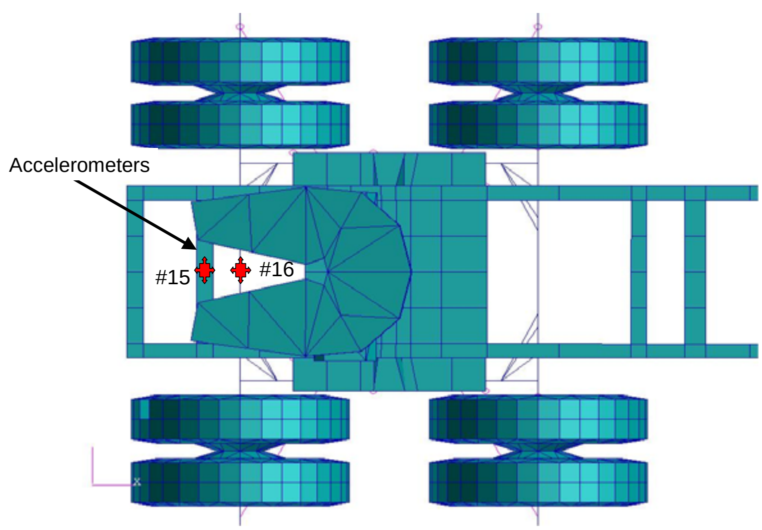

Figure 3.13. Position of accelerometers on tractor.

Seven accelerometers were placed on each side of the deck, close to the barriers (Figure 3.14). The longitudinal position is determined by FE mesh of the deck. The positions of the transducers coincide with the nodes.

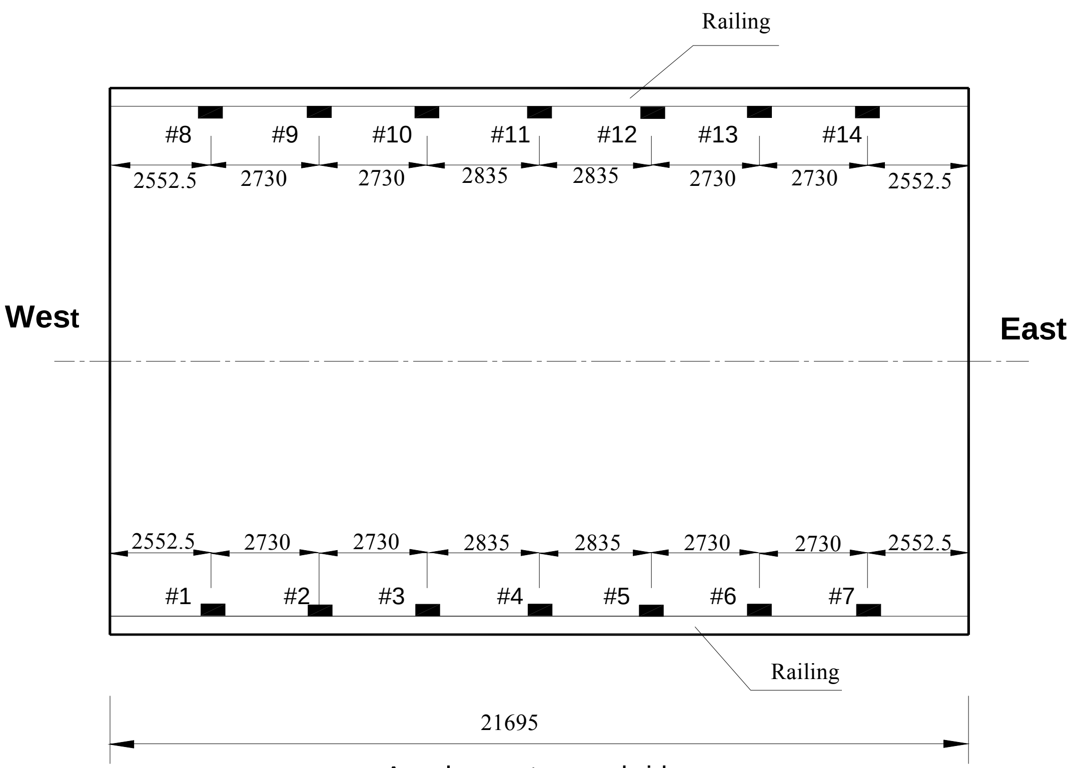

Accelerometers on bridge

Figure 3.14. Position of accelerometers on bridge deck in mm.

Positions of all accelerometers are listed in Table 3.4.

Table 3.4. Positions of accelerometers.

Accelerometer #	position	Attached to	Presented in Figure
1	Bridge deck	Top surface	Figure 3.14
2	Bridge deck	Top surface	Figure 3.14
3	Bridge deck	Top surface	Figure 3.14
4	Bridge deck	Top surface	Figure 3.14
5	Bridge deck	Top surface	Figure 3.14
6	Bridge deck	Top surface	Figure 3.14
7	Bridge deck	Top surface	Figure 3.14
8	Bridge deck	Top surface	Figure 3.14
9	Bridge deck	Top surface	Figure 3.14
10	Bridge deck	Top surface	Figure 3.14
11	Bridge deck	Top surface	Figure 3.14
12	Bridge deck	Top surface	Figure 3.14
13	Bridge deck	Top surface	Figure 3.14
14	Bridge deck	Top surface	Figure 3.14
15	Tractor	Middle of transverse beam	Figure 3.13
16	Tractor	Middle of rear axle	Figure 3.13
17	Trailer	Middle of the nearest transverse beam to rear axle of trailer	
18	Trailer	Middle of rear axle	

The plan for this in situ experiment was developed in cooperation with the FDOT Structures Lab. The experiment was based on the information collected in the literature review [4], [7], [8], [9], [13], [14], [19], [39].

3.4. Results of static tests

The main idea of the elastic superposition principle is that the results (for displacements and strains) for a combined loading state should be equal to the sum of results for separated loadings. The displacements or strains caused by the side-by-side trucks located in both lanes should be equal to the sum of the displacements or strains caused by a truck placed in the westbound lane and another in the east bound lane. The scheme of this situation is presented below in Figure 3.15.

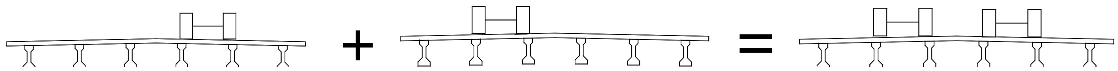

Figure 3.15. Principle of superposition.

Table 3.5 presents the displacements at the bottom of girder #3 (Figure 3.9) recorded by two types of instruments in static tests. The difference between the readings from the Noptel and LVDT devices, for the case when the truck was positioned on the west lane, is attributed to the torsion of the girder #3. Rotation of the girder's cross-section causes additional vertical displacements with opposite signs on both flange edges. These results have been confirmed by numerical calculations.

Table 3.5. Verification of superposition principle by deflection.

	Single truck on west lane	Single truck on east lane	Sum of single truck on west and east lane	Trucks side by side on both lanes
Noptel	1.41 mm	1.82 mm	3.23 mm	3.15 mm
LVDT	0.86 mm	1.83 mm	2.69 mm	2.73 mm

Measured strains also support the validity of the principle of superposition, which is shown in the Figure 3.16.

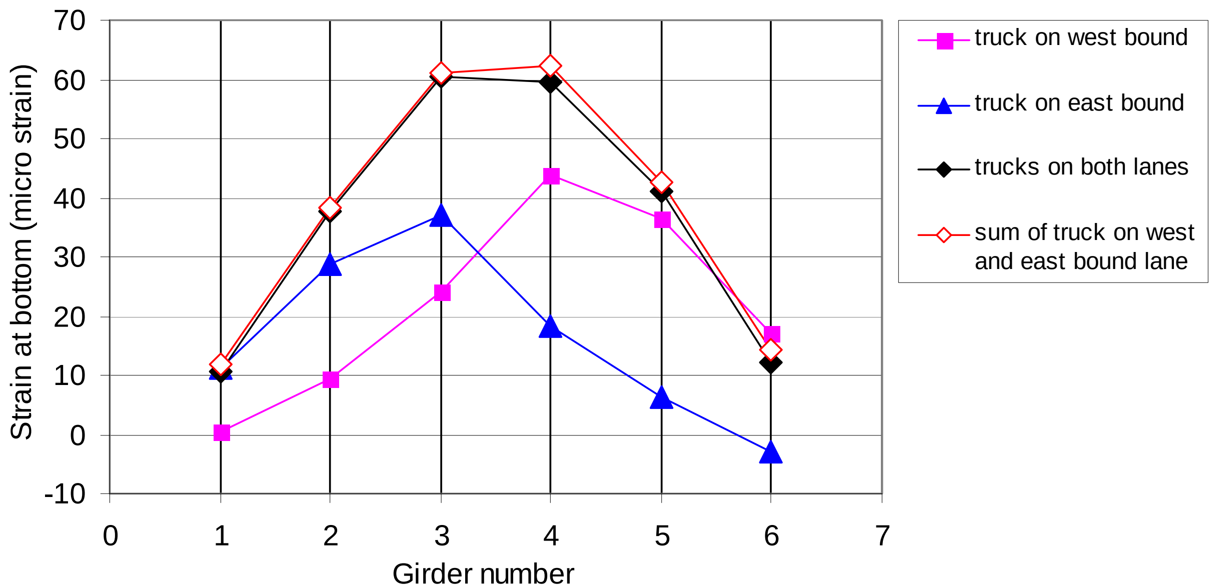

Figure 3.16. Verification of superposition principle for strains.

In figure 3.16, it can be observed that the structural response is not strictly symmetrical about the centerline of the roadway. The response when the truck is positioned on the eastbound lane is smaller than that when it is on the west bound lane. The nonsymmetrical response is attributed to the non-uniform distribution of material properties and boundary conditions. This effect was confirmed by the core test.

A wheel load distribution factor (DF), which is critical for bridge design and load rating, represents the distribution of the vehicular load among the load carrying components of the bridge. The distribution factor is obtained by [30]:

$$DF = \frac{\varepsilon_i}{\sum_{j=1}^{n} \left(\frac{EI_j}{EI_i} \right) \varepsilon_j} \tag{3.1}$$

where:

ε_i and ε_j are the measured strains of the *i*-th and the *j*-th girder,

EI_i and EI_j denote bending stiffness of the *i*-th and the *j*-th girders.

Based on equation (3.1) and the measured strain from the static test, the DFs were calculated for four loading cases for each girder (see Section 3.2). In the calculations it was assumed that the bending stiffness (EI) is the same for all six girders. The DFs are presented in Table 3.6.

Table 3.6. The distribution factor calculated from the measured strains.

Distribution factor (DF)	Single truck on west lane	Single truck on east lane	Truck on center of roadway	2 Trucks side by side on both lanes
Girder 1	0.0081	0.2301	0.0383	0.1906
Girder 2	0.1437	0.5826	0.2826	0.6816
Girder 3	0.3643	0.7503	0.6349	1.0922
Girder 4	0.6685	0.3688	0.6561	1.0764
Girder 5	0.5534	0.1254	0.3052	0.7411
Girder 6	0.2598	-0.0574	0.0828	0.2182

For bridges with concrete prestressed girders for two or more traffic lanes, the AASHTO specifications [2] give the distribution factor as:

$$DF = \frac{S}{5.5} \tag{3.2}$$

where:

S = spacing of beams or girders in feet

The comparison of the measured distribution factor and that given by AASHTO code is shown in Figure 3.17.

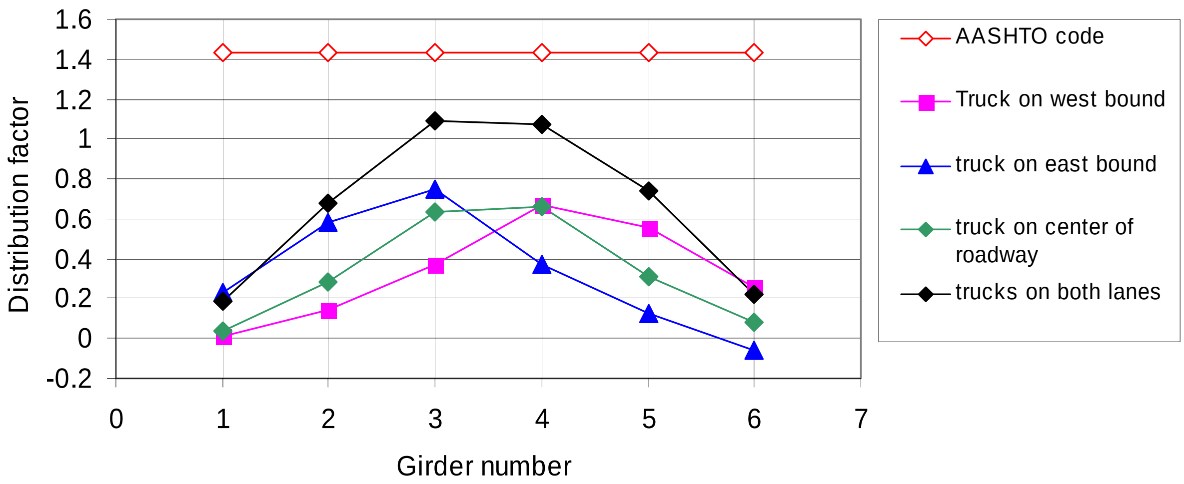

Figure 3.17. Wheel load distribution factors.

3.5. Results of dynamic tests

A total of twelve dynamic tests were conducted and most of the tests were repeated for cross checking. For convenience, all the dynamic tests are renamed in Table 3.7. All results were presented in the Interim Report and are attached in APPENDIX A - Experimental data. Obtained data were used to calculate the impact factors in a way presented in the next section.

Table 3.7. Configuration of dynamic tests.

Case #	Runs #	Type	No. of trucks	Position	Velocity	Piece of wood
1	2	dynamic	1	center of westbound lane	30 mph	No
2	2	dynamic	1	center of westbound lane	50 mph	No
3	2	dynamic	1	center of westbound lane	30 mph	Yes
4	2	dynamic	1	center of westbound lane	50 mph	Yes
5	2	dynamic	1	center of deck	30 mph	No
6	2	dynamic	1	center of deck	50 mph	No
7	2	dynamic	1	center of deck	30 mph	Yes
8	2	dynamic	1	center of deck	50 mph	Yes
9	1	dynamic	2	centers of both lanes	30 mph	No
10	1	dynamic	2	centers of both lanes	50 mph	No
11	1	dynamic	1 empty	center of westbound lane	50 mph	Yes
12	1	dynamic	1 empty	center of deck	50 mph	Yes

As an example, results for test #10 (Table 3.7) are presented below. This test was performed using two trucks running side by side in centers of both lanes at 50 mph (80 km/h) without plank. The previous cases have confirmed that the truck speed has influence on the dynamic response of the bridge. In this case the measured deflection at the middle of girder #3 increases about 25% more than static deflection (Figure 3.18). Strain histories for section #2, presented in Figure 3.19, indicate unsymmetrical response of the structure which, is believed, results from the unsymmetrical distribution of the materials and boundary conditions. The unsymmetrical property appears not only for the dynamic cases, but also for the static cases (Appendix A). It is noted that the strain amplitude for girder # 6 decreases slowly while for girder #1 it increases slowly after the trucks leave the first span. The main reason could be the small difference between the speeds of the trucks. The confirmation of this fact is demonstrated in the Figure 3.20, where time lag for curves corresponding to the girders 1 and 6 is visible.

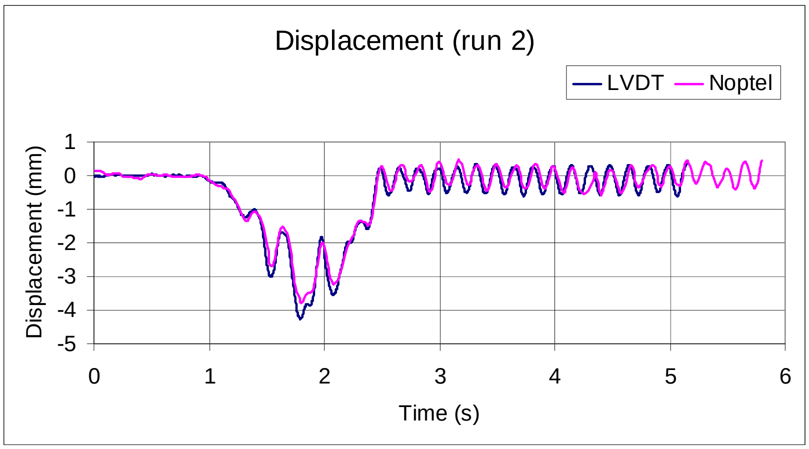

Figure 3.18. Displacement at the middle of girder #3 for case #10.

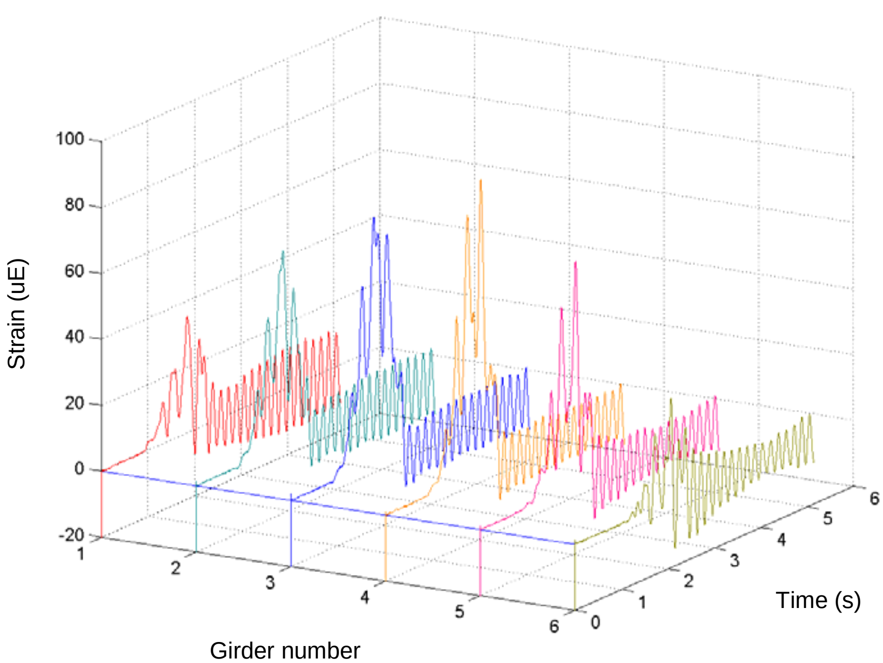

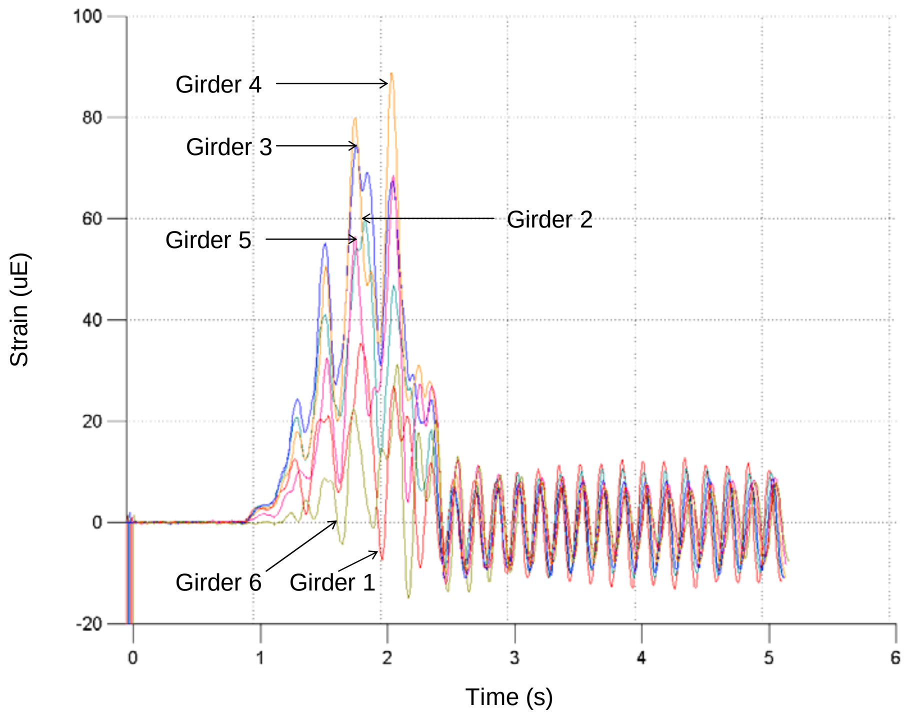

Figure 3.19. Strain histories measured at bottom of girders in section #2 for case #10 (run 1).

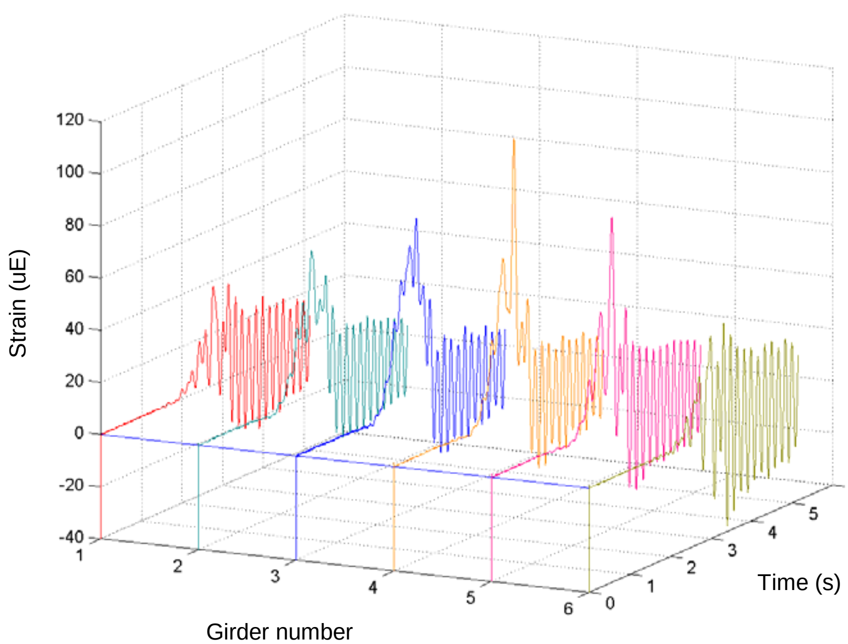

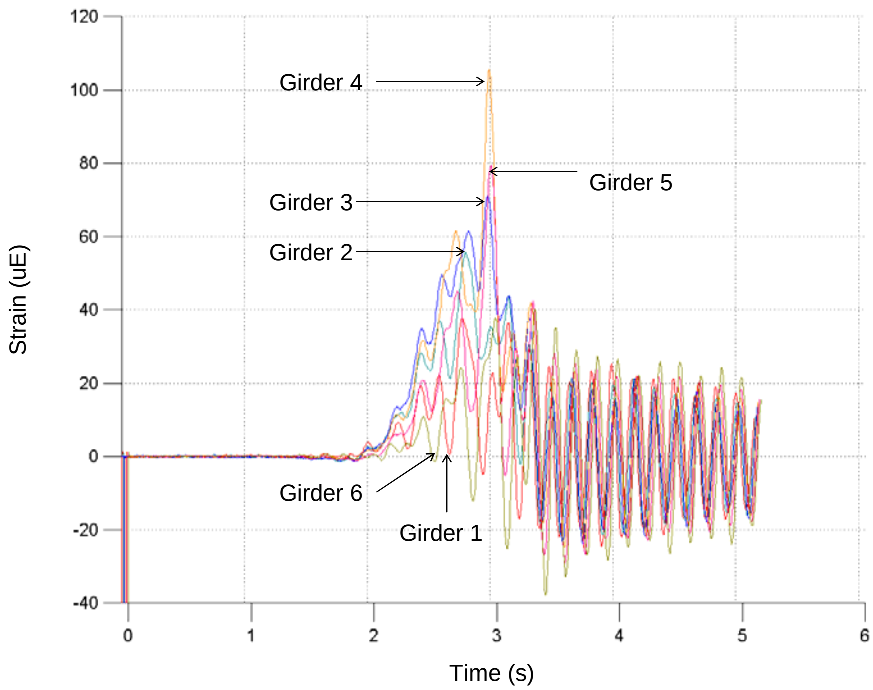

Figure 3.20. Strain histories measured at bottom of girders in section #4 for case #10 (run 1).

3.6. Impact factor and data reduction

The Load Allowance (impact factor) IM is defined as:

$$IM = \frac{R_d - R_s}{R_s} \times 100\% \tag{3.3}$$

where:

R_S = maximum static response,

R_d = maximum dynamic response.

The impact factor was first calculated separately for each girder under each loading case using displacement and strain readings at the middle of the first span (section 2). Different load cases give different impact factors for each girder. This fact raises the question: which value is representative and has practical importance for the whole bridge? To answer this question a consistent calculation process leading to data reduction was implemented. The data reduction is presented first for a set of cases where only one truck was passing over the bridge at 50 mph and without a plank (cases # 2 and 6). Next, the same procedure was implemented for other sets: one truck at 50 mph with plank, two trucks at 50 mph and for a speed of 30 mph. For each set of results, the number of trucks, the speed and the road conditions (with or without a plank) are the same except for the positions of the truck (westbound lane or center of the roadway). Additionally, for the calculation of the impact factor only, we added results for the eastbound lane case assuming symmetrical response of the bridge (even though it is actually not). The results of the eastbound lane case are a mirror of those of the westbound lane case. In this way one set of results includes all possible positions of the truck on the bridge.

Three subsequent Figures (3.21, 3.22, and 3.23) show a set of results including three cases. For each case, the static strains, dynamic strains and impact factors calculated from formula (3.3) are presented and plotted for each girder. All three figures show extremely large values of an impact factor for edge girders. However, these values refer to the small dynamic (and static) strains and should be neglected. Although some researchers present the results in this way [30], it must be admitted that it is very confusing and ambiguous. For a multi-girder bridge, we want to know which girders with small dynamic and static response can be disregarded. There is a need for objective criterion specifying which of these eighteen values of impact factor is representative for the considered set of cases.

Case 2 – one truck westbound lane
Static & 50mph

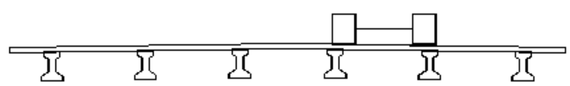

Case Ia - one truck right lane - static & 50mph			
girder	ε^S - static	ε^D - dynamic	IM [%]
1	0.53	6.90	1195.4
2	9.46	20.70	118.8
3	24.12	42.60	76.6
4	44.00	64.00	45.5
5	36.43	56.60	55.4
6	17.10	29.90	74.9
total	**131.64**	**220.70**	

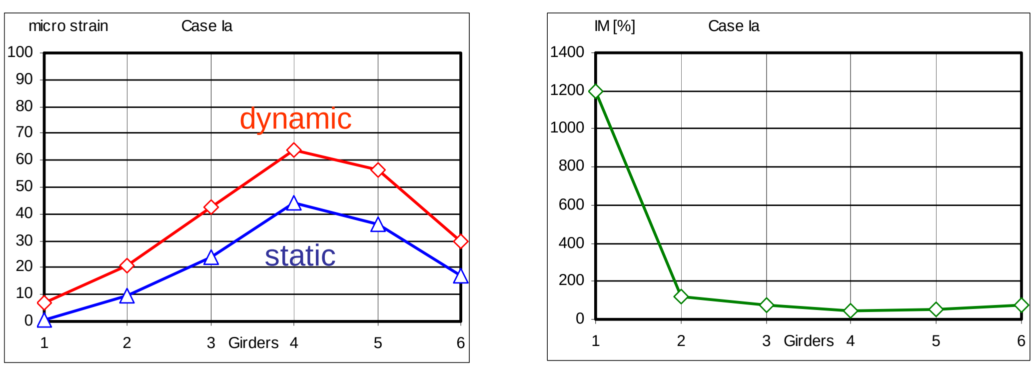

Figure 3.21. Calculation of impact factor for case 2.

Case 6 – one truck center – static & 50mph

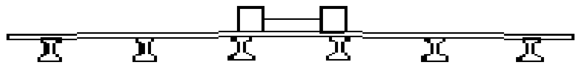

Case Ib - one truck center - static & 50mph			
girder	ε^S - static	ε^D- dynamic	IM [%]
1	2.21	16.20	633.5
2	16.30	35.10	115.4
3	36.62	64.00	74.8
4	37.84	69.20	82.9
5	17.60	43.40	146.5
6	4.78	17.70	270.5
total	**115.34**	**245.60**	

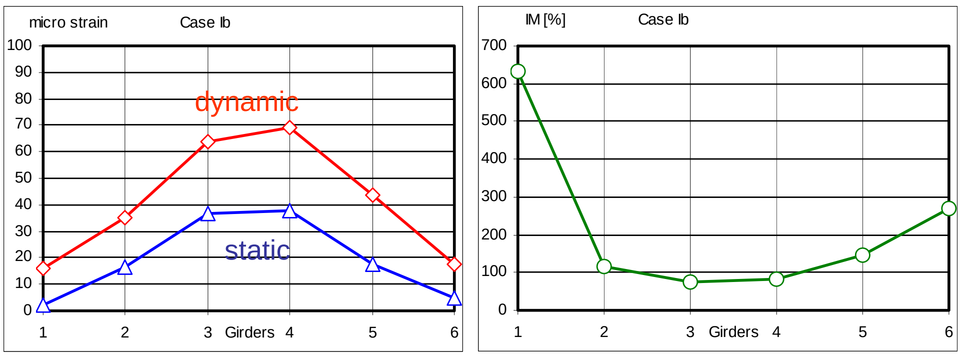

Figure 3.22. Calculation of impact factor for case 6.

Mirror of case 2 – one truck eastbound lane
static & 50mph – mirror of case Ia

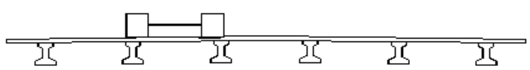

Case Ic - one truck left lane - static & 50mph			
girder	ε^S - static	ε^D- dynamic	IM [%]
1	17.10	29.90	74.9
2	36.43	56.60	55.4
3	44.00	64.00	45.5
4	24.12	42.60	76.6
5	9.46	20.70	118.8
6	0.53	6.90	1195.4
total	**131.64**	**220.70**	

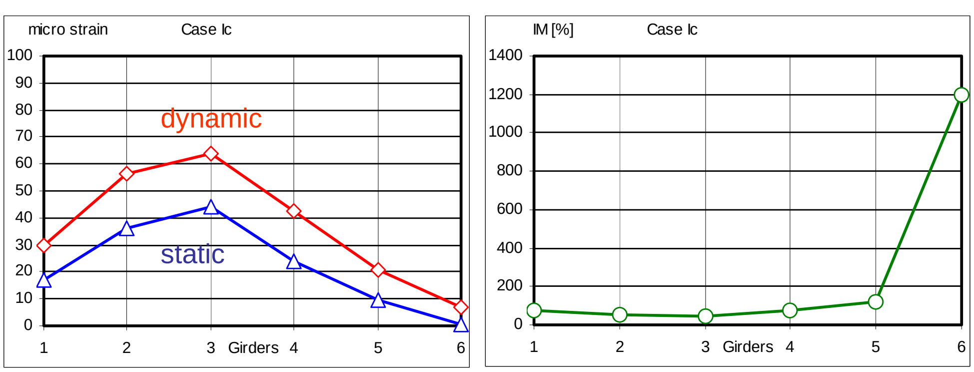

Figure 3.23. Calculation of impact factor for mirror of case 2.

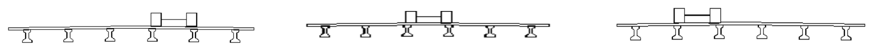

	Case Ia - one truck right lane		Case Ib - one truck center		Case Ic - one truck left lane	
girder	ε^D - dyn.	IM [%]	ε^D - dyn.	IM [%]	ε^D - dyn.	IM [%]
1	6.90	1195.4	16.20	633.5	29.90	74.9
2	20.70	118.8	35.10	115.4	56.60	55.4
3	42.60	76.6	64.00	74.8	64.00	45.5
4	64.00	45.5	69.20	82.9	42.60	76.6
5	56.60	55.4	43.40	146.5	20.70	118.8
6	29.90	74.9	17.70	270.5	6.90	1195.4
total	**220.70**		**245.60**		**220.70**	

Resultant IM

Criterion ---> max (ε^D - dynamic)

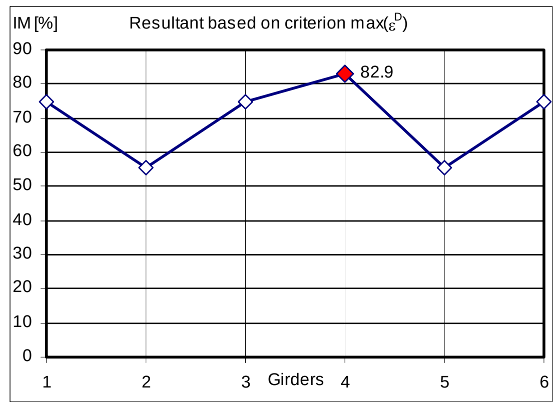

Figure 3.24. Resultant impact factors for girders.

The criterion applied in this research is defined by the symbolic formula

$$\text{Criterion ---> max } (\varepsilon^D \text{ - dynamic}) \tag{3.4}$$

It specifies that the representative is the value of the impact factor which corresponds to the largest dynamic strain. Figure 3.24 shows the application of this process. Initially for each girder we have three values of a calculated impact factor. The resultant is that value which corresponds to the maximum dynamic strain, ε^D. In this way we receive the diagram presented in Figure 3.24 showing six resultant impact factors for six girders. The next step is to determine which of these six values is representative. Again using the criterion (3.4) we decide that the representative value is:

$$IM = 82.9\ \%$$

for girder #4. The value refers to the maximum dynamic strain, ε^D =69.2. This strain was recorded in girder #4, for the case #6 – one truck on the center of the bridge. That value is representative for the selected bridge (bridge #500133, Figure 3.1) and selected truck (Figure 3.4) running with a speed of 50 mph, without a plank. For the considered vehicle - bridge configuration we received the highest dynamic strain for the pass through the center of the roadway. Although we cannot assume that it is typical for all bridges, for the one considered it is safer to drive along the traffic lane than through the center of the deck. That practical conclusion should be included as the recommendation in a permit.

Table 3.8 presents resultant impact factors calculated in the way presented above, for all considered sets of results. Values for cases without a plank correspond to the actual road surface conditions while the plank simulates extremely bad road surface conditions which can be caused by delaminations, spot wholes or threshold. The cases for two trucks will be excluded from the further analysis as they give a smaller impact factor than one truck cases and additionally are practically impossible.

Table 3.8. Resultant impact factors for bridge #500133.

	SPEED	ONE TRUCK	TWO TRUCKS
NO PLANK	30 mph	2.5%	20.0%
	50 mph	82.3%	50.5%
PLANK	30 mph	79.2%	
	50 mph	164.0%	

Comparing results of 30 mph and 50 mph tests, it can be seen that the vehicle speed is a very important factor. Since increased speed can cause high dynamic effects, reduction of speed is one option in an overweight permit process to ensure safety. It is also noted that for a speed of 50 mph we received impact factors much greater than those specified in the bridge code [2]

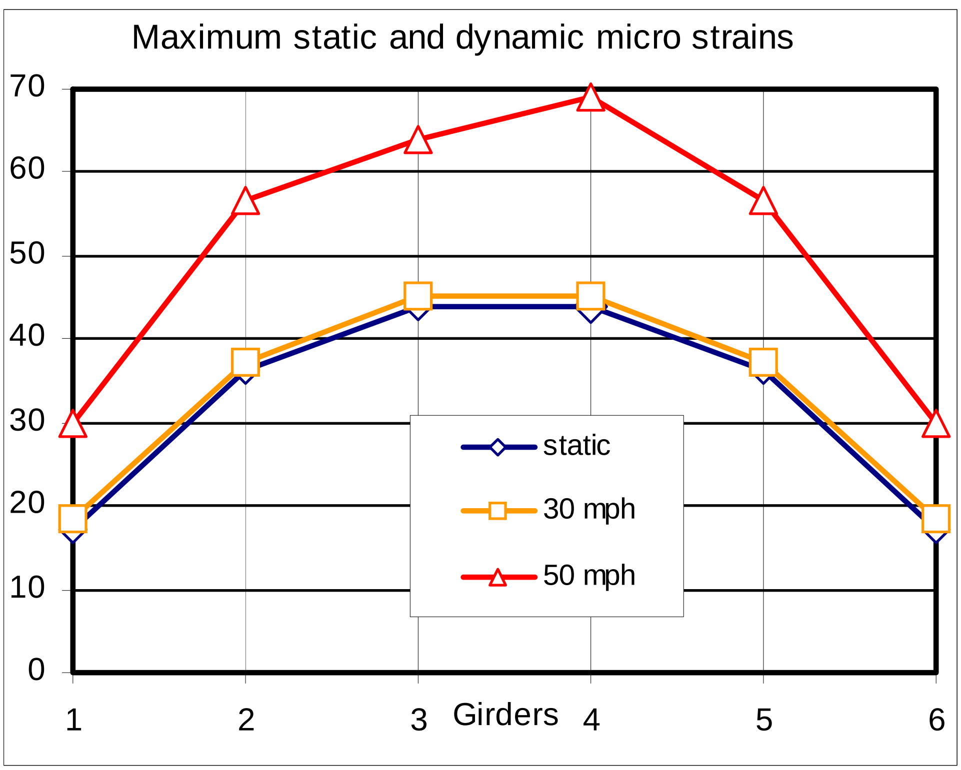

Figure 3.25. Maximum static and dynamic microstrains for one truck recorded in section #2 .

The videos recorded on site reveal that a significant hammering effect is caused by the bouncing of the concrete blocks triggered by the abutment threshold. This effect increases the dynamic interaction between the wheels and the deck. Figure 3.25 presents the maximum strains recorded in section #2 for each girder. It shows that for a speed of 30 mph the load bouncing was not triggered yet and the dynamic response is small, resulting in calculated impact factor of only 2.5%. For two trucks traveling at a speed of 30 mph, the tests produced an impact factor of 30%, less than that specified in [2].

Finally, excluding impact factors for two-truck cases and 30 mph cases from Table 3.8, we reach one impact factor 82.9% for the bridge #500133 with good surface conditions. The presented data reduction process was also applied for results of FE calculations.

3.7. Modal analysis

In the tests accelerations were recorded at 14 points located on the bridge deck (see Section 3.3). Directly obtained results in time domain were later transformed to frequency domain. Frequency domain technique is widely used for the determination of natural frequencies and mode shapes because of its simplicity. The technique is based on the fact that the frequency response functions (FRF) go through extreme values around the natural frequency. The frequency at which this extreme value occurs is a good estimation for the natural frequency of the structure. In the context of free vibration, the FRF is replaced by the spectra of responses [33]. In such a way, the natural frequencies are simply determined by the observation of the peak values on the graphs of the power spectra density, which are obtained by converting the measured accelerations to frequency domain by discrete Fourier transform (DFT).

A discretely sampled signal, p_n, can be expressed as a summation of N harmonic functions [12]:

$$p_n = \sum_{j=0}^{N-1} P_j e^{i(j\omega_0 t_n)} = \sum_{j=0}^{N-1} P_j e^{i(2\pi nj/N)} \tag{3.5}$$

where: $\omega_0 = 2\pi/T_0$ and $j\omega_0$ is the circular frequency of the j-th harmonic signal. Complex-valued coefficient P_j, which defines the amplitude and phase of the j-th harmonic, can be expressed as follows:

$$P_j = \frac{1}{T_0}\sum_{n=0}^{N-1} p_n e^{-i(j\omega_0 t_n)}\Delta t = \frac{1}{N}\sum_{n=0}^{N-1} p_n e^{-i(2\pi nj/N)} \tag{3.6}$$

P_n and P_j are called a *discrete Fourier transform (DFT) pair.* Equation (3.6) is the DFT of the signal p_n, and the equation (3.5) is the inverse DFT.

Figure 3.26 shows an acceleration history measured by accelerometer #4 subjected to one truck traveling at the center of the roadway at 50 mph without plank (case 6). Figure 3.27 presents the corresponding power spectra density. There are three frequency peaks at 6.00 Hz, 7.78 Hz and 13.17 Hz, respectively. However, due to the resolution, some close frequencies can not be identified by this method.

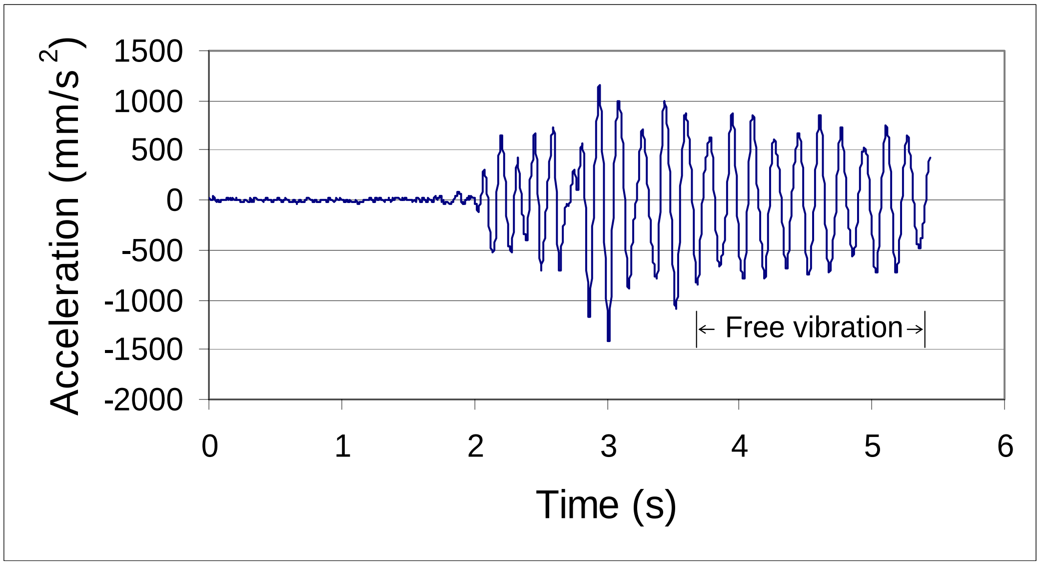

Figure 3.26. Acceleration history for Case 6 measured by accelerometer #4.

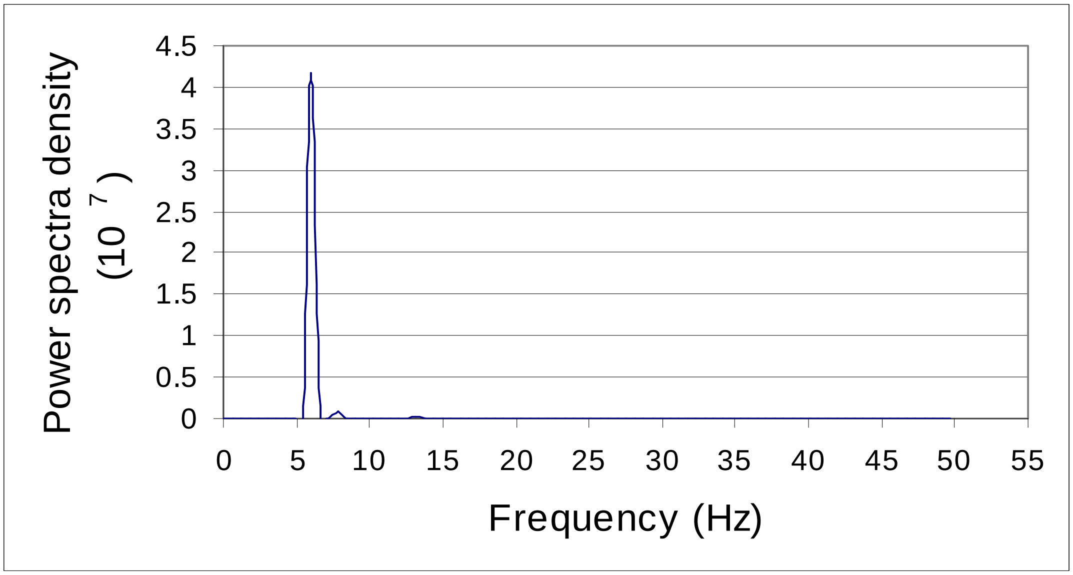

Figure 3.27. Power spectra density of free vibration measured by accelerometer #4.

To retrieve the mode shapes, one sensor reading was first selected as the reference signal. The components of natural mode shapes were normalized and determined by the ratios of the amplitudes of the interested signals over the reference signal. It was decided to use accelerometer #4 as the reference sensor to determine the first and third mode shapes while accelerometer #11 was chosen for the second mode shape. The positions where the #4 and #11 are located are the ones having the highest modal amplitude for the considered modes and therefore, are less sensitive to disturbance due to noise in the data. The calculated mode shapes are presented in Table 3.9 and plotted in Figure 3.28, 3.29 and 3.30.

Table 3.9. Mode shapes.

Position Number	Mode 1 (6.00Hz)	Mode 2 (7.78Hz)	Mode 3 (13.17Hz)
1	0.3741	0.3964	0.4243
2	0.6846	0.5903	0.7311
3	0.9169	0.7228	0.9402
4	1.0000	0.7695	1.000
5	0.9148	0.7045	0.9745
6	0.6805	0.5594	0.7675
7	0.3477	0.3087	0.3919
8	0.2801	0.4463	-0.3251
9	0.5419	0.7621	-0.7368
10	0.7061	0.9582	-0.9622
11	0.7616	1.000	-1.0654
12	0.6958	0.9119	-0.9819
13	0.5219	0.6825	-0.7850
14	0.2679	0.3444	-0.4516

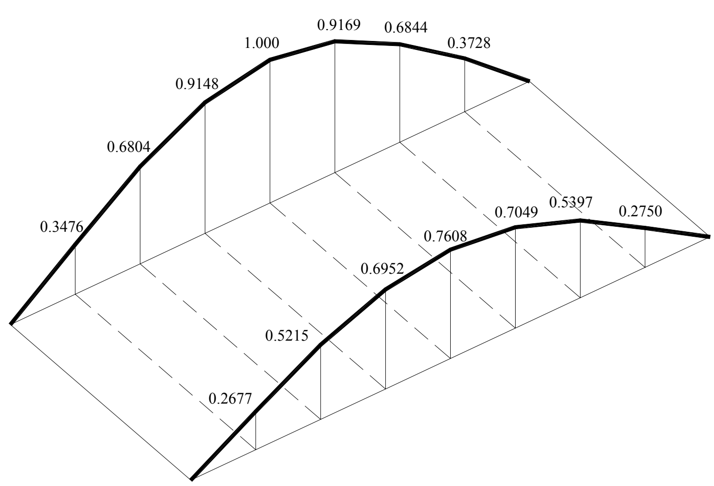

Figure 3.28. Mode shape 1 (6.00 Hz).

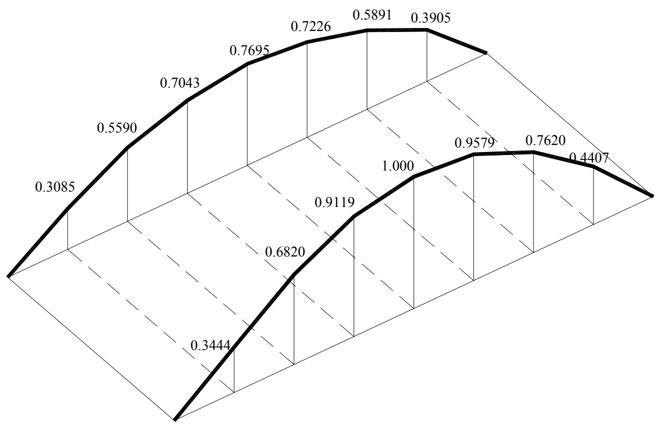

Figure 3.29. Mode shape 2 (7.78 Hz).

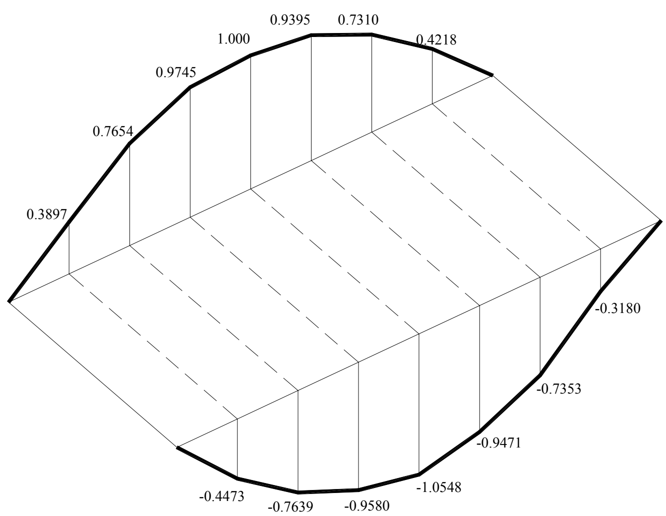

Figure 3.30. Mode shape 3 (13.17 Hz).

Mode 1 and 2 look very similar but it should be noticed that since accelerometers were located only along deck edges there is no representation for the interior part of the bridge. The mode 2 is actually a double flexural mode, undergoing a deformation also in the transverse direction [32].

It is evident, from mode 1 and mode 2, that the bridge exhibits a non-symmetric response. The amplitude of the mode shapes on the south edge is different from that on the north edge.

3.8. Estimation of damping ratio

Damping ratio is estimated by using autocorrelation method. Each mode is isolated and filtered around its natural frequency. The autocorrelation function is then computed for each mode [27]. For a sampled signal, the autocorrelation function is given by:

$$Rx(k) = \frac{1}{N-k}\left(\sum_{i=1}^{N-k} x(i)x(i+k)\right) \tag{3.7}$$

where: $x(i)$ is the sampled signal and *N* is the total number of sampled points.
The damping ratio is estimated by:

$$\xi = \frac{1}{2\pi m}\ln\frac{Rx(\tau)}{Rx(\tau + m\tau)} \tag{3.8}$$

where: $Rx(\tau)$ is the value of the autocorrelation function at time τ and *m* is the number of cycles. Figures 3.31, 3.32 and 3.33 present the normalized autocorrelation functions of the three modes respectively.

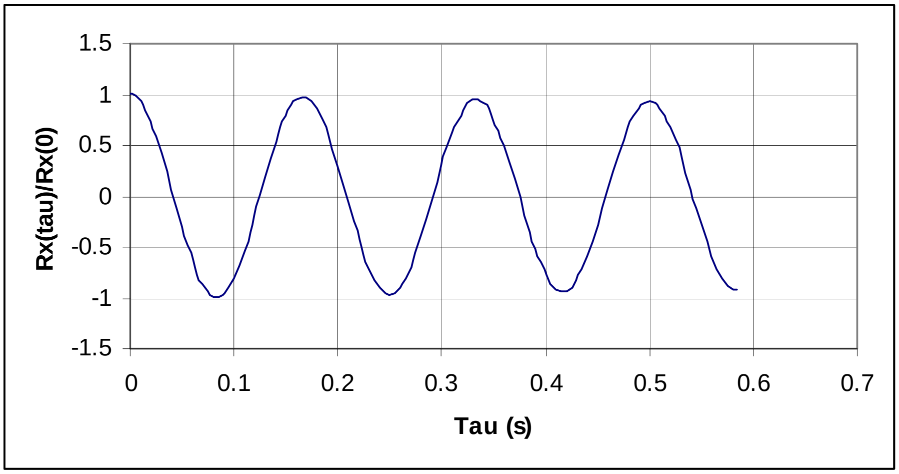

Figure 3.31. Autocorrelation function of the mode 1.

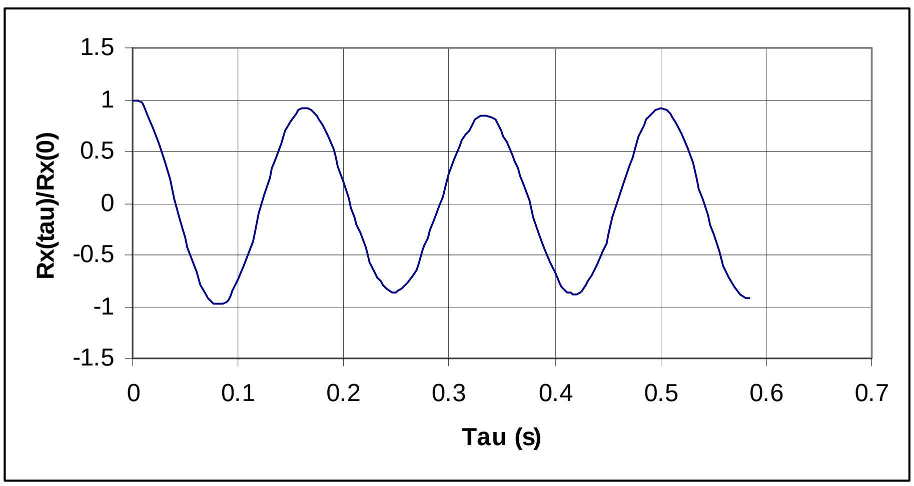

Figure 3.32. Autocorrelation function of the mode 2.

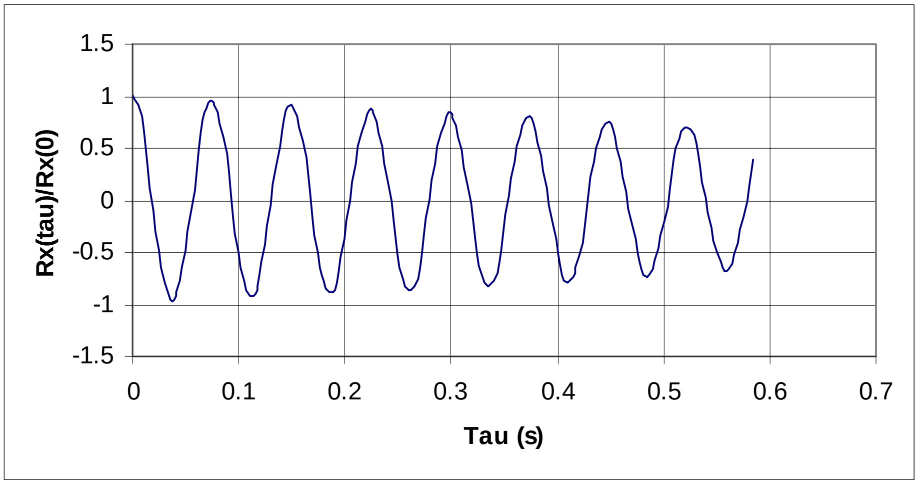

Figure 3.33. Autocorrelation function of the mode 3.

The damping ratios are estimated as 0.37%, 1.35% and 0.79% for the three modes, respectively.

Natural frequencies, mode shapes and damping ratio are inherent properties of the structure and do not depend on load configurations. The same natural frequency and similar mode shapes were identified from the recorded signals when the bridge subjected to other load cases.

4. DEVELOPMENT OF FE MODELS

4.1. Application of FE analysis for bridge dynamics

Nonlinear finite element methods are commonly used today to solve engineering problems. One such area is the efficient management of highway facilities, especially bridges, where the knowledge of exact load effect, load carrying capacity, and condition of bridges helps make management decisions and establish permissible weight limits.

Moving vehicles will cause an additional dynamic effect on bridges. This dynamic effect is accounted for in bridge design codes like AASHTO (American Association of State Highway and Transportation Officials) by introducing a dynamic impact factor. However, this impact factor is believed to result in conservative solutions for overweight vehicles like cranes. Therefore, an accurate prediction of bridge dynamic responses, bridge vehicle interaction, and dynamic loads imposed by moving cranes is of great interest to bridge designers and maintenance engineers. The interest arises from a good balance between economy and safety.

Actual field tests are still the most reliable source of information and the only method of final validation. However, the high cost of such experiments and difficulties with collecting extensive data from field tests lead to increasing interest in analytical and computational methods. A reliable, analytical investigation can reduce costs dramatically and allow for faster introduction of new solutions.

The traditional bridge analysis is based on the simplifications of geometry, material models, boundary conditions and loading. The interaction between a vehicle and bridge structure is usually simplified to point loads without reference to the dynamic characteristics of vehicles (suspension system) and surface roughness. The estimated dynamic effects are questioned by engineers.

A thorough investigation of the dynamic responses of bridges and bridge-vehicle interaction requires consideration of complex mechanical phenomena. The behavior of bridge-vehicle systems is represented by a complex mathematical model consisting of a set of nonlinear partial differential equations, boundary conditions, initial conditions, geometric features, and material properties. These equations cannot be solved in closed analytical form. However, an approximation of the exact solution can be obtained with numerical methods, with the finite element method being the most common among them.

In order to study and validate the dynamic response of highway bridges with a medium span (spans 20-30 m) subjected to moving vehicles, finite element analysis was chosen as a research approach. The emphasis was placed on development of finite element (FE) models of selected highway bridges, development and improvement of FE model of vehicles, numerical simulation of vehicle-bridge interaction, validation of FE models using the field test results, as well as the determination of actual impact factors.

4.2. FE modeling procedures

Today, large commercial finite element software enables the development of detailed, three-dimensional models of large engineering structures with a large number of elements, consistent stiffness and mass distribution, and different types of constraints and damping options. The FEM development methodology is articulated around three consecutive stages: data collection and model development followed by model validation. Figure 4.1 depicts the complete process scheme.

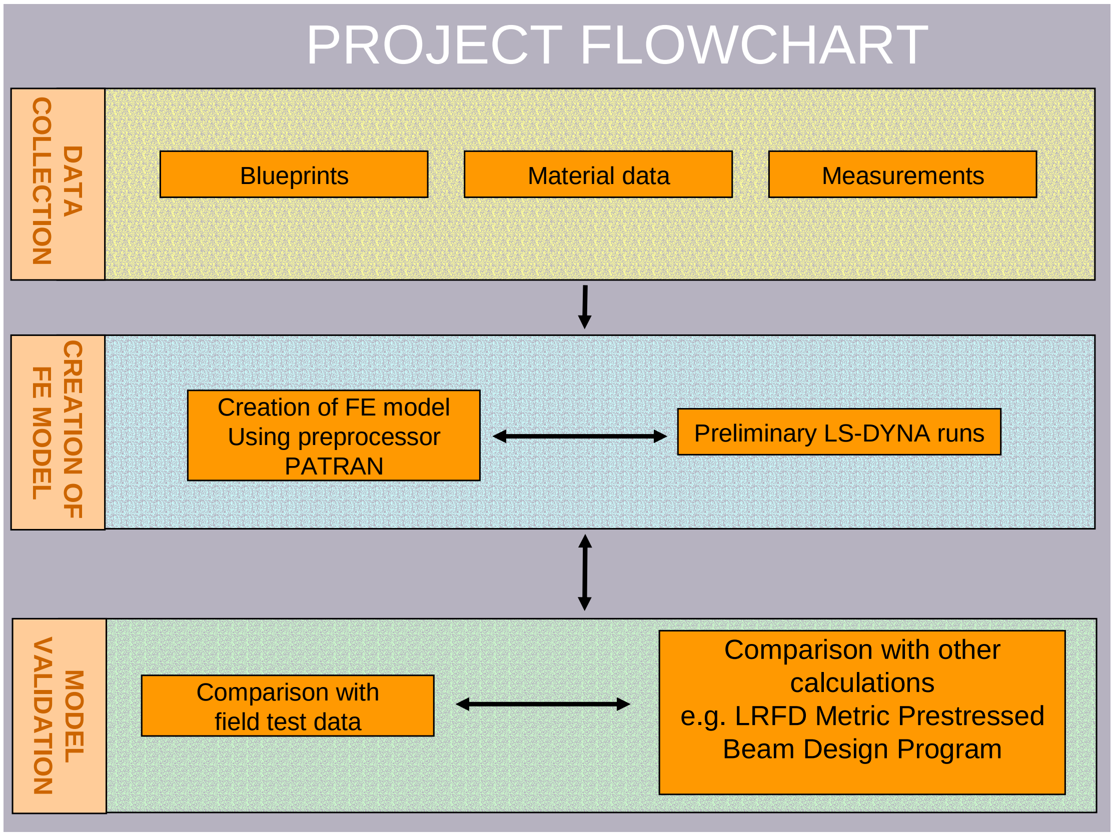

Figure 4.1. Flowchart for development of FE model.

In stage I, the information and data of the bridge and truck had to be collected for FE model development. Some data were taken directly from original blueprints and drawings, while some information was collected by measurement. In addition to geometric data such as component dimensions and positions of rebars and prestressed tendons, properties like thickness, material type, weight, and stiffness of springs were also collected.

In stage II, the finite element mesh was developed from the geometrical data; and then verified for errors. The material properties and constraints were assigned to complete the finite element model. Similar work was performed on the bridge, tractor and trailer separately. Later on, all parts were assembled to form the complete finite element model of the bridge-vehicle system.

In stage III, static and dynamic field tests were conducted on the selected bridge. Accelerations, displacements, and strains at selected points were monitored and recorded which were used to determine the responses of the bridge subjected to static and dynamic loads and subsequently to determine the actual impact factor. Additionally, the field test results were used to validate the FE models. A reasonable correlation between the FE simulation results and actual field test results was established and the model was modified (see Sections 4.5 and 4.7). The correlation was improved when actual values of concrete parameters were established from the laboratory core test. Model validation, experimental data and numerical results are strongly connected among themselves. The model validation process is presented in Section 4.5 for the truck model and in Section 4.7 for the bridge model.

The stages I, II, and III are discussed in detail in the following chapters. Subsequent paragraphs present software tools used in this research and the next section describes computer resources available in the research.

Graphical preprocessor MSC PATRAN

MSC.PATRAN by the MacNeal-Schwendler Corporation is the pre- and post-processing core of the MSC analysis software system. The MSC.PATRAN code is dedicated to build FE models applicable for different commercial solvers such as ABAQUS, ANSYS, DYTRAN, MARC, NASTRAN, PAMCRASH and SAMCEF. By using MSC.Patran, engineers can develop finite element models from their computer-aided design (CAD) parts; generate input files for simulation and visualize the simulation results. PATRAN supports all leading CAD software and analysis software programs. It is fast, easy-to-use and highly customizable, enabling engineers to develop their models quickly and directly incorporate MSC.Software products into their specific engineering processes. MSC.Patran has a comprehensive library of commands to generate and manipulate geometric entities including points, curves, surfaces and solids. Various creation options include translate, rotate, scale, mirror, glide, normal, extract, fillet, XYZ, extrude, revolve, decompose, intersect, manifold, project and many more. It has custom forms such as Loads, Boundary conditions, Element properties, Material properties, Multi-point Constraints (MPCs), Solution type, and parameters for code-specific data input. Mesh generation is especially convenient due to the numerous options and geometric tools embraced in PATRAN which allows the user to directly access model geometry and to quickly develop meshes. The “functional assignments” allow for the application of loads and boundary conditions, as well as the selection of element and material properties. Most of the model definitions can be easily formulated using PATRAN except for some of the LS-DYNA options regarding MPCs, loads and boundary conditions. These options have to be added manually in the key file or using the program LS-POST. To develop an FE model with LS-DYNA preference, an additional package called LS-DYNA 3D Module has to be installed in PATRAN. With this module, PATRAN is able to generate a key file which is used as an input deck for LS-DYNA solver. Figure 4.2 shows the MSC.PATRAN viewport.

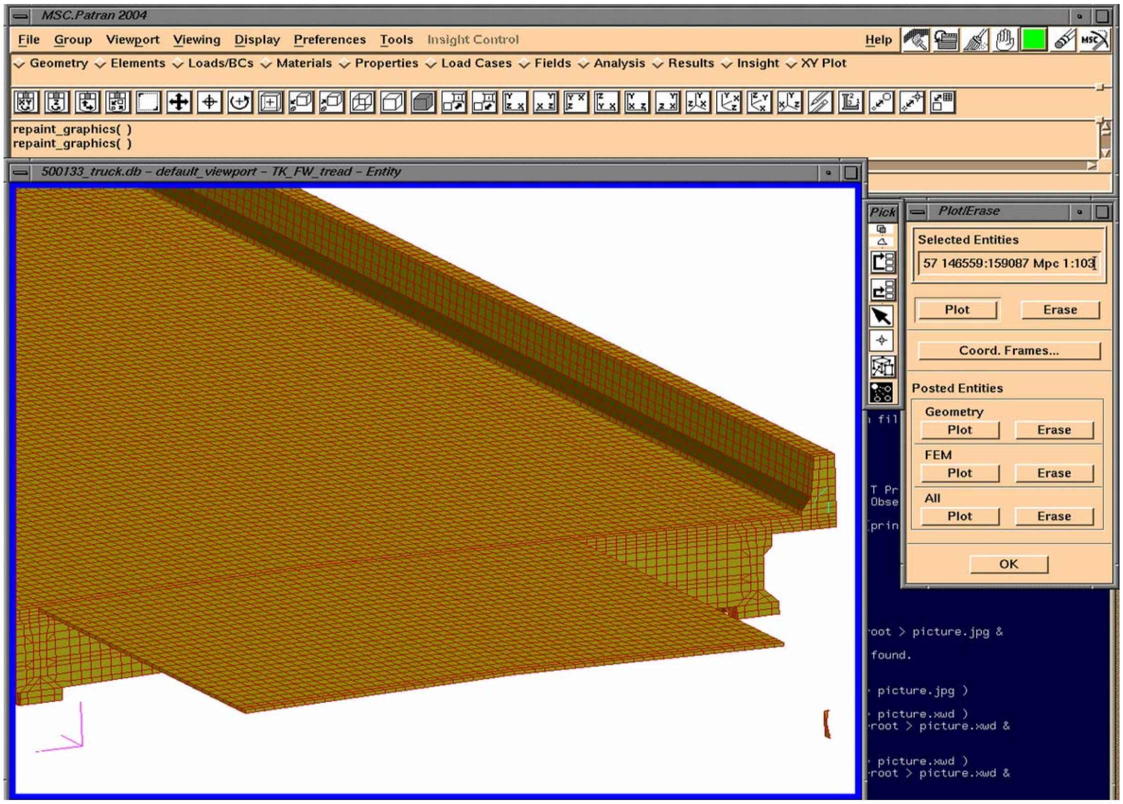

Figure 4.2. MSC.PATRAN Viewport.

Explicit finite element program LS-DYNA

Since the 1950's, when the finite element method was first applied for linear problems, the method has been continuously developed and is now an essential component of computer-aided design. In the infancy of the finite element methods, the excitement was mixed with the disdain of classical researchers. For example, for many years the Journal of Applied Mechanics rejected papers on the finite element method considering them as speculative and not scientific [5]. At the same time, the possibility of dealing with the complex geometry of real designs was attracting more and more researchers, especially engineers.

The history of nonlinear finite element methods is tied with the evolution of the computer age and is well represented by the development of codes - the fruits of the theory. Many of today's commercial nonlinear codes were developed at universities [5] and national research laboratories.

Until about 1990, the commercial finite element programs were focused on statics and implicit methods for dynamics. A new branch of modern nonlinear software is the explicit finite element codes. The first explicit finite element methods were strongly influenced by the work in the Department of Energy (DOE) laboratories and so-called hydro-codes [41], which were based on Eulerian mechanics. A new era of programming explicit finite element codes began at Lawrence Livermore National Laboratories by John Hallquist. The first version of his DYNA code was released in 1976. In contrast to other national laboratories, Livermore did not have restrictive dissemination polices and very soon, DYNA-2D and DYNA-3D were widely spread at universities and research laboratories throughout the world. Hallquist's improvements including effective contact-impact algorithms, application of one-point quadrature elements with consistent hourglass control and the high degree of vectorization, opened new possibilities for engineering simulations. The code contains over one hundred material models and numerous contact-impact algorithms, links, MPCs, and special elements such as airbag, which make it a leading analytical tool solving nonlinear dynamic problems.

The DYNA codes were first commercialized in the 1980s, by a French firm, ESI Group. ESI's product called PAMCRASH included many routines from WHAMS. In 1989 John Hallquist left Livermore and established his own firm Livermore Software Technology Corporation (LSTC), which distributes LS-DYNA, a commercial version of DYNA-3D.

Post processor LS-POST

LS-POST is an interactive post-processor for the program LS-DYNA. LS-POST reads the binary plot files generated by the LS-DYNA analysis codes and plots contours, time histories, and deformed shapes. Contours of a large number of quantities may be plotted on meshes consisting of plate, shell, and solid type elements. LS-POST can compute a variety of strain measures, reaction forces along constrained boundaries, and momentum. The graphic user interface of LS-POST is carefully crafted to create a user friendly environment. It supports the latest OpenGL standards to provide fast rendering for fringe plots and animation of results. It is available for all computer platforms. Figure 4.3 shows LS-POST viewport.

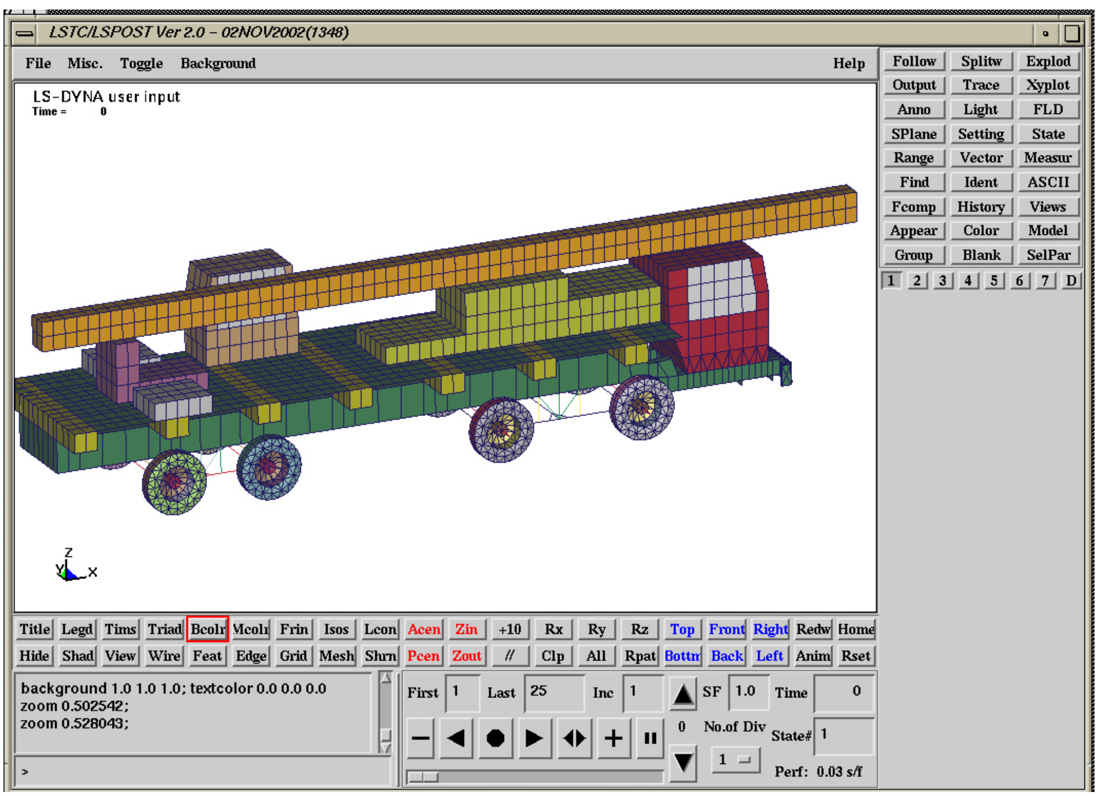

Figure 4.3. LS-POST Viewport.

4.3. Computational resources

The successful development of finite element codes would not be possible without the computer revolution. The decreasing cost of computer time and the increasing speed of computers make present computer simulations highly cost-effective.

In the mid 1970s a simulation of a model with only 300 elements and termination time of 20 ms took about 30 hours of computer time, using the most advanced hardware at that time [5]. The cost of such calculation was about $30,000, which was equivalent of three-year salary of an Assistant Professor.

For comparison, Table 4.1 presents an example of today's performance of a highly paralyzed MPP Version of LS-DYNA on a FSU supercomputer IBM SP-3 for a bus model developed in the previous project. The FSU supercomputer IBM SP-3 has 168 Power3 processors running at 375 MHz, each with 1/2 GB of memory. There is also a bigger and faster cluster IBM-SP4, also used in this project. SP-4 has 512 Power4 processors with 1 GB memory each. In addition to the access to FSU supercomputer, the CIA Laboratory has 5 SGI Octane Workstations and on SGI Origin 2000 main frame machine (see Figure 4.4). One run took from 8 to 24 hours on the supercomputer using 16 processors.

Table 4.1. Performance of the MPP version of LS-DYNA on IBM SP-3.

No. of CPUs	Hours, Minutes	Speed-up
SP3 - 1CPU	34h, 10 min	1.00
SP3 - 2CPUs	21h, 31min	1.58
SP3 - 4CPUs	9h, 42min	3.52
SP3 - 8CPUs	4h, 58min	6.87
SP3 - 16CPUs	2h, 31min	13.57
SP3 - 32CPUs	1h, 34min	21.8
SP3 - 64CPUs	1h, 9min	29.71
SGI Octane2 - 1 CPU	60h, 22min	0.56
SGI Origin 2000-10 CPUs	6h, 26min	5.31

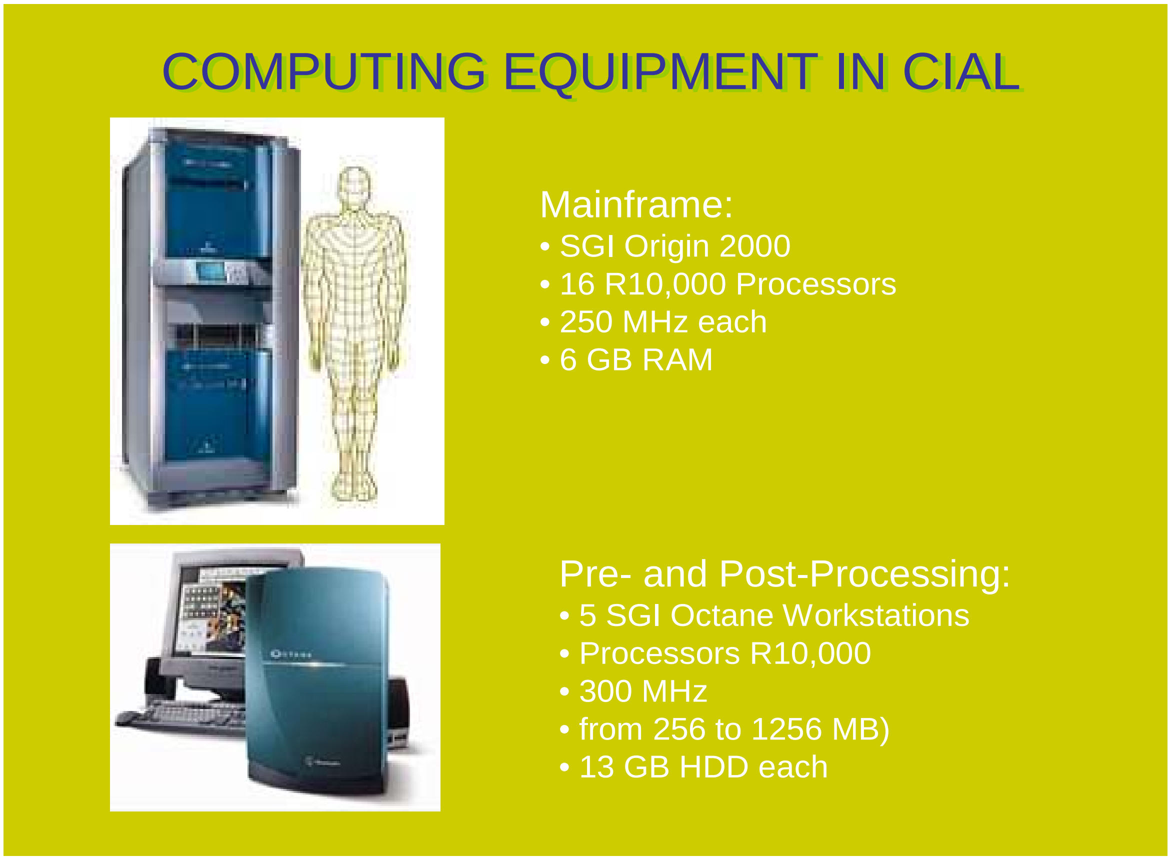

Figure 4.4. Computer resources available in CIA Lab.

Due to the domain-decomposition technique implemented in the MPP Version of LS-DYNA, it is possible to take full advantage of the massively parallel processing (MPP) supercomputers with their numerous processors. The domain-decomposition technique means that the mesh of the model is partitioned into sub-domains and, in most cases; each domain is assigned to one processor [22], [21].

Highly optimized software and continuously improving computer hardware, allow for fast, effective, and detailed finite element analyses. Integration of commercial FE codes with CAD programs and graphical preprocessors facilitates the arduous process of model development. Additionally, numerous graphical postprocessors enable for an impressive output visualization and better interpretation of results. However, the user of the finite element software must still be able to evaluate the suitability of a model for a particular analysis and understand its limitations.

4.4. Development of FE model for FDOT truck

This Section explains the development of a FE model of the FDOT truck used for the field test. A geometric model of a similar tractor in Autocad format was purchased from the website www.3dcadbrower.com. Development of the FE mesh started with the geometric model after amplification of necessary modifications. The truck model development was based on the experience gained from our previous research 'Crashworthiness and safety of public transit buses' conducted in the CIAL lab. The trailer model was developed based on the measured geometric data, along with the drawings obtained from the FDOT Structural Lab. The tractor and the trailer models were developed separately. Special emphasis was placed on the suspension system and the wheel models. After assembling the tractor and trailer parts together, all FE meshes were verified for consistencies and refined to improve the mesh quality. Next, decisions regarding element formulations, material models, material characteristics, contact algorithms, MPCs and connections, loading and boundary conditions, solution parameters and others were determined to complete the whole model of the truck.

Importing geometry data

Importing geometric data included two steps. The first step was to convert the data from Autocad format to the IGES format, the standard graphic file exchange format, using AnthroCAM. In the second step, geometric data was imported into MSC/PATRAN. Figure 4.5 shows the geometry model of the tractor imported in MSC.PATRAN.

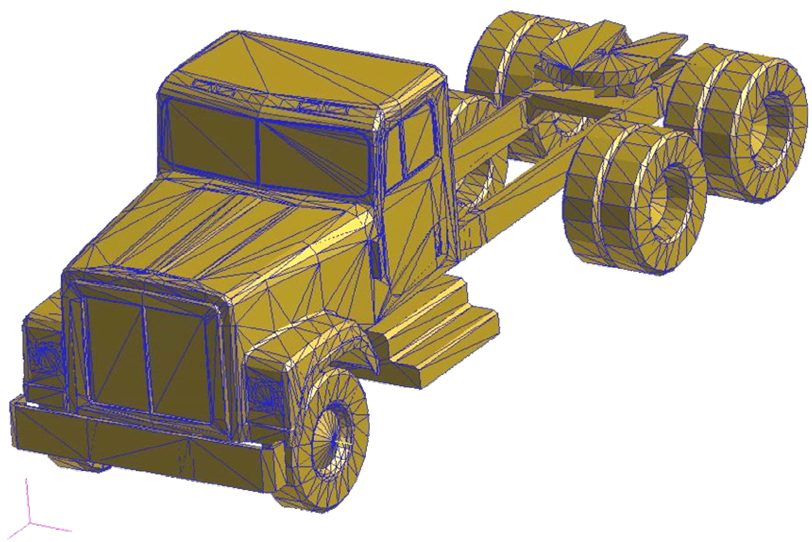

Figure 4.5. Geometry model of the tractor similar to FDOT tractor used in the field test.

Development of the FE Mesh

Creation of FE meshes is the first step in development of a finite element model. Only a well-defined FE model, with carefully established parameters, can realistically represent the behavior of the system. The process involves a repetition of creation, verification, and refinement of the FE meshes.

Different types of elements, such as Point, Bar, Tri, Quad, Tet, Wed, and Hex, were defined in PATRAN. Figure 4.6 shows the MSC.PATRAN viewport with the finite elements form used for creating finite element mesh.

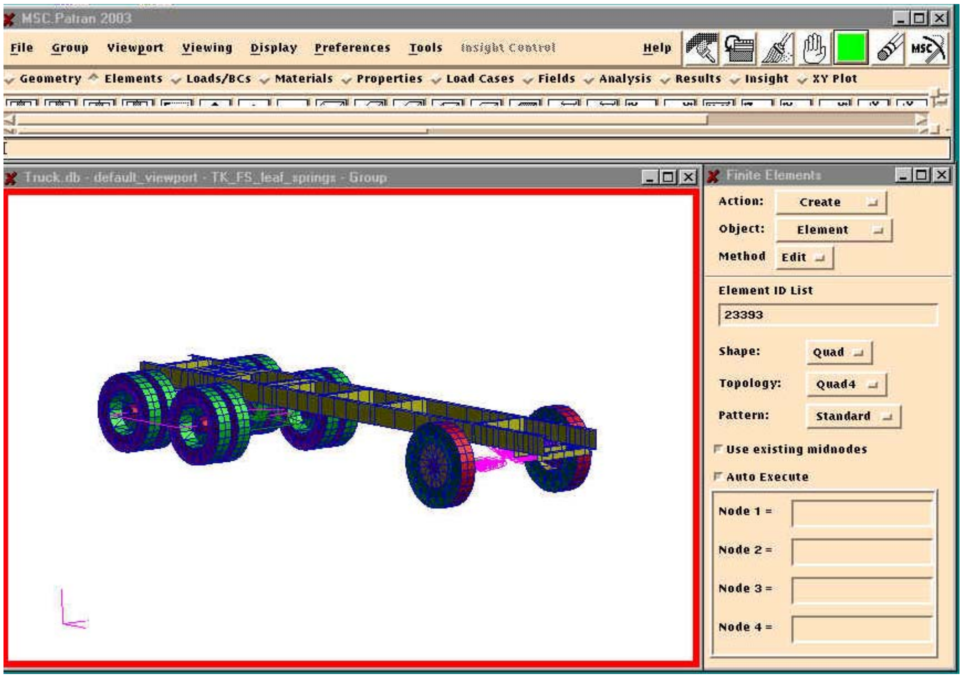

Figure 4.6. Finite Element mesh development.

An FE model of the tractor was developed based on measurements of the actual vehicle and a geometry model imported from Internet resources. The tractor model consists of beam, shell, and solid elements. Triangle elements were applied for the driver's compartment to represent its shape. The frame was meshed with regular quadratic elements. Some changes have been made according to the dimensions of the actual truck. Solid elements are used to represent the mass of the engine and rubber pads.

The trailer model was developed based on the drawings provided by the FDOT Structures Lab, along with in situ measurements. Shell elements were applied to create three dimensional structure of the frame. Up to 1616 elements were created for trailer (suspension and wheel are not included). The size of elements was controlled to make sure the shortest side of each element is longer than 100 mm. Elements that are too small result in time steps that are too short and therefore unacceptable calculation time.

The actual truck and its FE model are shown in Figure 4.7. A total of 12,870 elements, and 9 material types are included in the model. The wheel models consist of tread, sidewall, rim, and drum with airbag applied. The suspension system is represented by a series of beam elements and MPCs (Multi Point Constraint). Because the modeling of suspension and wheel is critical in this project, it will be described in detail in the next paragraphs.

Figure 4.7. The actual truck and its FE model.

Development of FE models for wheels

The wheel models are important for the simulation of truck-bridge interaction. The mechanical characteristics of wheels have influence on the dynamic reactions coming to the bridge deck. The major wheel components include tire, rim and drum as illustrated in Figure 4.8.

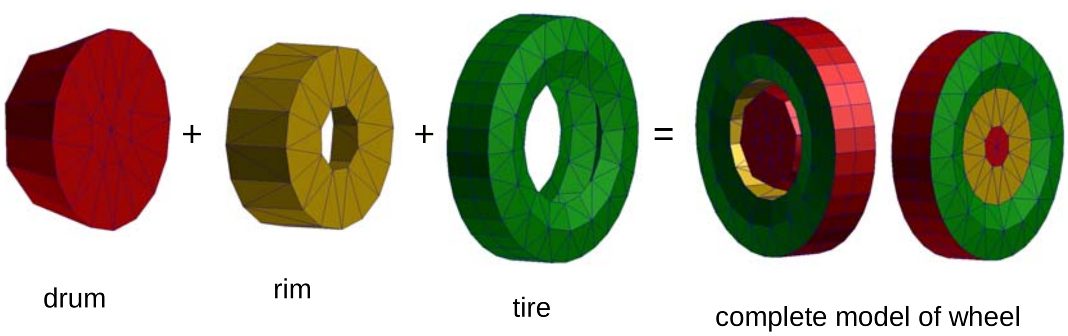

Figure 4.8. Development process of FE model for front wheel.

The tire and rim are modeled using shell elements while the drum is modeled with wedge elements (six node solid elements). Two layers of shell elements with different materials are created for tires with nodes at the same position. One layer is made of elastic material with average properties for rubber. The second material model called fabric is dedicated to simulate thin shells which have stiffness only for tension such as fabrics or a cord net in the tire. A linear elastic model with properties for steel is used for the rim and drum.

In order to realistically simulate the interaction between the tire and bridge surface, internal pressure is appropriately represented by applying AIRBAG option to the wheel model [22]. In LS-DYNA AIRBAG option is described as a volume enclosed by faces of shell or solid elements. In the wheel model, tread, sidewall of tire and some parts of steel rim define the enclosed volume for the AIRBAG. Because the enclosed space consists of shell elements, the norlams of all these elements must be oriented outward from the volume to make sure that the air pressure is applied in the correct direction. Two important values for the airbag are internal pressure and the damping factor. The value of applied internal pressure was read from the actual tire. The damping value is determined based on experience on another project in which a drop test of the wheel was conducted for validation of FE model of bus tires.

Development of FE models for suspension system

Due to the complex and irregular shape of the suspension system, it was decided to use structural elements such as beam and truss elements instead of shell or solid elements. Elements representing different parts are connected together using Multi Point Constraints (MPCs) [22] allowing for different interaction between connected nodes. Figures 4.9, 4.10 and 4.11 show models of the front, middle and rear suspension systems, respectively.

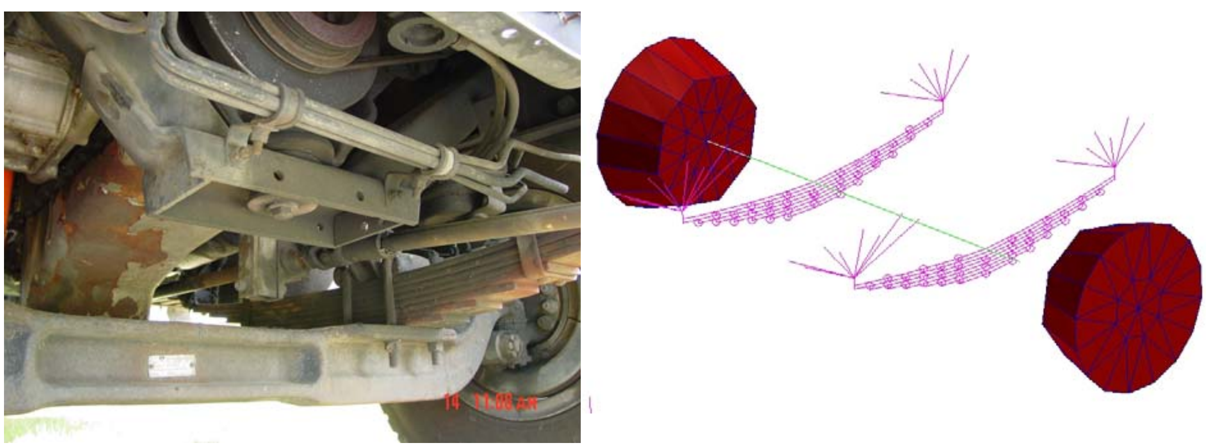

Figure 4.9. Front suspension and its FE model.

.

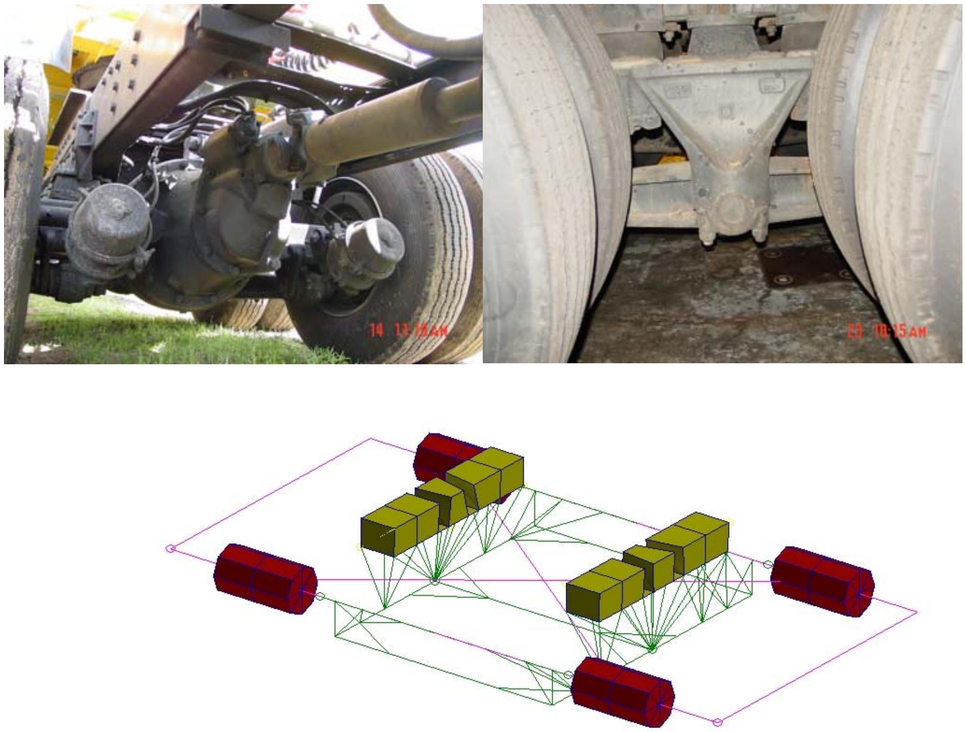

Figure 4.10. Middle suspension

The basic idea for development of middle suspension is similar to that for the front suspension. However, a special frame is created and attached to the main frame with springs and dampers and rubber pads. Figure 4.11 illustrates the rear suspension.

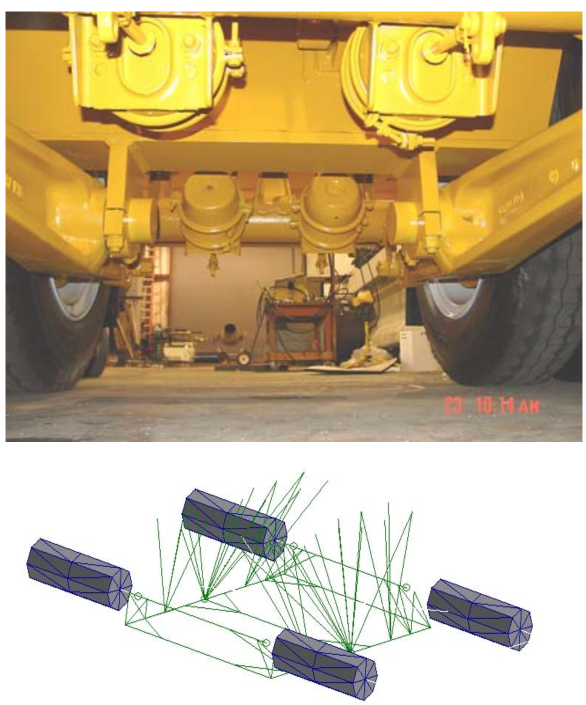

Figure 4.11. Rear suspension.

A lot of effort was made to simulate the rotation of wheels in the FE model. Figure 4.12 shows a trajectory for one of the selected nodes on the front tire and Figure 4.13 shows the wheel behavior when crossing the plank. The rotation of the wheels in the model is executed by a combination of appropriate MPCs. This is the feature which makes our model different from all models developed by other researchers (see Chapter 2). Although it is difficult to represent all dynamic characteristics of the suspension systems, we believe that our model has good potential for representation of the vertical movements. The interaction between truck components is well represented by springs, dampers and tire models. The estimation of spring and damper coefficients was based on the available data, mostly limited to the comparison of numerical results with the results from the field test (Section 4.5). There is a need for additional dynamic tests for suspensions of heavy vehicles to better represent their characteristics in the FE model.

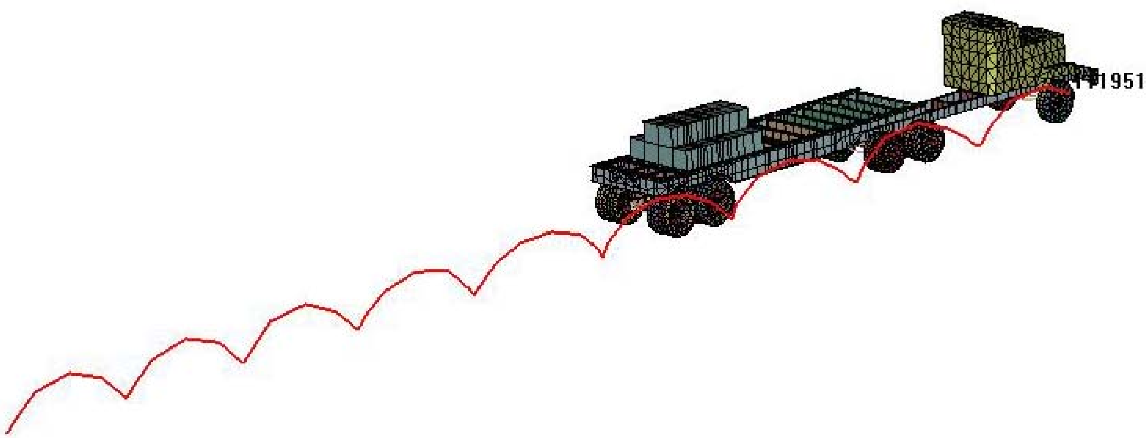

Figure 4.12. Characteristic cycloids drawn by a node on the front tire.

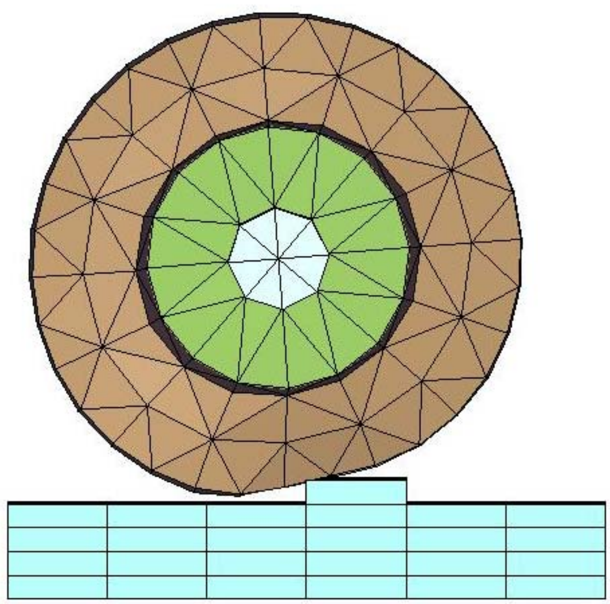

Figure 4.13. Deformation of the tire passing over a plank.

Groups of elements (parts) for the truck model

The models of trucks were developed as a set of components built simultaneously. Such a procedure saves time and allows for engaging a group of people into parallel work. It is convenient to check each part before assembly. Preliminary runs could identify human errors such as mesh inconsistencies, connection failures, duplicated elements, and elements with bad shape. A summary of the final FE model of the truck is provided in Table 4.2, where the number of elements, nodes and parts are presented. A "part" in LS-DYNA is the name for a group of finite elements with the same properties such as material, element thickness and element type. It is called "property" set in PATRAN.

Table 4.2. Summary of the final FE model of the FDOT truck.

No.	Entity	Number
1	Number of parts (LS-DYNA)/ Property sets (PATRAN)	157
2	Number of material models	9
3	Number of MPCs	103
4	Number of nodes	6312
5	Number of solid elements	438
6	Number of shell elements	11827
7	Number of beam elements	605
8	Total number of elements	12870

4.5. Validation of truck model

The truck model validation began with checking the mass distribution. Figure 4.14 presents the numbering of the axles and the axle spacing. To calculate the reactions, ten nodes on the five truck axels were selected to be constrained in the vertical displacement and gravity was applied to the truck as the load. The rapid application of gravity caused transient vibrations which were quickly damped by using global damping with a high damping factor of 30. The reactions for each axle were calculated using the node reactions. Figure 4.15 shows the time history of the axle load for the truck loaded with 12 concrete blocks. To reduce the difference between the FE analysis and the measurement, the FE model was modified by changing the thicknesses of some shell elements and cross-sectional properties of beam elements. The whole process was repeated until a good correlation of results was achieved. Table 4.3 shows the comparison of the axle loads from FE simulation and measurement, for the truck loaded with 12 concrete blocks. The FE analysis results match well with those from measurement.

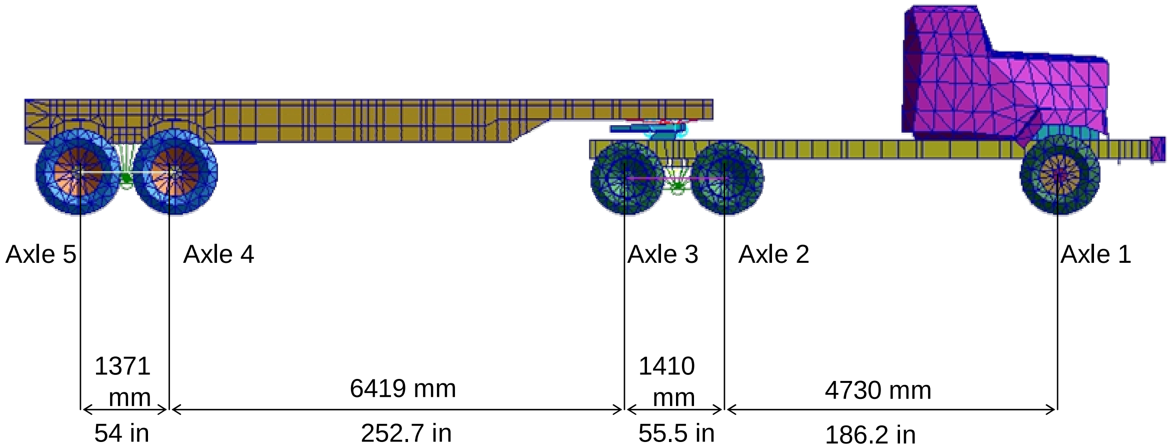

Figure 4.14. The axle spacing.

Table 4.3. Comparison of the axle loads from FE analysis and measurement.

Axle force		FE model [kN]		Measured by FDOT [kN]	Difference [kN]	Error [%]
Front	1st	51.53	51.53	50.62	0.91	1.80 %
Drive	2nd	45.14	101.30	100.44	0.86	0.86 %
	3rd	56.16				
Rear	4th	94.19	170.60	169.88	0.72	0.42 %
	5th	76.41				
Total		323.43	323.43	320.94	2.49	0.78 %

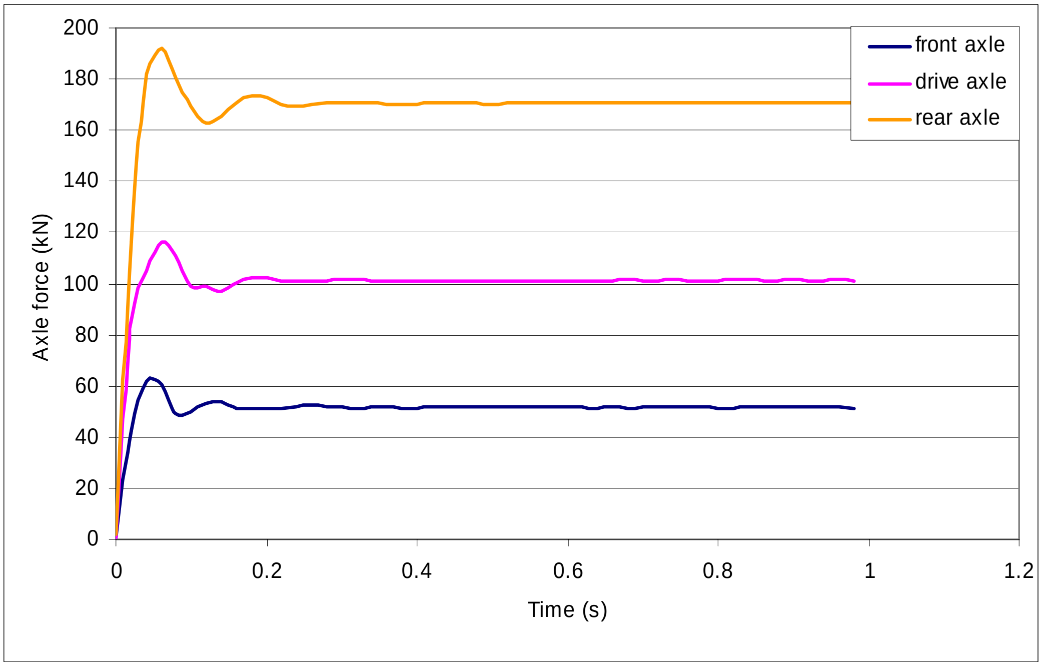

Figure 4.15. Time history of reactions for truck loaded with 12 blocks.

A drop test was carried out to check if the suspension systems were modeled realistically and if all the connections and MPCs worked properly. In the simulation, the truck model was dropped from the height of 25.4 mm (1 in). Figures 4.16 and 4.17 show time histories of spring and damper forces in the trailer suspension. After 1 second, the spring is subjected to a constant compressive force while the damping force tents to zero because the velocity goes to zero.

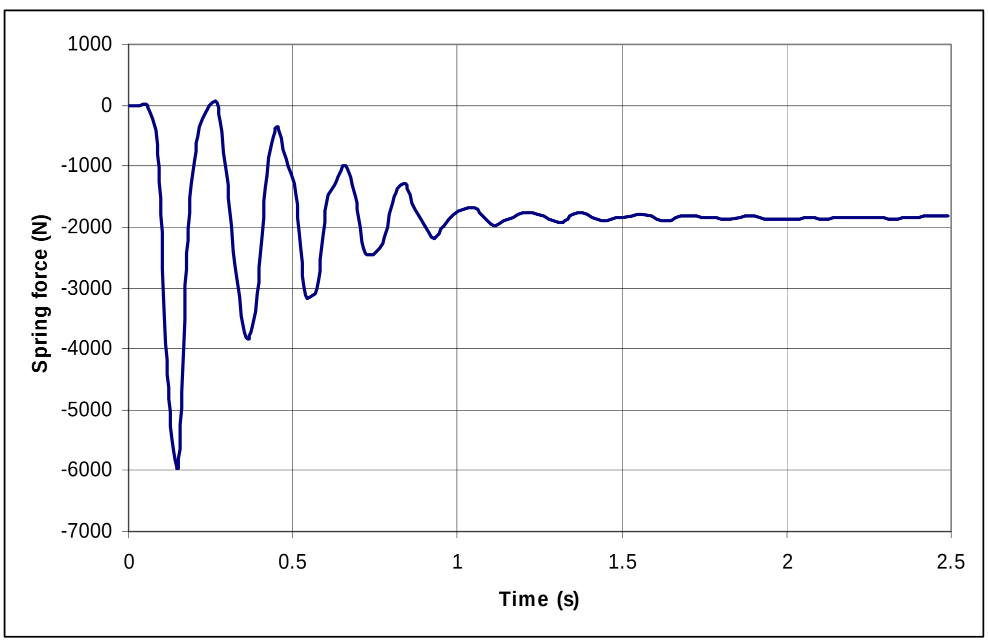

Figure 4.16. Time history of a selected spring force in the trailer suspension.

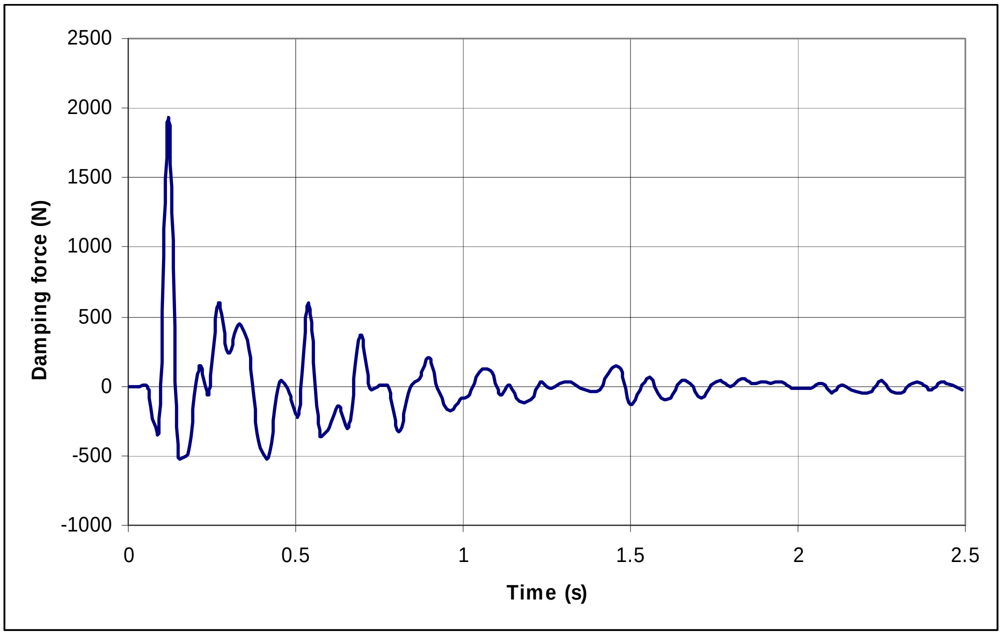

Figure 4.17. Time histories of a damper force in the trailer suspension.

Another way of validating the truck FE model was to compare the accelerations on the truck axles from numerical analysis and field testing (Figure 3.13). The calculated accelerations were received by derivation of the velocity histories of the nodes located close to the positions of actual accelerometers used in the experiment (Section 3.3). The truck model was also validated by comparison of the simulated bridge behavior subjected to the moving truck with corresponding experiment results. That comparison is a validation of both bridge and truck models and is presented in Section 4.8.

4.6. Development of FE model of the tested bridge

A Finite Element (FE) model of the tested bridge was developed based on the blueprints provided by FDOT. The bridge structure is already described in Chapter 3.

The FE model of one span consists of 5 structural elements: slab, barriers, beams, diaphragms and neoprene pads. Figures 4.18 to 4.22 show FE models for these bridge components. Concrete parts are modeled using 3D solid elements. Reinforcement and strands in girders are represented by 1D beam elements. Neoprene pads are modeled (see Figure 4.22) using solid 3D elements and material model MAT6 for viscoelastic material [22].

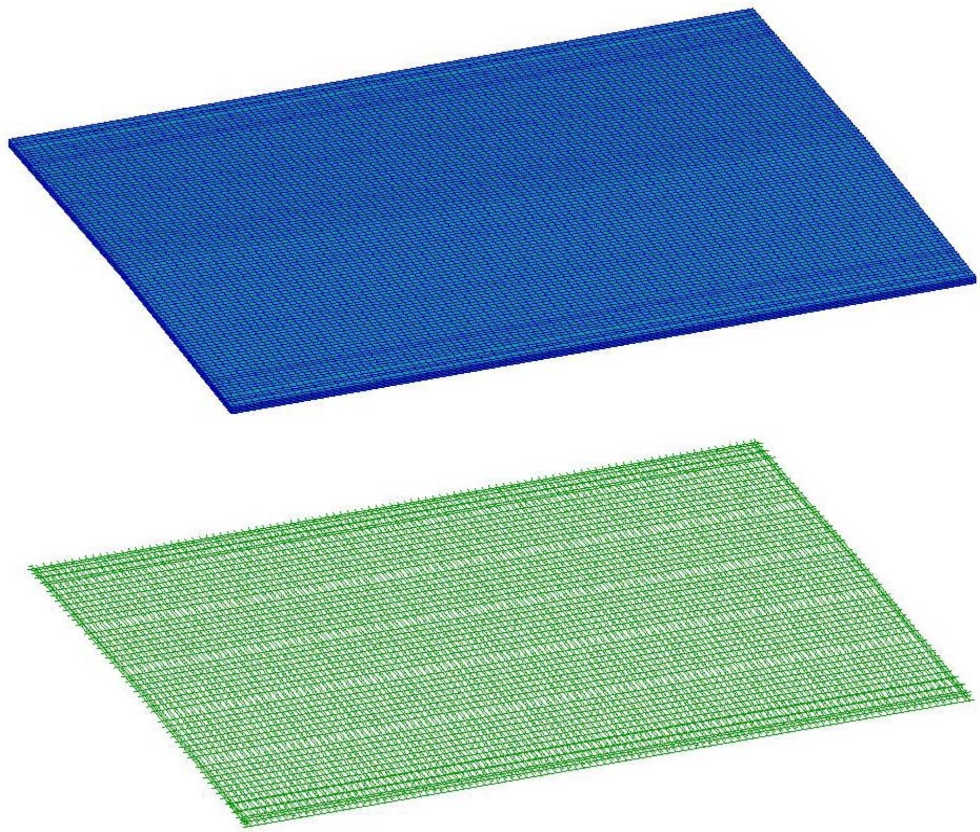

.
Figure 4.18. FE model of slab, concrete and reinforcement.

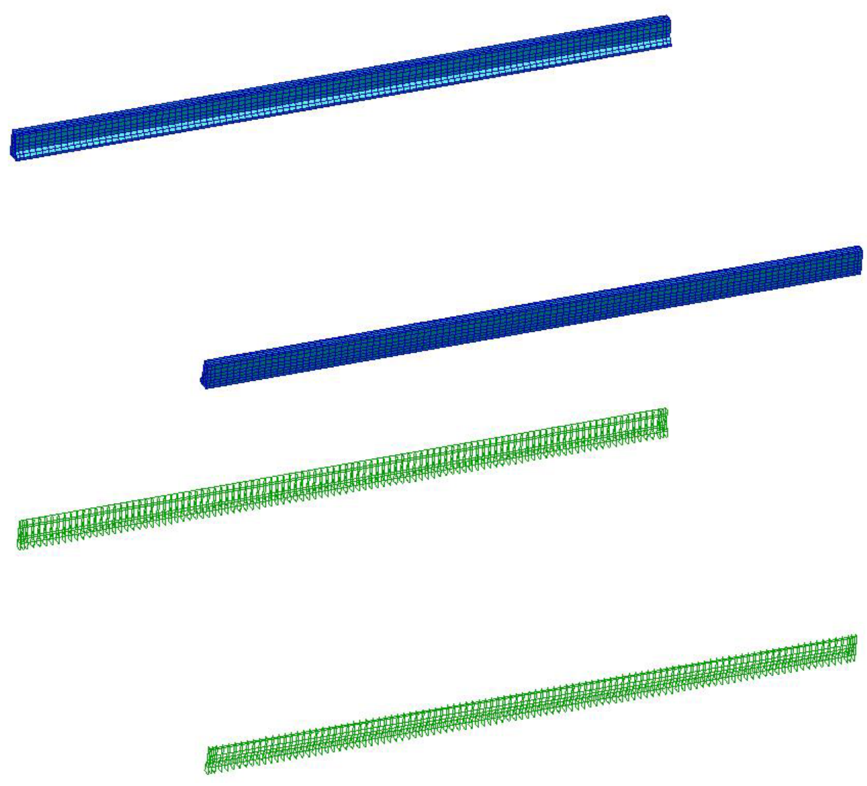

Figure 4.19. FE model of barriers, concrete and reinforcement.

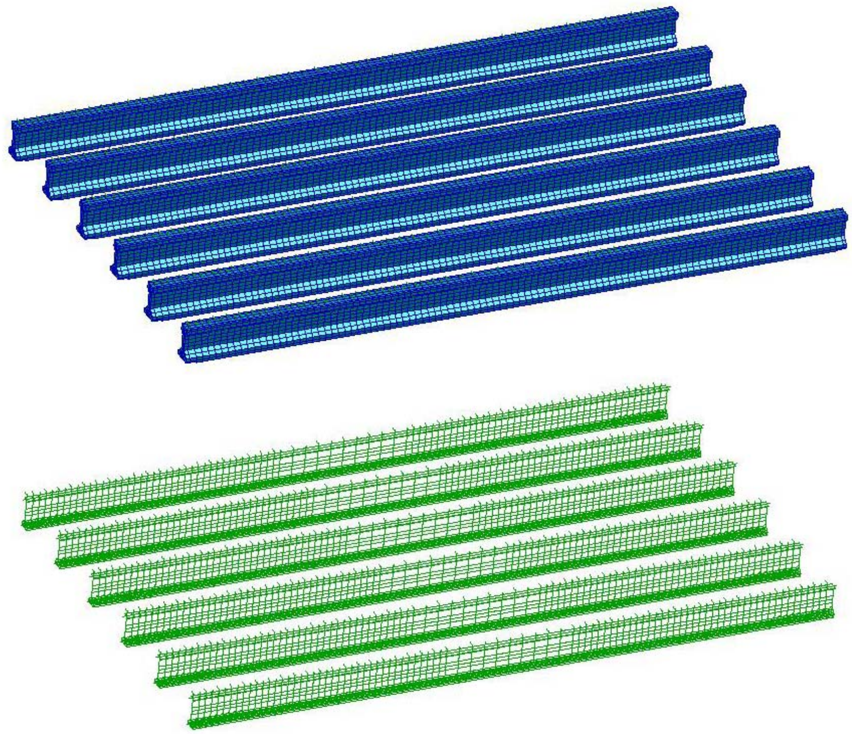

Figure 4.20. FE model of girders, concrete and reinforcement.

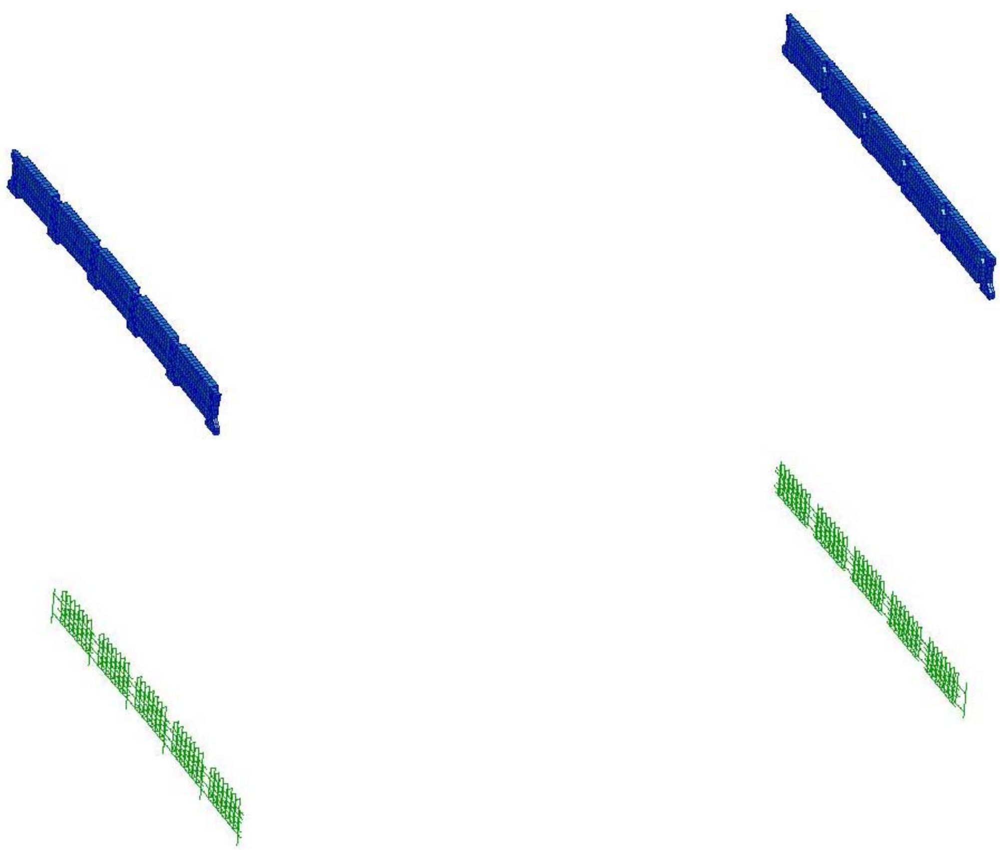

Figure 4.21. FE model of diaphragms, concrete and reinforcement.

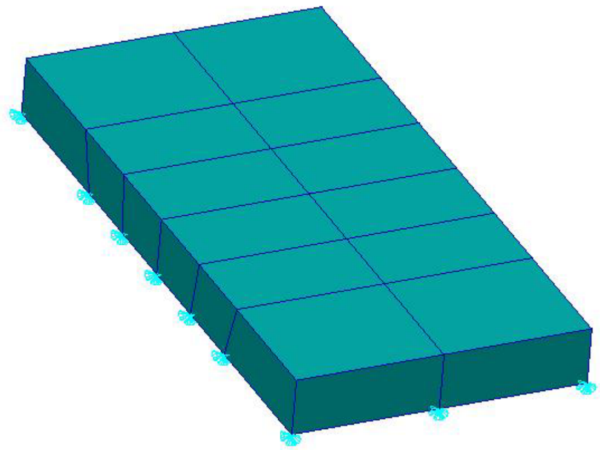

Figure 4.22. FE model of a neoprene pad with boundary conditions.

Figure 4.23 presents the top and bottom views of the entire slab with all structural components.

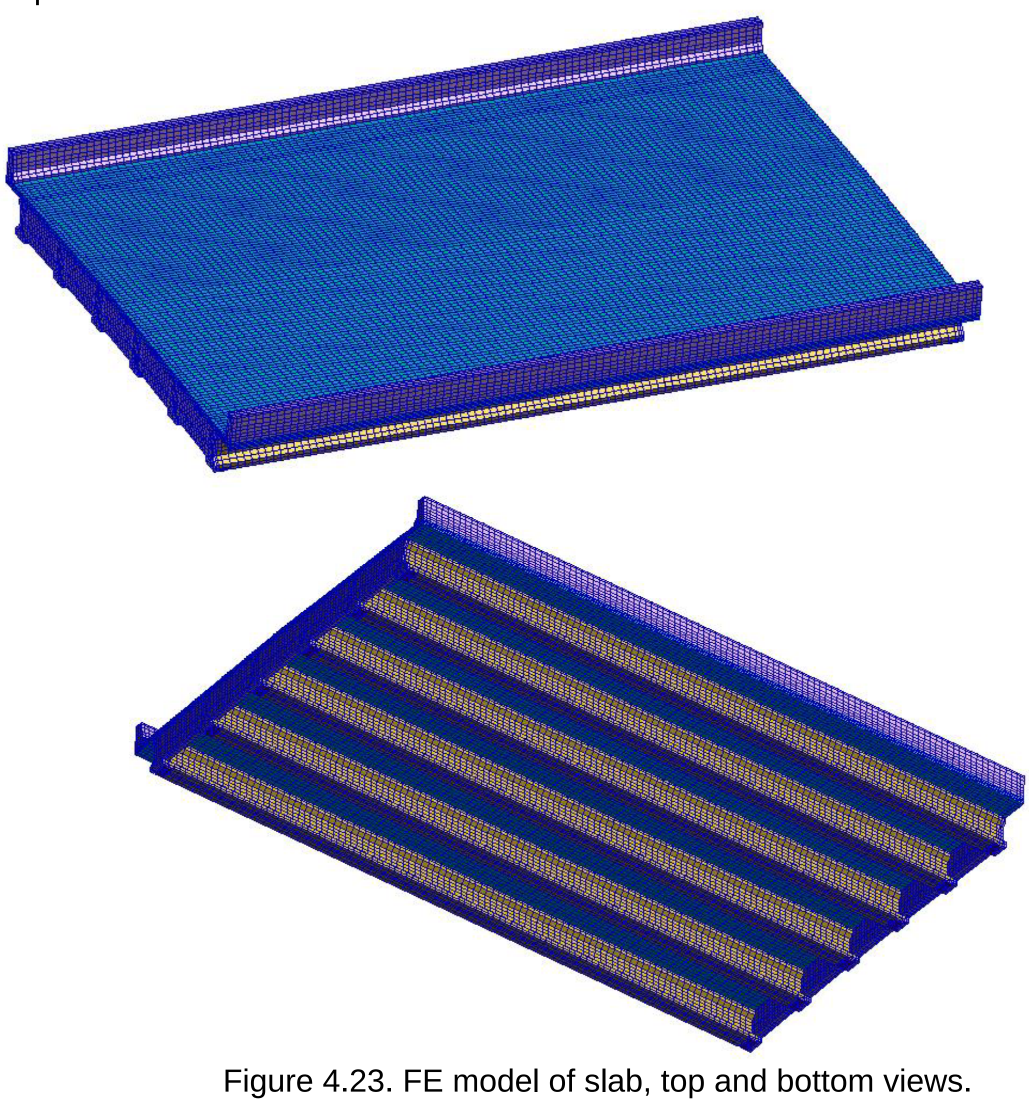

Figure 4.23. FE model of slab, top and bottom views.

Concrete elements

Concrete parts are modeled using 8 and 6 node solid, fully integrated elements. For the slab and beams most of the elements have a longitudinal dimension of 210 mm (see Figure 4.24). Only elements at the areas close to the ends of the span have different longitudinal dimensions, corresponding to the diaphragm dimensions. The dimension of 210 mm was chosen as the most suitable considering the location of the reinforcement, requirements for contact between tires and top surface of the deck and total number of FE elements.

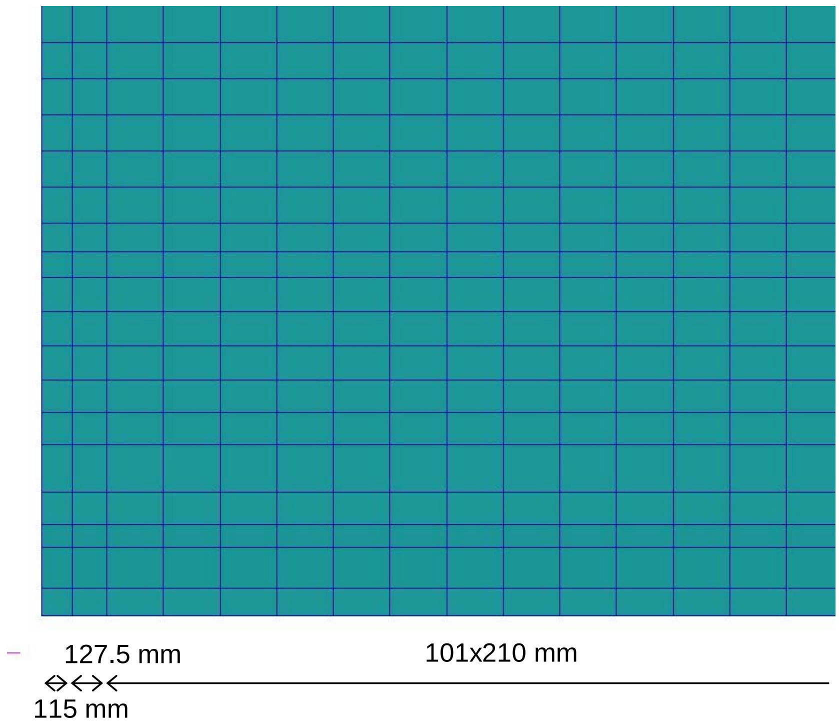

Figure 4.24. Top view of the part of the slab showing FE element division.

Four layers of solid elements are used for the slab as shown in Figure 4.25, which also presents FE element division in the beam cross-section. The number of FE elements and location of nodes in the beam cross-section was determined in pursuance of the location of rebars and strands in the actual beam (see Figure 4.26). Initially, the material properties of concrete were estimated from the design strength using the formula given by AASHTO:

$$E_c = 0.043 y_c^{1.5} \sqrt{f_c^{'}} \tag{4.1}$$

y_c = density of concrete (Kg/m^3)
$f_c^{'}$ = specified strength of concrete (MPa)

The Young's modulus of the concrete for the slab was estimated as 26725 MPa and as 28397 MPa for the girders. A discrepancy was observed between the FE analysis and field testing. Several samples were taken from the bridge and tested by FDOT Structures Lab. The actual material properties were applied in the FE model. It was assumed that the behavior of the actual bridge in the field test would be in the elastic range. If ultimate loading is investigated, one of more complex material models for concrete available in LS-DYNA will be used in the future.

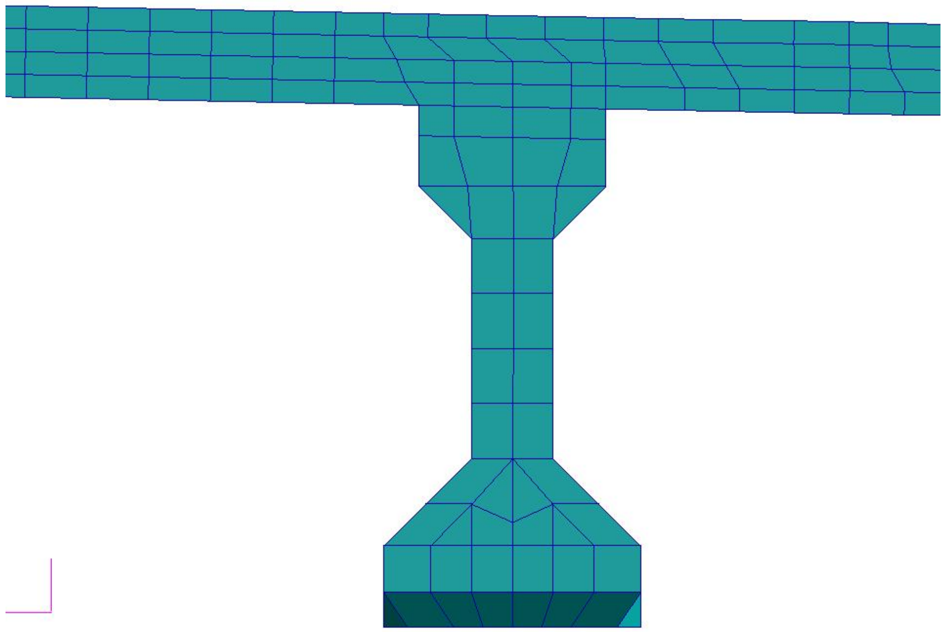

Figure 4.25. Part of the cross-section of slab and beam.

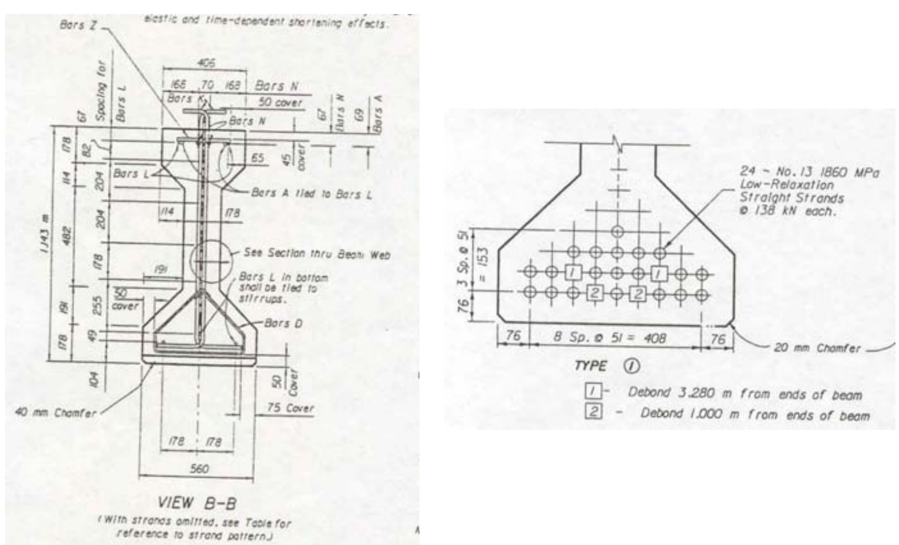

Figure 4.26. Location of rebars and strands in beam cross-section.

Rebars

Three types of rebars are present in the bridge structure: 10M, 15M, and 20M. All rebars are modeled using one-dimensional beam elements with nodes coinciding with corresponding nodes of concrete solid elements. Original location of the rebars is modified in the FE model due to finite number of elements and geometric limits of the FE mesh. Elastic material model with properties for steel was applied. As an example, Figure 4.27 presents a portion of rebars in the barrier model.

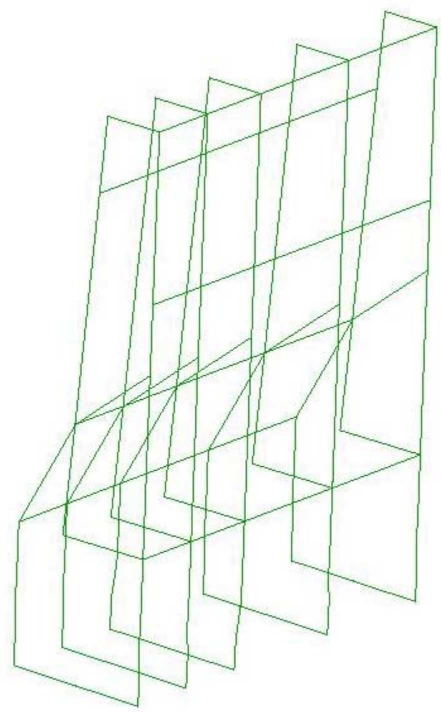

Figure 4.27. Rebars in barrier model.

Prestressed strands

In the modeled bridge, there are six prestressed ASHTO type III beams. Each beam has 24 No.13 1860 MPa low-relaxation strait strands at the bottom (Figure 4.26). Additionally, there are two No. 9 strands in the top of each beam. Strands are modeled using rod elements, with nodes coinciding with the appropriate nodes of solid elements. The mesh size requirement makes the beam cross-section too small to locate all 24 strands, so some of the strands are grouped as it is shown in Figure 4.28. Shaded dots show the node locations where grouped strands are positioned. Numbers indicate how many strands are represented at the location. These numbers (1, 2.5 and 3) are used as multipliers of cross-sectional area for No. 13 strands. Figure 4.28 shows how strand properties were relocated from their original positions (red dots) to the final position (indicated with blue and black dots). Number 9 strands present at the top part of the beams are grouped into one location since their original locations are very close (Figure 4.26).

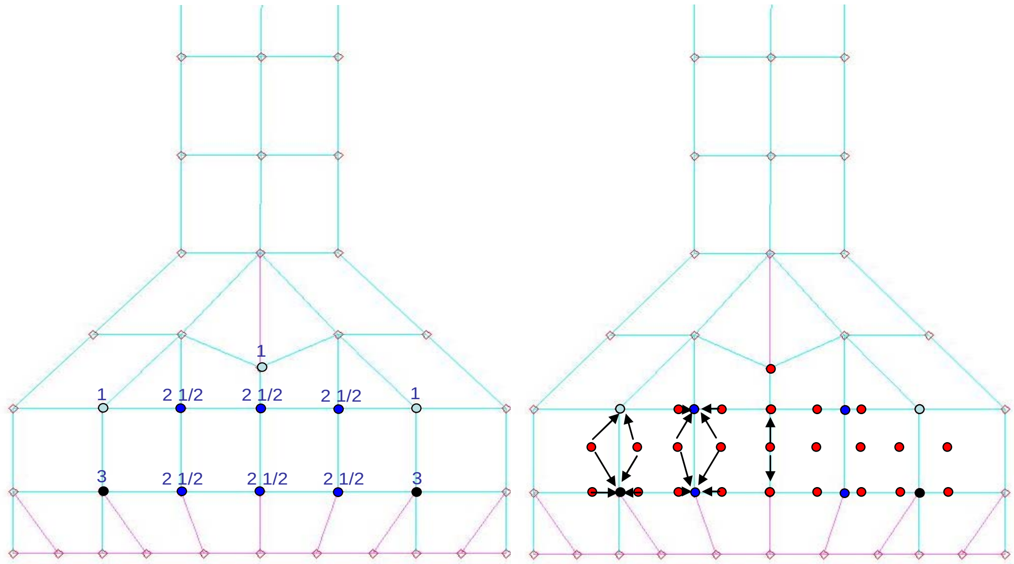

Figure 4.28. Distribution of strand properties to adjacent node locations.

To introduce prestressing forces in rod elements, a special material model called *MAT_CABLE_DISCRETE_BEAM was applied [22]. This material model is usually used to model cables and ropes, in which there is no stiffness for compression. Additionally, it allows for introducing initial tensile force by defining appropriate initial elongation. After trials and errors, the initial elongation of 1.4 mm was found appropriate for an element size of 210 mm. This value gives stress in strands close to the values estimated from MathCAD program: LRFD English Prestressed Beam Design [17]. The value of deflection (camber) was bigger than in the actual beam as the reological effects could not be taken into account in the FE model. The relation between the initial elongation and stresses in strands or beam deflection is nonlinear when the deformation caused by prestressing is taken into account. The effect of the prestressed strands is crucial for ultimate loading capacity analysis (not conducted in this research). Because considered vibrations are within the limits of the linearly elastic response (Section 3.5), the effect of the strands is small and can be neglected. The strands were excluded from the further numerical analysis to simplify obtaining the results (no need to calculate the initial state without loading but with gravity and prestress forces).

Second span

The second span was developed in the preprocessor Patran using the option "copy groups – mirror". In this way, the second span was a mirror of the first span with a symmetry plane at the end of the first span. Not only elements and nodes were copied but also all properties and boundary conditions. The two-span model is presented in Figures 4.29 and 4.30. In the actual bridge all girders are simply supported and the deck is cast as continuous with continuous reinforcement. Visual inspection of the bridge indicated distinct cracks in the deck at the joints. In the model between the spans a gap was created and contact between adjacent elements applied. For barriers, the opening was equal to 20 mm as specified in the blueprints. The gaps between slabs and diaphragms were determined as 1 mm. The gaps simulated a construction joint where there were forces only when it was closing. Because the girders are simply supported and the deck is separated by a crack opening, the influence of the adjacent span is limited. Most of the calculations were conducted for models consisting of one span only.

Figure 4.29. FE model consisting of two spans (top view).

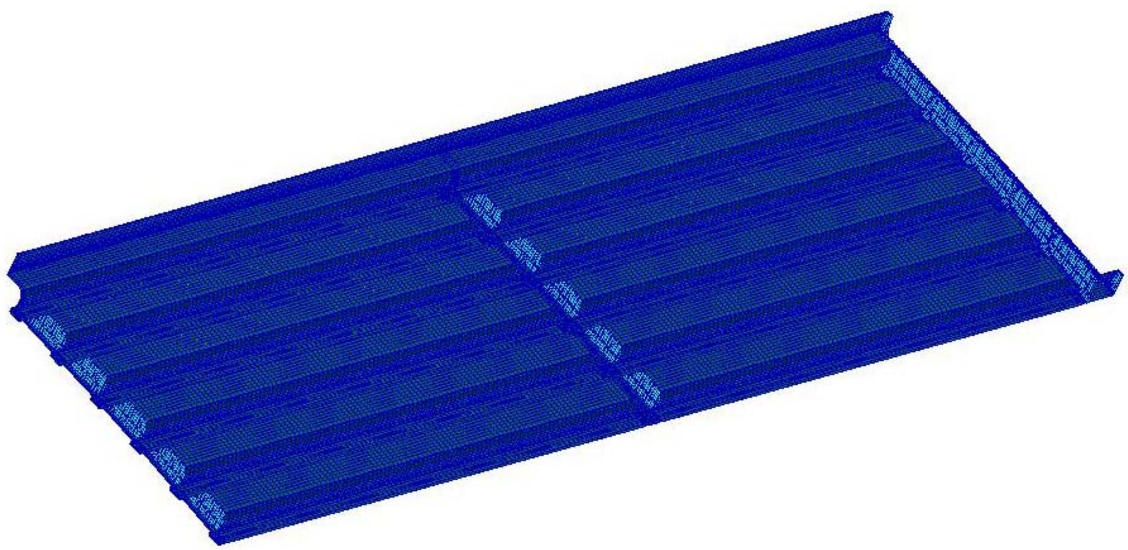

Figure 4.30. FE model consisting of two spans (bottom view).

4.7. Validation of bridge model

The bridge model validation started with checking the behavior of girder subjected to prestress forces. The FE simulation results were compared with the results from LRFD English Prestressed Beam Design [17]. Number 9 strands (Figure 4.26) were excluded in the validated model (they were present in other models) since it was not possible to include them in the input data set for the beam design program. Initial elongation of strand elements of 0.67% (1.4 mm for strand elements with the length 210 mm) was applied. This initial value was established using trial and error method. It is 15% larger than directly calculated for the strands. The difference compensates for reduction of stresses caused by shortening of the strands due to the deformation of the girder. Figure 4.31 shows time history for z (vertical) displacement in the middle of the beam (LS-DYNA analysis). The static value is 30 mm and is positive (camber). Figure

4.32 presents axial force for one of the beam elements representing steel No. 13 strands (LS-DYNA analysis). The static value is 140 kN. These values correspond to the state of the beam after the strands release. Figure 4.33 shows the estimated camber at a different stage using FDOT program. After release, the camber at the middle point is 31 mm. After considering the prestress loss, the FDOT program gives 122 kN in the strands.

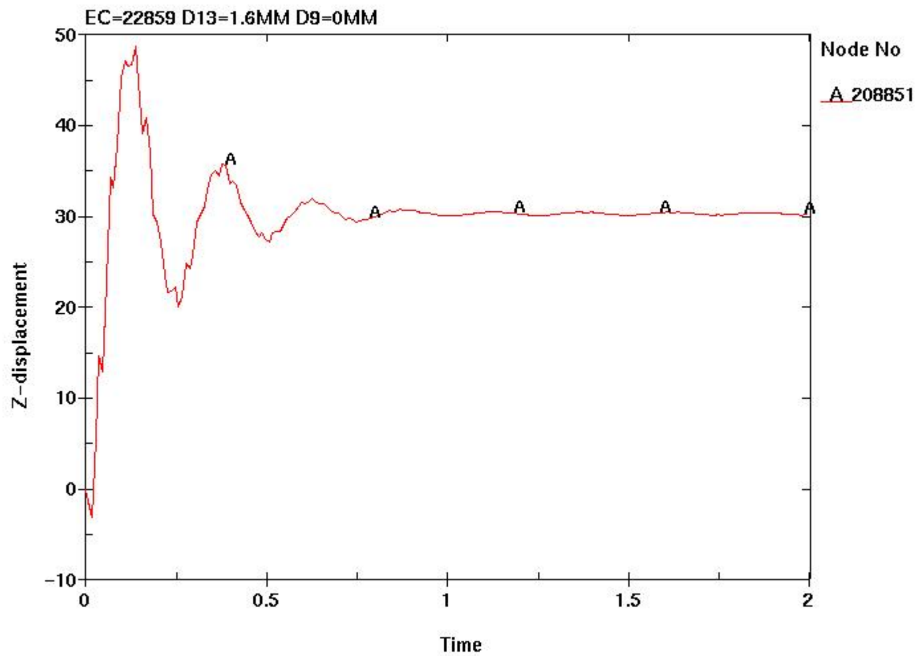

Figure 4.31. Z displacement in the middle of the beam.

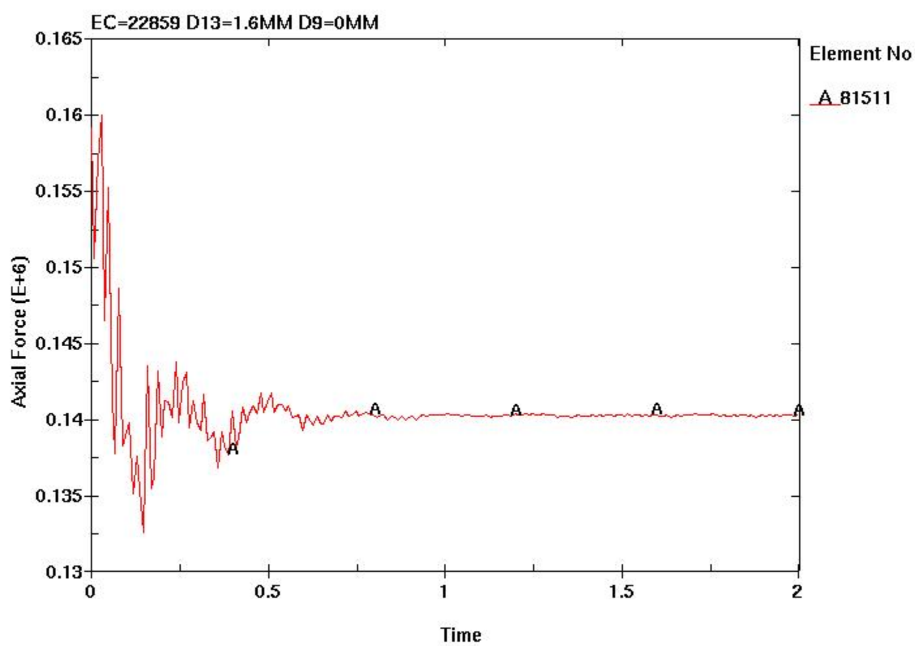

Figure 4.32. Axial force in strands [N].

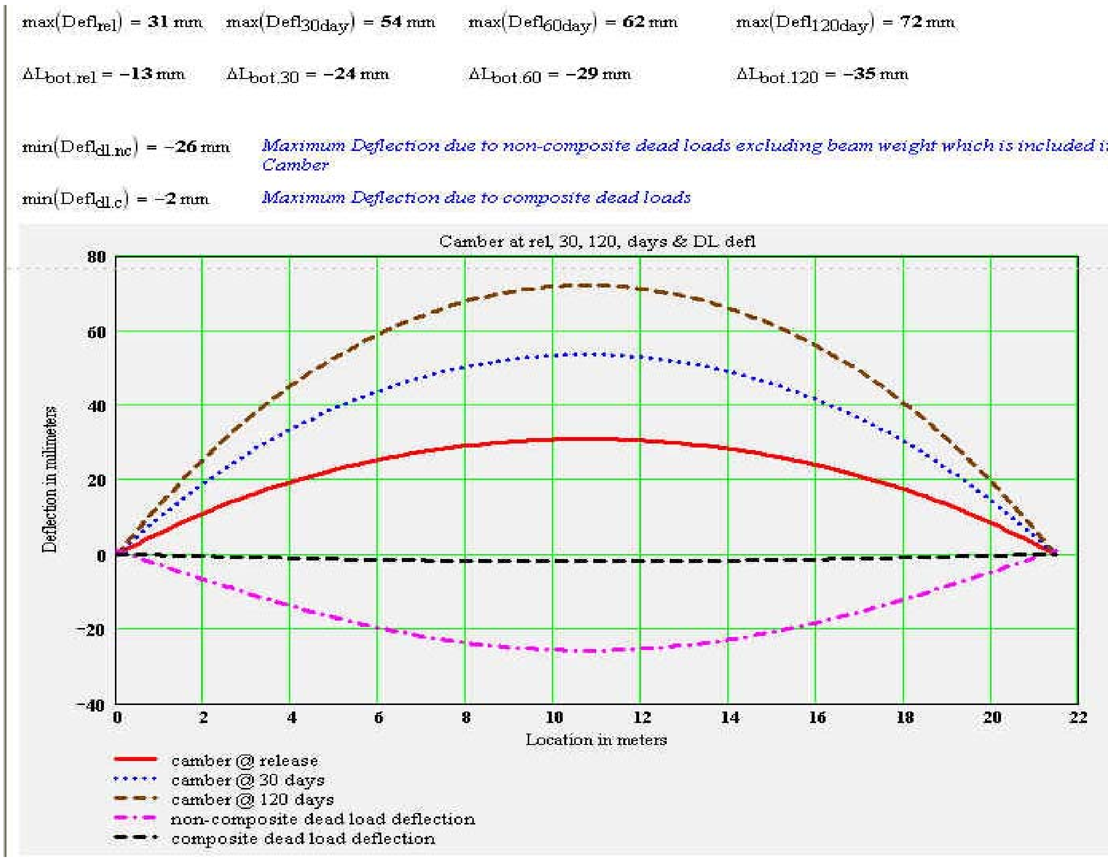

Figure 4.33. The camber of girder at different stages estimated form LRFD English Prestressed Beam Design.

As it was mentioned before in Section 4.6, we are interested in the load effect caused by the vehicular load. The initial stress state due to prestress has a small effect on the determination of the vehicular load effect if linear elastic model for concrete is used and the deformation is small. Some test runs for the static case were performed to validate the above conclusion. Three scenarios were set up: (1) the bridge subjected to prestress, gravity and one truck positioned at the center of the roadway (2) the bridge subjected to only prestress and gravity (3) the bridge subjected to only one truck positioned at the center of the roadway. The strains at the middle of the first span are presented in Figure 4.34. It is shown that the strain increment due to the vehicular load, received as a difference of results for cases (1) and (2) is almost equal to that caused only by the vehicular load, case (3). The prestress was excluded from the further numerical analysis to simplify obtaining the results.

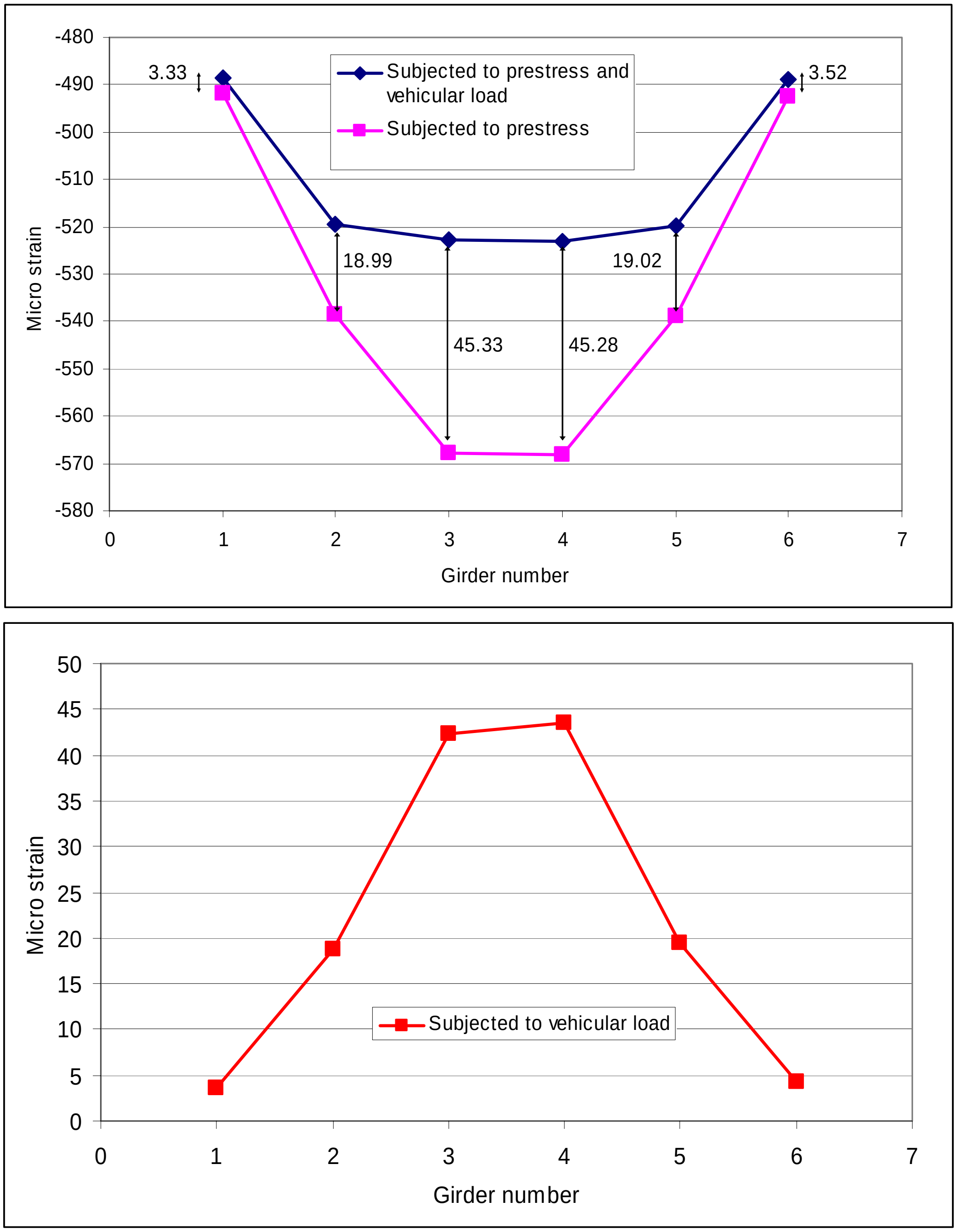

Figure 4.34. Comparison of results with and without prestress.

One method for bridge model validation is to check the static response. Estimated concrete properties from the blueprint were used in FE analysis at the beginning of the project. Some discrepancies were observed between numerical and experimental results for static loading. The discrepancy indicated that the stiffness of the FE model was smaller than the actual structure. Four core samples, two from the slab and two from the girders, were taken by the FDOT Structures Lab team for the lab test (Figure 4.35). Each sample was 3.2” in diameter and 6.25” in height. Two strain gauges were attached vertically and other two were glued peripherally. Two additional LVDTs were used to cross check the shortening of the sample.

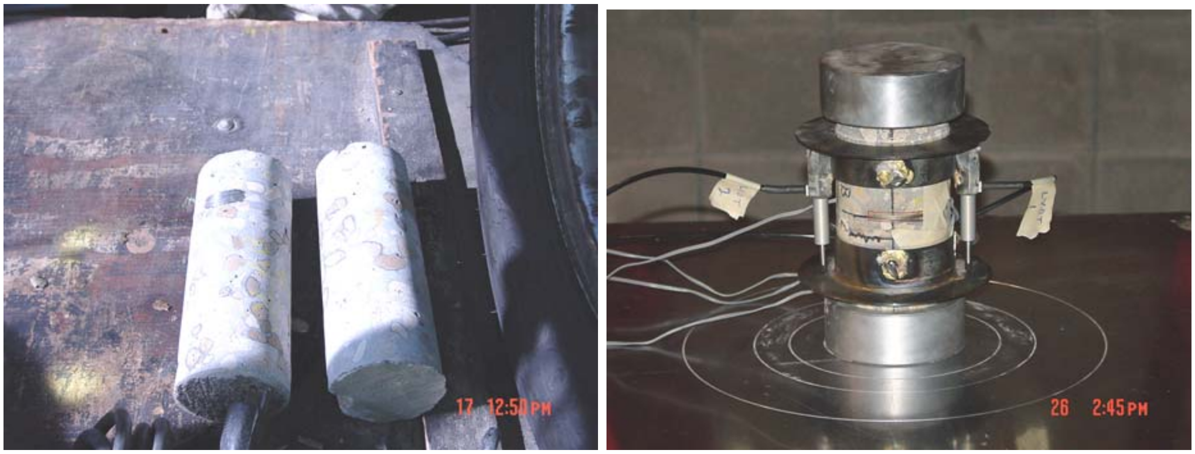

Figure 4.35. The core test samples and the strain gauge set up.

Each sample was loaded at the rate of 300 lb/second until failure. Figure 4.36 shows the results for one sample from the girder. The actual concrete properties are summarized in Table 4.4.

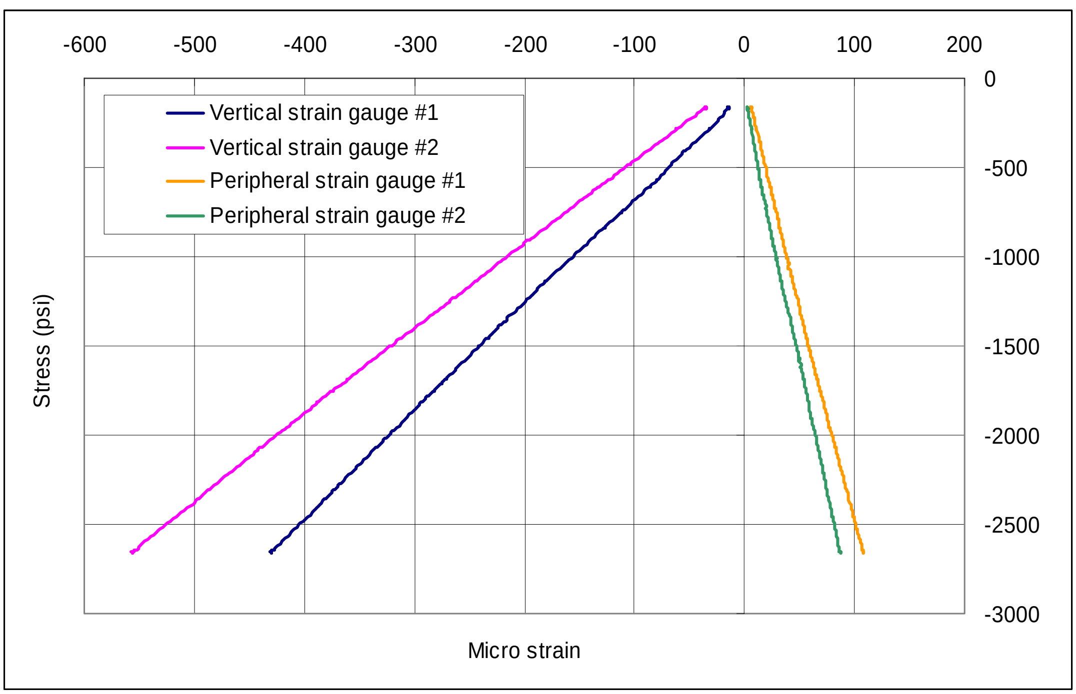

Figure 4.36. Experimental results for one girder sample.

Table 4.4. The actual material properties of the concrete.

	Modulus (E)	Poisson's ratio (ν)	Strength ($f_c^{'}$)
Beam	37.5 GPa (5441.9 ksi)	0.22	63.7 MPa (9.24 ksi)
Slab	40.5 GPa (5871.8 ksi)	0.20	55.9 MPa (8.11 ksi)

It is noted that the strength is much higher than the design strength and the Young's modulus is higher than that estimated by using AASHTO code. The finite element model was improved by incorporating the actual material properties. The new results from the computer simulation matched better with the experimental data. Figure 4.37 shows the comparison of strains at the middle span.

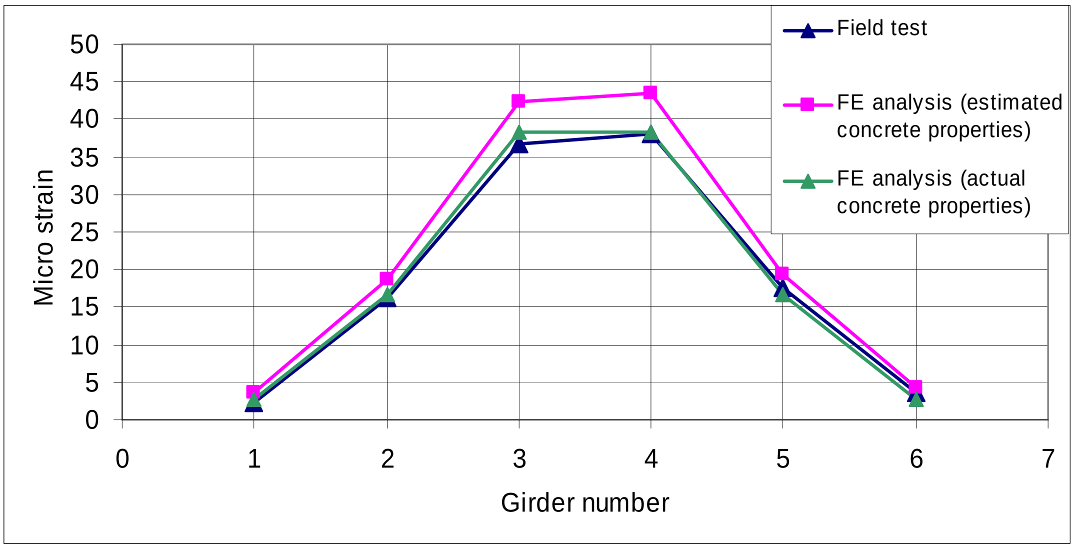

Figure 4.37. Comparison of the field measurement and the FE analysis for the static case (one truck at the center of the roadway).

To further check the validity of the bridge model, the natural frequencies and modes were retrieved by using the LS-DYNA implicit algorithm and were compared with the field test measurement. The first two modes correspond to bending and torsion deformation (Figure 4.38). The first (6.11Hz), the third (8.21Hz) and the sixth mode (12.66 Hz) from FE analysis correspond to the three modes retrieved from the experiment as 6 Hz, 7.78 Hz and 13.17 Hz (Figure 4.39). The FE analysis and the experimental results match well.

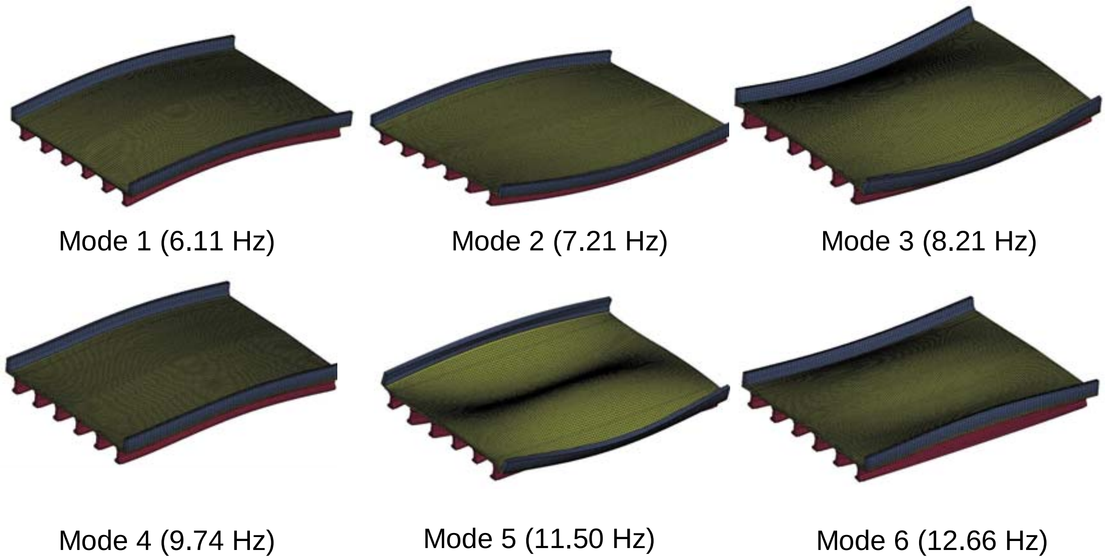

Figure 4.38. The first six natural vibration modes for tested bridge.

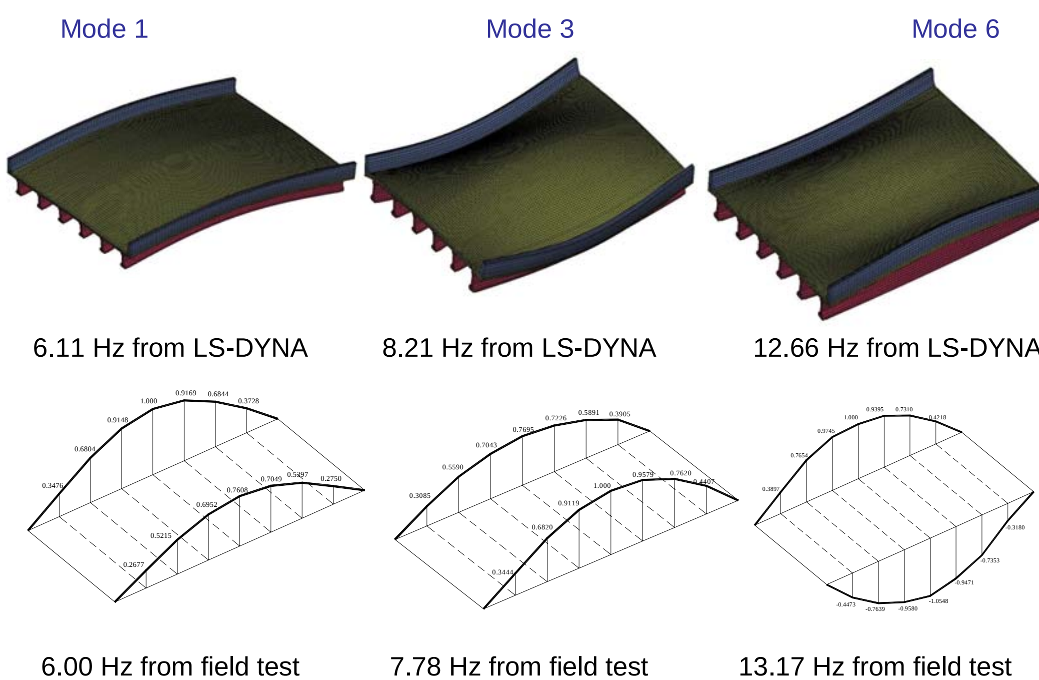

Figure 4.39. Comparison of natural vibration modes received based on calculation and experiment.

4.8. Comparison of the FE analysis and the field test

After the truck and the bridge models were validated separately, they were assembled together to simulate vehicle-bridge interaction for static and dynamic cases conducted in the filed test.

Static cases

Even though LS-DYNA is dedicated to transient dynamics, it still can be used to analyze static cases if global damping with large scaling factor is used. After a short time, the response of the structure reaches stable state corresponding to the static response.

One truck at the center of the roadway

Figure 4.40 shows girder strains from the FE simulation for the case where one truck is at the center of the roadway. Figure 4.41 presents the comparison of the FE analysis with the field test.

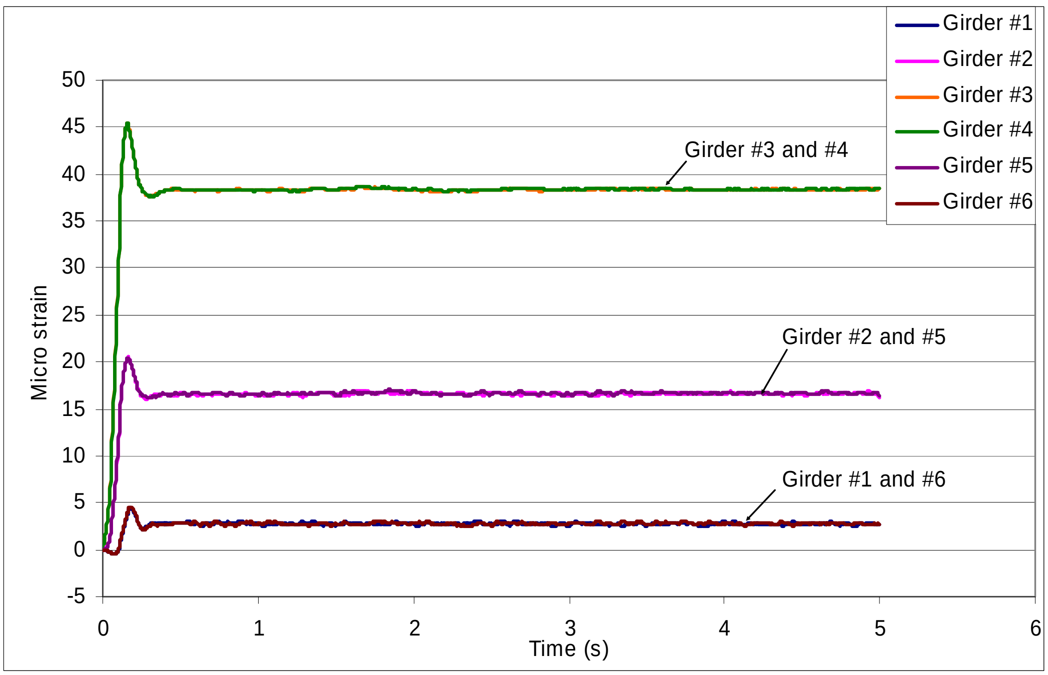

Figure 4.40. Strains at the middle span from FE simulation under one truck positioned at the center of the roadway.

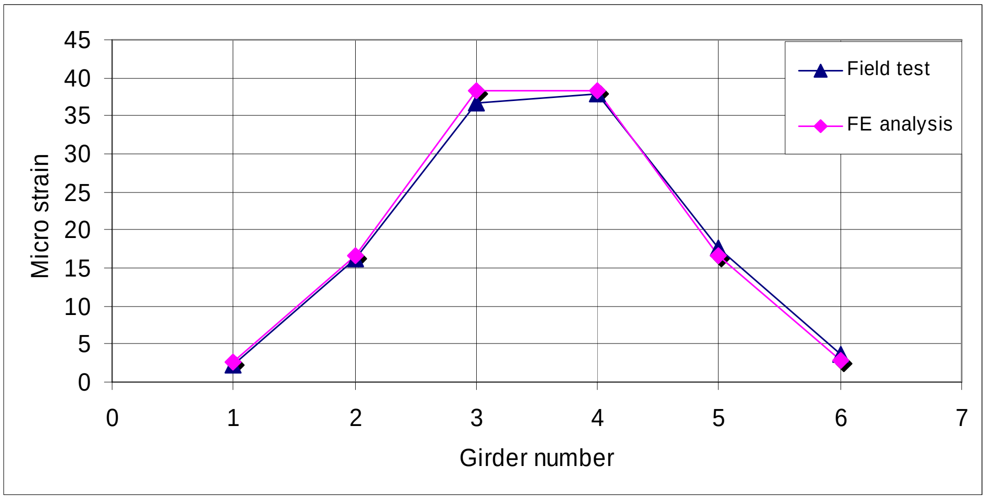

Figure 4.41. Comparison of strains from field test and FE analysis at the middle span under one truck positioned at the center of the roadway.

One truck on the westbound lane

The comparison of strains at the middle span subjected to one truck on the westbound lane is presented in Figure 4.42.

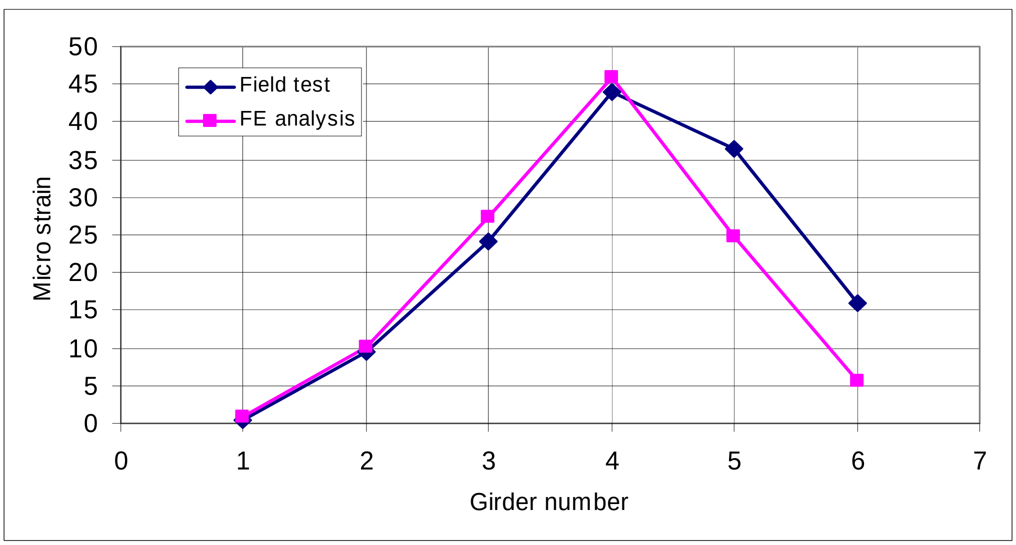

Figure 4.42. Comparison of strains from field test and FE analysis at the middle span subjected to one truck positioned on the westbound lane.

The field test has demonstrated a non-symmetric response of the structure subject to symmetric loading. The nonsymmetrical response is believed to be due to the non-uniform distribution of stiffness (Chapter 3). However, our bridge model is strictly symmetrical about the center line. This explains the discrepancy of the results at girders #5 and #6. It is concluded from Figure 4.42, that the stiffness of girders #5 and #6 is smaller than for other girders.

Two trucks on both lanes

The comparison of strains at the middle span subjected to two trucks on both lanes is presented in Figure 4.43.

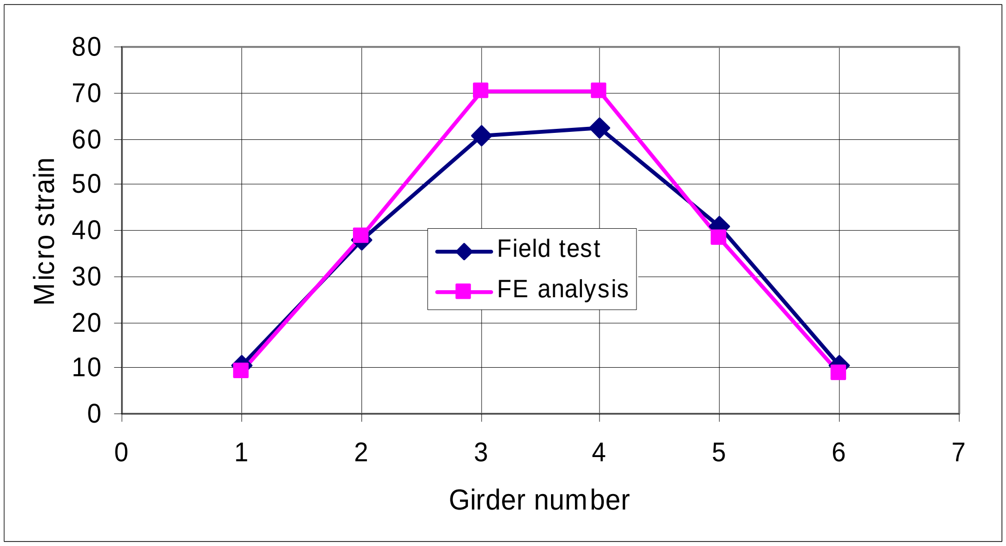

Figure 4.43. Comparison of strains from field test and FE analysis at the middle span subjected to two trucks positioned on both lanes.

Dynamic cases

During the field test and later inspections, a distinct approach depression and 10 to 15 mm threshold before the bridge (Figure 4.44) were discovered. This kind of non-horizontal road profile caused significant truck-bridge system vibration when the truck speed was high. An extremely high impact factor was obtained in the field test for cases at 50 mph (Chapter 3).

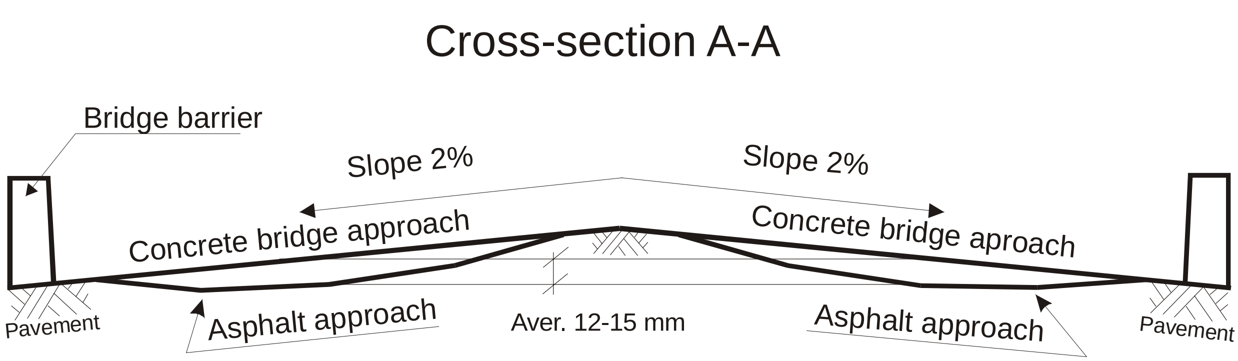

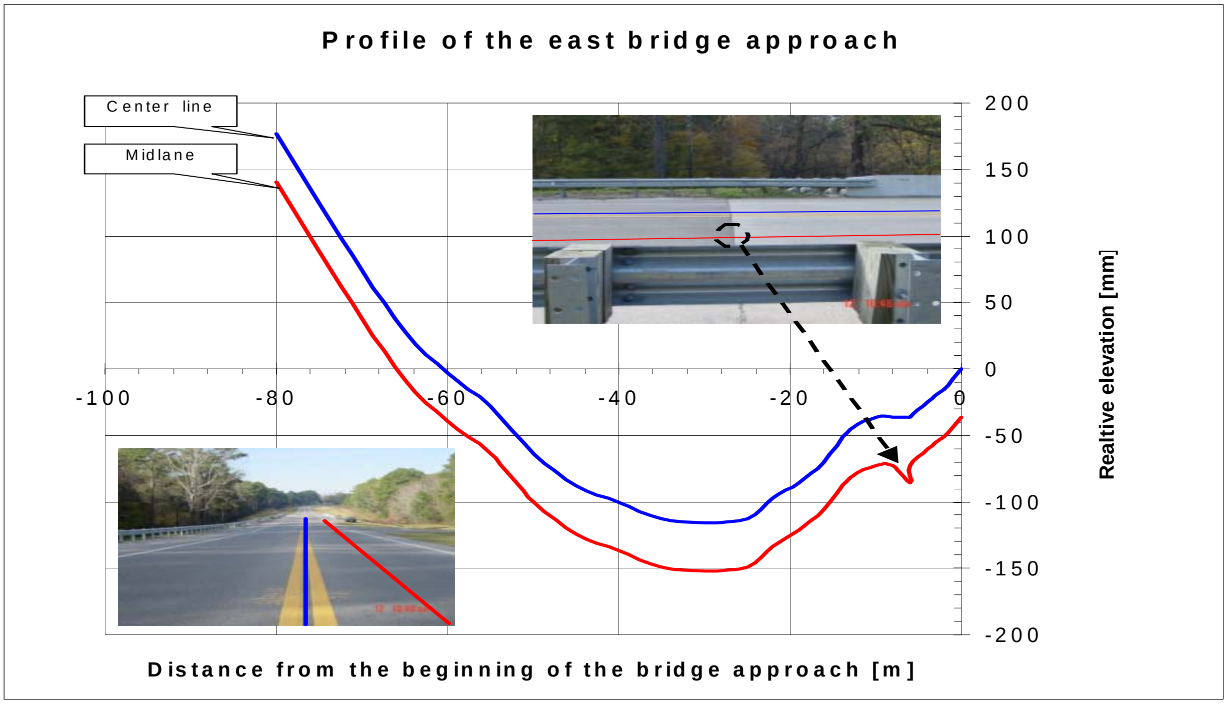

Figure 4.44. Profile of the east approach before Mosquito creek bridge.

To enhance the numerical results the road profile was incorporated into the FE model and an additional approach slab was created before the bridge (Figure 4.45).

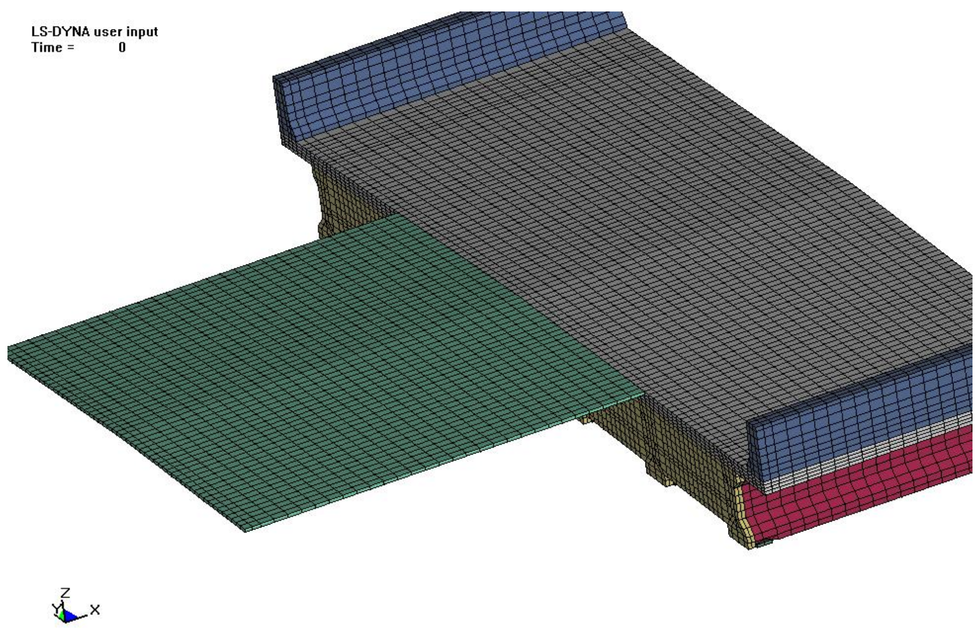

Figure 4.45. Approach slab added before the bridge.

One truck crossing on the center of the roadway at 30 mph

Figure 4.46 shows the comparison of the acceleration history at the rear axle of the tractor (accelerometer 16, chapter 3.3). Comparison of these results with experimental data also validates the truck model (chapter 4.5).

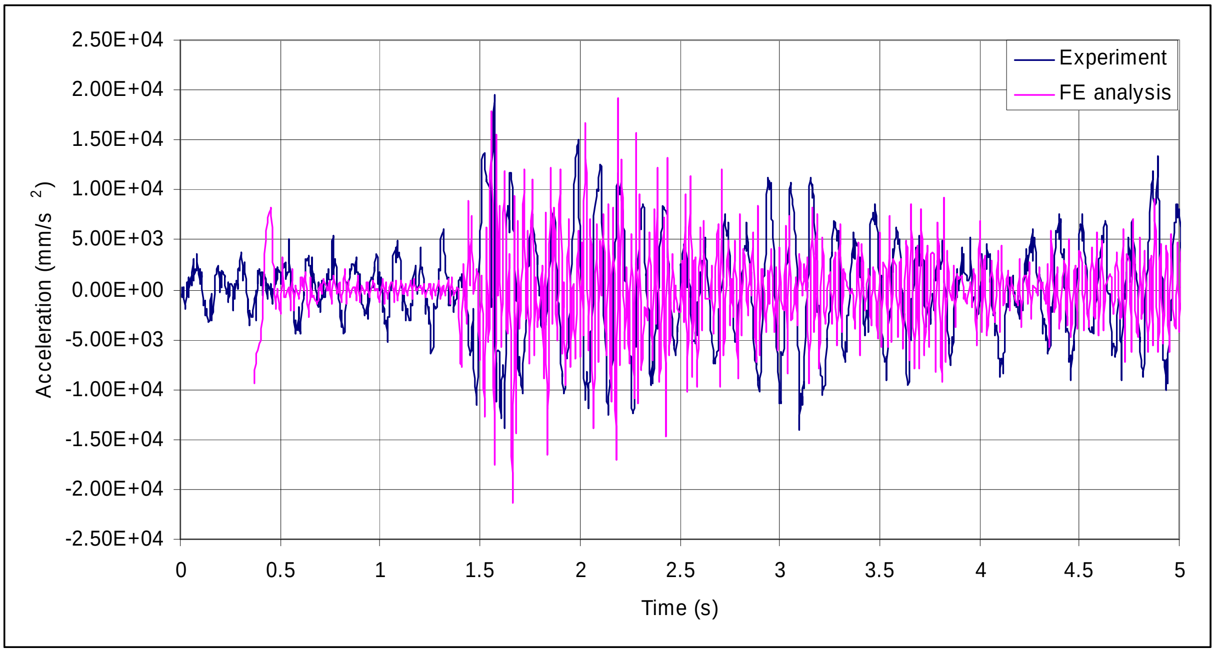

Figure 4.46. Comparison of vertical acceleration histories for the rear axle of the tractor passing at 30mph.

Because the position of the truck on the bridge during the field test was not registered it is difficult to match numerical and experimental results along the time abscissa axis. Experimental results for the first 1.5s show higher vibration in the truck due to the actual road surface conditions.

Figure 4.47 shows the comparison of the accelerations recorded and calculated at the middle of the first span (accelerometer 11, Chapter 3.3). For the first 2s, when the truck approaches the bridge, there is no vibration in the numerical signal. This is because in the FE model there is no connection between the horizontal rigid wall standing for the road and the bridge structure. In the real environment the vibration from the road is transmitted to the bridge superstructure before the truck enters the bridge.

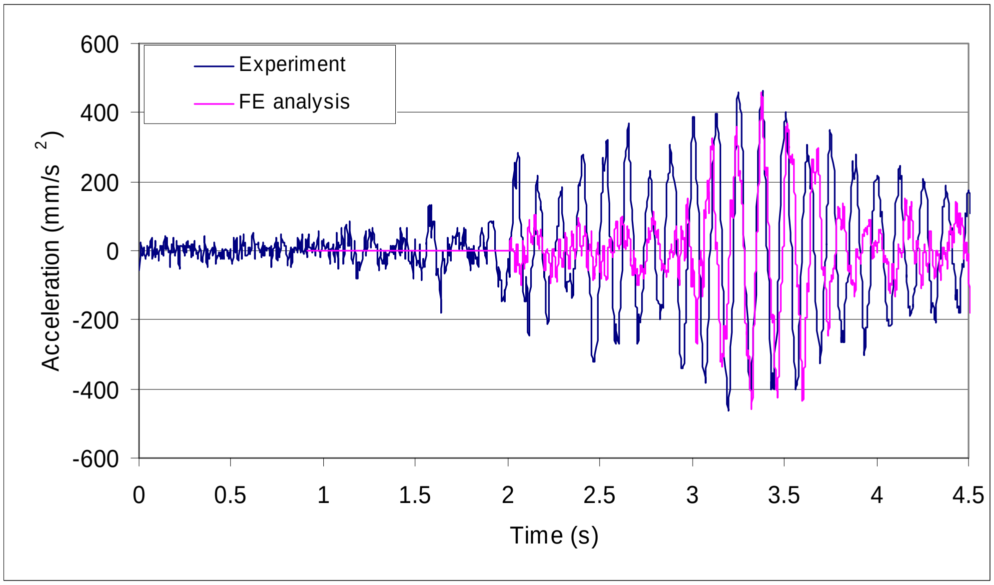

Figure 4.47. Comparison of recorded and calculated accelerations at the middle point on the slab (accelerometer #11).

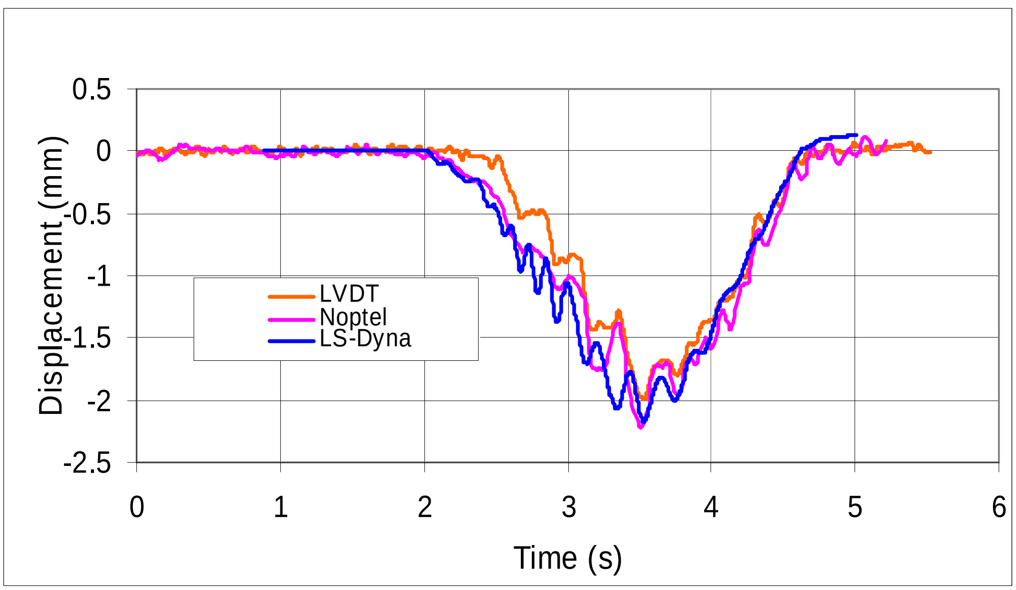

Figure 4.48. Comparison of experimental recordings and numerical results for displacement at the middle point of the girder #3.

Figure 4.49 shows the comparison of the strain histories for all six girders. The largest differences between experimental and numerical results are recognized for the edge girders #1 and #6. Experimental data shows that the actual girders are more flexible that their FE models. This is probably it is because in the FE model girders, slab and barriers are fully connected into one monolithic superstructure. In the real structure the action, especially between the barrier and the slab, can be not fully composite.

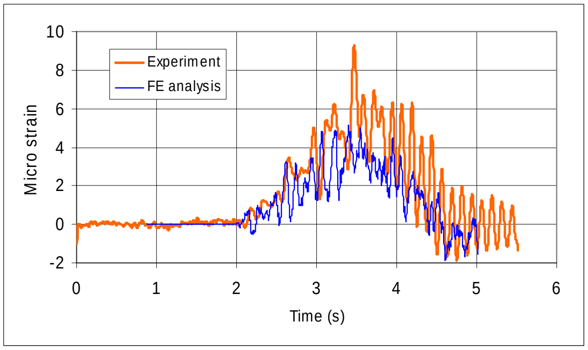

Strain for girder #1

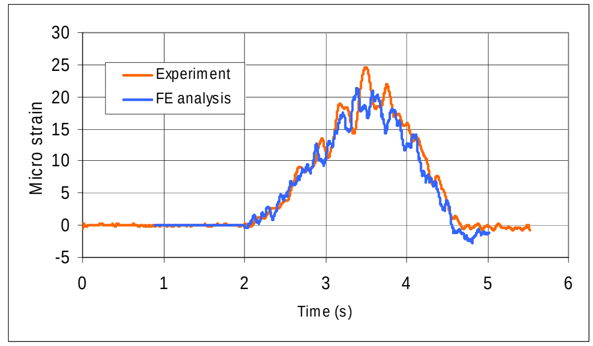

Strain for girder #2

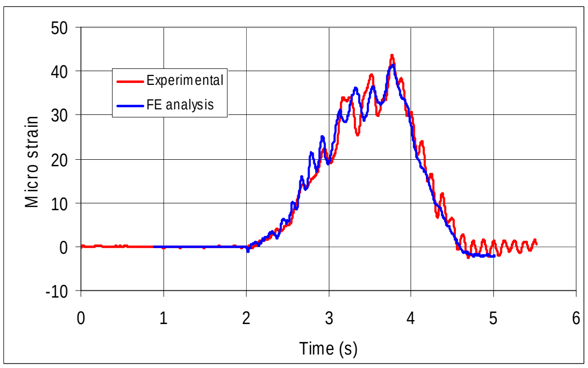

Strain for girder #3

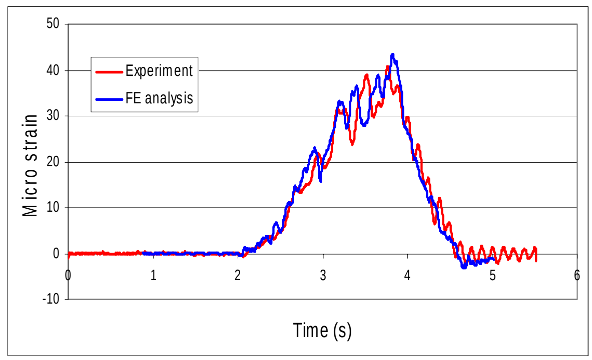

Strain for girder #4

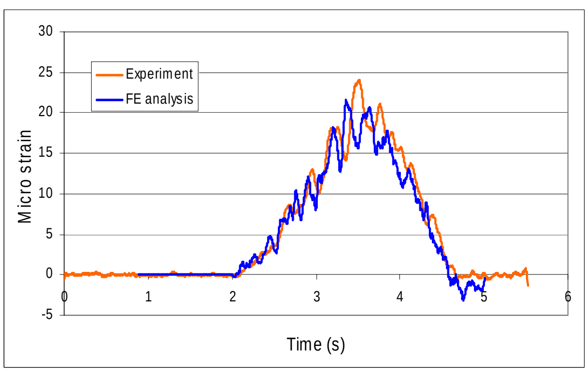

Strain for girder #5

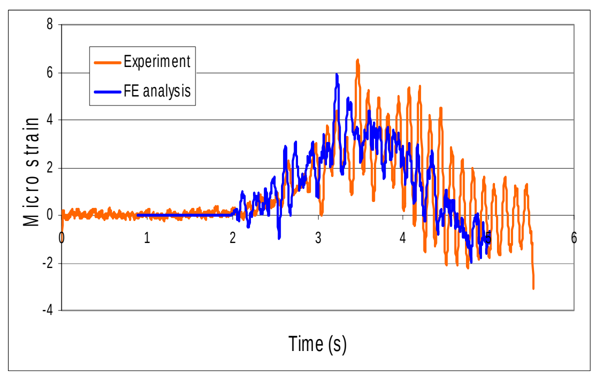

Strain for girder #6

Figure 4.49. Comparison of the strain histories for all six girders.

One truck crossing on the west bound lane at 50 mph

It is noted that for a speed of 50 mph, we received impact factors in the experiment much greater than those specified in the bridge codes. The videos recorded during the test reveal that a significant hammering effect is caused by bouncing of the concrete blocks triggered by the abutment threshold. This effect increases the dynamic interaction between the wheels and the deck. The truck FE model was improved by allowing the concrete blocks to bounce up and down. Figure 4.50 shows the comparison of the deflection at the middle of girder #3, while Figure 4.51 presents the strain comparison for the girder #4.

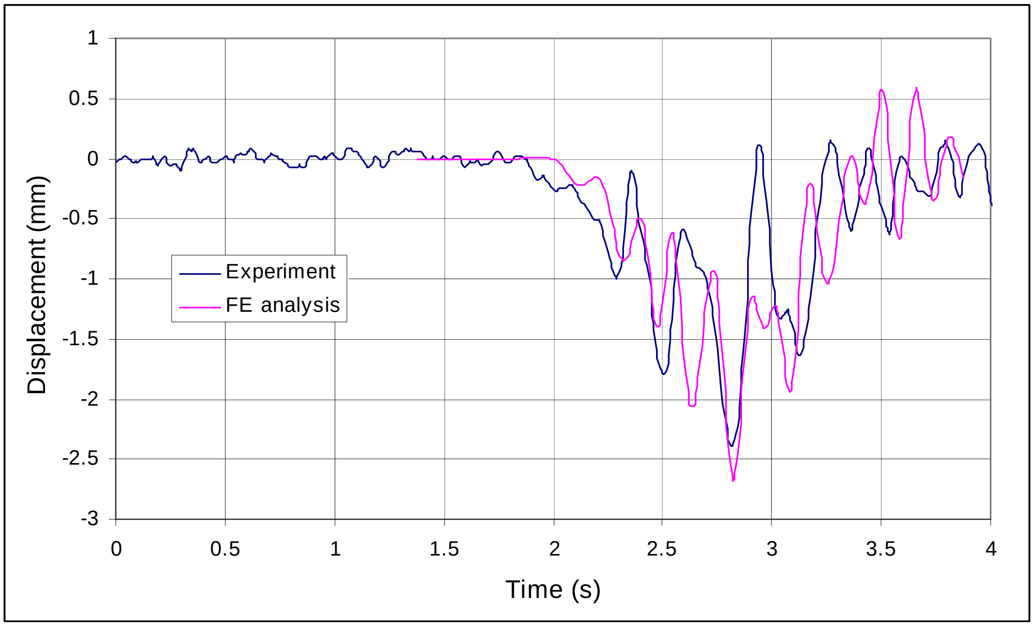

Figure 4.50. Comparison of the displacement at the middle point on the girder #3.

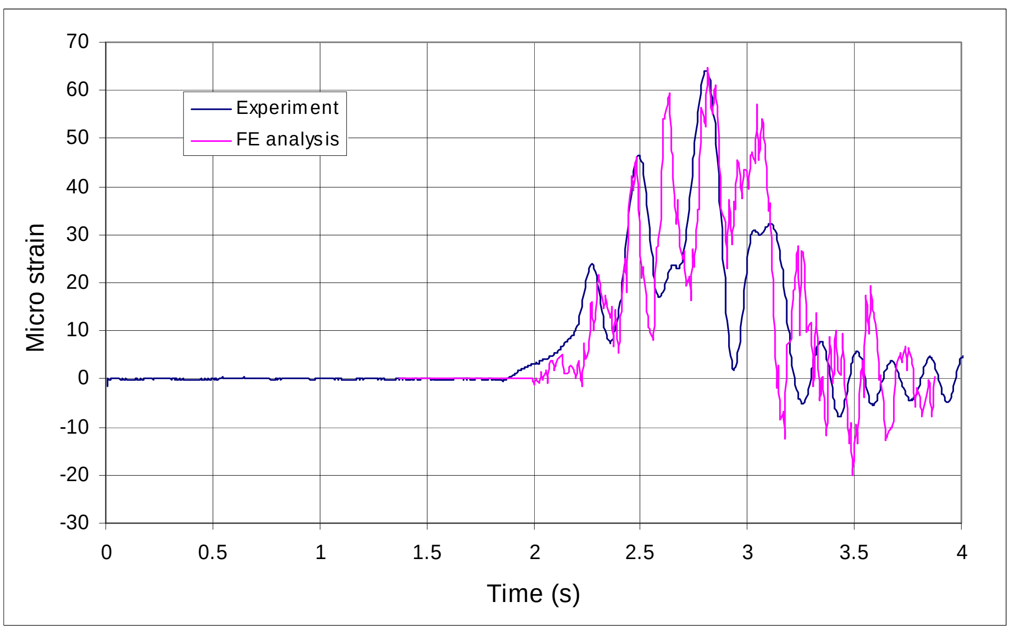

Figure 4.51. Comparison of the strain history for girder #4.

One truck crossing on the west bound lane at 50 mph with plank (FE model allowing the concrete blocks to bounce up and down)

Figures 4.52 and 4.53 show the comparison of the experimental and numerical results for the case when one truck is crossing the bridge at 50 mph. A plank is included to represent the extreme road surface conditions. It is the most complex case with large dynamic effects. Although there is the phase difference between the results, the amplitudes are at the same range.

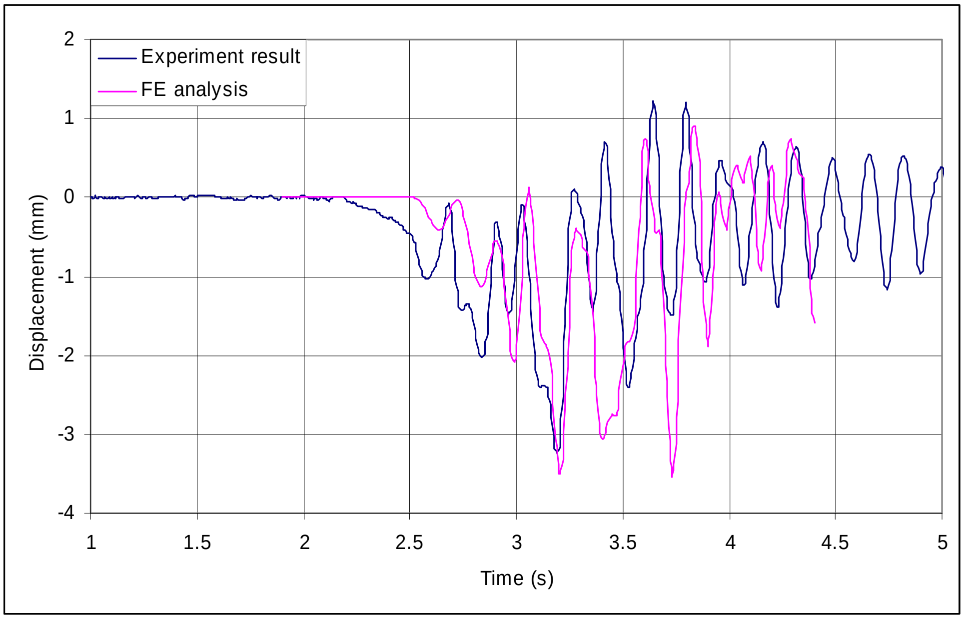

Figure 4.52. Comparison of the displacement at the middle point on the girder #3.

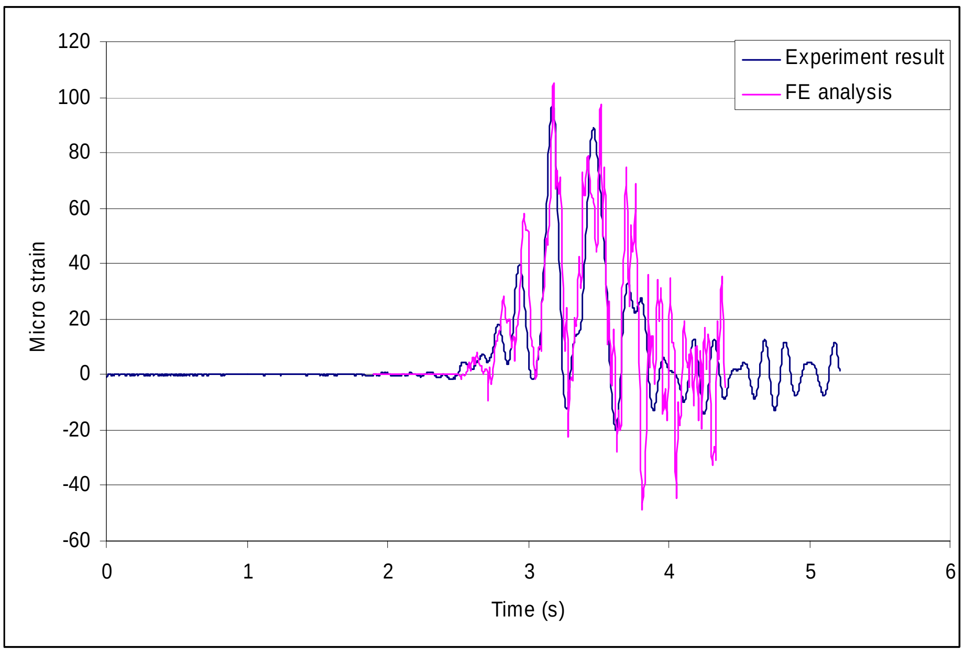

Figure 4.53. Comparison of the strain history for girder #4.

4.9. FE models of additional trucks

With the help of Mr. Jean Ducher, the Project Manager, a crane (LTM 1080) was selected for FE development (Figure 4.54). The crane was recommended by the Florida Crane Owners Council (FCOC). Blueprints and technical specifications were obtained from the FCOC and the manufacturer.

Figure 4.54. The selected crane (LTM 1080) for FE development.

The total weight of LTM 1080 crane is 89,700 lbs (402 kN). Models for the third and fourth vehicles were based on this model, with additional loadings of 5 and 10 kips respectively. The additional loads were evenly applied to the two rear axles. The first four models developed are shown in Figure 4.55.

Different values of the suspension stiffness were considered and two truck types #5 and #6 (Table 4.5) were added. The following types of suspension stiffness were applied:

- original stiffness for truck #1 with very high stiffness
- HS20–44 truck suspension stiffness. The spring factors and damping coefficients are taken from the literature [46]
- higher stiffness - truck #5 – The stiffness is a value between the HS20-44 suspension and the very stiff suspension.
- the highest stiffness – truck #6 – The suspension is very stiff, and the springs can be treated as rigid bodies.

The parameters for each suspension are listed in Table 4.6.

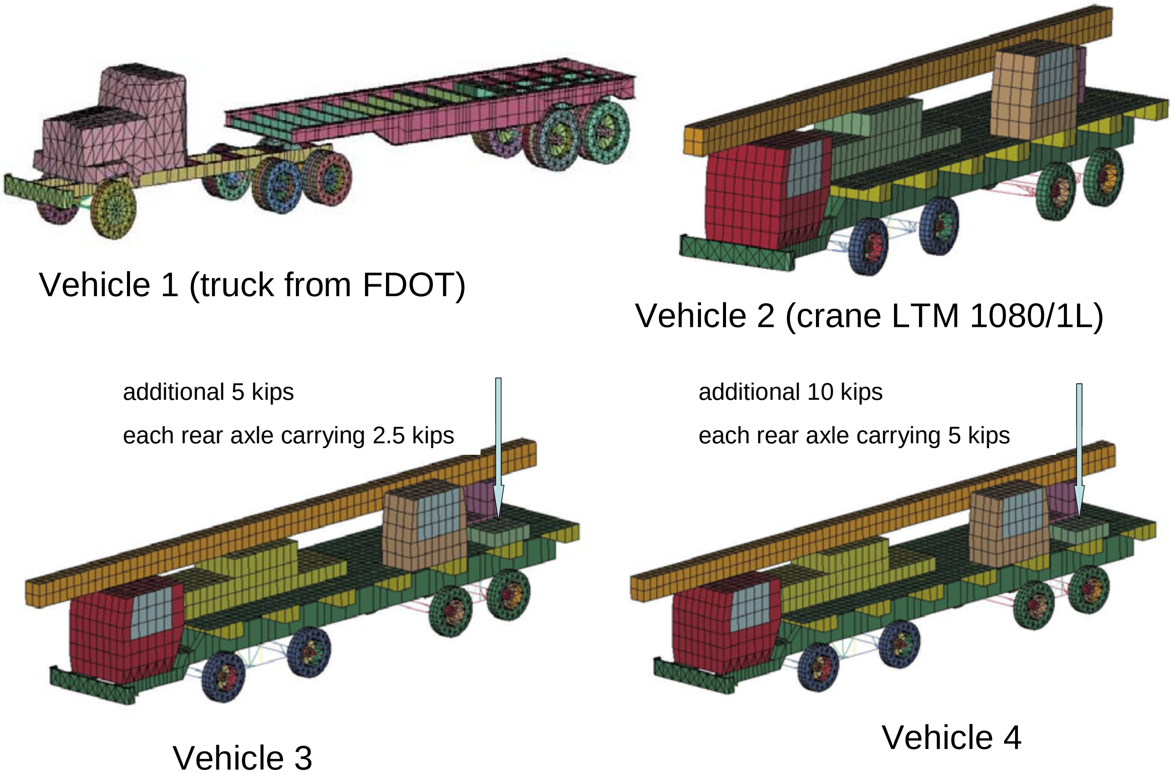

Figure 4.55. First four FE models of heavy vehicles.

Table 4.5. Description of selected heavy vehicles.

VEHICLE TYPES	
1	truck with trailer, with total weight of approximately 319kN (71700 lbs), from FDOT
2	crane LTM 1080/1L, total weight of 399kN (89700 lbs), recommended by the FCOC, suspension HS20-44
3	crane LTM 1080/1L plus additional weight, total weight of 421kN (94700 lbs) (additional 5 kips applied to Vehicle 2 with each rear axle carrying 2.5 kips), suspension HS20-44
4	crane LTM 1080/1L plus additional weight, total weight of 444kN (99700 lbs), (additional 10 kips applied to Vehicle 2 with each rear axle carrying 5 kips), suspension HS20-44
5	crane LTM 1080/1L, total weight of 399kN (89700 lbs), recommended by the FCOC, suspension HS20-44 (vehicle #2) with higher suspension stiffness
6	crane LTM 1080/1L, total weight of 399kN (89700 lbs), recommended by the FCOC, suspension HS20-44 (vehicle #2) with the highest suspension stiffness

Table 4.6. Suspension parameters.

	Truck #1 original suspension	Trucks #2, 3, 4 HS20-44	Truck #5 Higher stiffness	Truck #6 The highest stiffness
Spring Stiffness	167 x 10^6 N/m	8 X 10^6 N/m	80 X 10^6 N/m (10 times HS20-44)	160 X 10^6 N/m (20 times HS20-44)
Dampers	2X10^4 N*s/m	2X10^4 N*s/m	2X10^4 N*s/m	2X10^4 N*s/m

Table 4.7. The axle reaction forces for crane LTM1080-1L (vehicle #2)

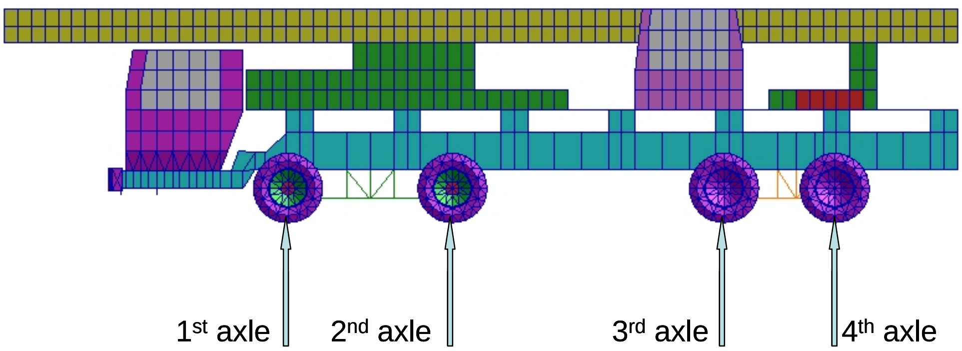

Axle	FE model [kN]	Provided by manufacturer [kN]	Difference [kN]	Error [%]
1-st	101.71	100.84	0.87	0.86
2-nd	101.68	100.55	1.13	1.1
3-rd	97.94	99.28	-1.34	-1.3
4-th	97.91	98.49	-0.58	-0.59
Total weight	399.24	399.16	0.08	0.02

Reactions were the only actual data we could receive for the additional vehicle models. Because of that, the model validation was limited to comparison of calculated and measured reactions. The results of that comparison are presented in Tables 4.7, 4.8 and 4.9.

Table 4.8. VEHICLE #2 with an additional 5 kips (22.24 kN) load added to the third and forth axle (vehicle #3).

Axle	FE model [kN]	Provided by manufacturer [kN]	Difference [kN]	Error [%]
1-st	100.29	100.84	-0.55	-0.55
2-nd	100.30	100.55	-0.25	-0.25
3-rd	110.41	110.4	0.01	0.01
4-th	110.42	109.61	0.81	0.74
Total weight	**421.42**	**421.4**	**0.02**	**0.005**

Table 4.9. VEHICLE #2 with an additional 10 kips (44.48 kN) added to the third and forth axle (vehicle #4).

Axle	FE model [kN]	Provided by manufacturer [kN]	Difference [kN]	Error [%]
1-st	98.92	100.84	-1.92	-1.9
2-nd	98.90	100.55	-1.65	-1.64
3-rd	122.91	121.52	1.39	1.14
4-th	122.89	120.73	2.16	1.79
Total weight	**443.62**	**443.64**	**-0.02**	**-0.005**

4.10. FE models of additional bridges

After visiting 10 bridges in northern Florida, the bridge 500126 on US 27 over Ochlockonee river was selected for further finite element development. This 11-span bridge, completed in 2001, is in very good condition (Figure 4.56).

Figure 4.56. Selected bridge (No. 500126) for FE development.

Two other bridge models, suggested by the FDOT, were completed. They are four meters longer than the bridge #500133 and the bridge #500126, respectively. Table 4.10 depicts all four bridge models developed in this research.

During the visual inspection of the bridge #500126, it was noticed that there was an small approach depression before the bridge. This kind of non-horizontal road profile could cause additional truck vibration (and also for the bridge), which has been observed in the experiment on Mosquito Creek bridge. In order to capture the real dynamic response and obtain good simulated results, this vertical profile was surveyed by CIAL members with the help from FDOT who arranged the bridge lane closure. Figure 4.57 shows the approach depression before bridge #500126, and Figure 4.58 presents the vertical profiles of the first two spans.

Table 4.10. Finite element models of bridges.

BRIDGE CLASS		
1	6 AASHTO III girders, length of span 21.700 m (71.14 ft)	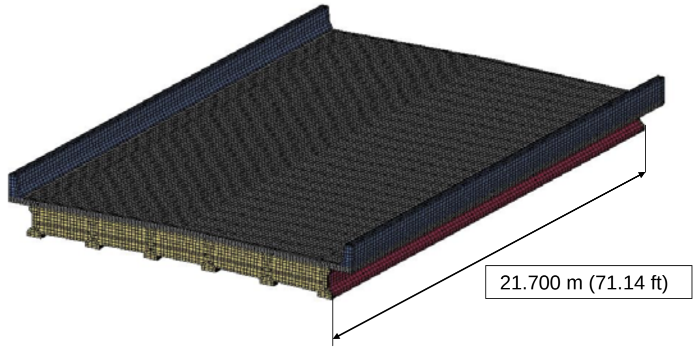
2	6 AASHTO III girders, length of span 25.700 m (84.26 ft)	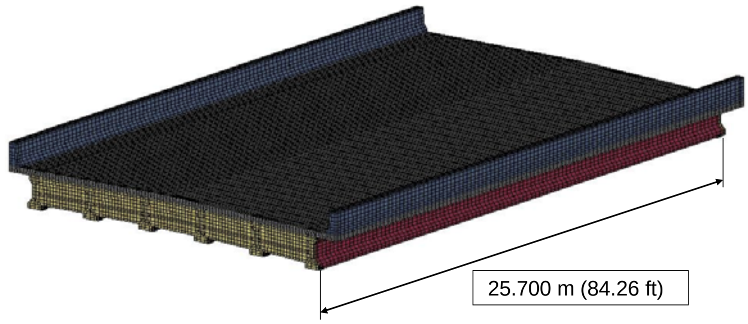
3	5 AASHTO III girders, length of span 19.260 m (63.15 ft)	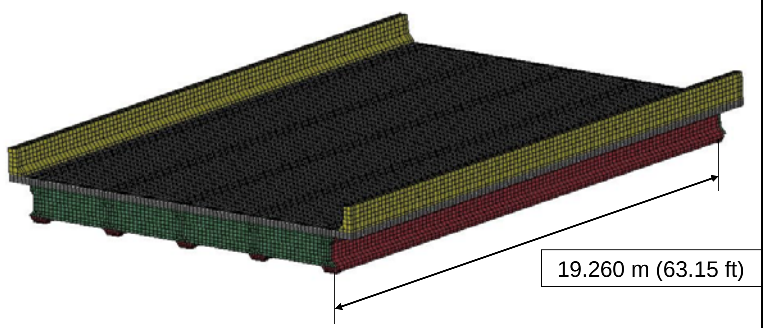
4	5 AASHTO III girders, length of span 23.260 m (76.26 ft)	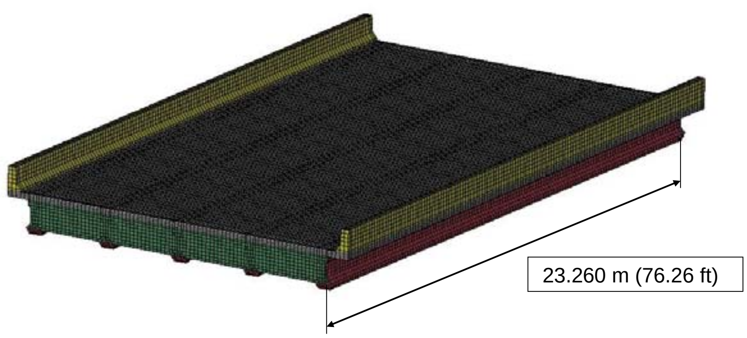

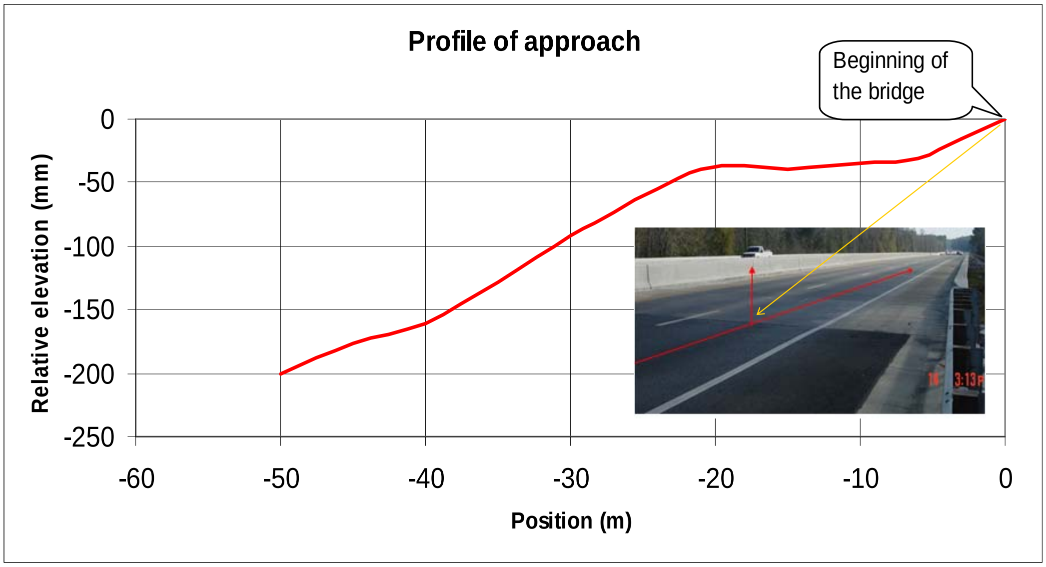

Figure 4.57. Vertical profile of the approach before bridge #500126.

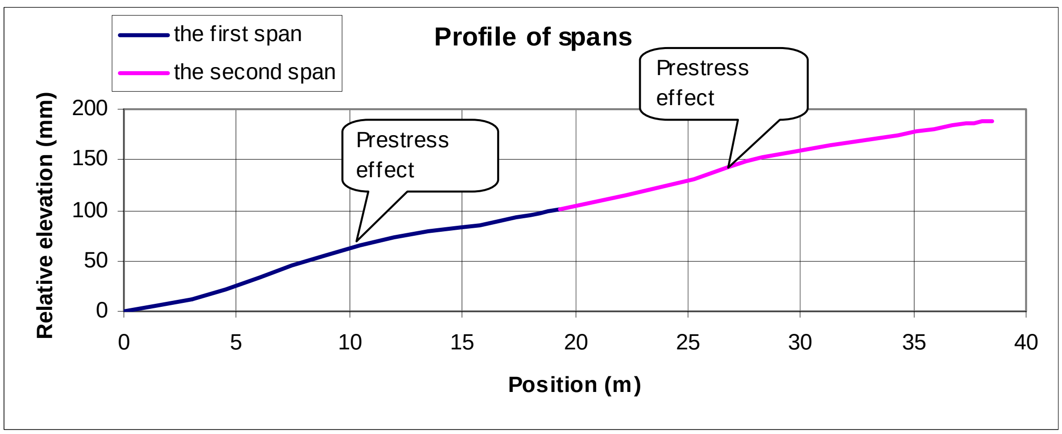

Figure 4.58. Vertical profile of the first two spans of bridge #500126.

Modal analysis presented below provides validation for the newly developed FE bridge models. Figure 4.59 presents the first two natural vibration modes calculated for the three models of additional bridges. Table 4.11 lists the first two natural frequencies for each of the four available bridge models. The fundamental frequencies obtained from FE analysis were compared with those from approximate formula. The comparison indicates a good correlation.

Bridge 500133

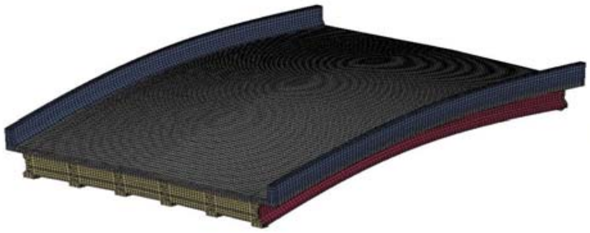

Frequency 6.11 Hz

Frequency 7.21 Hz

500133 + 4

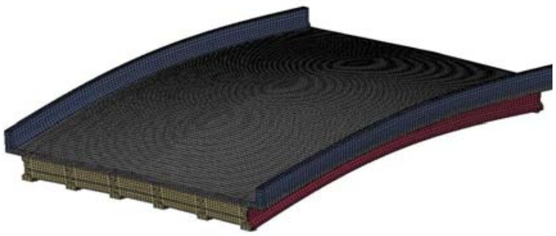

Frequency 5.23 Hz

Frequency 5.97 Hz

Bridge 500126

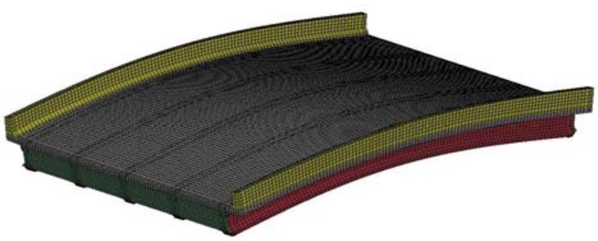

Frequency 7.35 Hz

Frequency 9.70 Hz

500126 + 4

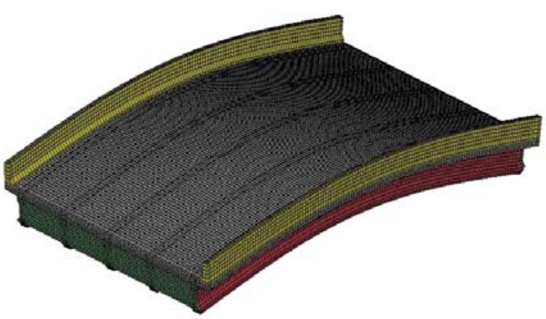

Frequency 5.15 Hz

Frequency 6.90 Hz

Figure 4.59. Natural vibration modes corresponding to the first two natural frequencies.

Table 4.11. Natural frequencies for the four bridge models.

	Bridge 500126 (19.26 m)	Bridge 500133 (21.7 m)	4 meters longer than bridge 500126 (23.26 m)	4 meters longer than bridge 500133 (25.7 m)
1st mode from FE model	7.35 Hz	6.11 Hz	5.15 Hz	4.50 Hz
2nd mode from FE model	9.70 Hz	7.21 Hz	6.90 Hz	5.90 Hz
1st mode from approximate formula	7.09 Hz	6.28 Hz	4.81 Hz	4.44 Hz

5. RESULTS OF FE ANALYSIS

5.1. Case matrix

The case matrix was refined based on the discussion conducted in the CIA Lab on 10.05.2004. The new matrix was developed for the previously selected four bridges described in Table 5.1 and Table 4.10, and for six trucks depicted in Table 4.5. The total case number was doubled from 16 to 32. The distribution of the additional loading for truck #3 and #4 was changed to ensure the additional loads were evenly applied to the two rear axles.

Table 5.1. Description of selected bridges.

BRIDGE CLASS	
1	6 AASHTO III girders, length of span 21.700 m (71.14 ft)
2	6 AASHTO III girders, length of span 25.700 m (84.26 ft)
3	5 AASHTO III girders, length of span 19.260 m (63.15 ft)
4	5 AASHTO III girders, length of span 23.260 m (76.26 ft)

Experiences gained during the field test and preliminary calculations imply that the following six variables could have a significant influence on impact factor IM. They are:

1. span length,
2. vehicle speed,
3. suspension parameters,
4. truck weight,
5. truck position on bridge lanes,
6. road surface condition.

The case matrix was designed to study the influence of some of these parameters. Different values of the suspension stiffness were considered and two truck types #5 and #6 were added (table 4.5). The parameters for each suspension, listed in Table 4.6 include:

- Original stiffness for truck #1 with very high stiffness.
- HS20–44 truck suspension stiffness. The spring factors and damping coefficients are taken from the literature.
- Higher stiffness - truck #5 – The stiffness is a value between the HS20-44 suspension and the very stiff suspension.
- The highest stiffness – truck #6 – The suspension is very stiff and the springs can be treated as rigid bodies.

However, for case #19, #25 and #31, softer springs than the original suspension were used in line with what newer cranes have.

Tables 5.2, 5.3 and 5.4 present the case matrix for calculations. The FE Model of the bridge #4 was excluded from further analysis. This model, already completed, can be used in future calculation, if needed. Additionally, for the truck #1 the loading was modified. Based on the recorded video from the field test it was found that the dynamic effect was amplified by the concrete blocks jumping up and down during the crossing of the bridge. This bouncing (hammering) effect was included in the calculations for the truck #1.

Table 5.2. Eight cases with speed 35 mph selected for two actual bridges and four trucks.

SPEED V=35mph	Truck #1 (FDOT truck) 71.7 Kips Original suspension	Truck #2 (crane 1080/1L) 89.7 Kips HS20-44 suspension	Truck #3 (truck #2 + 5 Kips) 94.7 Kips HS20-44 suspension	Truck #4 (truck #2 + 10 Kips) 99.7 Kips HS20-44 suspension
Bridge #1 (21.7m)	Case 1	Case 2	Case 3	Case 4
Bridge #3 (19.26 m)	Case 5	Case 6	Case 7	Case 8

Table 5.3. Six cases with speed 45 mph for bridge #1.

SPEED V=45mph	Truck #1 (FDOT truck) 71.7 Kips Original suspension	Truck #2 (crane 1080/1L) 89.7 Kips HS20-44 suspension	Truck #3 (truck #2 + 5 Kips) 94.7 Kips HS20-44 suspension	Truck #4 (truck #2 + 10 Kips) 99.7 Kips HS20-44 suspension	Truck #5 (truck #2 with higher stiffness	Truck #6 (truck #2 with very high stiffness)
Bridge #1 (21.7m)	Case 9	Case 10	Case 11	Case 12	Case 13	Case 14

Table 5.4. Eighteen cases with speed 55 mph for three bridges.

SPEED V=55mph	Truck #1 (FDOT truck) 71.7 Kips Original suspension	Truck #2 (crane 1080/1L) 89.7 Kips HS20-44 suspension	Truck #3 (truck #2 + 5 Kips) 94.7 Kips HS20-44 suspension	Truck #4 (truck #2 + 10 Kips) 99.7 Kips HS20-44 suspension	Truck #5 (truck #2 with softer stiffness	Truck #6 (truck #2 with very high stiffness)
Bridge #1 (21.7m)	Case 15	Case 16	Case 17	Case 18	Case 19	Case 20
Bridge #2 (25.7m)	Case 21	Case 22	Case 23	Case 24	Case 25	Case 26
Bridge #3 (19.26m)	Case 27	Case 28	Case 29	Case 30	Case 31	Case 32

Each case is defined by the selected vehicle-bridge configuration and the specific speed. In each case a run of one truck through the center of the traffic lane was simulated as a most representative situation for the impact factor estimation. As an example, Figure 5.1 shows the view of truck #1 running with 55mph through bridge #1, as specified for case #15.

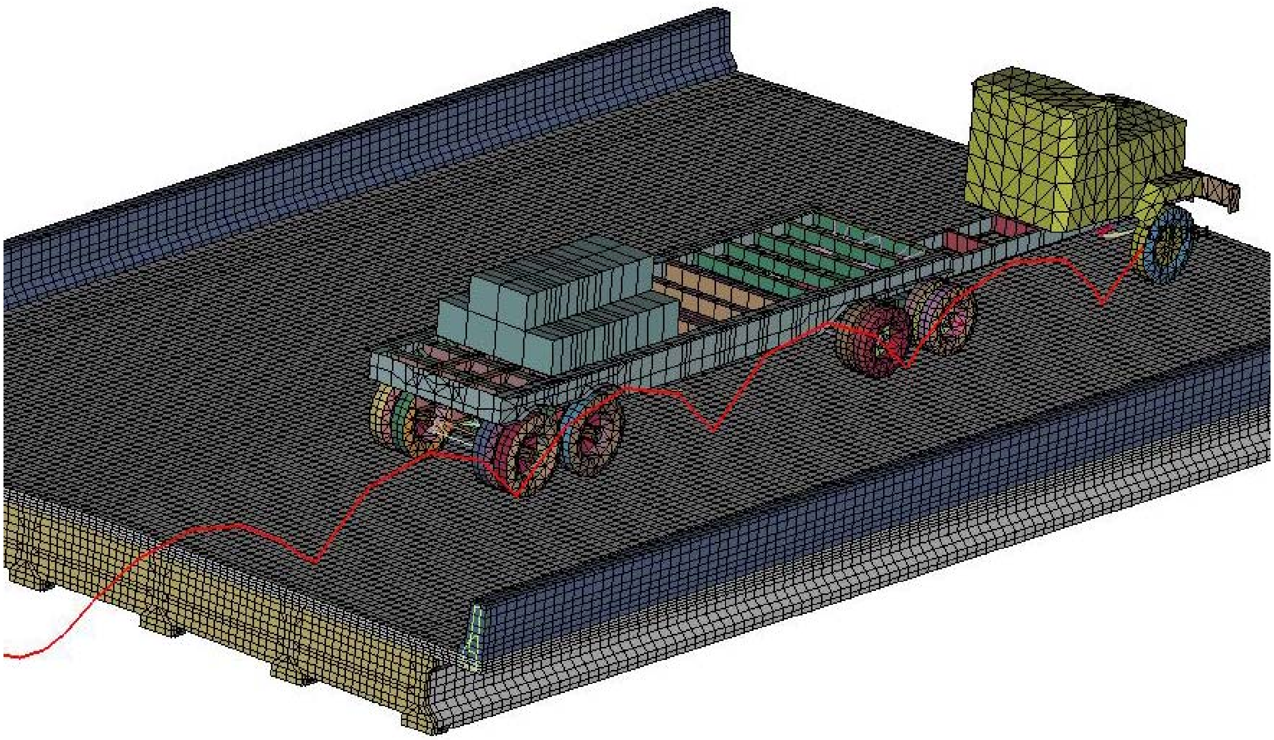

Figure 5.1. View of truck #1 running with 55 mph through bridge #1.

5.2. Summary of numerical results

The results of calculations for each case described in Tables 5.2, 5.3, and 5.4 are presented in the separate sections of Appendix B: Numerical Results. FE simulation provides a lot of data representing mechanical properties (displacement, velocity, acceleration, stress, strain) at any location of the models at any selected moment. Data presented in Appendix B is limited to the quantities at the bottom of each girder in the middle of the span, which are practically used for the calculation of the impact factors (see equation 3.3). In Appendix B, for each case, the presented data includes the time histories of micro strains in all girders, the time histories of stresses, the comparison of maximum static and dynamic strains, as well as the impact factors.

Tables 5.5, 5.6, and 5.7 list the calculated values of the representative impact factors for all cases. These values correspond to the maximum dynamic strain and are determined using the procedure described in Section 3.6.

.

Table 5.5. Calculated impact factors for cases with a speed of 35 mph.

SPEED V=35mph	Truck #1 (FDOT truck) 71.7 Kips Original suspension	Truck #2 (crane 1080/1L) 89.7 Kips HS20-44 suspension	Truck #3 (truck #2 + 5 Kips) 94.7 Kips HS20-44 suspension	Truck #4 (truck #2 + 10 Kips) 99.7 Kips HS20-44 suspension
Bridge #1 (21.7m)	23.7% threshold load bouncing	10.6% No threshold No bouncing	7.0% No threshold No bouncing	2.7% No threshold No bouncing
Bridge #3 (19.26 m)	25.9% threshold load bouncing	11.0% No threshold No bouncing	7.2% No threshold No bouncing	3.7% No threshold No bouncing

Table 5.6. Calculated impact factors for cases with a speed of 45 mph.

SPEED V=45mph	Truck #1 (FDOT truck) 71.7 Kips Original suspension	Truck #2 (crane 1080/1L) 89.7 Kips HS20-44 suspension	Truck #3 (truck #2 + 5 Kips) 94.7 Kips HS20-44 suspension	Truck #4 (truck #2 + 10 Kips) 99.7 Kips HS20-44 suspension	Truck #5 (truck #2 with Higher stiffness)	Truck #6 (truck #2 with very high stiffness)
Bridge #1 (21.7m)	34.8% threshold load bouncing	11.3% No threshold No bouncing	8.3% No threshold No bouncing	2.9% No threshold No bouncing	11.9% No threshold No bouncing	7.6% No threshold No bouncing

Table 5.7. Calculated impact factors for cases with a speed of 55 mph.

SPEED V=55mph	Truck #1 (FDOT truck) 71.7 Kips Original suspension	Truck #2 (crane 1080/1L) 89.7 Kips HS20-44 suspension	Truck #3 (truck #2 + 5 Kips) 94.7 Kips HS20-44 suspension	Truck #4 (truck #2 + 10 Kips) 99.7 Kips HS20-44 suspension	Truck #5 (truck #2 with softer stiffness)	Truck #6 (truck #2 with very high stiffness)
Bridge #1 (21.7m)	60.2% threshold load bouncing	12.7% No threshold No bouncing	10.1% No threshold No bouncing	3.5% No threshold No bouncing	11.1% No threshold No bouncing	8.9% No threshold No bouncing
Bridge #2 (25.7 m)	51.4% threshold load bouncing	7.9% No threshold No bouncing	6.2% No threshold No bouncing	3.0% No threshold No bouncing	6.5% No threshold No bouncing	6.3% No threshold No bouncing
Bridge #3 (19.26 m)	85.0% threshold load bouncing	15.3% No threshold No bouncing	11.5% No threshold No bouncing	4.2% No threshold No bouncing	13.6% No threshold No bouncing	12.9% No threshold No bouncing

In the subsequent sections the variation of the impact factor due to different parameters is discussed. Displayed diagrams show some tendencies and help to extrapolate received results to other vehicle-bridge cases. Solid lines depict interpolated relations, related to values within the range of calculated results. Dotted lines indicate expected tendencies extrapolated from the calculated values of the impact factor. Diagrams presented below are received using very limited data. To more precisely represent relations between the impact factor and selected parameters, more cases should be considered, especially for the extrapolated (dotted) segments of the curves. All results presented in this chapter were received based on the assumption that all road surfaces are in good condition.

5.3. Effect of truck speed

Diagrams in Figures 5.2 and 5.3 show the dependence of the impact factor on speed for bridges #1 and #3 and for three trucks #2, #3, and #4. Figure 5.4 presents results for two bridges #1 and #3 and the truck #1 with the load bouncing effect. The results show that heavier vehicles lead to smaller impact factors (see Section 5.4). For the trucks #2, #3, and #4, for which bouncing effect is not included, the impact factor grows linearly when the speed increases [43]. For the truck #1 (Figure 5.4) the relation seems to be nonlinear as a result of the hammering effect caused by the bouncing of loading. The impact factor increases rapidly when the speed is above 50mph and is much higher than the value predicted by the AASHTO code.

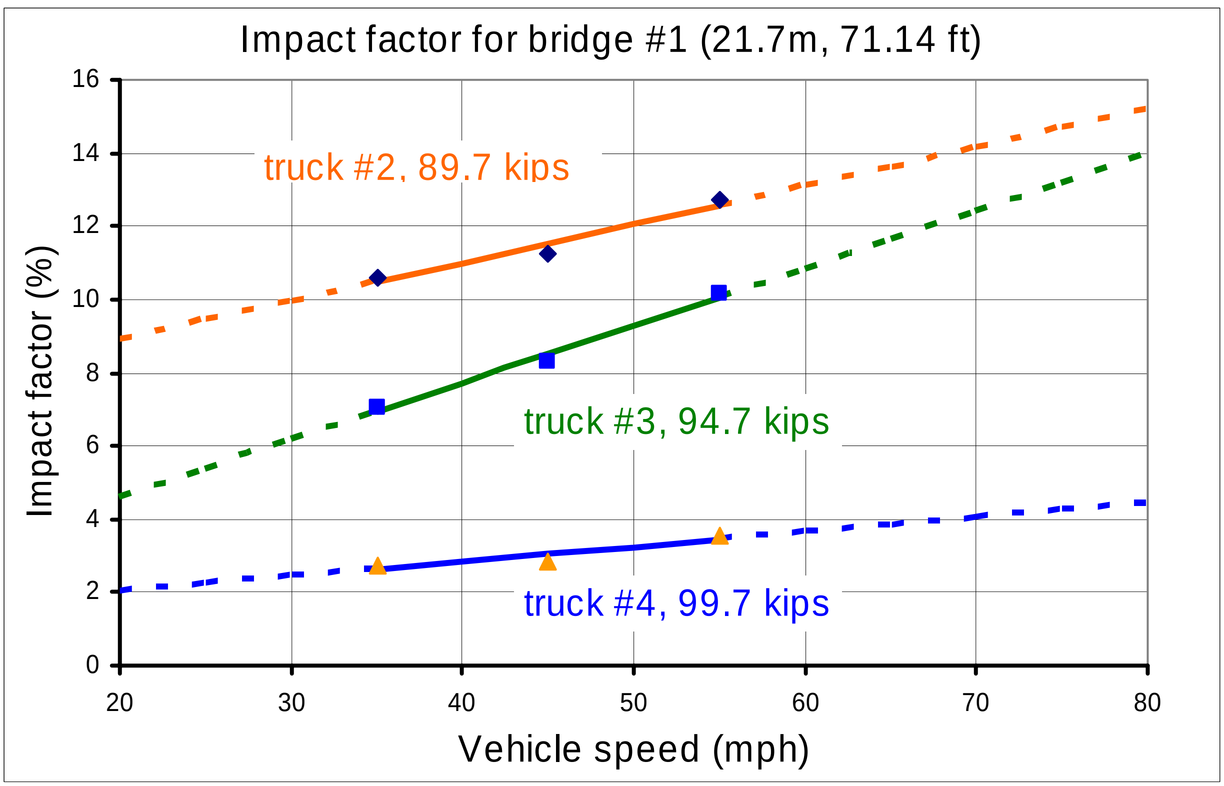

Figure 5.2. Dependence of impact factor on speed for bridge #1.

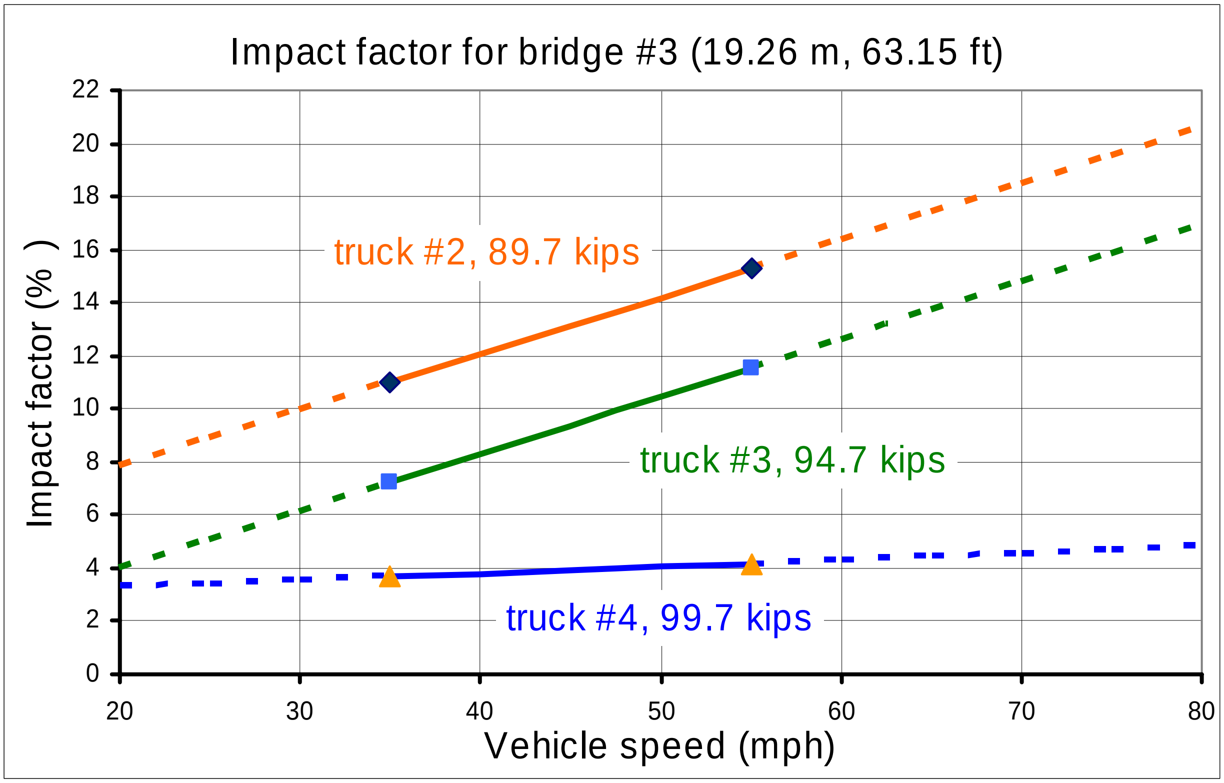

Figure 5.3. Dependence of impact factor on speed for bridge #3.

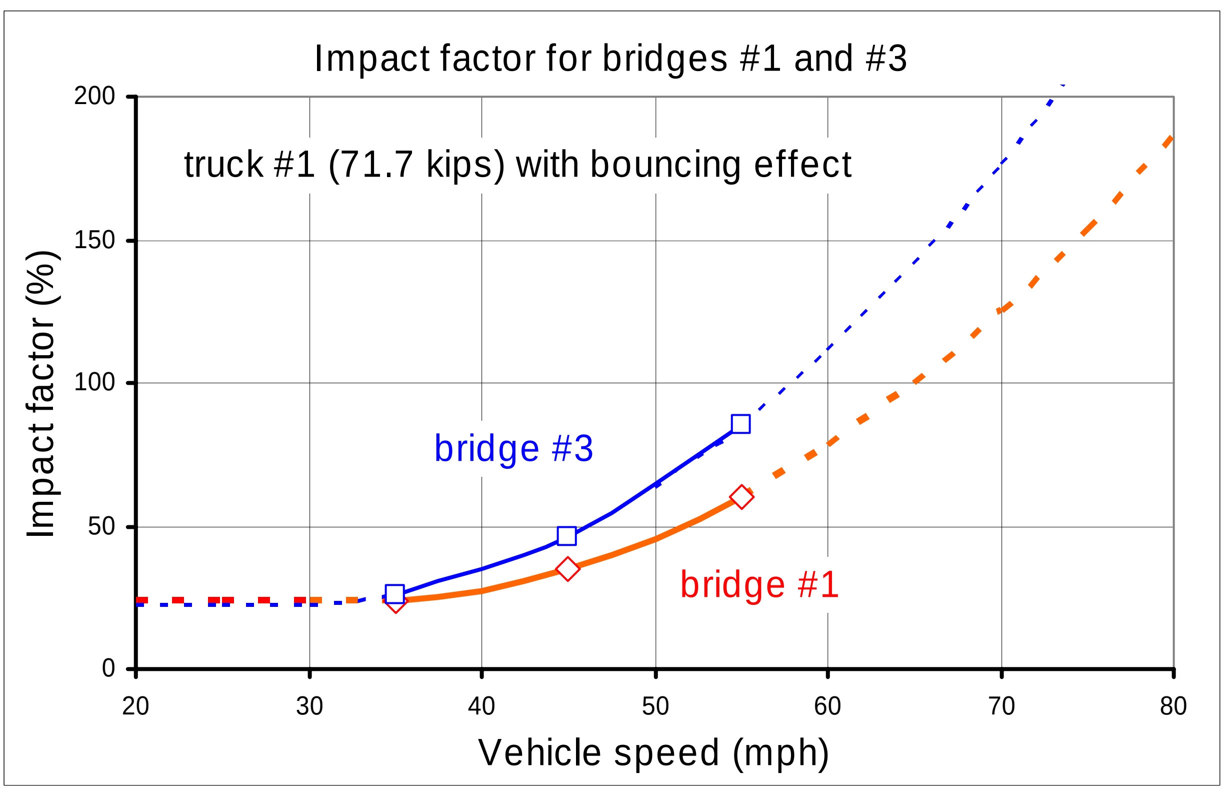

Figure 5.4. Dependence of impact factor on speed for bridges #1 and #3.

5.4. Effect of truck weight

The next three diagrams in Figures 5.5, 5.6, and 5.7 give the variation of the impact factor for three bridges with varying vehicle weight. All three diagrams show that the impact factor increases as the vehicle weight decreases. This tendency is well known and it is due to the fact that growing vehicle weight causes smaller increments of the dynamic strain component compared to the static strain. Figure 5.8 shows analogous results presented in [24], where authors investigated a variation of the impact factors for moments and shear forces in girders based on their own calculations. Although values received in [24] are much higher, the tendency is similar to what is presented in Figures 5.5, 5.6, and 5.7.

The relation between the impact factor and the vehicle weight is dependant upon other parameters such as the vehicle speed. The results given in Figure 5.5 were calculated for three different speeds of 35, 45, and 55 mph. Figure 5.6 shows only results for a speed of 55 mph and Figure 5.7 for two speeds, 35 and 55 mph. For the cranes of interest, the AASHTO code overestimates the impact factor.

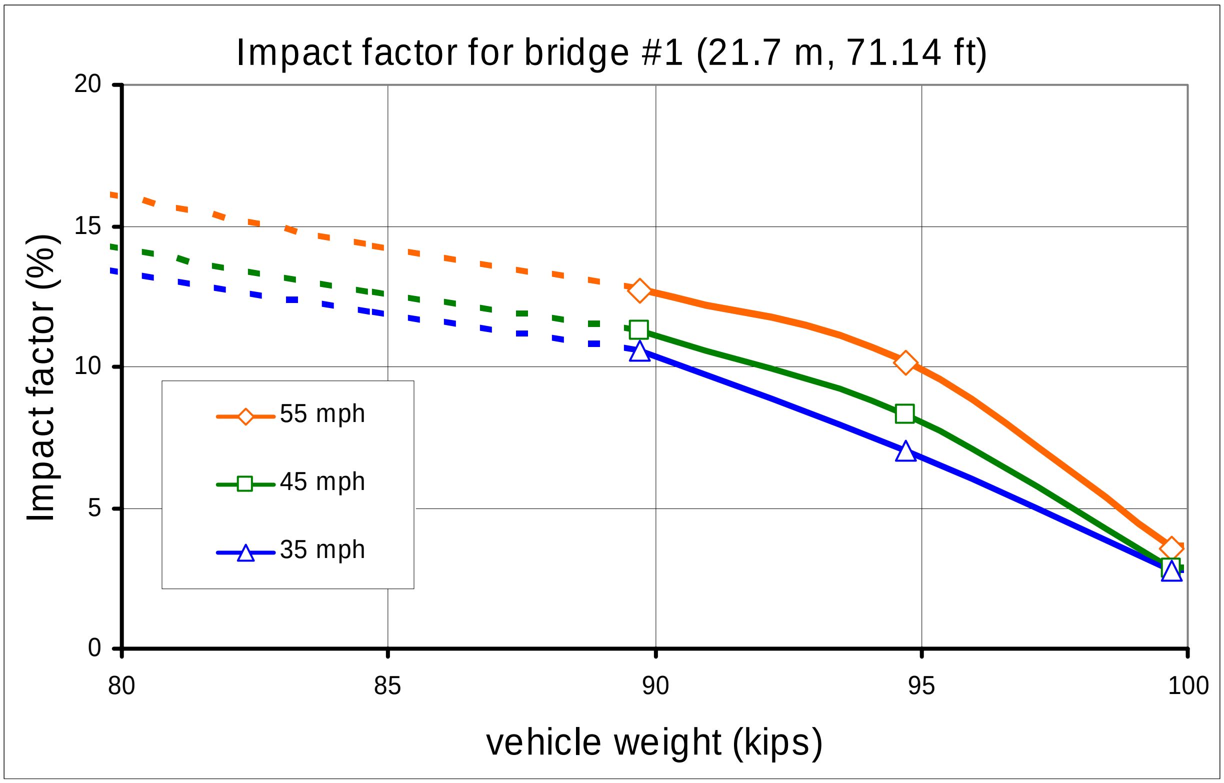

Figure 5.5. Dependence of impact factor on truck weight for bridge #1.

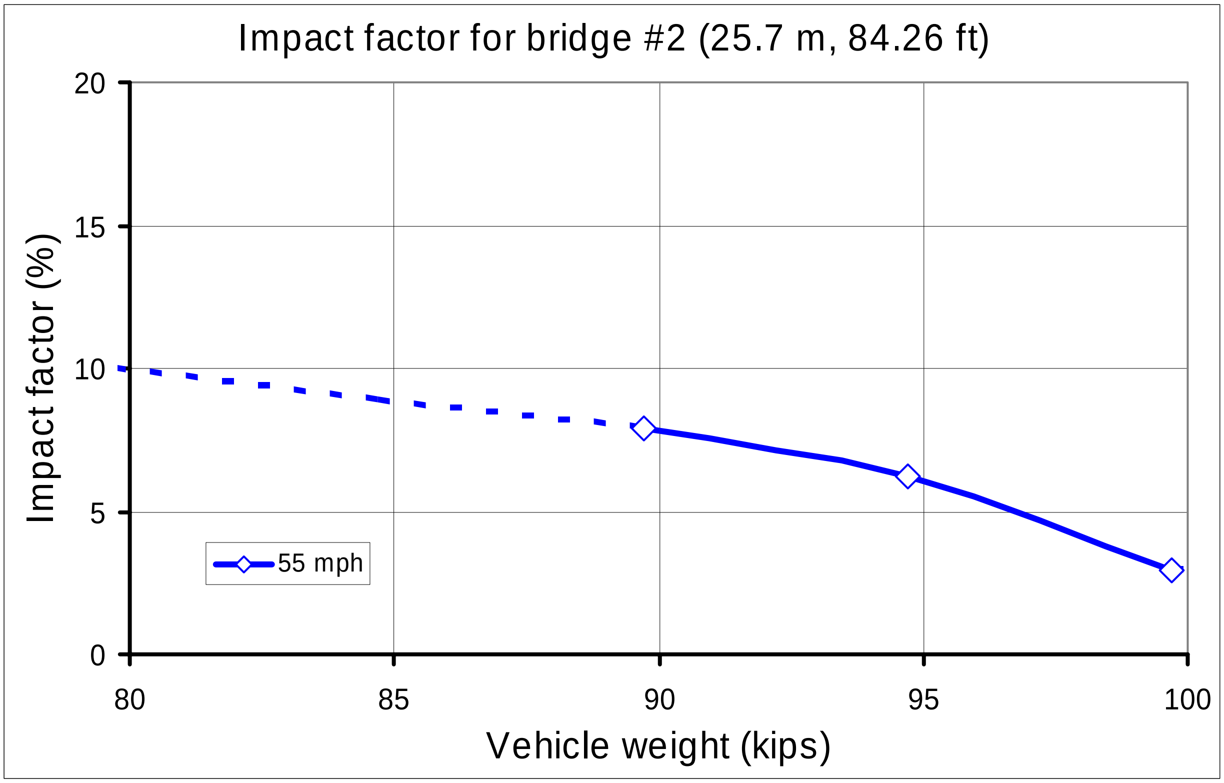

Figure 5.6. Dependence of impact factor on truck weight for bridge #2.

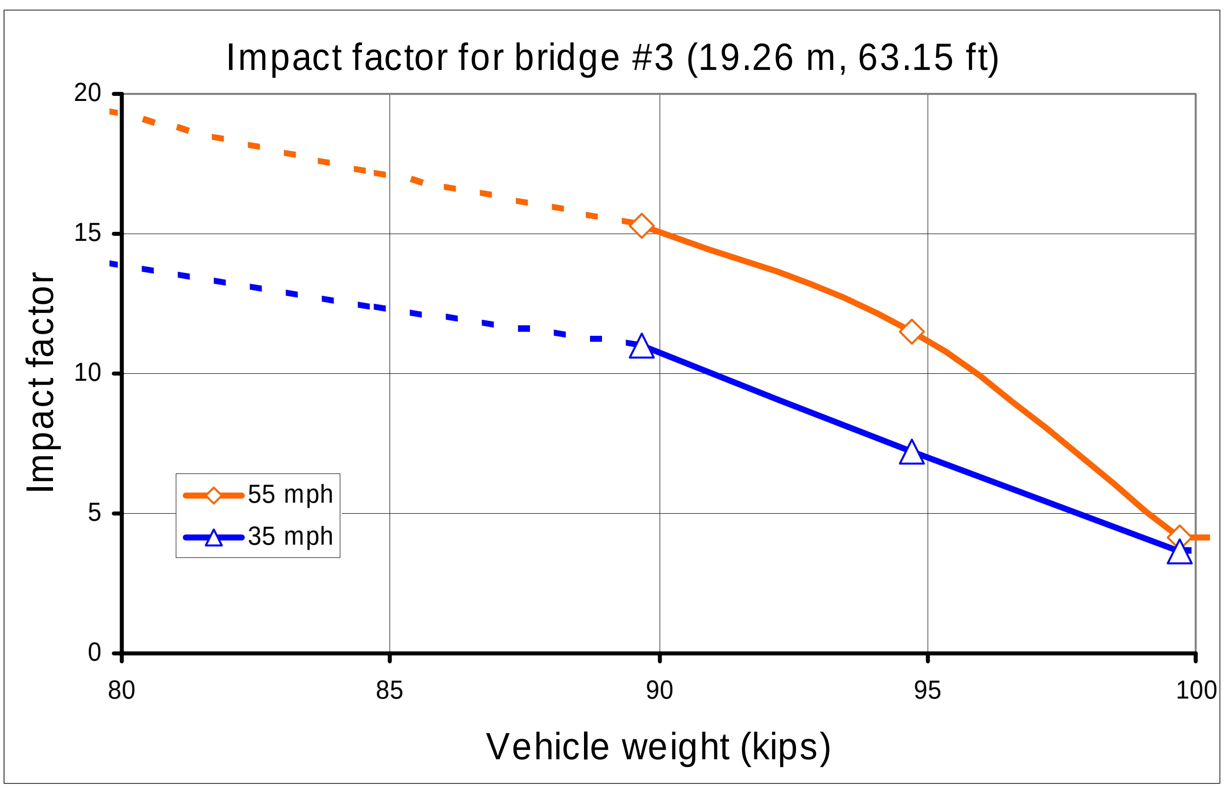

Figure 5.7. Dependence of impact factor on truck weight for bridge #3.

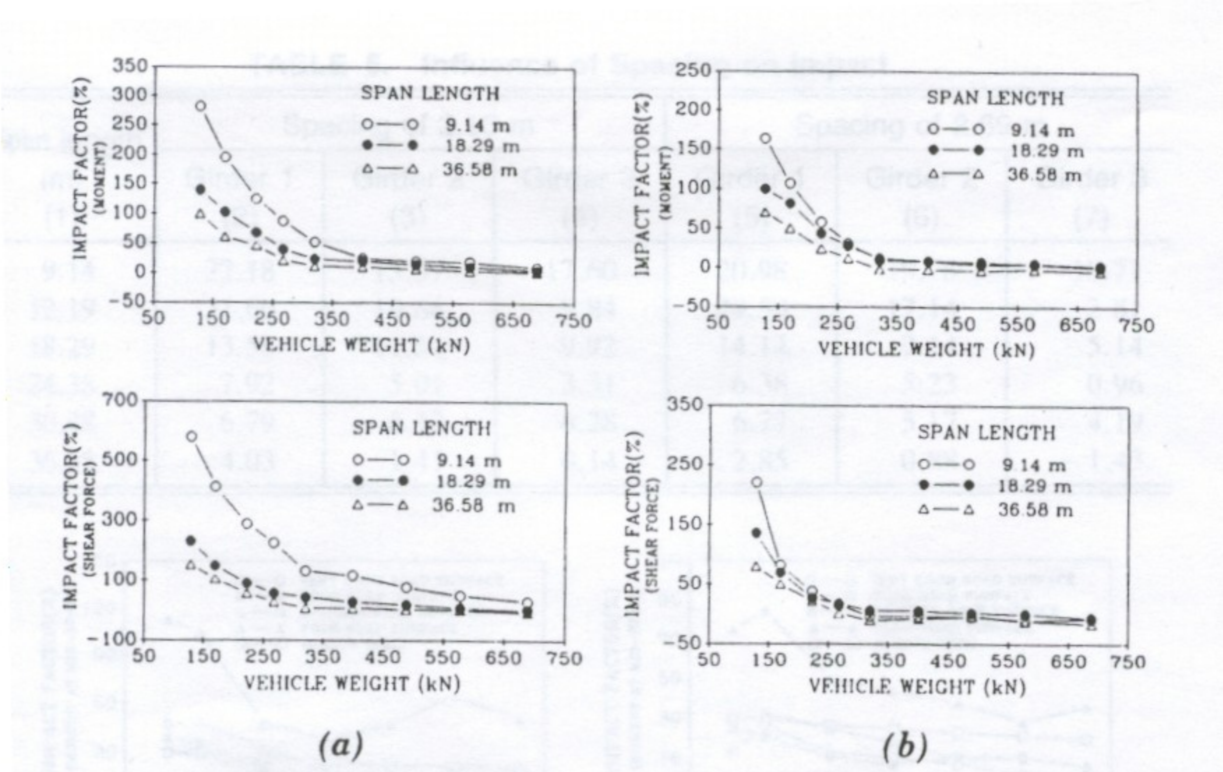

Figure 5.8. Effect of vehicle weight on impact factor [24].

5.5. Effect of bridge length

Bridge length is another important parameter that influences the impact factor. Figures 5.9 and 5.10 show relationships between the impact factor and the bridge length for different trucks and different speeds. As expected, with an increase of bridge length, the impact factors decrease gradually. For middle and long span bridges (longer than 20m), the impact factor due to heavy cranes is distinctly lower than that predicted by AASHTO code, provided that the road surface is in good condition. A curve named “AASHTO code” was added for comparison. It shows results calculated using the following AASHTO formula [1]:

$$IM = \frac{15.24}{L + 38.1} \times 100\% \tag{5.1}$$

Where L is the loaded length in meters. IM is not greater than 0.3.

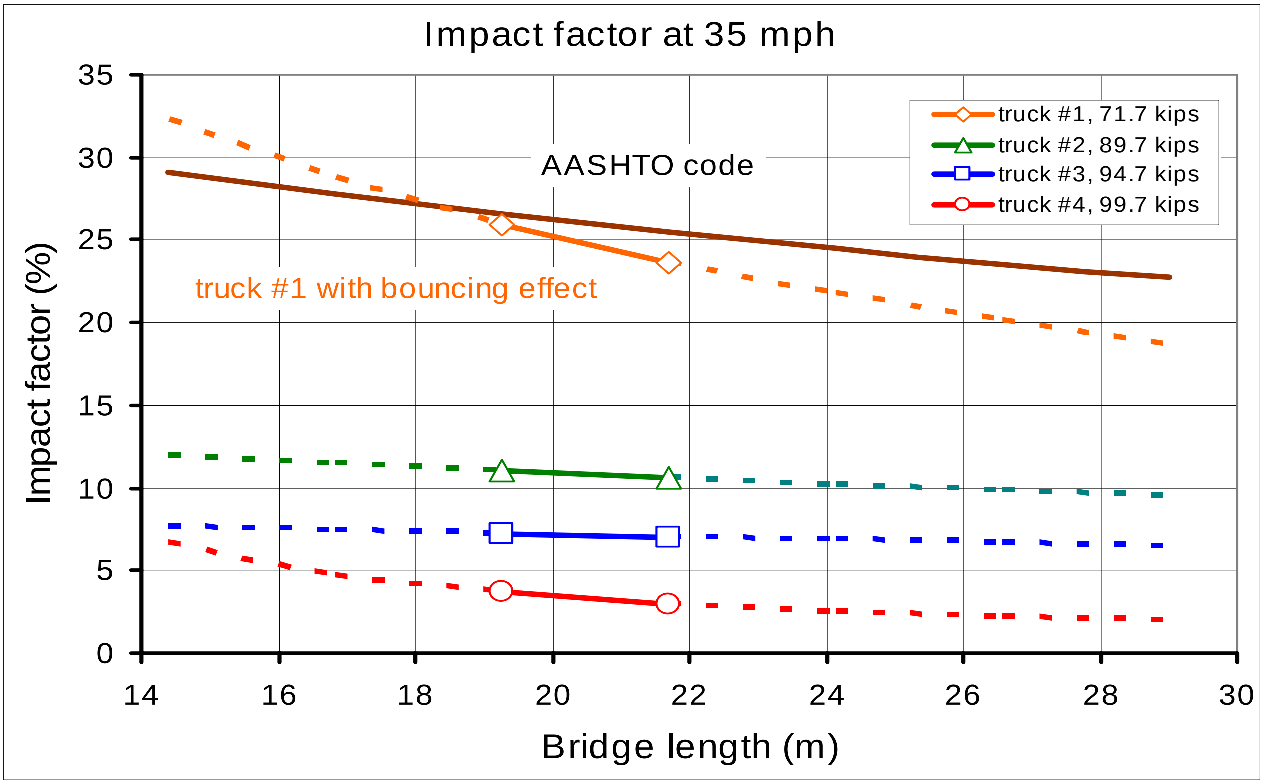

Figure 5.9. Dependence of impact factor on bridge length at truck speed of 35 mph.

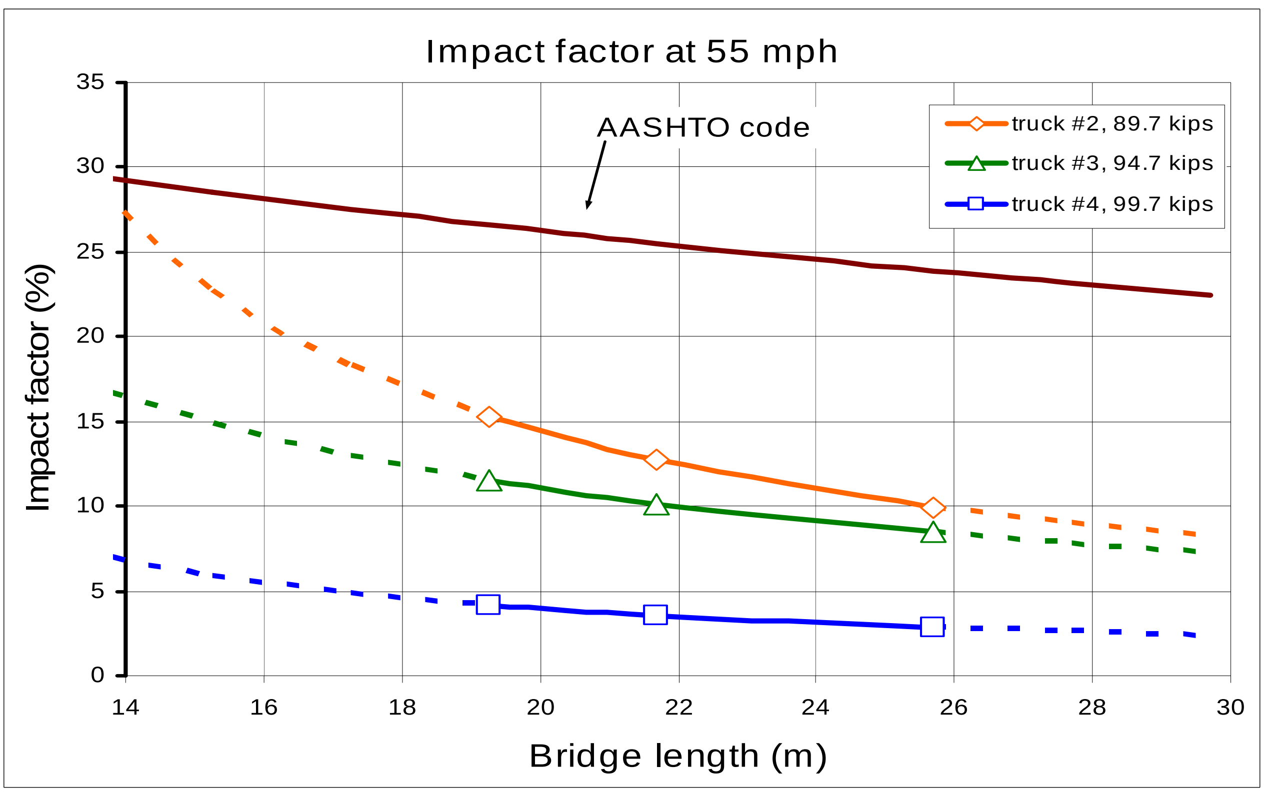

Figure 5.10. Dependence of impact factor on bridge length at truck speed of 55 mph.

5.6. Effect of suspension stiffness

Figures 5.11 and 5.12 show values of the impact factor for different suspension stiffnesses. The abscissa in the Figures is the ratio of the truck (crane) stiffness to HS20-44 suspension stiffness in which the spring factor is taken as $8x10^6$ N/m.

Due to the limited data, it is difficult to interpolate the results into the cases corresponding to the trucks with other suspension properties. It must also be pointed out that the truck suspension system is usually complex and dependent on many parameters describing the stiffness and damping properties.

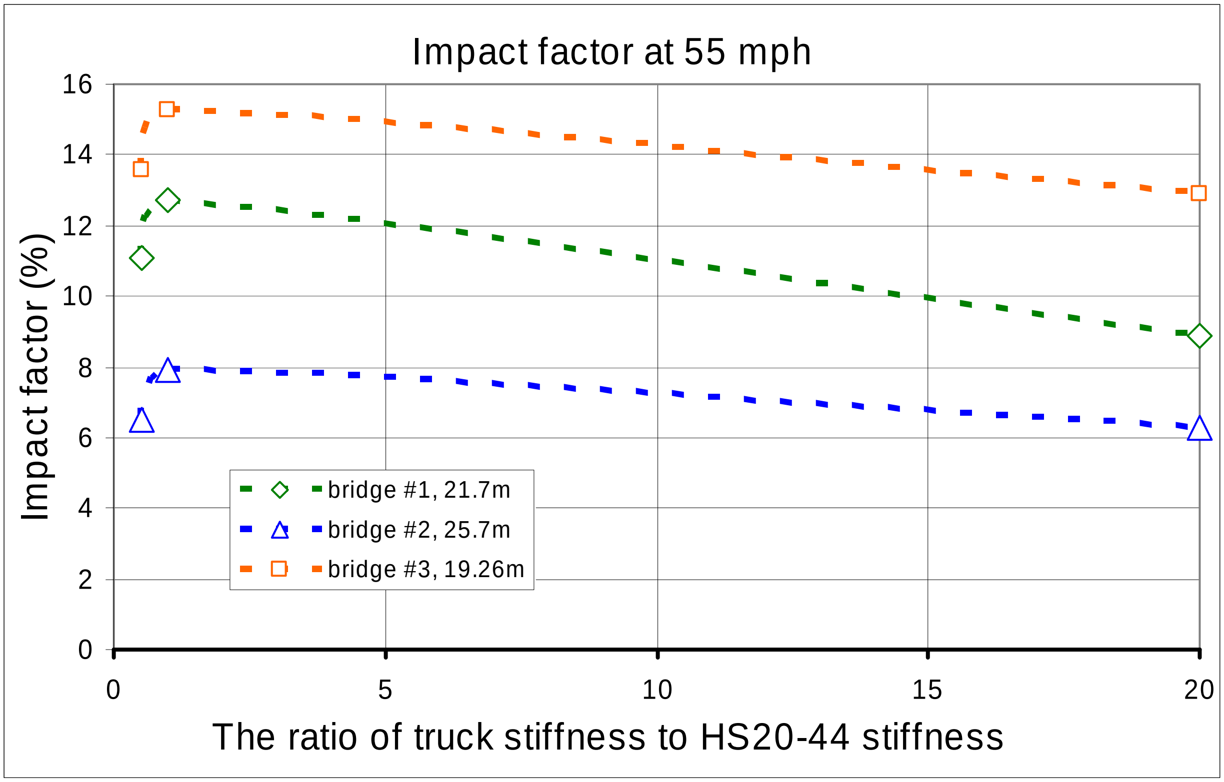

Figure 5.11. Dependence of impact factor on suspension stiffness at 55 mph.

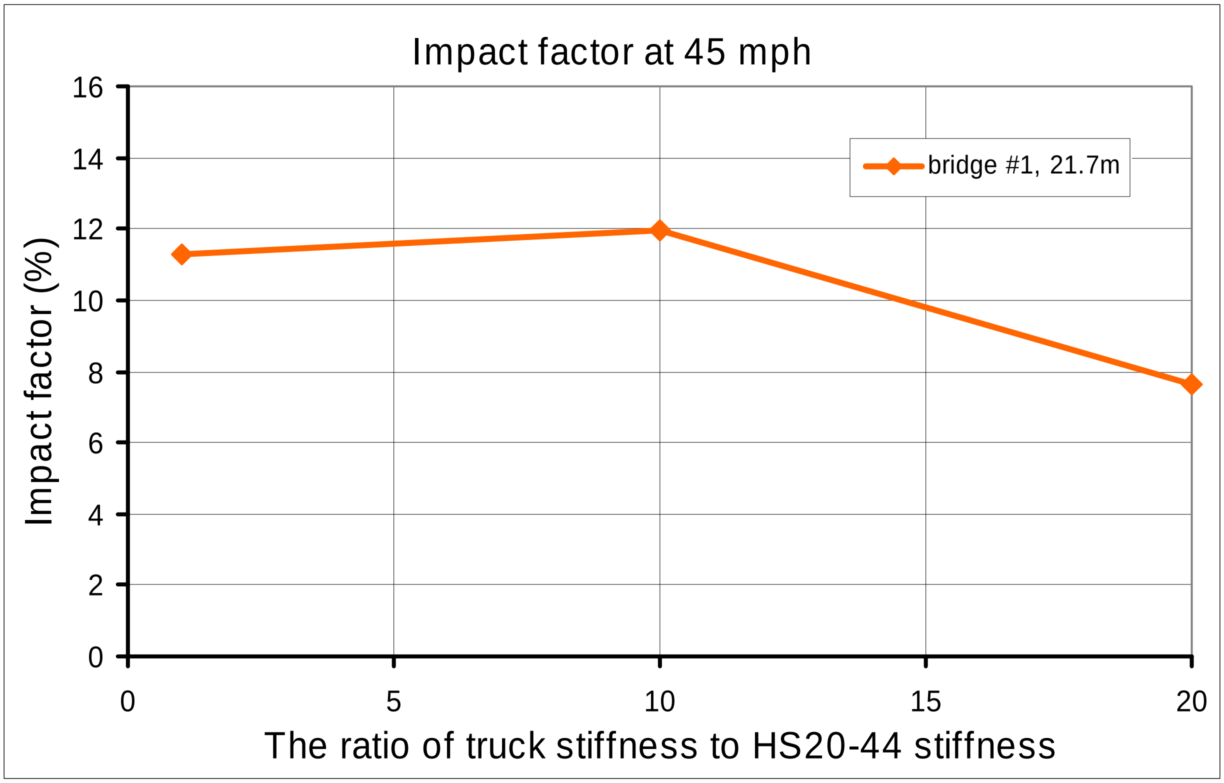

Figure 5.12. Dependence of impact factor on suspension stiffness at 45 mph.

6. SUMMARY AND CONCLUSIONS

6.1. Summary of the results

Dynamic effects in bridges due to moving vehicles may be attributed to the three major sources as it is presented schematically in Figure 6.1:

1. pure motion of constant reaction forces exerted by a vehicle along a perfectly smooth bridge surface,
2. change in time of reactions due to interaction in the wheel suspension assembly, and
3. impact forces exerted by the wheels on the bridge and triggered by road surface imperfections and discontinuities (hammering effect).

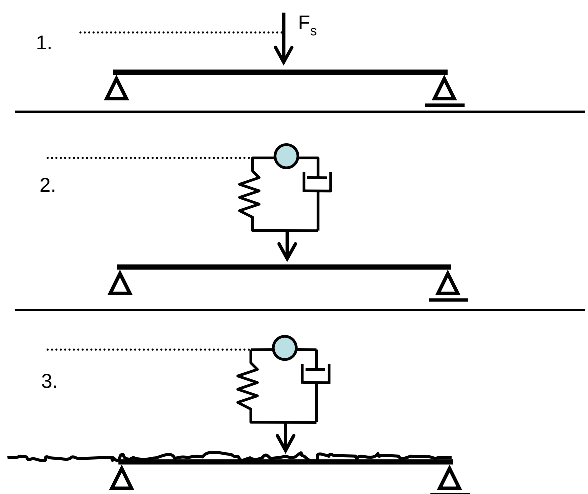

Figure 6.1. Schematic representation of wheel forces.

All three effects are combined at the same time resulting in a complex dynamic loading of the bridge. The first source alone has a negligible effect on the bridge response since even the highest practical vehicle velocities are much lower than the theoretical values of critical velocities [37] causing extensive vibration.

The second phenomenon is related to the characteristics of a vehicle suspension and vehicle velocity. Its effect on the bridge dynamic response depends on bridge characteristics such as a span length, number of girders and position of the loading vehicle. This factor is dominant when the road surface is in good condition and the hammering effect (third factor) is not present. Continuous variation of reactions in time affects the impact factor in a predictable way which can be evaluated by the consideration of numerous vehicle – bridge cases with different values of affecting parameters.

The most significant dynamic effects expressed by the impact factor come from the third cause: impact forces induced by geometric surface imperfections.

Both the vehicle and bridge can be described by several parameters which affect the wheel reactions or the bridge response. Based on both experimental and numerical results, several variables were determined to have an influence on the dynamic effects of the investigated vehicle – bridge interaction. They are listed in Table 6.1 and can be divided into two groups: one related to vehicles and one to bridges.

Table 6.1. Parameters affecting vehicle bridge interaction.

Vehicle	Bridge
V1. speed	B1. road surface condition
V2. weight	B2. number of girders (deck width)
V3. suspension parameters	B3. span length
V4. trucks position on bridge lanes	

Parameters V1, V2, V3, and B1 affect the cause of vibrations (i.e. the wheel reactions). The rest of parameters, V4, B2, and B3 are related to the bridge response. Some of the parameters like vehicle speed and weight or bridge length and number of girders can be easily expressed by numerical values. Suspension parameters and especially road surface condition are difficult to validate and assess numerically.

The parameter B1 (road surface condition) is difficult to evaluate and express by numerical values due to a wide variety of types of road surface imperfections. Moreover, it is also difficult to predict future changes of the road surface conditions. Road surface discontinuities, causing additional impact forces in vehicle-bridge interaction, include approach thresholds, deck joints, cracks, potholes, and delaminations. In addition, approach depression may have some magnifying effect. Severe road surface imperfections were represented by a plank in the field test and in numerical calculations. Impact factors exceeding design values (see Section 3.6) were obtained especially for high vehicle speed when additional bouncing effect of loading was induced. All numerical results for the 32 cases considered (see Section 5.1) were obtained for the bridge model without a plank. It should be remembered that conclusions drawn from this study are limited to the bridges with smooth road surface conditions only.

Suspension parameters of vehicles are difficult to evaluate because of the wide variety of heavy trucks. In addition, there is lack of information about the dynamic properties of actual suspension systems which could be used to establish stiffness and damping properties of one-dimensional springs and dampers representing complex suspension systems in the simplified FE model. This problem describes an area where further research should be continued and improvements are expected. Some ideas for experimental evaluation of dynamic suspension properties are presented in Section 6.3.

The numerical results presented in the preceding chapter were used to develop diagrams expressing relations between the impact factor and changing values of some parameters listed in Table 6.1. Dotted lines were obtained using linear extrapolation of the calculated results. These lines depict the area where additional vehicle – bridge cases should be calculated and further investigation performed to correctly predict the estimated trends. Presented diagrams with calculated quantities of impact factors can be used to evaluate the permissible limits for overload vehicles and serve as a helpful tool in the decision making process.

Diagrams presented in Chapter 5 confirm the following tendencies in variation of the impact factor:

- The impact factor increases when truck speed increases.
- With increase of the truck weight the impact factor decreases.

- o Increase of the span length is associated with gradual decrease of the impact factor.

6.2. Practical recommendations

Several conclusions can be drawn from experimental data and computational mechanics analysis. We suggest including the following recommendations in the process of issuing overweight permits:

1. Speed reduction. As shown in Section 3.6, higher vehicle speed can induce bouncing of loading initiated by even small road surface imperfections (as 15 mm deep approach threshold). Speed reduction for overloaded vehicles crossing a bridge can almost completely eliminate dynamic effects. We suggest including a recommendation to reduce speed to 35 mph in some permits for crossing over problematic bridges. The vehicle speed should be reduced before approaching a bridge.
2. Restrict driving to the right traffic lane. Field test for the bridge #500133 showed that in some cases dynamic stresses in girders can be larger if a vehicle is crossing the bridge along the center of the deck. It appears to be safer if the vehicle does not change the traffic lane on the bridge. This requirement should be included in the permit.
3. Evaluation of the road surface condition. Road surface condition is a critical factor affecting dynamic loading of the bridge. This factor cannot be evaluated without visual inspection and therefore cannot be considered in an everyday decision making process. However, it should be emphasized in the maintenance practice. Inexpensive maintenance tasks including elimination of bridge deck thresholds and bridge approach depressions are very cost effective and will significantly reduce actual dynamic impact factors.

The most practical, although incomplete data obtained in this research is presented in Section 5.2, where impact factors for different vehicle – bridge configurations are graphically summarized. This data can be extrapolated to include additional vehicle and bridge configurations. Suggestions for further research are presented in the next section.

6.3. Suggestions for further research

Three major sources of dynamic loading of bridges were listed and discussed in Section 6.1 of this report. Since motion of the trucks on idealized FE models of the bridges was described very well using almost ½ million finite elements in 32 bridge-vehicle configurations, no further refinement seems to be desirable nor cost effective. However, more efforts are needed in the other two areas, as listed in Section 6.1:

1. Detailed knowledge of actual loading exerted by truck wheels on Florida bridges. This information would include reactions under each wheel as a function of time, truck loading and suspension system, and
2. Detailed knowledge of bridge surface imperfections and their influence on dynamic loading. These imperfections include: common bridge approach depressions and deck thresholds, expansion joints, delaminations, discontinuities, pot holes and common trash (often idealized by a standard piece of wood) on the bridge deck.

Extensive validation, presented in Sections 4.7 and 4.8, shows that our detailed FE models of bridges can accurately predict the behavior of actual structures. Validation of FE models of heavy vehicles indicates potential for further improvements. Some advanced features of truck models developed in this research make them unique for analysis of vehicle – bridge interaction (Chapter 2). These include three dimensional models of wheels with rotation, tires modeled with two layers representing rubber and cord, application of internal pressure in tires, and usage of complex contact algorithms. Also three dimensional structures built of rigid elements, springs and dampers can potentially well represent vehicle suspension systems. However, reliability of these models depends on the correct assessment of stiffness and damping properties of the special elements applied in the FE models. It is difficult to evaluate these values based only on regular technical specifications provided by auto manufacturers.

Experimental procedure to assess actual dynamic reactions from the wheels should be included in overall data acquisition to further improve FE models of heavy vehicles in future research. The basic concept, consisting of two steps, is presented in Figure 6.2. In the first step a precise continuous measurement of distant ***d*** (Figure 6.2) is conducted and recorded while the vehicle is crossing a bridge. Figure 6.2 shows the concept of how to attach measuring devices. One of more sophisticated laser devices available on the market could be used, maybe after some modifications regarding wireless connection with a data acquisition unit. Changes in distance ***d*** correspond to deflection of the tire. They are caused by dynamic reactions coming from the deck to the wheels. In the second step registered deformations of tiers will be combined with dynamic reactions through parallel measurement of the distant ***d*** and the wheel weight under static loading and unloading. For the measurement of wheel reactions, a portable wheel weigher scale like one presented in Figure 6.3 can be used. The relation between reaction and change of ***d*** will allow for recalculation of time histories of the distant ***d(t)*** into time histories of reactions ***R(t)***. In this method reactions are related only to deflection of tiers by comparison of static measurements and dynamic recordings. This means that only damping properties of the tire are ignored while stiffness and

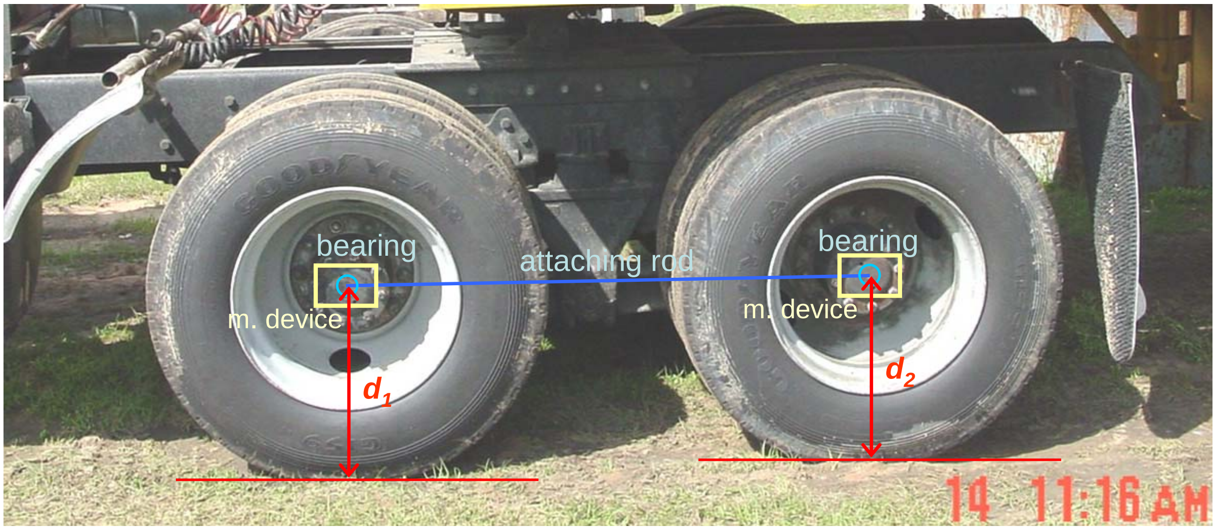

Figure 6.2. Setup for measurement of tire deformation.

damping properties of suspension systems are fully represented. This method has several advantages. First, it allows for numerous recordings of valuable data with different speed and loading configurations, for different road surface condition, and others. It does not require closure of traffic. The measurement indirectly gives time histories of resultant forces coming from wheels to the bridge deck. Collected data is straightforward and provides the magnitude of dynamic overloading. Impact factors for loading instead of bridge response can be calculated.

Figure 6.3. Portable wheel weigher scale.

Additionally, experimental time histories of reactions would allow for the simplification of FE models of heavy vehicles and at the same time consideration of more vehicle-bridge cases. The simplified FE truck models, well representing actual mass distribution and matching static reactions would additionally be loaded with changing in time forces, corresponding to dynamic increments of reactions. Such models would be simpler, without wheel rotation and complex suspension systems but at the same time would be more accurate. It is believed that improving truck models and increasing the number of vehicle – bridge cases, it will be possible to represent numerically all practical and important trends for impact factors of the Florida DOT bridges.

It is also proposed to focus future research on the bridge deck surface imperfections and the additional dynamic loading triggered by these imperfections. As an additional task, the depression of the east approach to the bridge #1 was surveyed. Elevations of this approach are shown in Figure 6.4. When combined with a 0.5 in threshold between asphalt and approach slab, this unexpected surface imperfection triggered additional dynamic load resulting in impact factor of 82.3% at 50 mph. This unintended and unexpected observation leads to a hypothesis that significant number of bridges in Florida may exhibit similar or even worse surface imperfections, some of which may produce additional, significant dynamic loading than others. More systematic approach and surveys of Florida bridge approach depressions and thresholds should be conducted. This research should also identify the most critical characteristics of surface imperfections, which trigger the biggest dynamic loading.

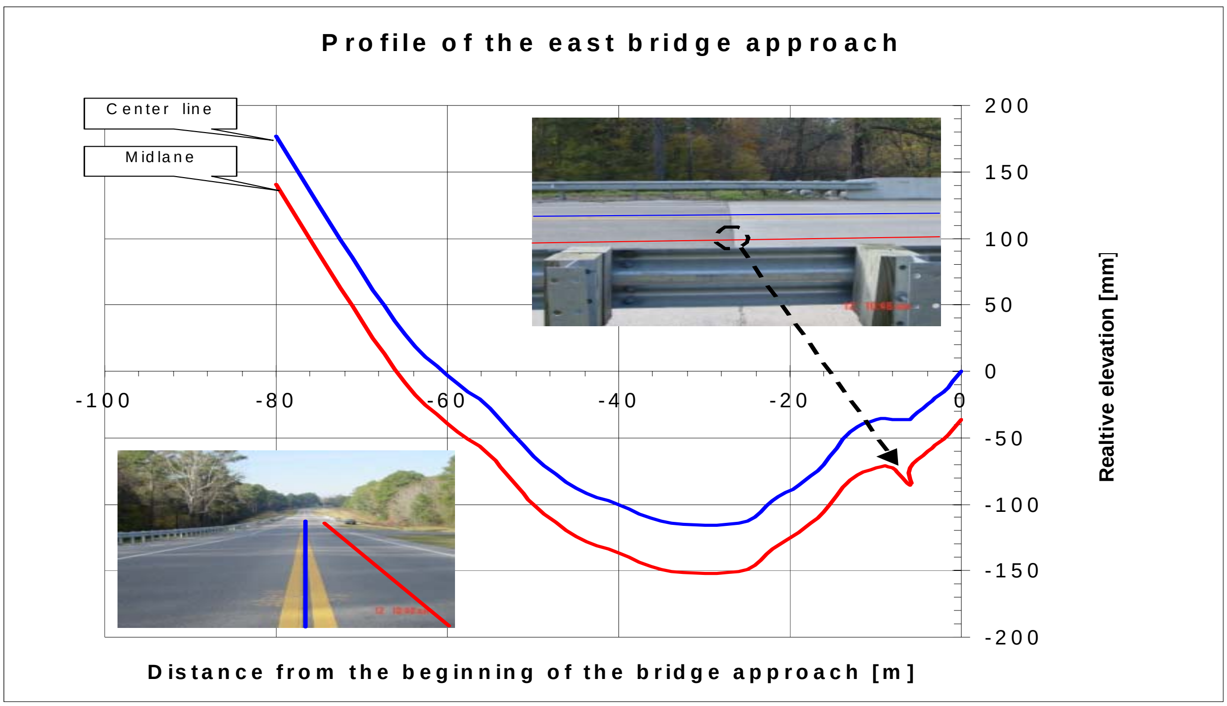

Figure 6.4. Relative elevations of the east approach to the bridge #1.

Reference

[1] AASHTO LRFD bridge design specifications. SI units, 1st edition, 1994.

[2] AASHTO Standard specifications for highway bridges. 17th edition, 2002.

[3] Alaylioglu H., Alaylioglu A., Dynamic structural assessment of a highway bridge via hybrid FE model and in situ testing, *Computers and Structures*, Vol. 63, No. 3, pp 439-453, 1997.

[4] Baumgaertner W., Bridge-truck interaction: simulation, measurements and load identification.

[5] Belytschko T., Liu W. K., Moran B., *Nonlinear Finite Elements for Continua and Structures*, John Wiley & Sons, LTD, Chichester, England, 2000.

[6] Bergmeister K., Santa U., Global monitoring concept for bridges, *Proceedings of SPIE*, Vol. 3995, pp. 14-25, 2000.

[7] Brady S.P., Gonzalez A., Znidaric A., O'Brien E.J., Impact factors on medium span bridges due to multiple vehicle presence, *7Th international symposium on heavy vehicle weight & dimensions*, Delft, The Netherlands, June 16-20, 2002.

[8] Brownjohn J. M.W., Lee J., Cheong B., Dynamic performance of a curved cable-stayed bridge, *Engineering Structures*, Vol. 21, pp. 1015-1027, 1999.

[9] Chan T.H.T., Law S.S., Yung T.H., Moving force identification using an existing prestressed concrete bridge, *Engineering Structures*, Vol. 22, pp.1261-1270, 2000.

[10] Cheng Y. S., Au F. T. K., Cheung Y. K. & Zheng D. Y., On the separation between moving vehicles and bridge, *Journal of Sound and Vibration*, Vol. 222(5), pp 781-801,1999.

[11] Chompooming K. & Yener M., The influence of roadway surface irregularities and vehicle deceleration on bridge dynamics using the method of lines, *Journal of Sound and Vibration*, Vol. 183(4), pp 567-589, 1995.

[12] Chopra A. K., Dynamics of Structures. Prentice Hall, Upper Saddle River, New Jersey, 2001.

[13] Chowdhury M. R., Ray J.C., Accelerometers for bridge load testing, *NDT&E International*, Vol. 36, pp.237-244, 2003.

[14] Clemente P., Marulo F., Lecce L. & Bifulco A., Experimental modal analysis of the Garigliano cable-stayed bridge, *Soil Dynamics and Earthquake Engineering*, Vol. 17, pp. 485-493, 1998.

[15] Das A., Dutta A. & Talukdar S., Efficient dynamic analysis of cable-stayed bridges under vehicular movement using space and time adaptivity, *Finite Elements in Analysis and Design*, Accepted February 9, 2003.

[16] Fafard M., & Bennur M., A general multi-axle vehicle model to study the bridge vehicle interaction, *Engineering Computations*, Vol. 14, No. 5, pp. 491-508, 1997.

[17] LRFD English Prestressed Beam Design, version 1.81, 2000.

[18] Green M.F., Cebon D., Dynamic interaction between heavy vehicles and bridges. *Computers & Structures*, Vol. 62, No.2, pp 253-264, 1997.

[19] Green M.F., Cebon D., Dynamic responses of highway bridges to heavy vehicle loads, theory and experimental validation, *Journal of Sound and Vibration*, Vol. 170(1), pp. 51-78, 1994.

[20] Guo W. H. & Xu Y. L., Fully computerized approach to study cable-stayed bridge vehicle interaction, *Journal of Sound and Vibration*, Vol. 248(4), pp 745-761, 2001.

[21] Hallquist, J.O., *LS-DYNA Theory Manual*, Livermore Software Technology Corporation, Livermore, CA, 1998.

[22] Hallquist, J.O., *LS-DYNA User's Manual*, *Nonlinear Dynamic Analysis of Structures in Three Dimensions*, Livermore Software Technology Corporation, Livermore, CA, 1999.

[23] Henchi K., Fafard M., Talbot M., Dhatt G. , An efficient algorithm for dynamic analysis of bridges under moving vehicles using a coupled modal and physical components approach, *Journal of Sound and Vibration*, Vol. 212(4), pp. 663-683, 1998.

[24] Huang D., Wang T-L., Shahawy M., Impact studies of multigirder concrete bridges, *Journal of Structural Engineering*, Vol. 119, pp 2387-2402, 1992.

[25] Huang D., Wang T-L., Shahawy M., Vibration of horizontally curved box girder bridges due to vehicles, *Computers & Structures*, Vol. 68, pp 513-528, 1998.

[26] Huber M. S., Bay J. A., Halling M. W., Womarc K. C., Use of velocity transducers in low-frequency modal testing of structures, *Proceedings of SPIE*, Vol. 3995, pp. 414-424, 2000. [2.16!]

[27] Lardies J. & Gouttebroze S. Indentification of modal parameters using wavelet transform, *International Journal of Mechanical Sciences*, Vol. 44, 2002, pp 263-2283.

[28] Li J.-Q., Leng X.-L. & Fang T., Evolutionary random response problem of a coupled vehicle-bridge system, *Archive of Applied Mathematics*, Vol. 72, pp 536-544, 2002.

[29] Marzougui D., Jin S., Livingston R. A., Development of an LS-DYNA nonlinear finite element model for use in damage detection and health monitoring of highway bridges, Health Monitoring and Management of Civil Infrastructural Systems, *Proceedings of SPIE*, Vol. 4337, pp.432-440, 2001.

[30] Nowak A. S., Kim S., Stankiewicz P. R., Analysis and diagnostic testing of a bridge, *Computers and Structures*, Vol. 77, pp.91-100, 2000.

[31] Paultre P., Chaalial O., Bridge dynamics and dynamic amplification factors – a review of analytical and experimental findings, *Canadian Journal of Civil Engineering*, Vol. 19, pp.260-278, 1992.

[32] Piombo B.A.D., Fasana A., Marchesiello S., & Ruzzene M., Modeling and identification of the dynamic response of supported bridge, *Mechanical Systems and Signal Processing*, Vol. 14(1), pp 75-89, 2000.

[33] Ren W., Zong Z., Output-only modal parameter identification of civil engineering structures, *Structural Engineering and Mechanics*, Vol. 17, No. 3-4, pp. 1-16, 2004.

[34] Robinson M. J., Halling M. W., Womarc K. C., Condition assessment of a six span full scale bridge using forced vibration, *Proceedings of SPIE*, Vol. 3995, pp.404-413 2000.

[35] Salawu O.S., Detection of structural damage through changes in frequency: a review, *Engineering Structures*, Vol. 19, No. 9, pp. 718-723, 1997.

[36] Salawu O.S., Williams C., Review of full scale dynamic testing of bridge structures, *Engineering Structures*, Vol. 17, No. 2, pp. 113-121, 1995.

[37] Szczesniak W., Ataman M., On the certain method of investigation of the aperiodic vibration of the elastic, simply supported beam, in a closed form – Krylov's problem, Theoretical Foundations of Civil Engineering, *Polish - Ukrainian Transactions*, Vol. 9, 2001.

[38] Tan G. H., Brameld G. H., Thambiratnam D. P., Development of an analytical model for treating vehicle-bridge interaction, *Engineering structure*, Vol. 20, No 1-2, pp 54-61, 1998.

[39] Tedesco J. W., Stallings J.M., EL-Mihimy M., Finite element method analysis of a concrete bridge repaired with fiber reinforced plastic laminates, *Computers and Structures*, Vol. 72, pp. 379-407, 1999.

[40] Wang T.-L., Huang D., Shahawy M., Huang K., Dynamic response of highway girder bridges, *Computers & Structures*, Vol. 60, No. 6, pp 1021-1027, 1996.

[41] Wilkins M.L., *Calculation of elastic-plastic flow, Methods of Computational Physics*, Vol.3, Academic Press, New York, 1964.

[42] Yang Y., Chang C.-H., Yau J.-D., An element for analyzing vehicle bridge systems considering vehicle's pitching effect, *International Journal for Numerical Methods in Engineering*, Vol. 46, pp 1031-1047, 1999.

[43] Yang Y., Liao S., Lin B., Impact formulation for vehicles moving over simple and continuous beams, *Journal of Structural Engineering*, Vol. 121, pp 1644-1650, 1995.

[44] Yang Y., Lin B.-H., Vehicle-bridge interaction analysis by dynamic condensation method, *Journal of Structural Engineering*, Vol. 121, No. 11, pp 1636-1643, 1995.

[45] Zaman M., Taheri M. R. & Khanna A., Dynamic response of cable-stayed bridges to moving vehicles using the structural impedance method, *Applied Mathematical Modeling*, Vol. 20, pp.876-889,1996.

[46] Zen H., Vibration of discretely stiffened skew plates and bridge vehicle interaction analysis, Dissertation, University of Oklahoma.

APPENDIX A
EXPERIMENTAL DATA

Table of contents

A.1. Static test results

A.1.1 Displacements and strains – verification of the superposition principle

The main idea of the elastic superposition principle is that the results (for displacements and strains) for combined loading state should be equal to the sum of results for separated loadings. Based on this principle, authors decided to compare received data. Additionally in this way they wanted to get the proof of the validity of recorded outcomes. Therefore, in the first stage the measured deflections in the middle of the first span were compared. The displacements caused by the side-by-side trucks located in both lanes should be equal to the sum of the displacement under a truck placed in the westbound lane and the second time located on the east bound lane. The scheme of this situation is presented below.

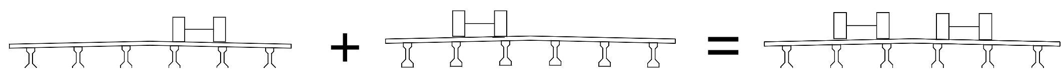

Table A.1 contains the comparison of results (from two kinds of instruments) for performed measurements. These deflections were measured for these cases at the same location (at the middle of girder 3, see Figure 3.9).

Table A.1. Verification of superposition principle by deflection.

	Single truck on west lane	Single truck on east lane	Sum of single truck on west and east lane	Trucks side by side on both lanes
Noptel	1.41 mm	1.82 mm	3.23 mm	3.15 mm
LVDT	0.86 mm	1.83 mm	2.69 mm	2.73 mm

In the second step, values of strains were compared to verify the validity of the mentioned principle. Results of this comparison are presented in the Figure A.1.

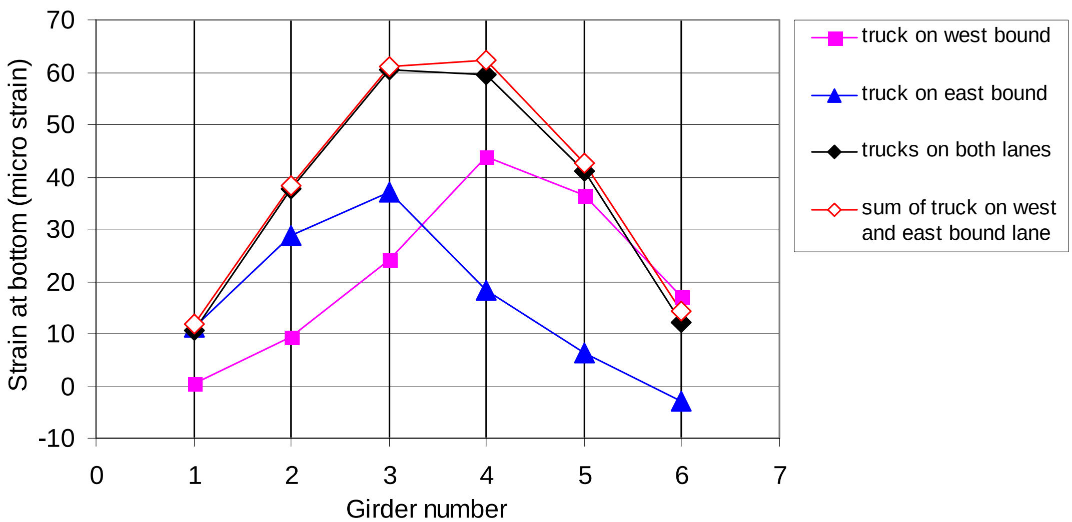

Figure A.1. Verification of superposition principle for strains.

It is noticed that the structural response is not strictly symmetrical about the centerline of roadway. The response when the truck is on the eastbound lane is smaller than that when on the west bound lane. The main reason for this unsymmetrical response can be attributed to the non-uniform distribution of material properties. This effect was confirmed by core testing. Additionally, the support conditions and the connection with the deck are not exactly the same for each girder.

A.1.2. Load distribution factor

The wheel load distribution factor (DF), which is critical for bridge design and load rating, represents the distribution of the vehicular load among the load carrying components of the bridge. It could be calculated using following formula:

$$DF = \frac{\varepsilon_i}{\sum_{j=1}^{n} \left(\frac{EI_j}{EI_i} \right) \varepsilon_j} \tag{A.1}$$

where:

ε_i and ε_j are the strains of the *i*-th girder and the *j*-th girder,

EI_i and EI_j are the bending stiffness of the *i*-th girder and the *j*-th girder.

Based on equation (A.1) and the strains measured in the testing, the DFs were calculated for four loading cases (see Chapter 3) with the assumption that the bending stiffness is the same for all six girders. The results are presented in Table A.2.

Table A.2. The distribution factor calculated from the measured strains.

Distribution factor (DF)	Single truck on west lane	Single truck on east lane	Truck on center of roadway	2 Trucks side by side on both lanes
Girder 1	0.0081	0.2301	0.0383	0.1906
Girder 2	0.1437	0.5826	0.2826	0.6816
Girder 3	0.3643	0.7503	0.6349	1.0922
Girder 4	0.6685	0.3688	0.6561	1.0764
Girder 5	0.5534	0.1254	0.3052	0.7411
Girder 6	0.2598	-0.0574	0.0828	0.2182

For bridges with concrete prestressed girders for two or more traffic lanes, the AASHTO specifications [A.2?] give the distribution factor as:

$$DF = \frac{S}{5.5} \tag{A.2}$$

where:

S = spacing of beams or girders in feet

The comparison of the measured distribution factor and that given by AASHTO code is shown in Figure A.2.

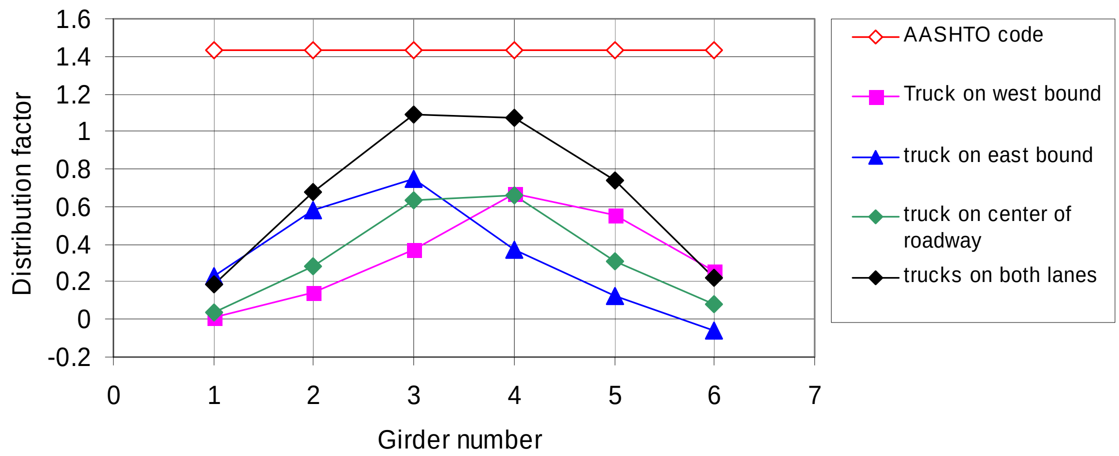

Figure A.2. Wheel load distribution factors.

A.1.3. Summary of static results

The bridge static response is verified by using the recorded displacement and strains at the middle of the first span. The measured deflection and strains confirms the validity of superposition principle, which indicates that the bridge response is in elastic range.

In the next step the measured distribution factor (DF) is compared with that predicted by AASHTO code. The AASHTO code gives a bigger value than actual one. It shows that from the static point of view the applied loading factor used in the experiment is safety and below the limit value.

It is expected that the results for the first two cases should be symmetrical (see Figures A.1 and A.2). However, the bridge exhibits an unsymmetrical response. It confirms once more that the material properties for concrete used are not the same in all bridge parts. Additionally it shows that the support conditions for the span are not the same.

A.2. Dynamic test results

A.2.1. Impact factor, deflection and strain analysis

A total of twelve dynamic tests, with one or two trucks, were conducted and most of the tests were repeated for cross checking. Displacements and strains were recorded and filtered by a frequency of 60 Hz. All outcomes for each case are presented and discussed separately in the following sections. Final conclusions from these tests are presented at the end of the chapter. The impact factor was calculated by:

$$IM = \frac{R_d - R_s}{R_s} \times 100\% \tag{A.3}$$

where:

R_S = maximum static response,

R_d = maximum dynamic response.

The vertical displacements in the section 2 for the girder #3 and the strains at the bottom of each girder in sections 2 and 4 were used to calculate the impact factor for different loading cases.

A.2.2. Case 1 - one truck on the west bound lane at 30 mph without plank

In this case the truck crossed the bridge on the west bound lane at 30 mph (48 km/h). Recorded values of displacements from two devices for two runs are presented in the Figure A.3. These values were used to calculate the dynamic impact factor for displacement (I_D). The obtained values for dynamic impact factor are presented in the Table A.3. The maximum value of I_D for this case is 0.57.

Figures A.4 and A.5 present the recorded values of longitudinal strains in section 2 and 4 as a function of time for the run #1 and in Figures A.6 and A.7 for the run #2. From these two runs it is clear that the higher values of strains are at the bottom of girder #4 in the middle span. According to the theoretical solutions this portion should be responsible for the maximum values of tension stresses. The obtained results are in accordance with the theory as the higher strains are observed in the section 4. It shows the correctness of obtained results since for both these cases the right side was loaded by the truck. This increase of strains in middle section compared to the first span is caused by the fact that when the truck is located at the first span some vibrations are transferred to the second span. For instance, maximum strains are observed in the first span at time 3.7s and at the same time the increase of strains in the section #4 (the second span) is visible. It means that some vibrations are transmitted by the continuous slab even though the girders are simply supported. For the girder # 1 in both cases, strain values are close to zero but the effect of transmitted vibrations is clearly visible. All obtained results are presented in Tables A.4 and A.5 and used to calculate the impact factor for strains (I_S) using formula (A.3). These values are presented in the Figure A.8. The value of the impact factor where the loading produces the maximum stress (strain) is most important. For this case the highest stress is developed at girder #4 and therefore the impact factor for the girder #4 (located in the section #4) which is I_S =0.18 is the most important. The impact factors for girder 1 and girder 2 are large but the strains of these two girders are small. For such cases, the significance of the large impact factors has no practical meaning and should be neglected.

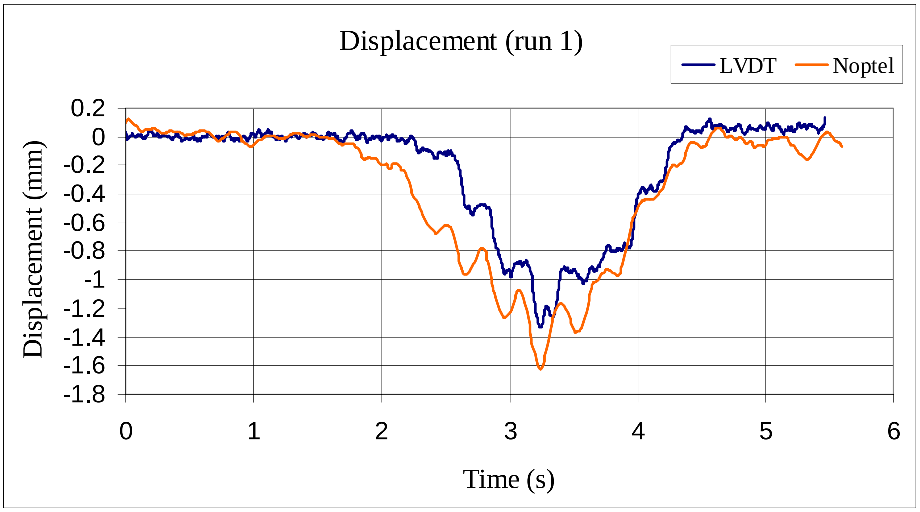

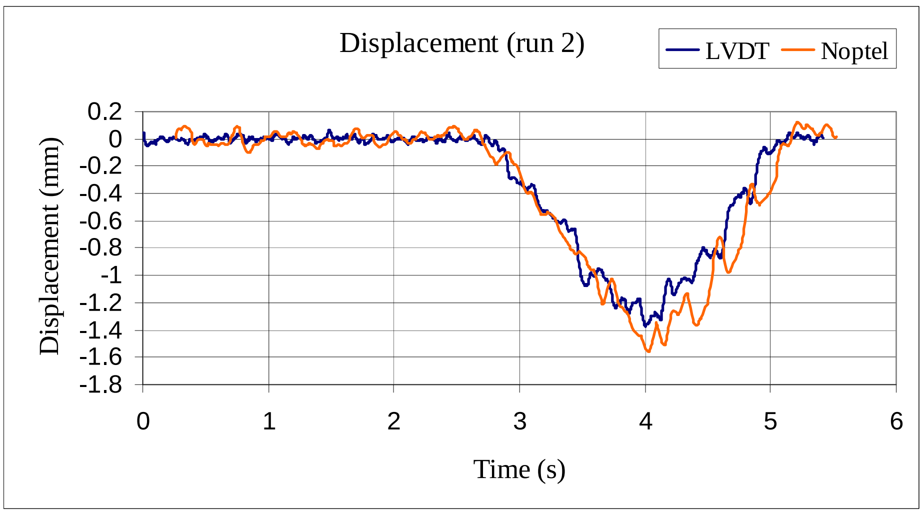

Figure A.3. The displacement of the point at the middle of girder #3 for case # 1.

Table A.3. The impact factor for girder # 3 from displacement history.

	LVDT (dynamic max) [mm]	LVDT (static) [mm]	Impact factor from LVDT I_D	Noptel (dynamic max) [mm]	Noptel (static) [mm]	Impact factor from Noptel I_D
Run 1	-1.33	-0.86	0.547	-1.62	-1.41	0.149
Run 2	-1.37		0.593	-1.55		0.099

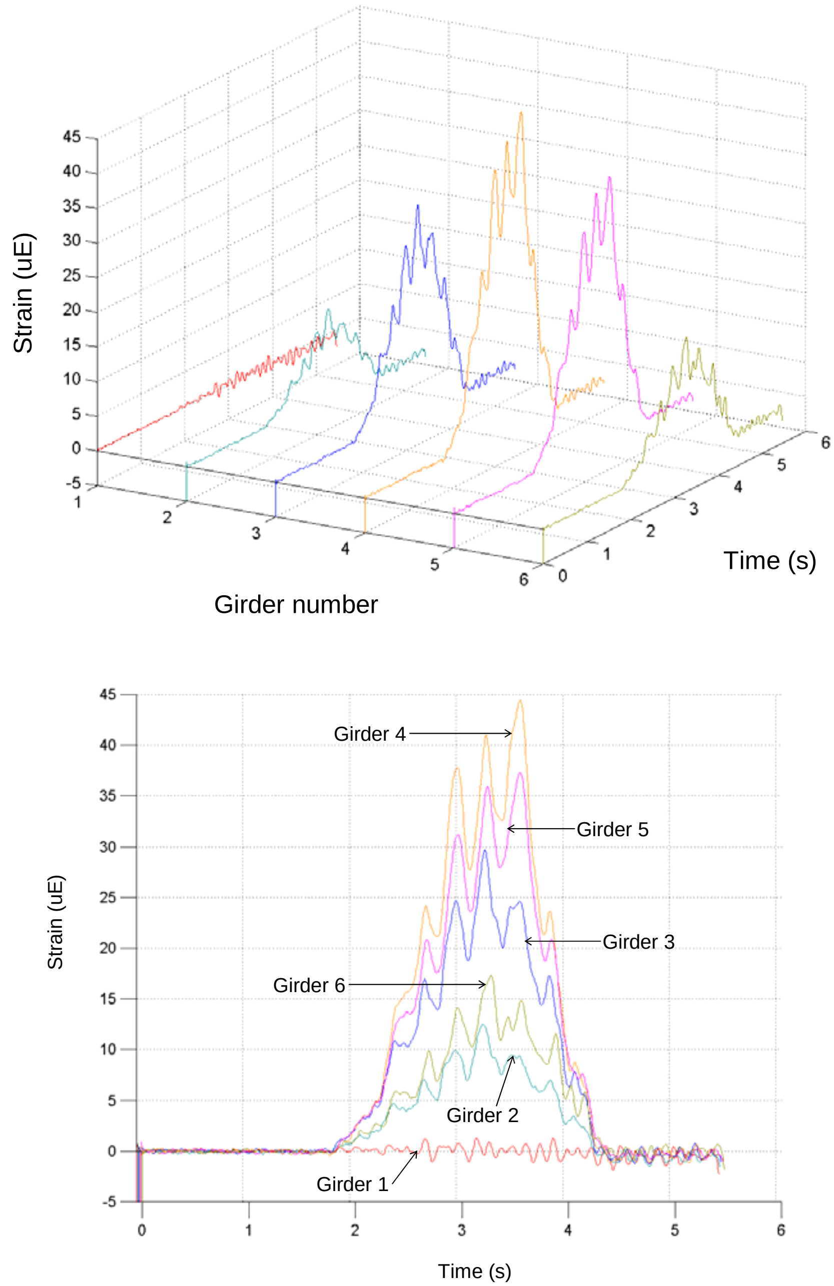

Figure A.4 Strain histories measured at bottom of girders in section # 2 (run 1).

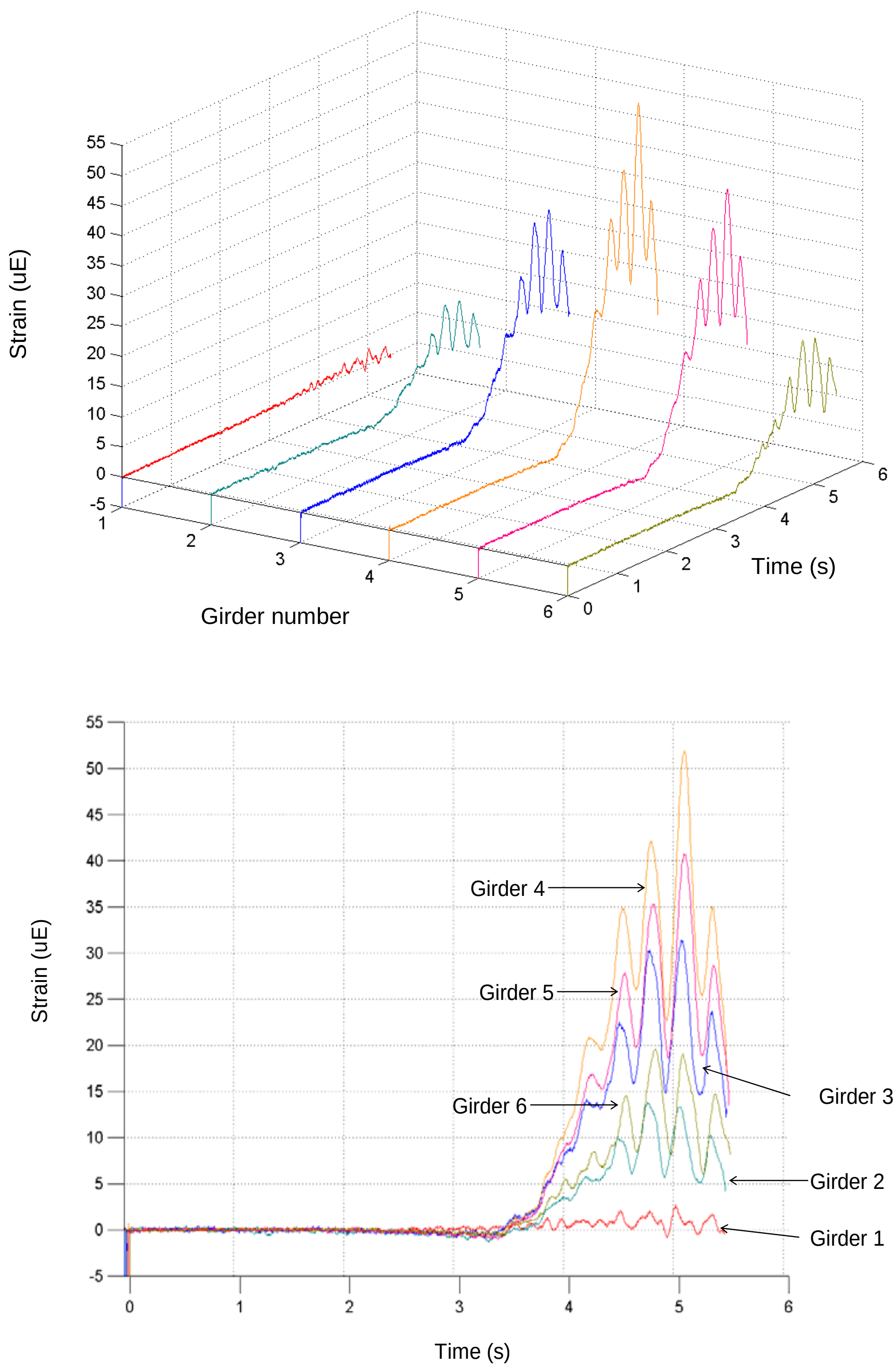

Figure A.5. Strain histories measured at bottom of girders in section # 4 (run #1).

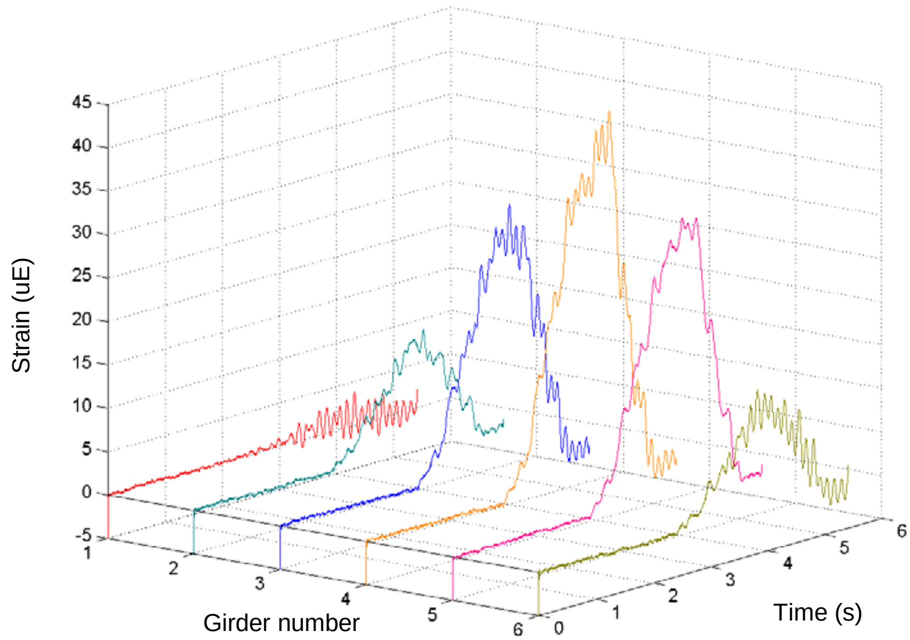

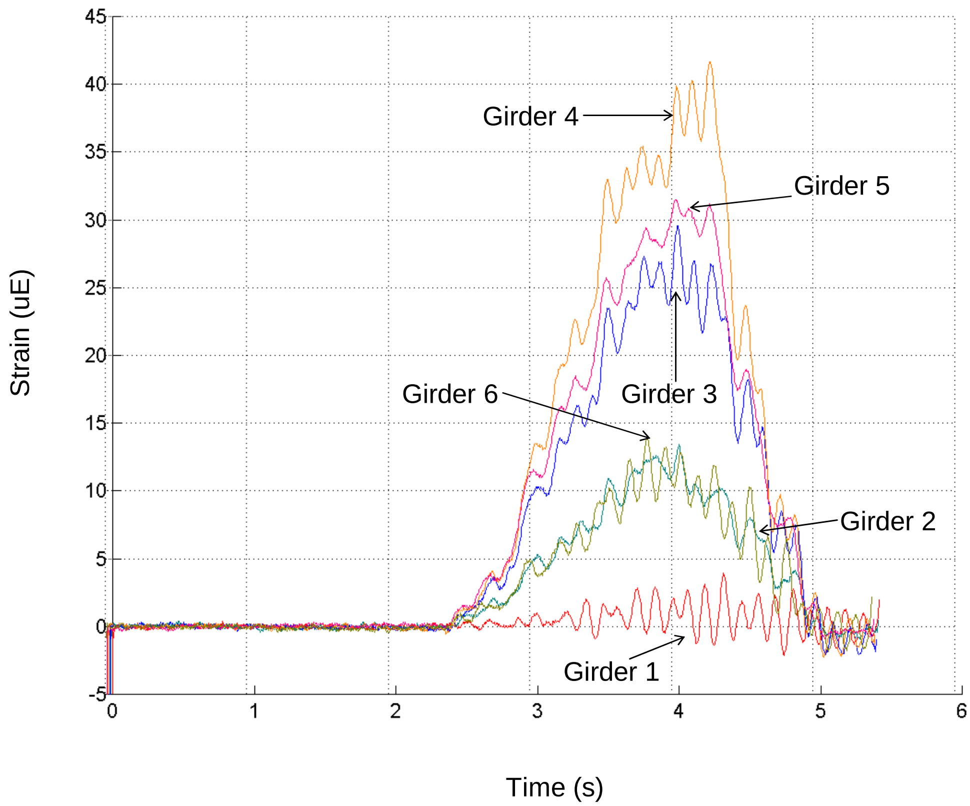

Figure A.6. Strain histories measured at bottom of girders in section # 2 (run #2).

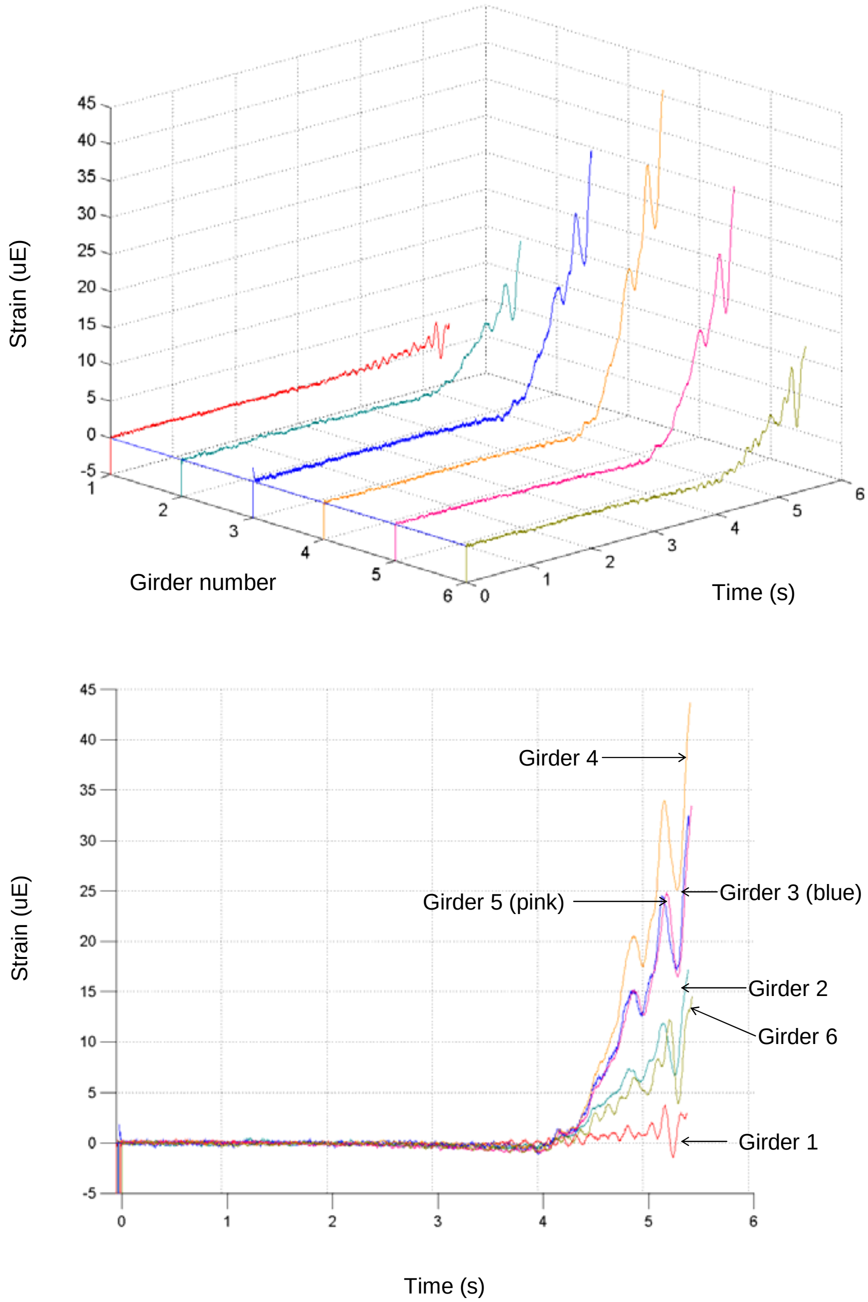

Figure A.7. Strain histories measured at bottom of girders in the section # 4 (run # 2).

Table A.4 The impact factor calculated from strain history for the first span (in the section #2)

Girder number	1			2			3			4			5			6		
	D	S	I_S	D	S	I_S	D	S	I_S	D	S	I_S	D	S	I_S	D	S	I_S
Run 1	1.3	0.5	1.47	12.5	9.5	0..32	29.7	24.1	0.23	45.1	44	0.03	37.3	36.4	0.02	18.4	17.1	0.08
Run 2	3.9		6.4	13.4		0.42	29.6		0.23	42.12		-0.04	31.5		-0.13	14.9		-0.13

Table A.5 The impact factor calculated from strain history for middle span (in the section #4)

Girder number	1			2			3			4			5			6		
	D	S	I_S	D	S	I_S	D	S	I_S	D	S	I_S	D	S	I_S	D	S	I_S
Run 1	2.7	0.5	4.13	13.8	9.5	0.46	31.4	24.1	0.30	52.	44	0.18	40.8	36.4	0.12	19.7	17.1	0.15
Run 2	NA			NA			NA			NA			NA			NA		

D = micro strains from dynamic case
S = micro strains from static case
I_S = impact factor for strains according to equation (A.3)

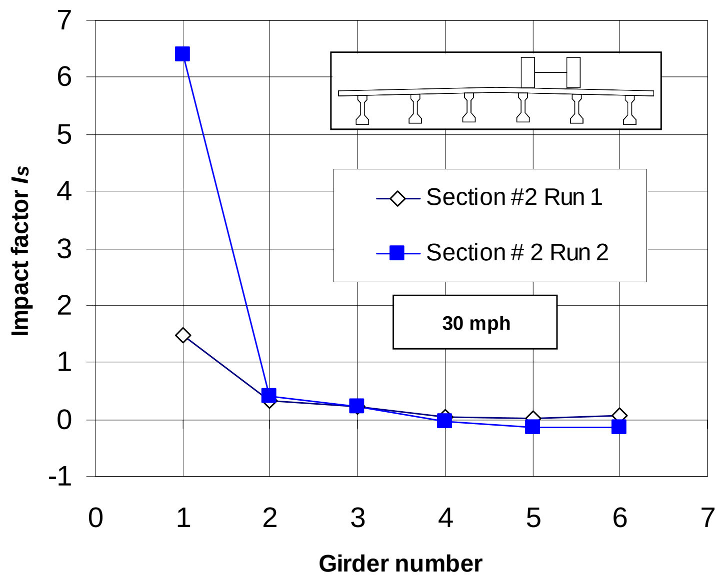

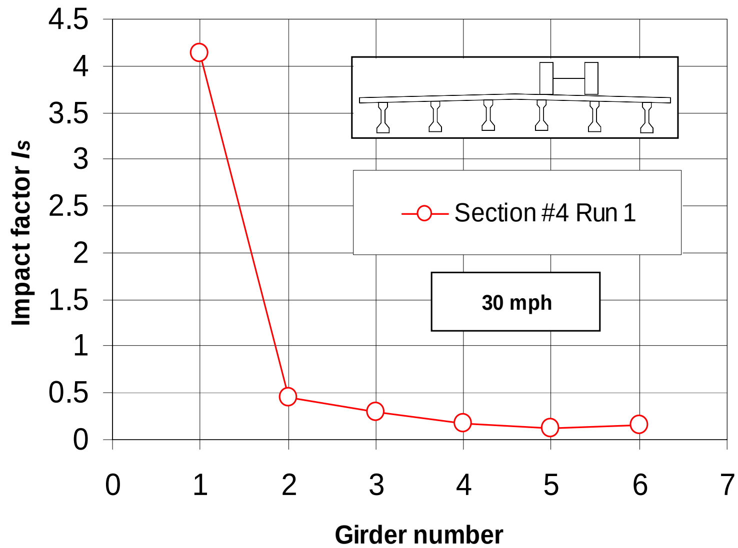

Figure A.8. Impact factor I_s for case #1 (speed 30mph).

A.2.3. Case 2 - one truck on the west bound lane at 50 mph without plank

In this case the truck crossed the bridge on the west bound at 50 mph (80 km/h). Results presented in Figures A.9 to A.13 show the same tendency as in the case 1. Girder # 4 is the one which carries the highest load. Additionally, it could be noted that the increase in the speed has caused an increase in the strains and hence the values of the impact factor (I_S). Furthermore, the impact factor calculated from maximum values of displacement (I_D) (see Table A.6) confirms this fact. Obtained maximum values of the impact factor are 1.56 for displacements and 1.78 for strains (see Table A.7). These big values of impact factors and visible vibrations (especially differences between next amplitudes) are related to the influence of external factors. Investigations of the bridge approach revealed the depression in this area and the visible threshold between the asphalt and concrete slab. These two factors cause additional vibrations, which are transferred from the truck wheels to the bridge slab. The suspension system of the test truck is not very flexible to absorb the shocks. This behavior of the suspension system is more apparent at higher speeds of the truck.

The visible decline in the strains in section # 2 (Figure A.10 and A.11) clearly shows that at this moment, the truck is leaving the first span and it starts vibrating freely. The first phase of this process takes about 1s, after that a small increase of vibrations in section # 2 is visible. This vibration amplification is caused by the influence of vibrations transferred from section #4, which is loaded by the crossing truck at the same time. These results are as expected.

Table A.6. The impact factor for girder # 3 from displacement history for case 2.

	LVDT (dynamic max) [mm]	LVDT (static) [mm]	Impact factor from LVDT I_D	Noptel (dynamic max) [mm]	Noptel (static) [mm]	Impact factor from Noptel I_D
Run 1	-1.99	-0.86	1.31	-2.39	-1.41	0.7
Run 2	-2.42		1.81	-2.66		0.89

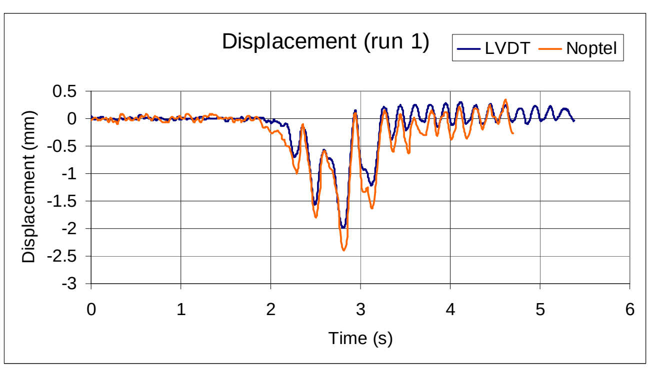

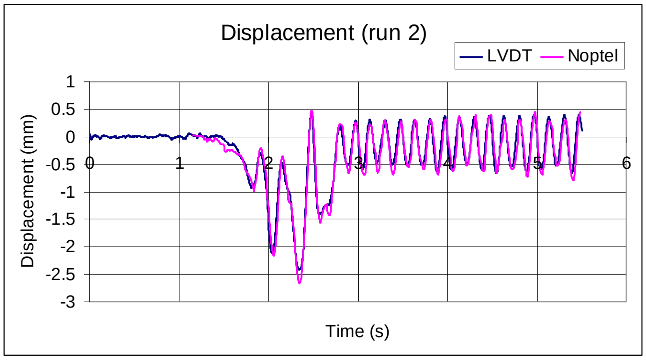

Figure A.9. The displacement of the point at the middle of girder #3 for case #2.

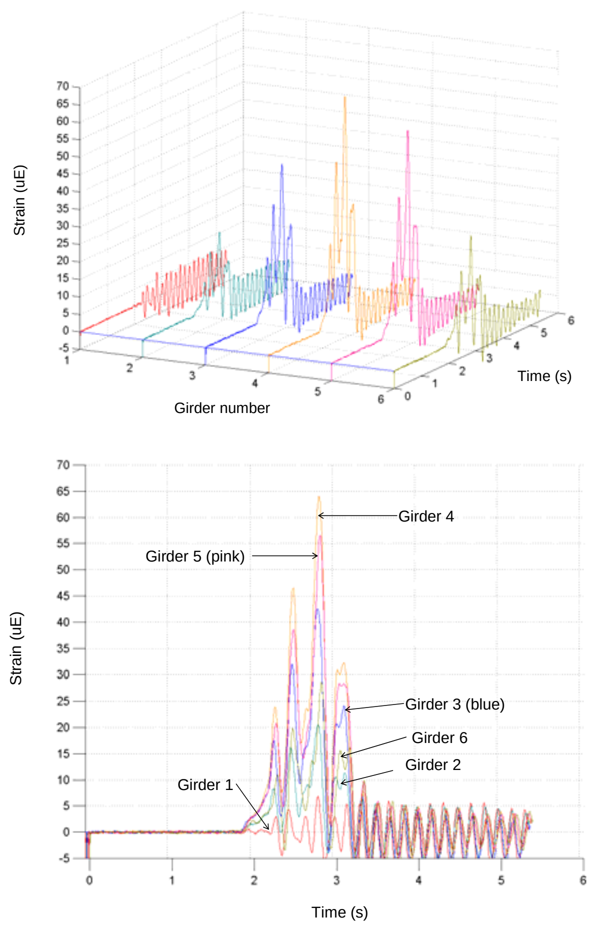

Figure A.10. Strain histories measured at bottom of girders in section # 2 for case # 2 (run 1).

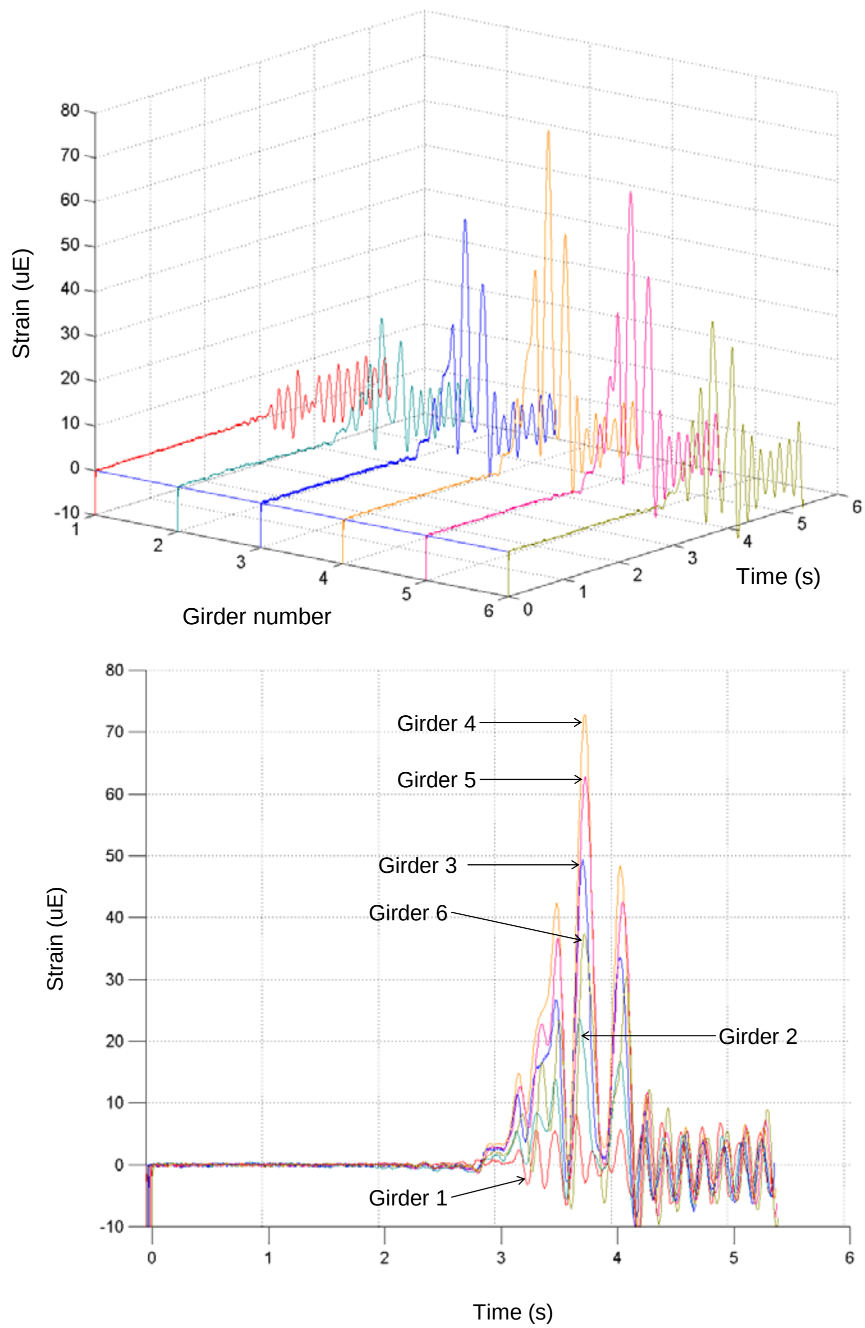

Figure A.11. Strain histories measured at bottom of girders in section # 4 for case # 2 (run 1).

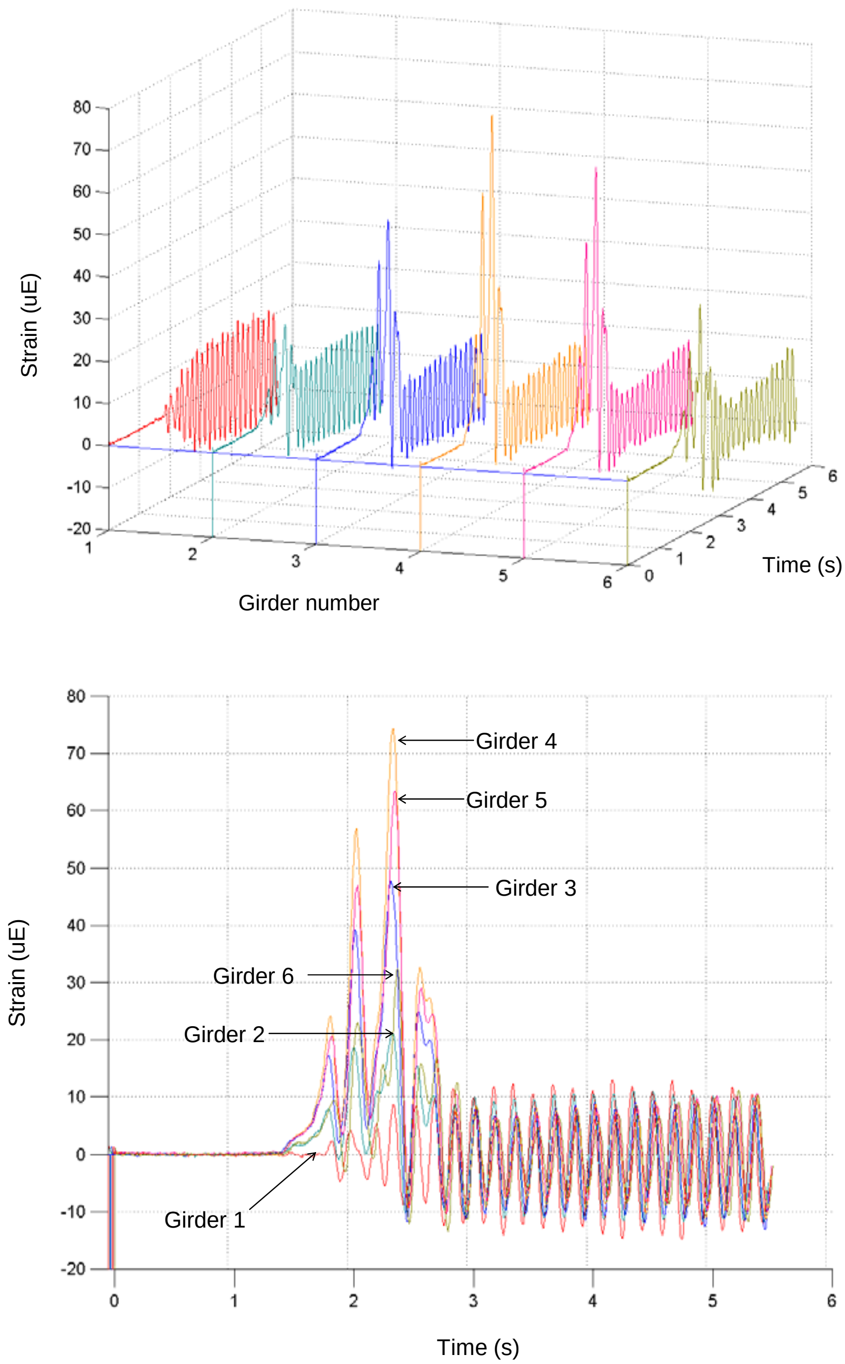

Figure A.12. Strain histories measured at bottom of girders in section # 2 for case # 2 (run 2).

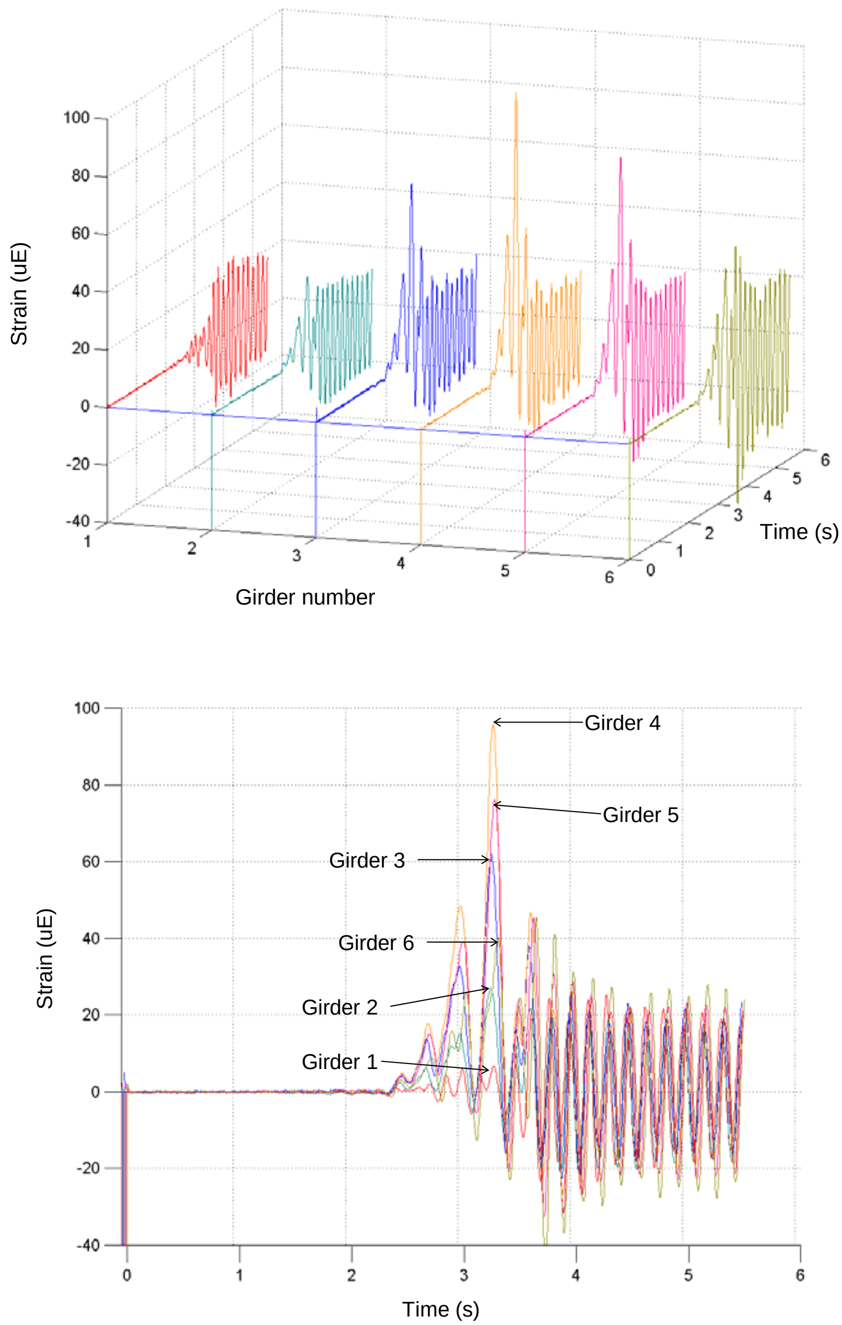

Figure A.13. Strain histories measured at bottom of girders in section # 4 for case # 2 (run 2).

Table A.7. The impact factor computed from strain history for the first span (in the section#2).

Girder number	1			2			3			4			5			6		
	D	S	I_S	D	S	I_S	D	S	I_S	D	S	I_S	D	S	I_S	D	S	I_S
Run 1	6.9	0.5	12.8	20.7	9.5	1.18	42.6	24.1	0.77	64.0	44.	0.46	56.6	36.4	0.56	29.9	17.1	0.75
Run 2	13.1		25.2	21.2		1.23	47.7		0.98	75.4		0.71	63.5		0.74	33.6		0.96

Table A.8. The impact factor computed from strain history for middle span (in the section #4).

Girder number	1			2			3			4			5			6		
	D	S	I_S	D	S	I_S	D	S	I_S	D	S	I_S	D	S	I_S	D	S	I_S
Run 1	8.2	0.5	15.4	23.6	9.5	1.48	49.4	24.1	1.05	72.9	44	0.66	62.7	36.4	0.72	37.4	17.1	1.19
Run 2	25.2		50.4	27.0		1.84	62.0		1.57	95.8		**1.18**	76.2		1.09	45.5		1.66

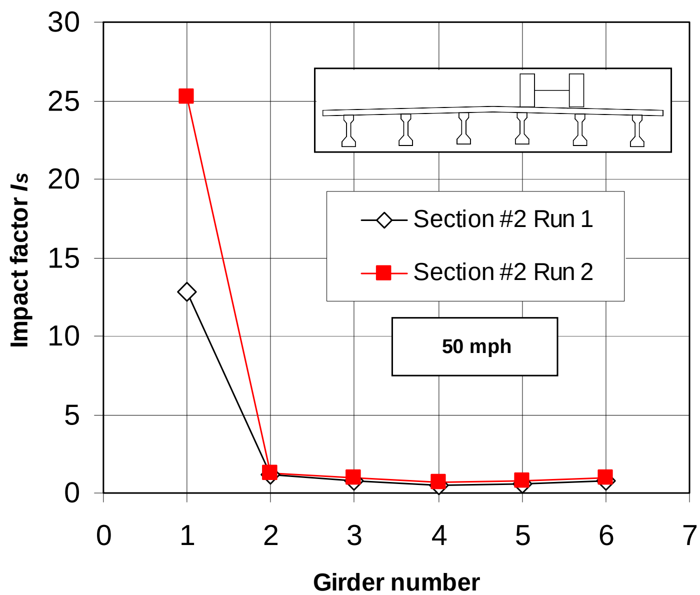

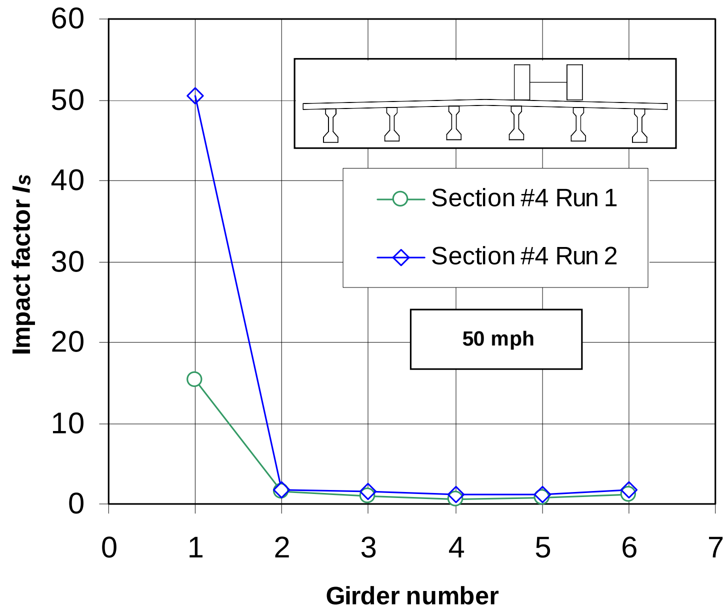

Figure A.14. Impact factor I_s for case #2 (speed 50mph).

A.2.4. Case 3 - One truck on the west bound lane at 30 mph with plank

In this case the truck crossed the bridge on the west bound lane at 30 mph (48 km/h). A wooden plank was placed on the slab of the first span to cause a bump. All other conditions were the same as in case 1. The main role of the plank was to stimulate extra vibrations on the suspension system of the crossing truck. The observed values of displacement and strains confirm the influence of this obstacle. It is clear that the deflection in the middle span is increased by about 80 % and the obtained curve is not as smooth as in the case #1. The effect of this obstacle is also evident from the observed strains. The increase in the strains compared to the strains in case # 1 is about 30 % for the section #2. The frequency for the case with plank as an obstacle is much higher compared to the case without the plank (this topic will be discussed in detail in the next section). The maximum values of the impact factor are 2.86 for displacement and 0.36 for strains. Similar to the previous cases, the girder # 4 is the most tensioned in this case. It shows that the tendency of the bridge behavior is as expected. However, the exciter (plank) causes the higher vibrations and hence higher value of the impact factor for the first span unlike in previous cases, always for the second span. The analysis of the strain amplitudes shows the downward character of these vibrations which is due to the natural damping (Figures A.15, A.16 & A.18) of concrete. The high impact factor demonstrates how dangerous can an accidentally left artificial obstacle on a bridge deck be.

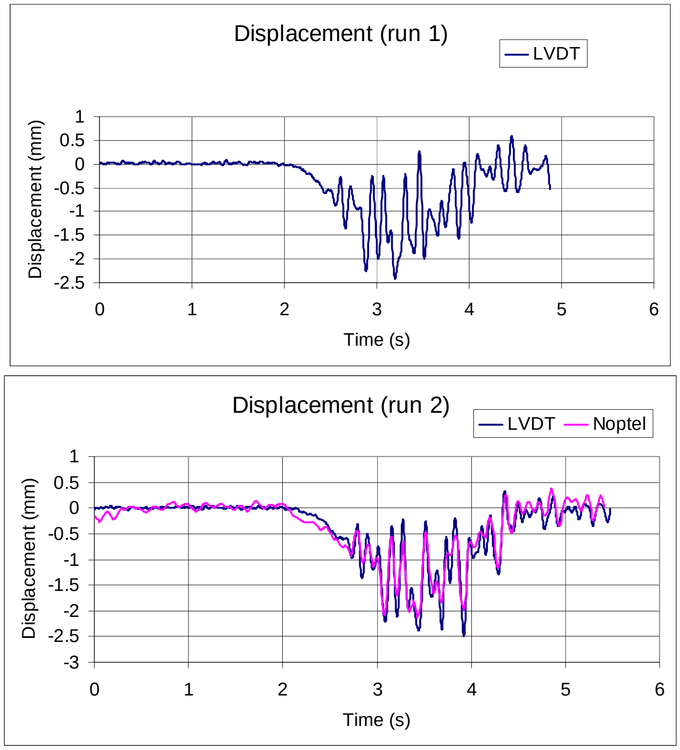

Figure A.15. The displacement of the point at the middle of girder #3 for case #3.

Table A.9. The impact factor for girder # 3 from displacement history for case # 3.

	LVDT (dynamic max) [mm]	LVDT (static) [mm]	Impact factor from LVDT I_D	Noptel (dynamic max) [mm]	Noptel (static) [mm]	Impact factor from Noptel I_D
Run 1	-2.41	-0.86	2.8	NA	-1.41	NA
Run 2	-2.50		2.91	-2.13		1.51

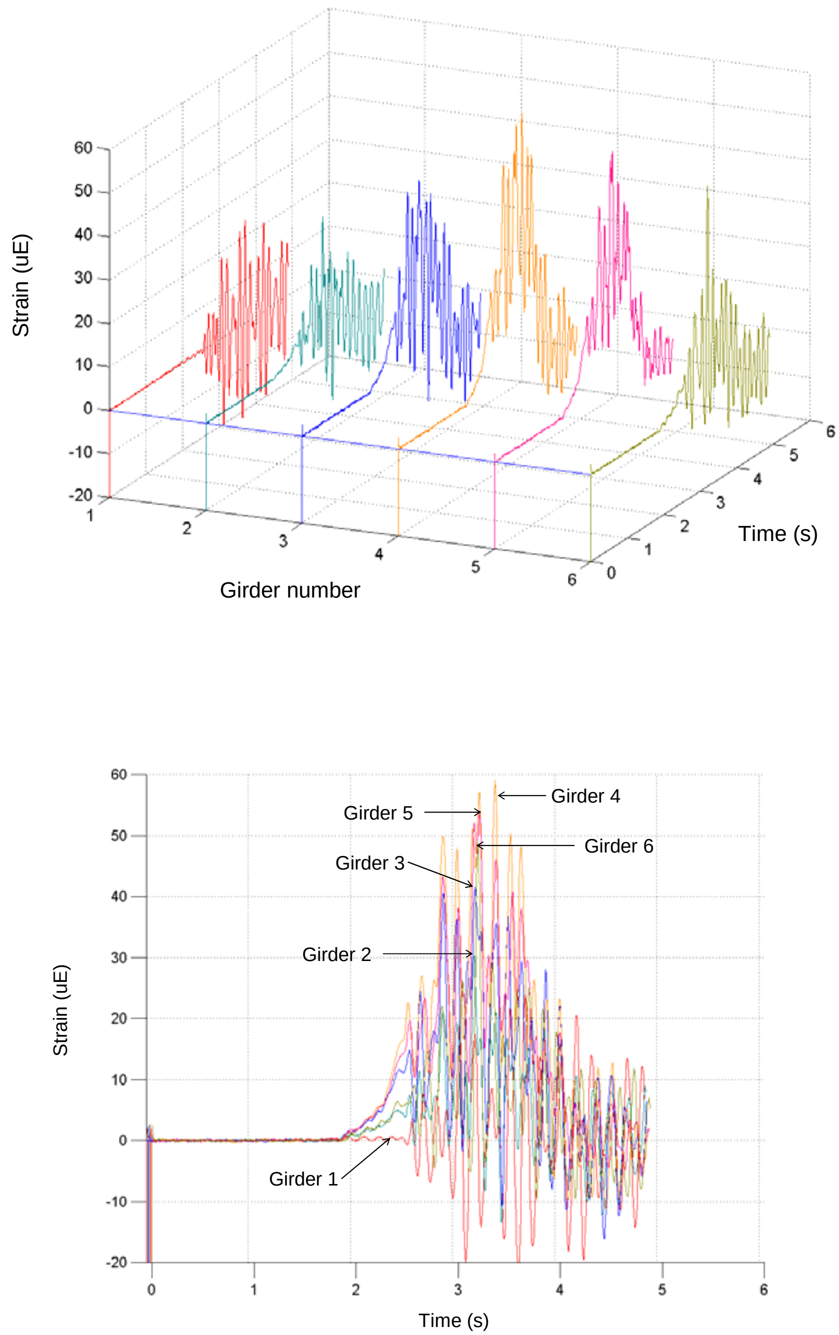

Figure A.16. Strain histories measured at bottom of girders in section # 2 for case # 3 (run 1).

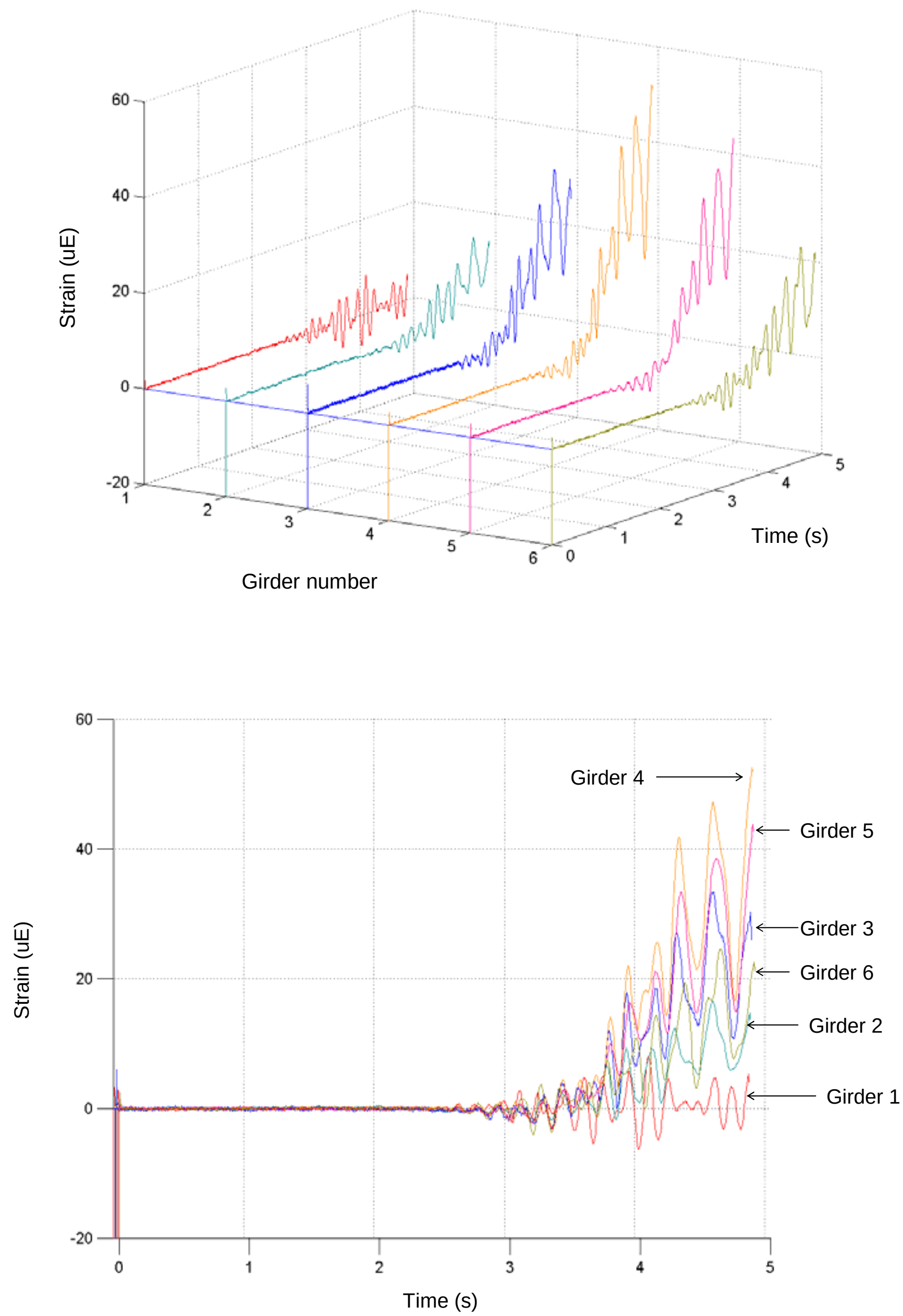

Figure A.17. Strain histories measured at bottom of girders in section # 4 for case # 3 (run 1).

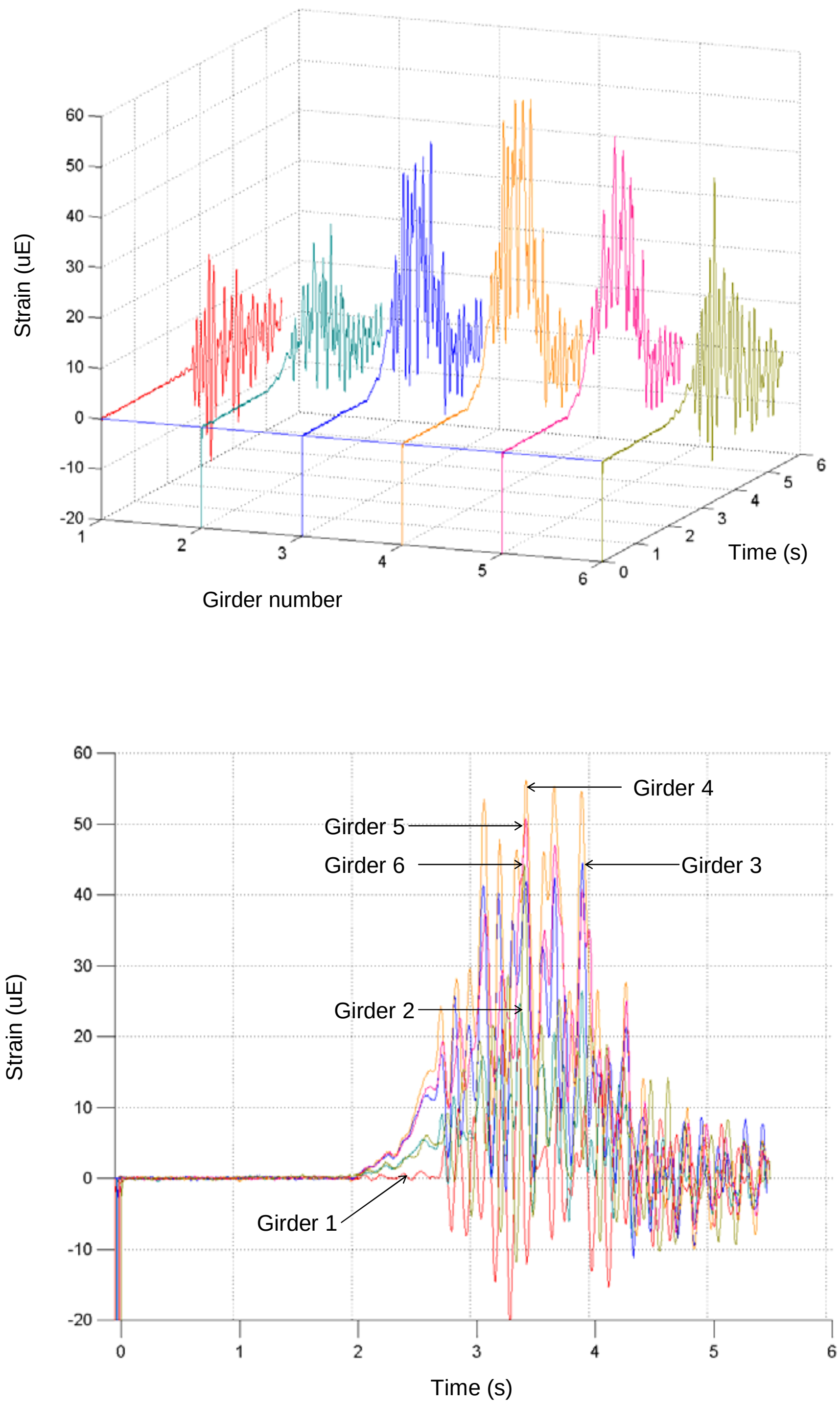

Figure A.18. Strain histories measured at bottom of girders in section # 2 for case # 3 (run 2).

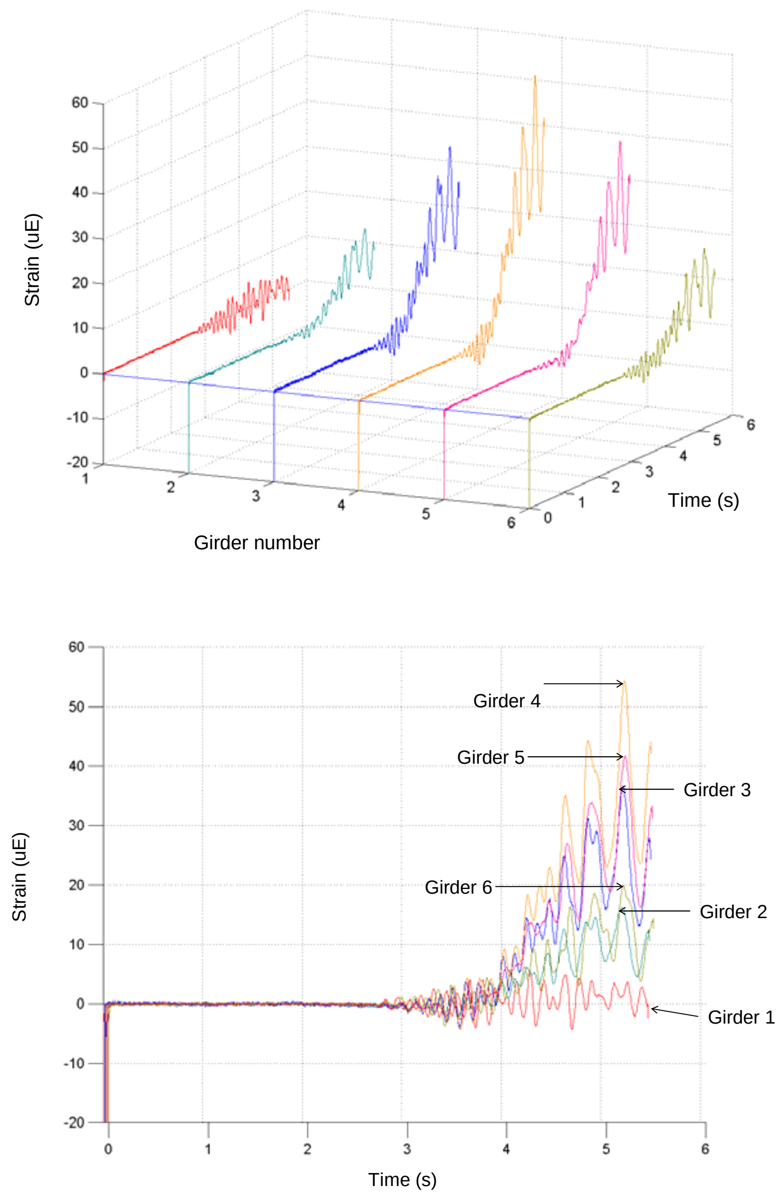

Figure A.19 Strain histories measured at bottom of girders in section # 4 for case # 3 (run 2).

Table A.10. The impact factor computed from strain history for the first span (in the section#2).

Girder number	1			2			3			4			5			6		
	D	S	I_S	D	S	I_S	D	S	I_S	D	S	I_S	D	S	I_S	D	S	I_S
Run 1	23.8	0.5	46.6	30.3	9.5	2.2	41.5	24.1	0.72	59.7	44	0.36	54.0	36.4	0.48	48.9	17.1	1.86
Run 2	21.0		41.0	26.4		1.78	44.5		0.85	56.7		0.29	50.8		0.4	44.4		1.6

Table A.11. The impact factor computed from strain history for the middle span (the section #4).

Girder number	1			2			3			4			5			6		
	D	S	I_S	D	S	I_S	D	S	I_S	D	S	I_S	D	S	I_S	D	S	I_S
Run 1	NA	0.5		NA	9.5		NA	24.1		NA	44		NA	36.4		NA	17.1	
Run 2	5.7		10.4	16.3		0.72	36.6		0.52	54.3		0.23	41.8		0.15	12.0		-0.3

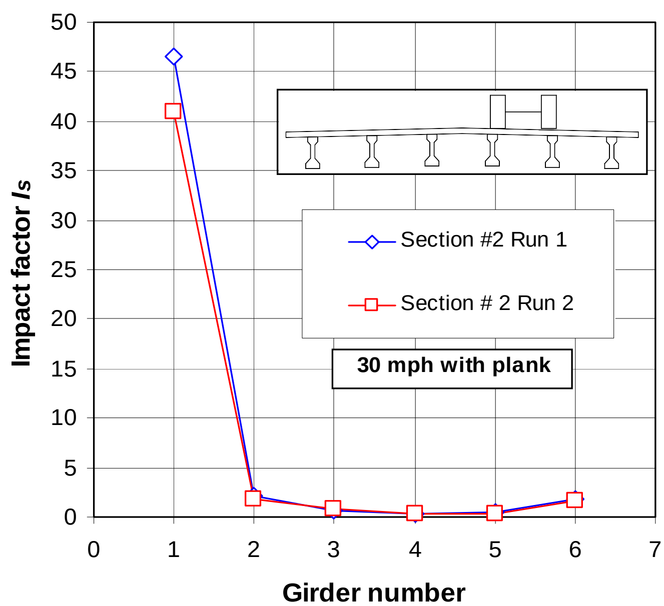

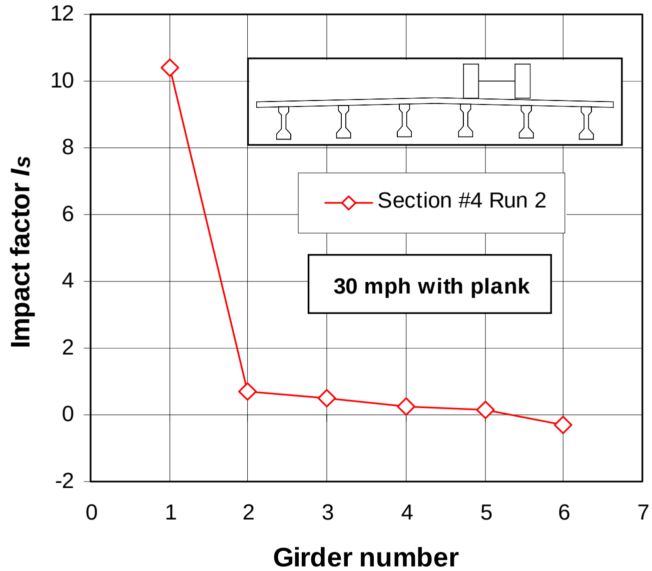

Figure A.20. Impact factor I_s for case #3 (speed 30mph with plank on the bridge deck).

A.2.5. Case 4 - One truck running on the west bound lane at 50 mph with plank

In this case the truck crossed the bridge on the west bound lane at 50 mph (80 km/h). As in case 3, a wooden plank was placed on the slab of the first span to cause a bump. All other conditions are the same like for case 2. The general tendency of the bridge behavior is similar as in the previous case. It was observed that the deflection of the span and strains in the girder # 4 increased up to about 35% and 50 % respectively. This phenomenon confirms the significant influence of the truck speed (see case # 2). The maximum values of the impact factor are 2.38 for displacement and 1.02 for strains. However, in this case the I_D is higher for the section # 4. It indicates that the amplitude of the vibrations for the first span is higher. Furthermore, the period between succeeding measuring points is shorter. Artificially caused vibrations in addition to the vibrations transmitted from the truck are too high to be extinguished by the bridge structure in such a short time. Therefore the values of strains in the section #4 transferred by the bridge deck are higher. Finally, decline in the vibrations takes place because the truck leaves the bridge and the effect of the wheel forces on the slab disappears.

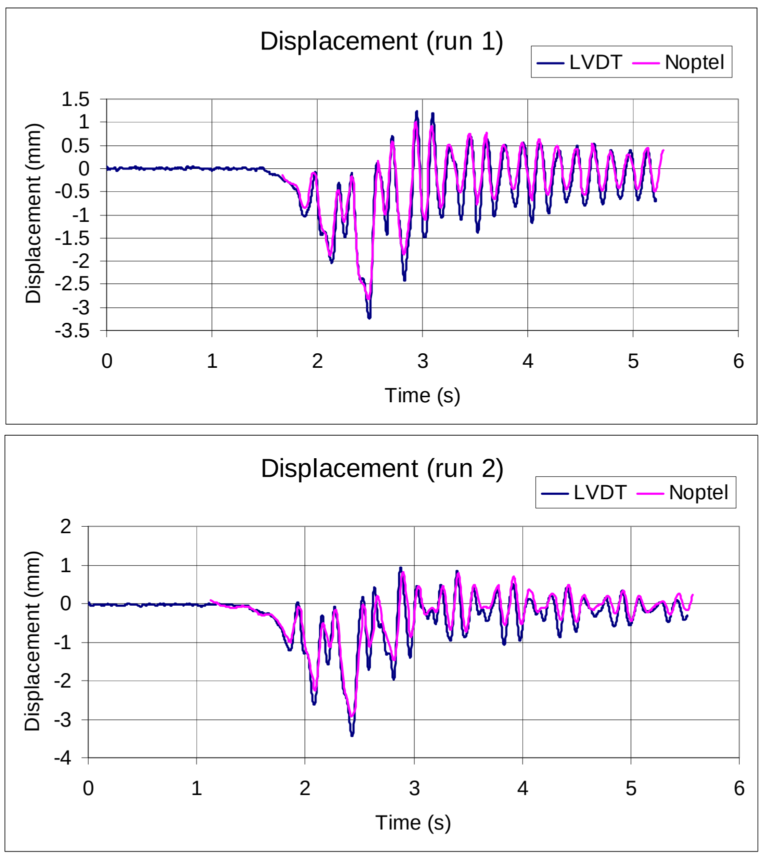

Figure A.21. The displacement of the point at the middle of girder #3 for case # 4.

Table A.12 The impact factor for girder # 3 from displacement history for case # 4.

	LVDT (dynamic max) [mm]	LVDT (static) [mm]	Impact factor from LVDT I_D	Noptel (dynamic max) [mm]	Noptel (static) [mm]	Impact factor from Noptel I_D
Run 1	-3.24	-0.86	2.77	-2.82	-1.41	1
Run 2	-3.44		2.0	-2.92		1.07

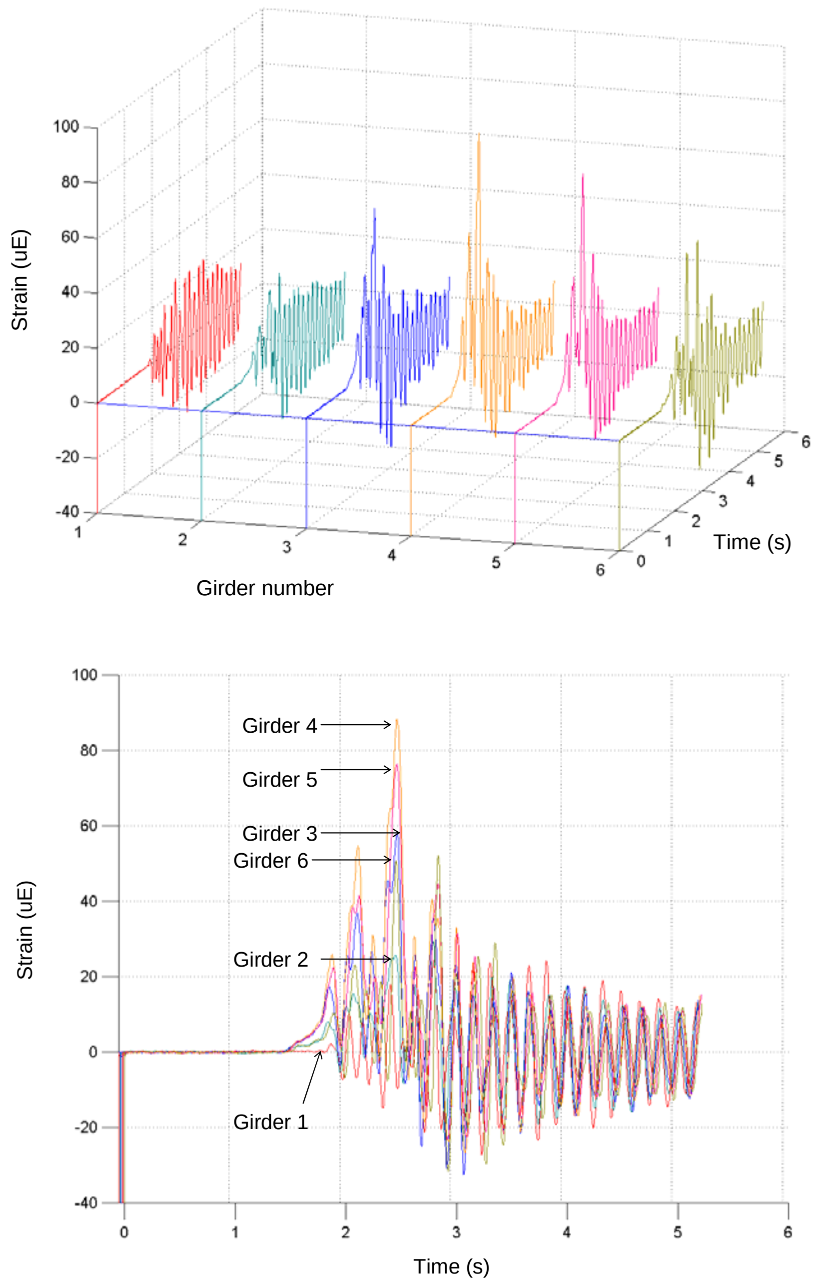

Figure A.22. Strain histories measured at bottom of girders in section # 2 for case # 4 (run 1).

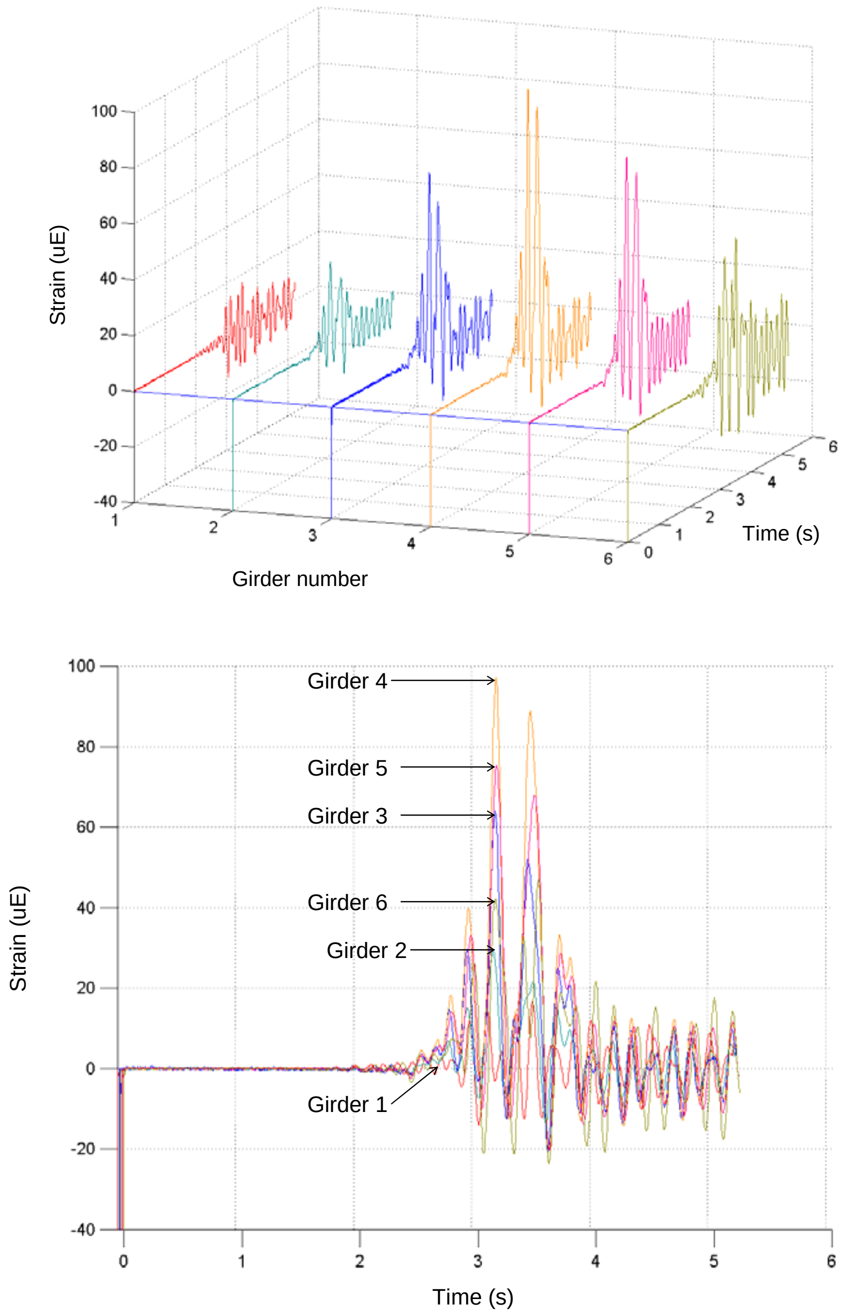

Figure A.23. Strain histories measured at bottom of girders in section # 4 for case # 4 (run 1).

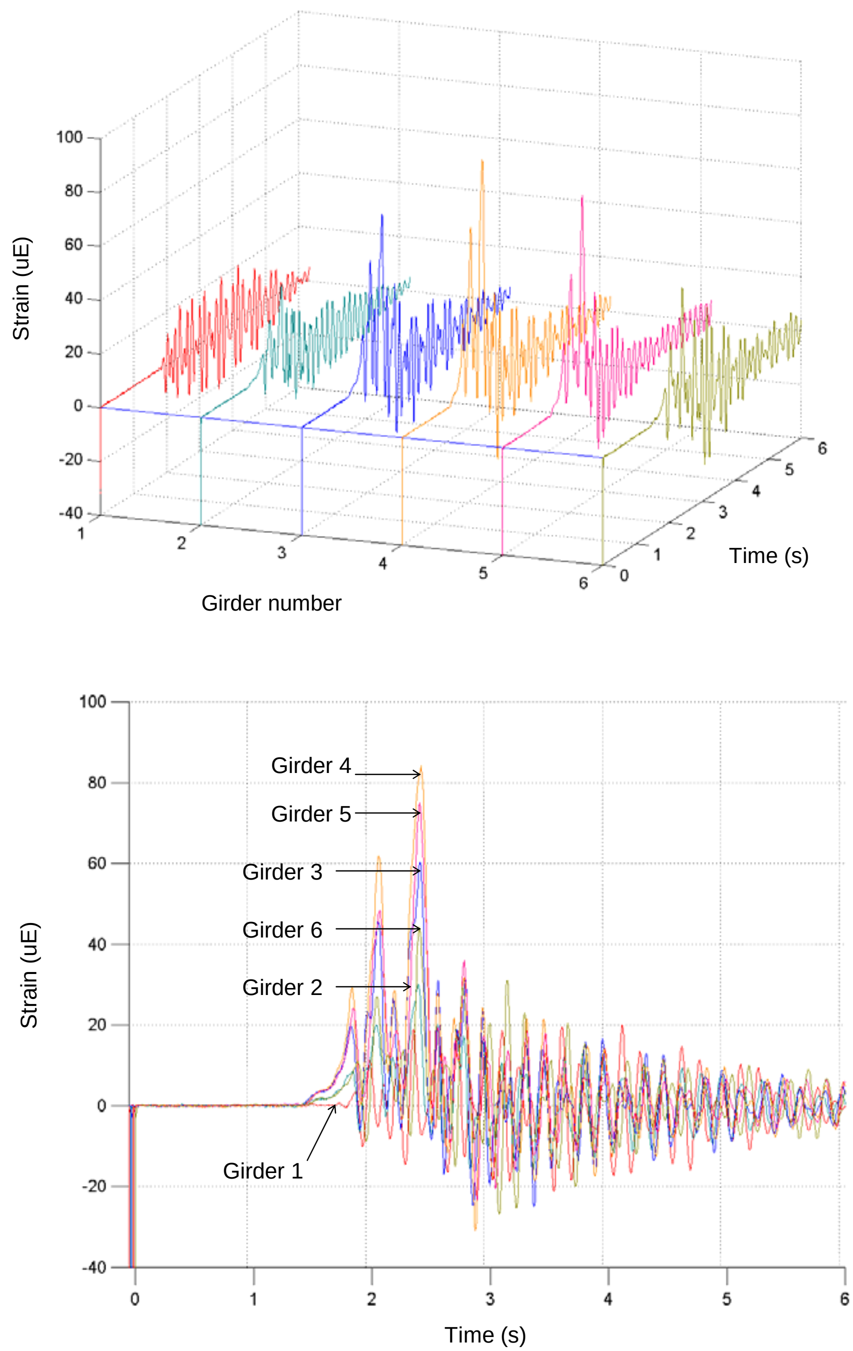

Figure A.24. Strain histories measured at bottom of girders in section # 2 for case # 4 (run 2).

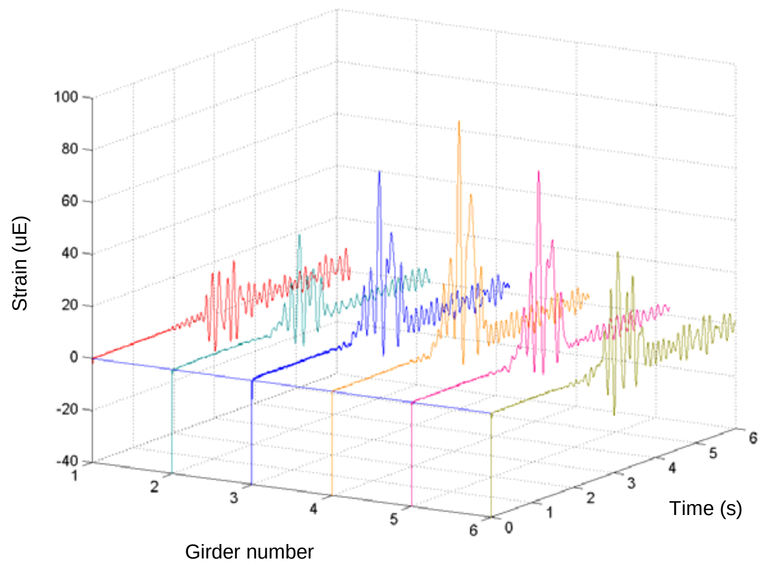

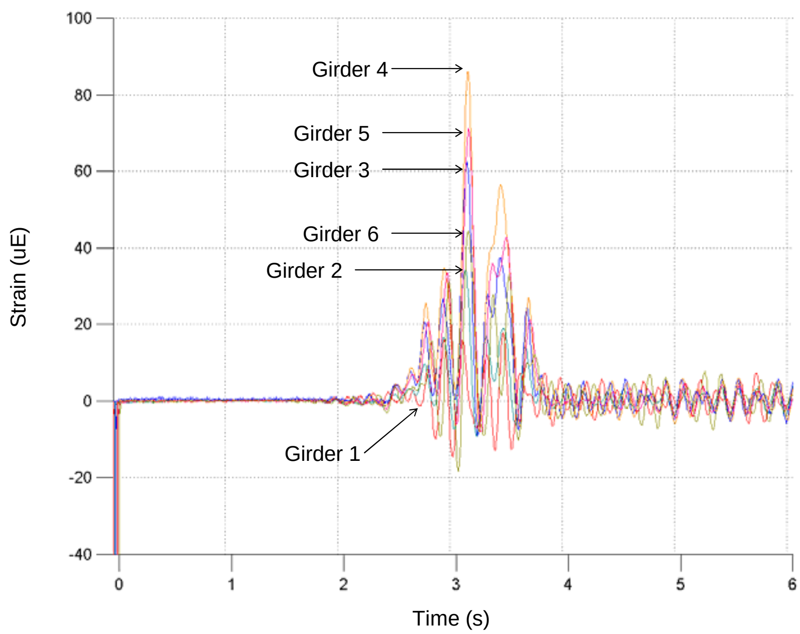

Figure A.25. Strain histories measured at bottom of girders in section #4 for case #4 (run 2).

Table A.13. The impact factor computed from strain history for the first span in the case # 4.

Girder number	1			2			3			4			5			6		
	D	S	I_S	D	S	I_S	D	S	I_S	D	S	I_S	D	S	I_S	D	S	I_S
Run 1	24.5	0.5	48.0	29.5	9.5	2.1	58.0	24.1	1.4	89.1	44	1.02	76.6	36.4	1.1	52.3	17.1	2.06
Run 2	20.1		39.2	30.2		2.2	60.3		1.5	84.6		0.92	74.9		1.06	45.1		1.6

Table A.14. The impact factor computed from strain history for the middle span in the case # 4.

Girder number	1			2			3			4			5			6		
	D	S	I_S	D	S	I_S	D	S	I_S	D	S	I_S	D	S	I_S	D	S	I_S
Run 1	16.9	0.5	32.8	29.5	9.5	2.1	64.0	24.1	1.7	97.2	44	1.2	75.4	36.4	1.07	47.2	17.1	1.76
Run 2	18.0		35.0	34.3		2.6	62.6		1.6	86.0		0.95	71.1		0.95	44.4		1.6

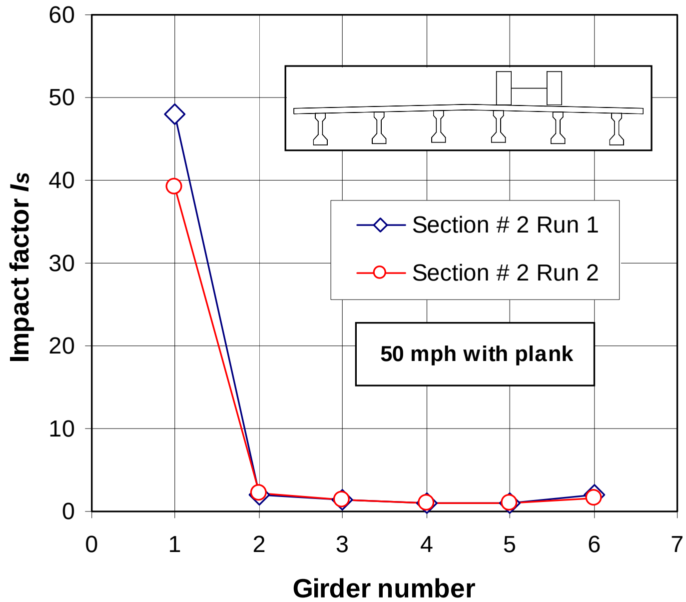

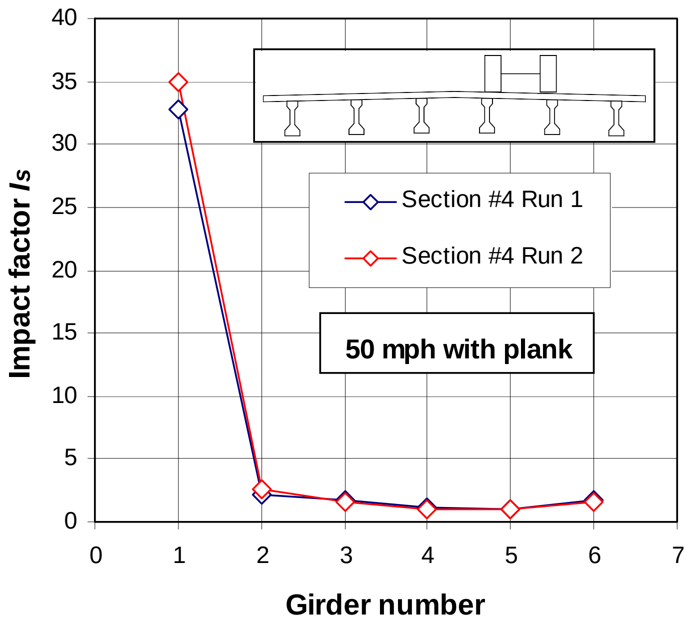

Figure A.26. Impact factor I_s for case #4 (speed 50mph with plank on the bridge deck).

A.2.6. Case 5 - One truck running on the center of roadway at 30 mph without plank

In this case the truck crossed the bridge on the center of the roadway at 30 mph (48 km/h). Comparing the span deflection it is clear that the displacement has increased. This situation was expected as mainly the girders 3 and 4 were loaded. This increase in the displacement is about 50% compared to case 1. Consequently, this fact affects the smaller value of the impact factor calculated (I_D) and amounts to 0.34 (table A.15). This test clearly shows the significant influence of the loading (truck) position on the bridge behavior.

For this case symmetrical results for recorded strains were expected. This situation took place for the run #1. Results are almost the same for next couples of girders: 1-6, 2-5 and 3-4 (Figures A.28 & A.29). Small differences are noticeable for the second run. This difference could be attributed to the inaccuracy in keeping constant speed of the truck for both the runs. Additionally it can be caused by measurement error. Obtained values of strains are about 10 % smaller than in the case #1. The maximum impact factor (I_S) computed from the strain history for the most loaded girders (3 & 4) equals 0.19 for the first span and 0.3 for the middle span (Tables A.16 & A.17). This increase for the second span confirms the existence of the same phenomena as in case 1, the transfer of vibrations.

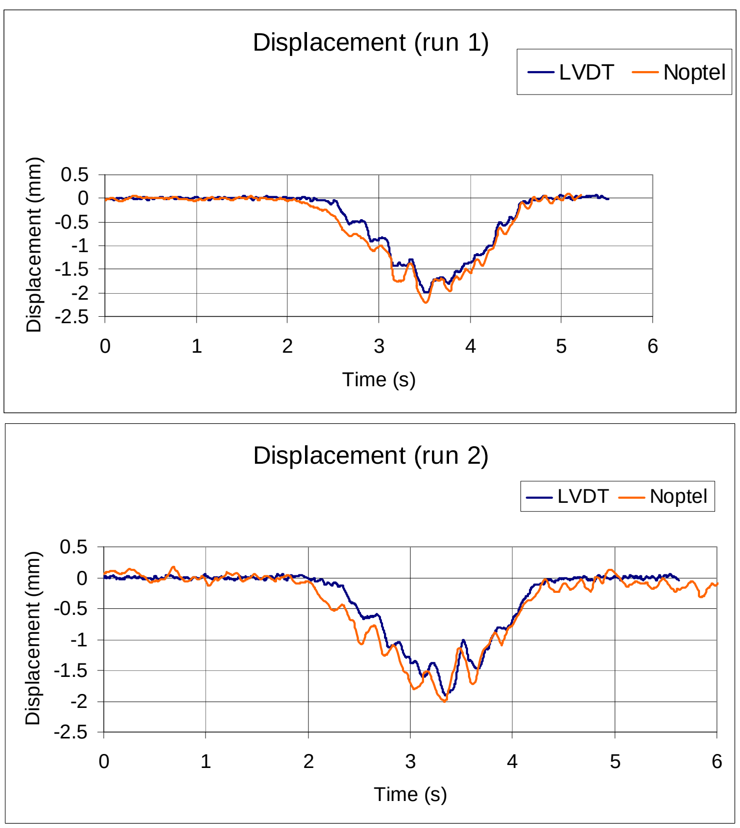

Figure A.27. The displacement of the point at the middle of girder #3 for the case # 5.

Table A.15. The impact factor for girder # 3 from displacement history for case # 5.

	LVDT (dynamic max) [mm]	LVDT (static) [mm]	Impact factor from LVDT I_D	Noptel (dynamic max) [mm]	Noptel (static) [mm]	Impact factor from Noptel I_D
Run 1	-1.99	-1.46	0.36	-2.22	-1.94	0.14
Run 2	-1.91		0.31	-2.01		0.04

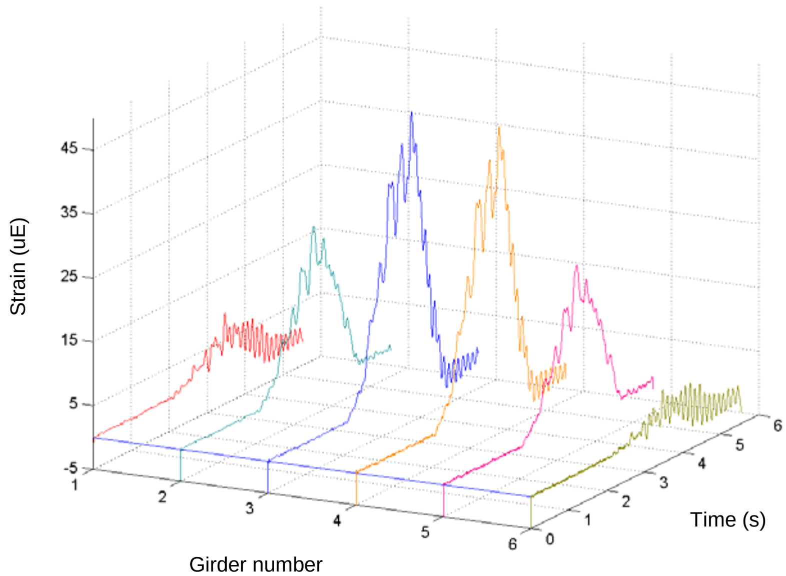

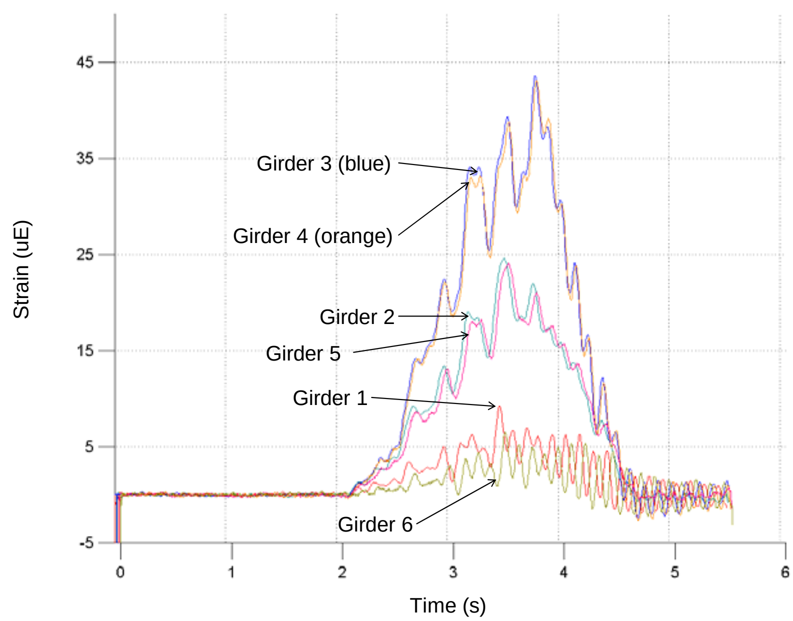

Figure A.28. Strain histories measured at bottom of girders in section # 2 for case # 5 (run 1).

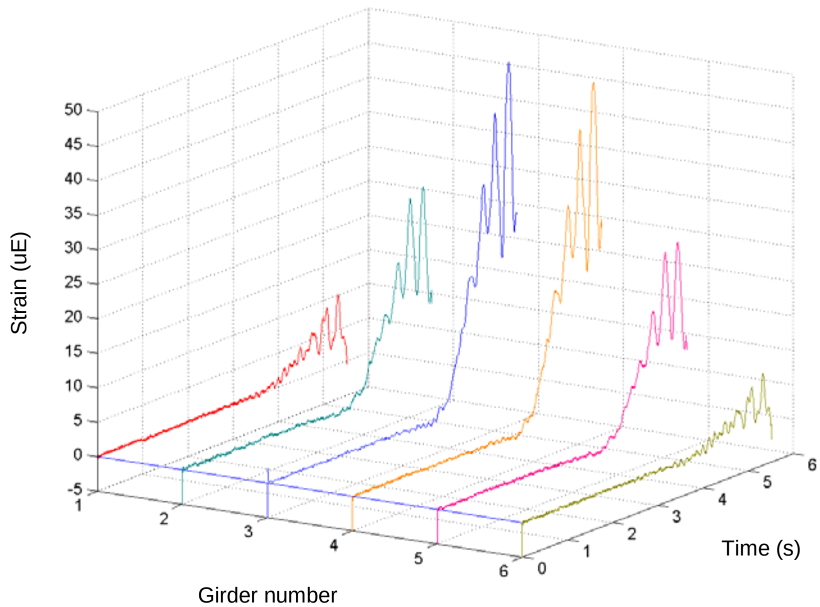

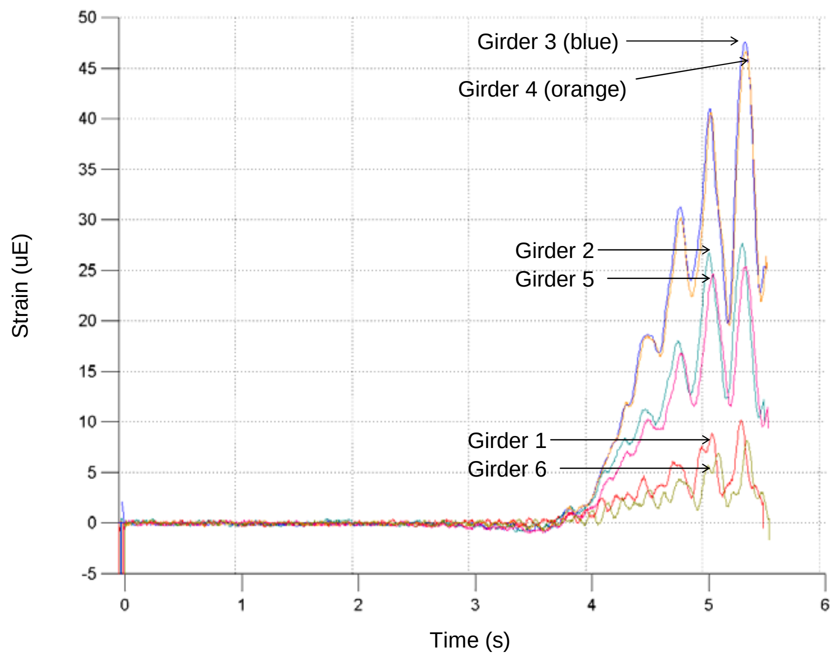

Figure A.29. Strain histories measured at bottom of girders in the section # 4 for case #5 (run1).

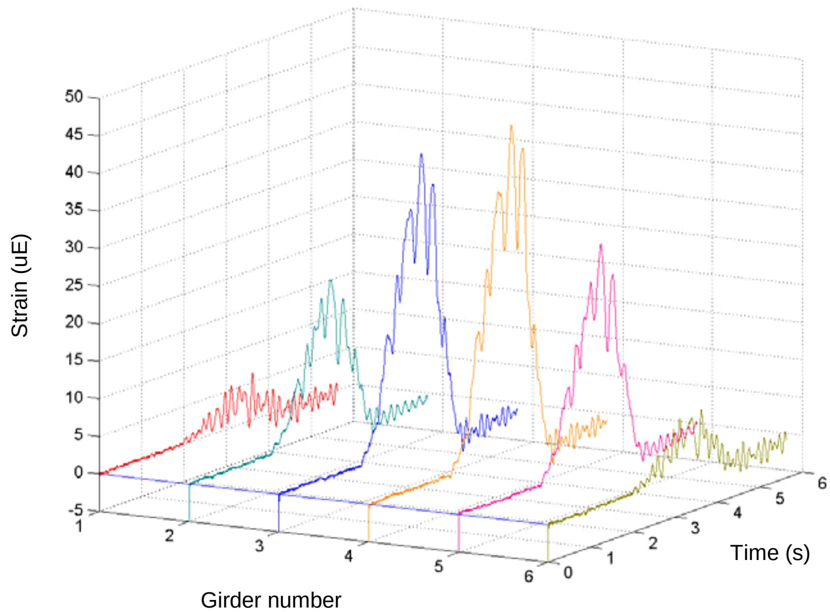

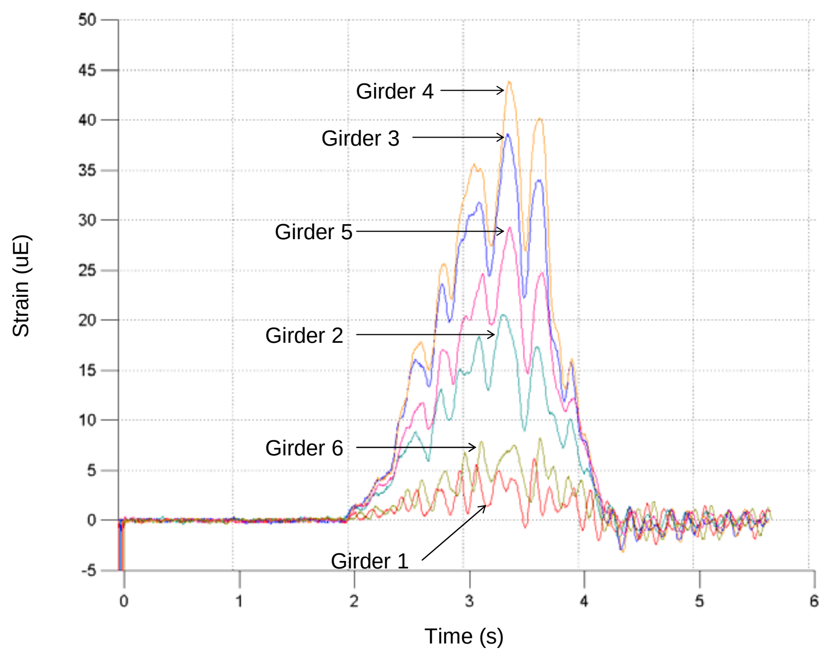

Figure A.30. Strain histories measured at bottom of girders in section #2 for case #5 (run 2).

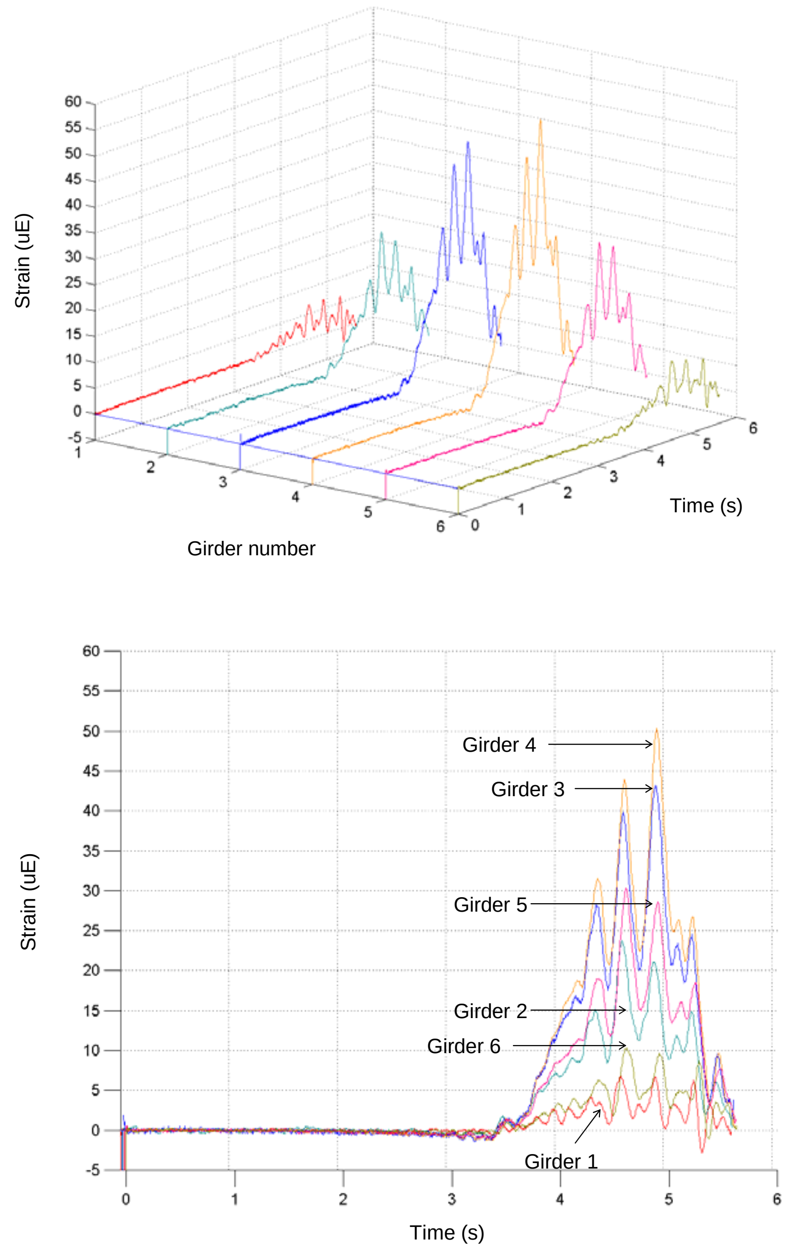

Figure A.31. Strain histories measured at bottom of girders in section #4 for case #5 (run 2).

Table A.16. The impact factor computed from strain history for the first span in the case #5.

Girder number	1			2			3			4			5			6		
	D	S	I_S	D	S	I_S	D	S	I_S	D	S	I_S	D	S	I_S	D	S	I_S
Run 1	9.3	2.2	3.2	24.6	16.3	0.51	43.6	36.6	0.19	41.9	37.9	0.11	24.1	17.6	0.37	7.4	4.8	0.54
Run 2	6.2		1.8	20.6		0.26	38.6		0.06	43.7		0.15	29.3		0.66	9.2		0.92

Table A.17. The impact factor computed from strain history for the middle span in the case 5.

Girder number	1			2			3			4			5			6		
	D	S	I_S	D	S	I_S	D	S	I_S	D	S	I_S	D	S	I_S	D	S	I_S
Run 1	10.3	2.2	3.68	27.6	16.3	0.7	47.6	36.6	0.3	46.6	37.8	0.23	25.4	17.6	0.44	8.2	4.8	0.71
Run 2	6.8		2.09	23.8		0.46	43.2		0.18	50.3		0.33	30.3		0.72	10.3		1.16

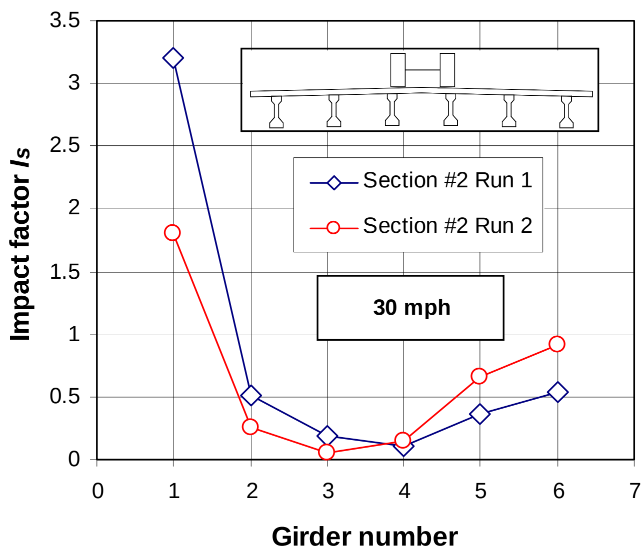

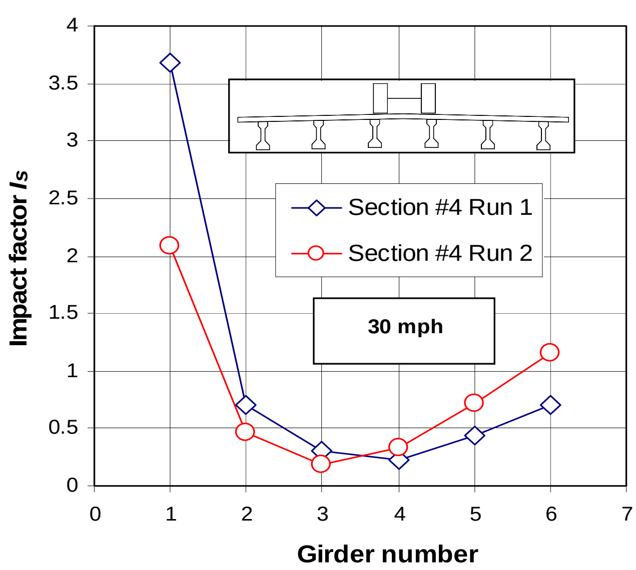

Figure A.32. Impact factor I_s for case # 5 (speed 30 mph without the plank on the bridge deck).

A.2.7. Case 6 - One truck running on the center of roadway at 50 mph without plank

This case is similar to the previous one; only the truck speed is higher and equals 50 mph (80 km/h). This speed increment causes the increase in the first span deflection by about 50 %. Furthermore it is noticeable that the calculated impact factor (I_D) increases to 1.38 (Table A.18). The increase in the impact factor is due to the increased speed of the truck in this case compared to case # 5. This also affects the strain history significantly. For both the recorded parameters there were appreciable changes in amplitude and the frequencies.

As in the previous test, symmetrical results for recorded strains were expected. However, the differences are noticeable for both runs. The reasons could be the same as mentioned in the case # 5. This consistency revealed the tendency of the strain increase for the first and second span. The increase in the strain for second span is obviously higher. Similar effects were also observed for the cases #1 and #2. It confirms the accuracy of the tests conducted and describes the real nature of the bridge behavior loaded by dynamic interacting forces. The maximum impact factor (I_S) computed from the strain history for the girder 3 equals 1.04 for the first span and 1.6 for the middle span (Tables A.19 & A.20). This increase in the impact factor for the second span (same as in the previous case) confirms the existence of the same phenomena as in the case 1, the transfer of vibrations.

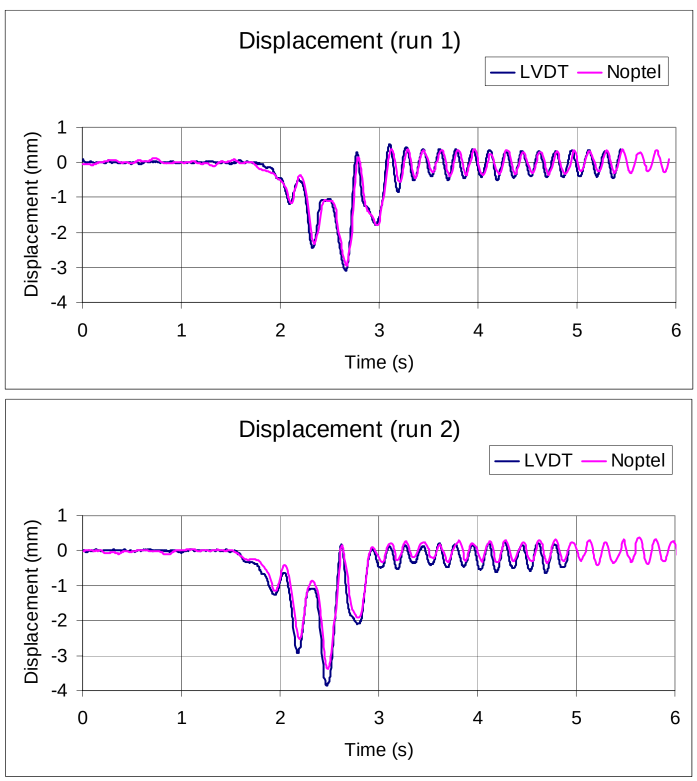

Figure A.33. The displacement of the point at the middle of girder #3 for case #6.

Table A.18. The impact factor for girder #3 from displacement history for case # 6.

	LVDT (dynamic max) [mm]	LVDT (static) [mm]	Impact factor from LVDT I_D	Noptel (dynamic max) [mm]	Noptel (static) [mm]	Impact factor from Noptel I_D
Run 1	-3.08	-1.46	1.12	-2.95	-1.94	0.52
Run 2	-3.86		1.65	-3.39		0.75

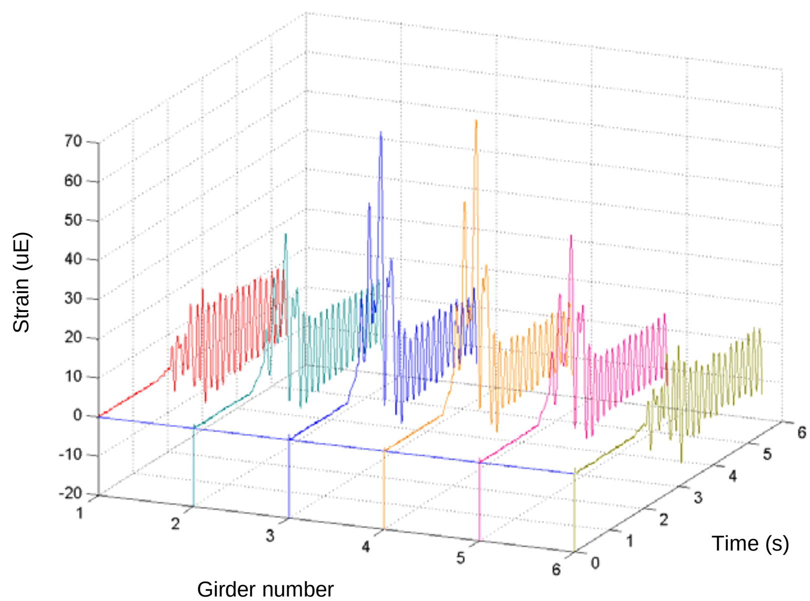

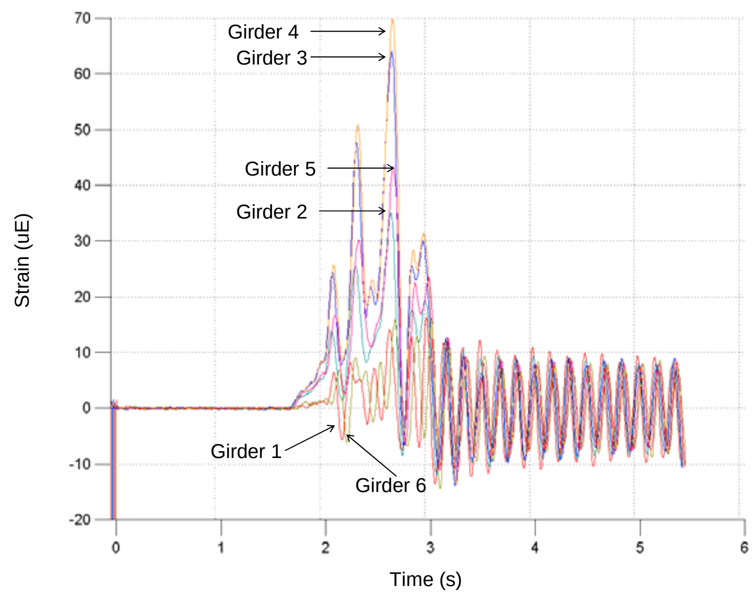

Figure A.34. Strain histories measured at bottom of girders in section #2 for case #6 (run 1).

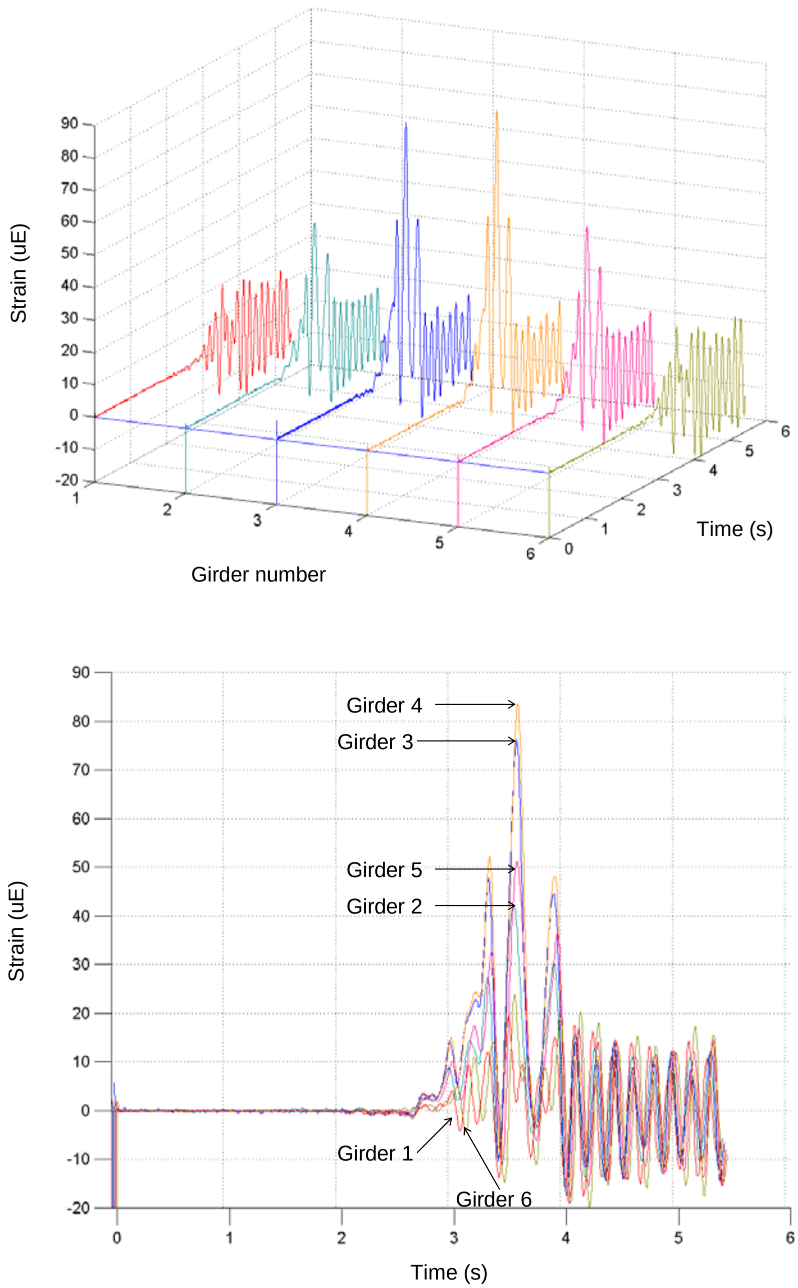

Figure A.35. Strain histories measured at bottom of girders in section #4 for case #6 (run 1).

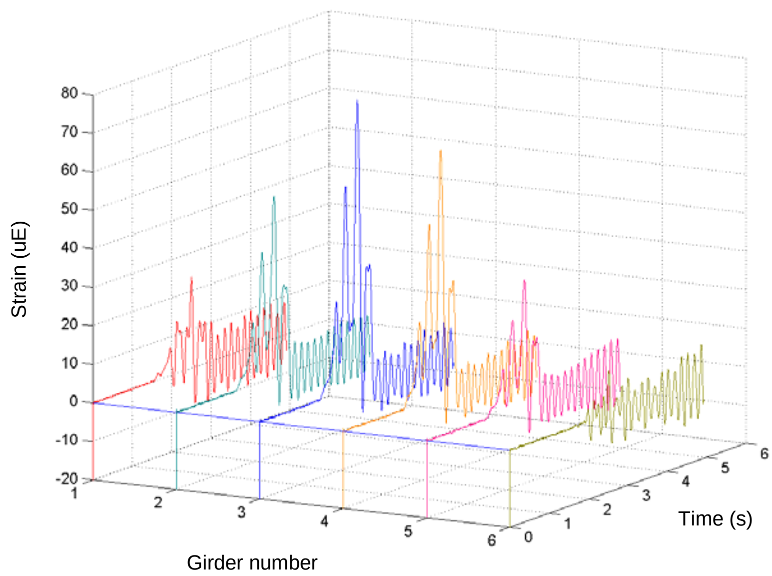

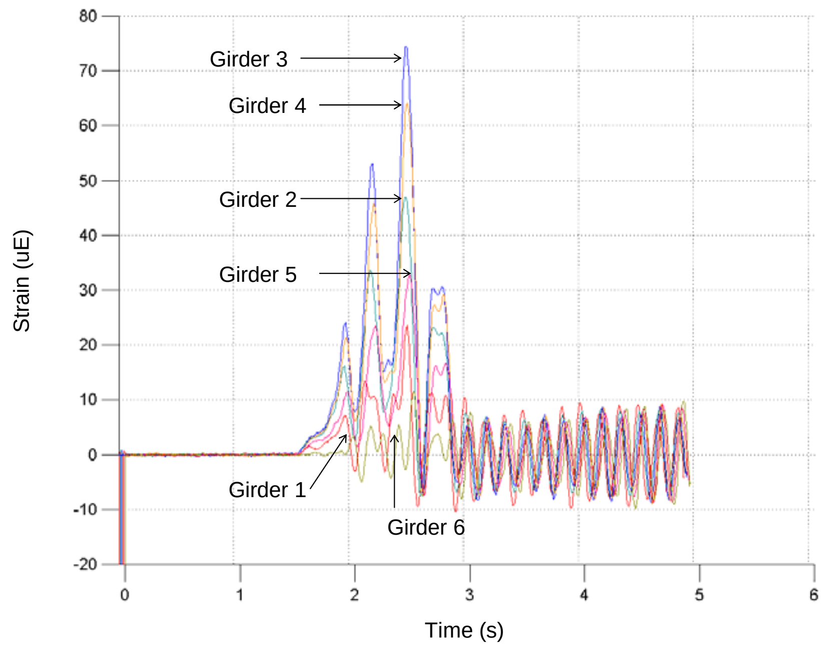

Figure A.36. Strain histories measured at bottom of girders in section #2 for case #6 (run 2).

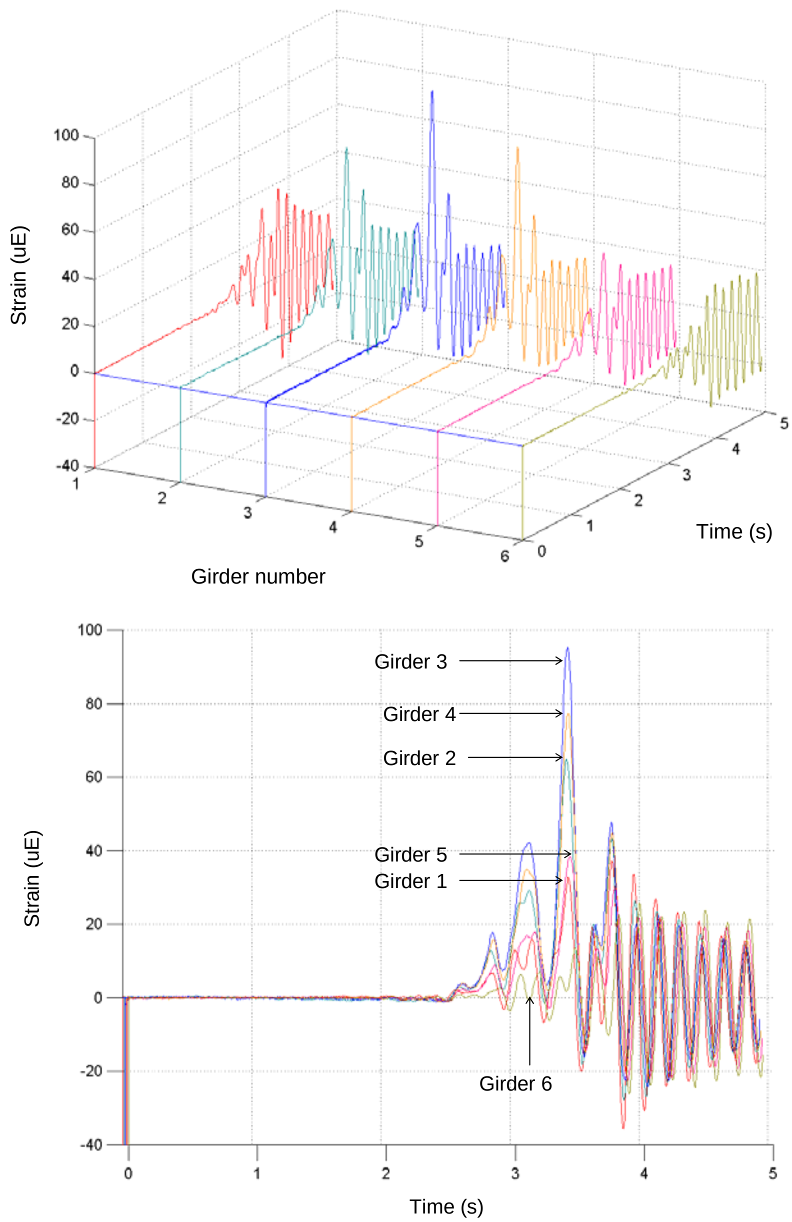

Figure A.37. Strain histories measured at bottom of girders in section #4 for case #6 (run 2).

Table A.19. The impact factor computed from strain history for the first span in the case #6.

Girder number	1			2			3			4			5			6		
	D	S	I_S	D	S	I_S	D	S	I_S	D	S	I_S	D	S	I_S	D	S	I_S
Run 1	16.2	2.2	6.36	35.1	16.3	1.15	64.0	36.6	0.75	69.2	37.8	0.83	43.4	17.6	1.47	17.7	4.8	2.69
Run 2	23.6		9.72	47.1		1.89	74.5		1.04	62.7		0.66	32.9		0.87	12.6		1.62

Table A.20. The impact factor computed from strain history for the middle span in the case #6.

Girder number	1			2			3			4			5			6		
	D	S	I_S	D	S	I_S	D	S	I_S	D	S	I_S	D	S	I_S	D	S	I_S
Run 1	19.5	2.2	7.86	42.0	16.3	1.58	76.2	36.6	1.08	83.5	37.8	1.21	51.2	17.6	1.91	24.0	4.8	4.0
Run 2	37.2		15.9	64.9		2.98	95.3		1.6	77.5		1.05	38.5		1.19	25.8		4.38

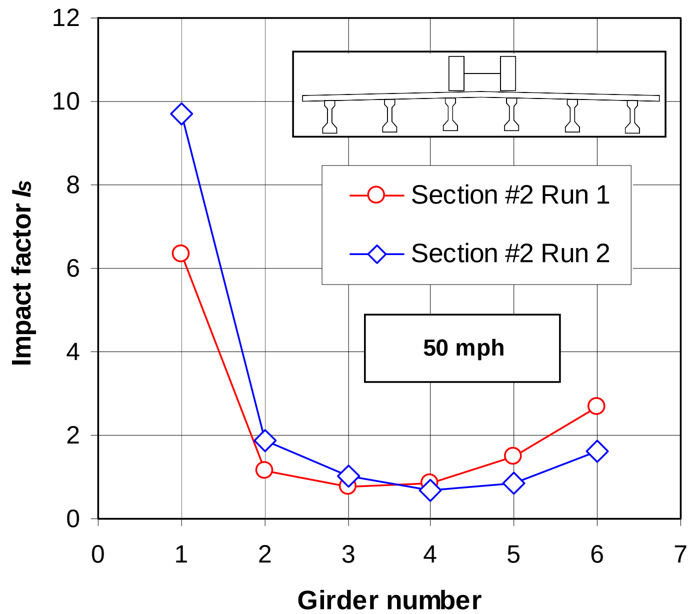

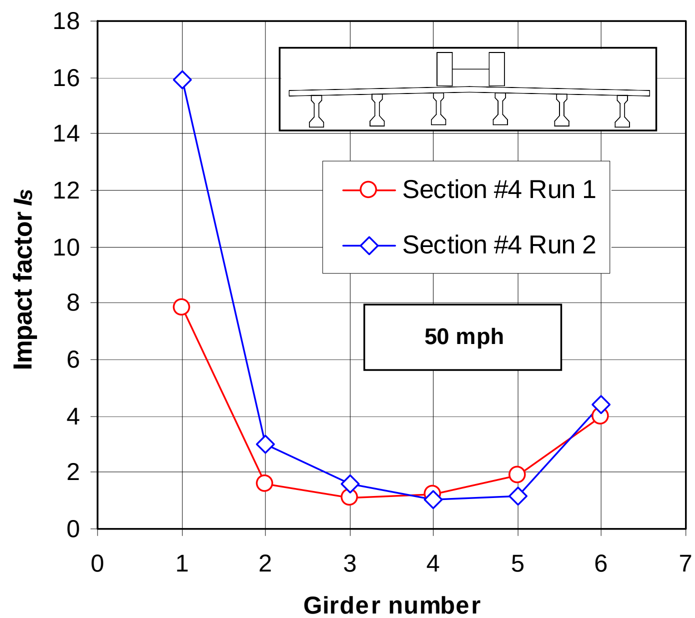

Figure A.38. Impact factor I_s for case # 6 (speed 50 mph without the plank on the bridge deck).

A.2.8. Case 7 - One truck running on the center of roadway at 30 mph with plank

In this case the plank was placed on the bridge deck. The truck crossed the bridge on the center of the roadway at 30 mph (48 km/h). The results were expected to be symmetric. This situation took place for the run 1 (see figures A.40 and A.41). Small differences are visible for the run 2 (Figure A.42 and A.43). The difference in the readings and unsymmetry could be due to the inaccuracy in maintaining the constant speed and driving accurately along the center line of the roadway for both the runs.

The impact factor I_D calculated from deflection for the first span reached the value 1.63. Obviously, this increase, compared to case 5 is closely related to the existence of the artificial obstacle like the plank. Increase in the deflection is about 100%. It confirms that additional vibrations created due to the plank are automatically transmitted to the bridge deck. It shows significant sensitivity of structures like bridges to extra-imposed forces. Furthermore, all figures verify bigger dynamic changes of displacement and strains amplitudes (the same like for all tests with the plank). Maximum impact factor (I_S) reached the value 0.63 for the second span. This fact is consistent with all analyzed cases and theoretical solutions for multi element beam structures.

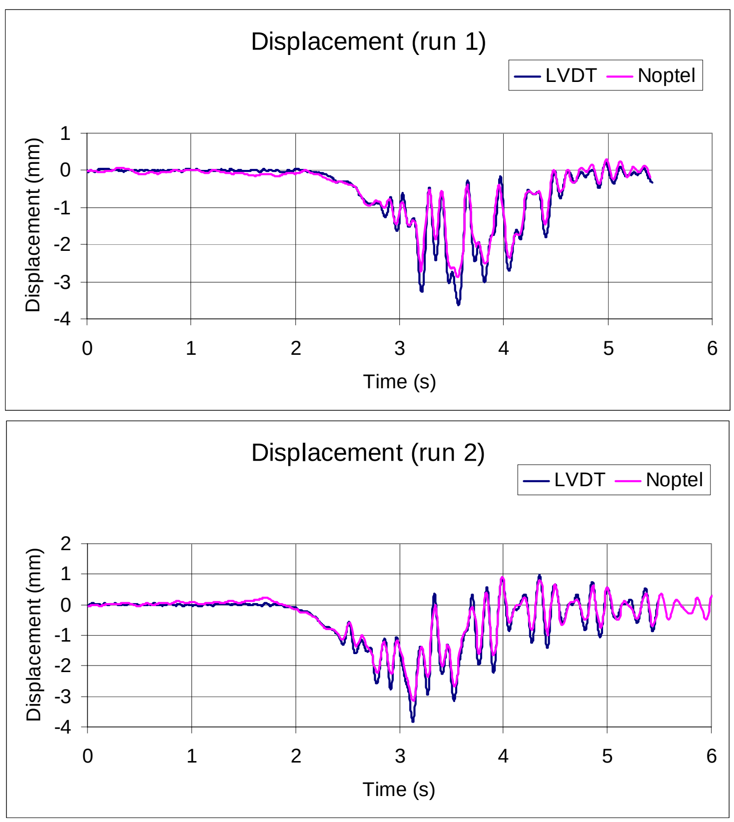

Figure A.39. The displacement of the point at the middle of girder #3 for case # 7.

Table A.21. The impact factor for girder # 3 from displacement history for case # 7.

	LVDT (dynamic max) [mm]	LVDT (static) [mm]	Impact factor from LVDT I_D	Noptel (dynamic max) [mm]	Noptel (static) [mm]	Impact factor from Noptel I_D
Run 1	-3.62	-1.46	1.48	-2.88	-1.94	0.48
Run 2	-3.83		1.63	-3.15		0.62

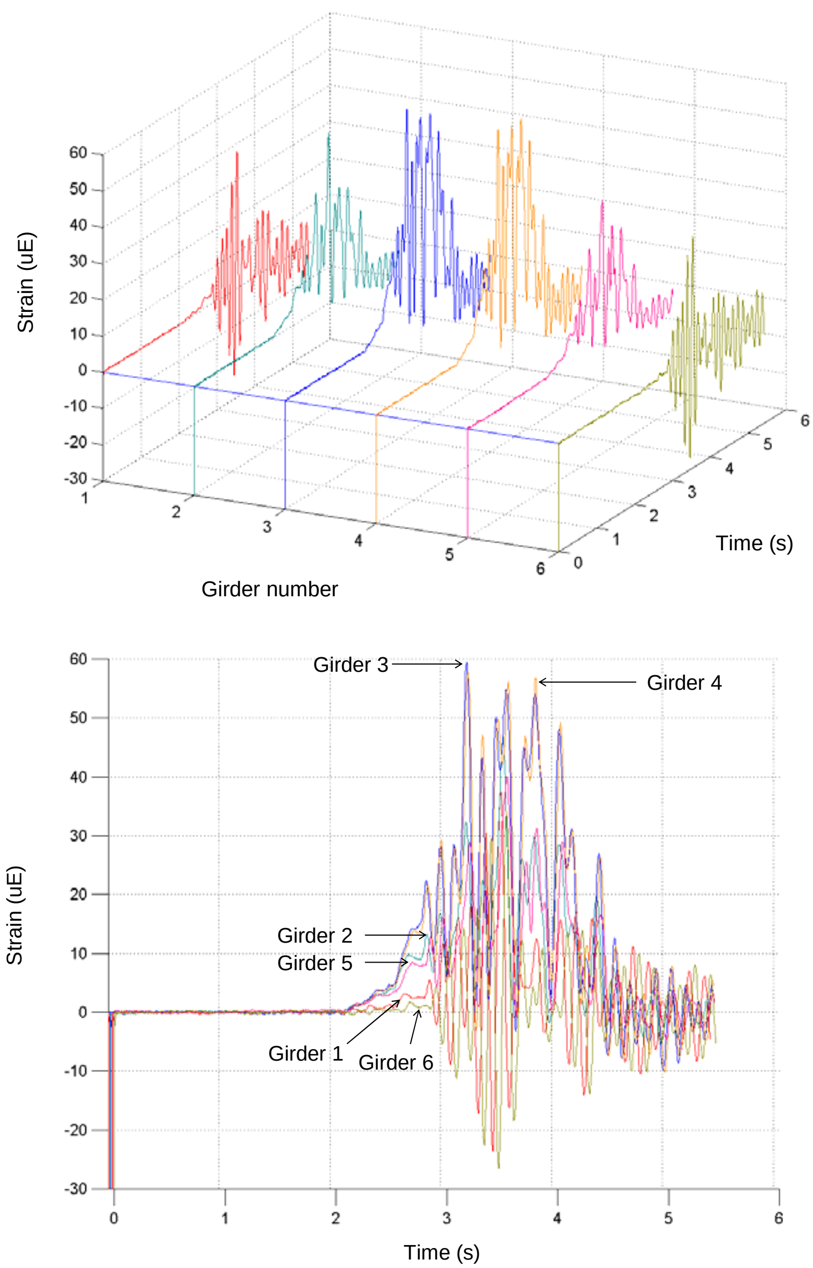

Figure A.40. Strain histories measured at bottom of girders in section #2 for case #7 (run 1).

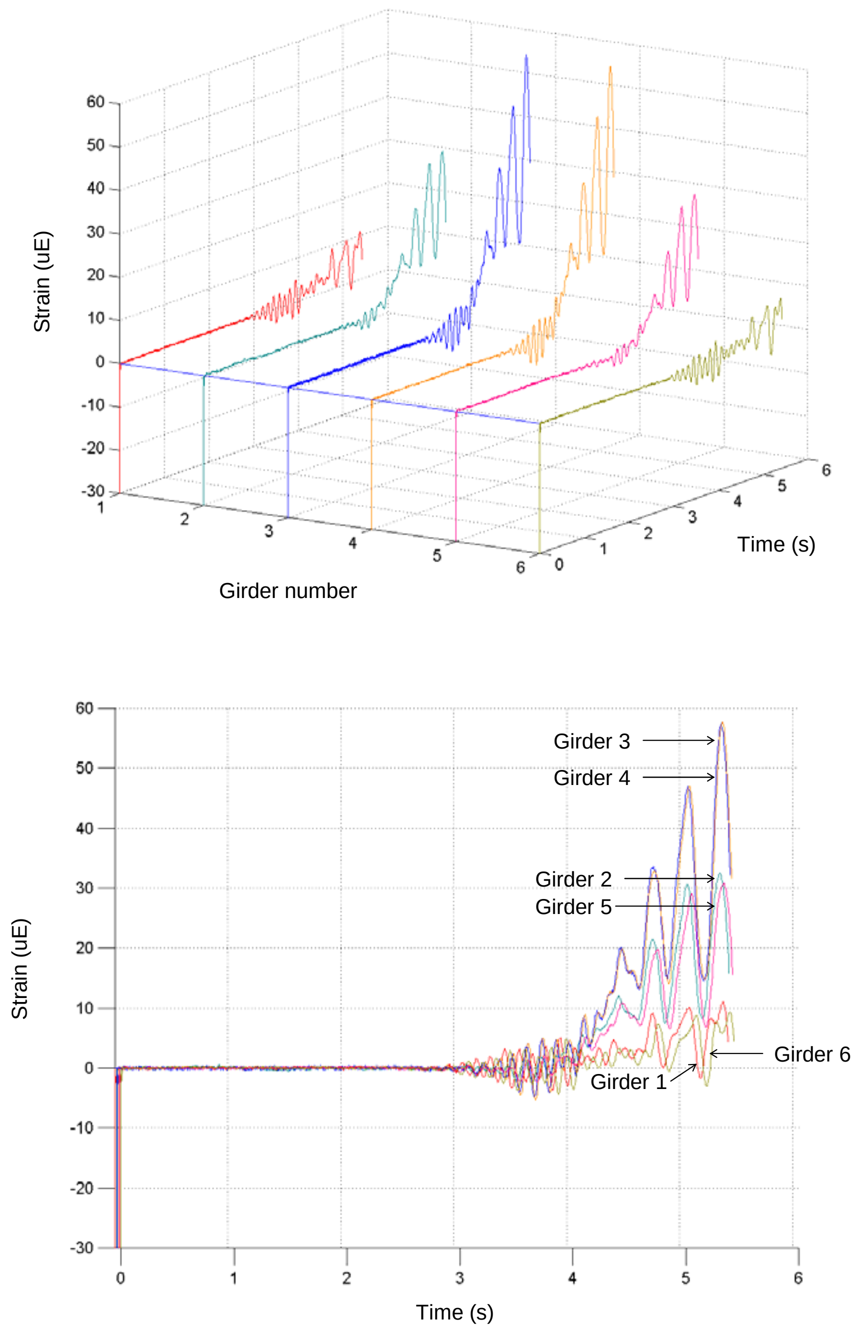

Figure A.41. Strain histories measured at bottom of girders in section #4 for case #7 (run 1).

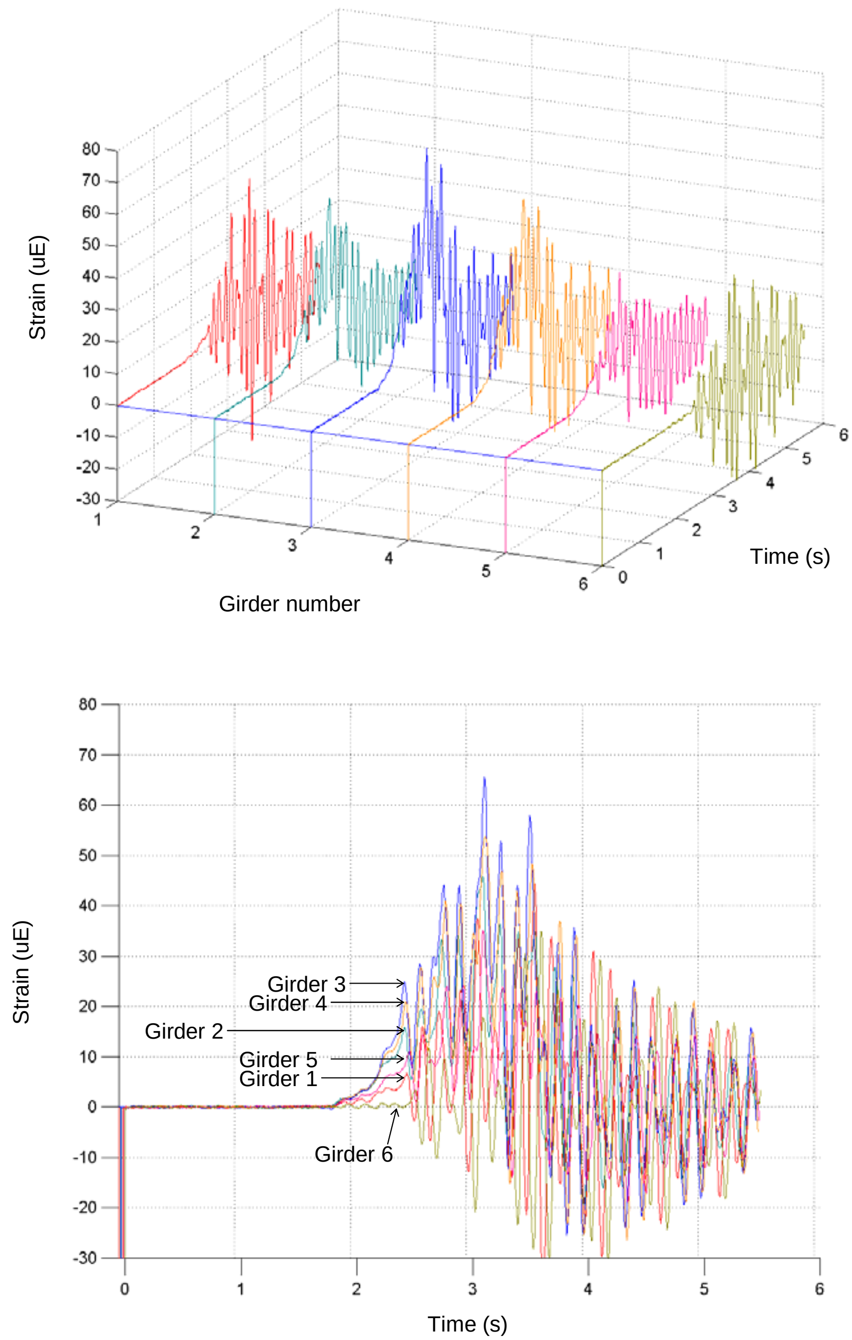

Figure A.42. Strain histories measured at bottom of girders in section #2 for case #7 (run 2).

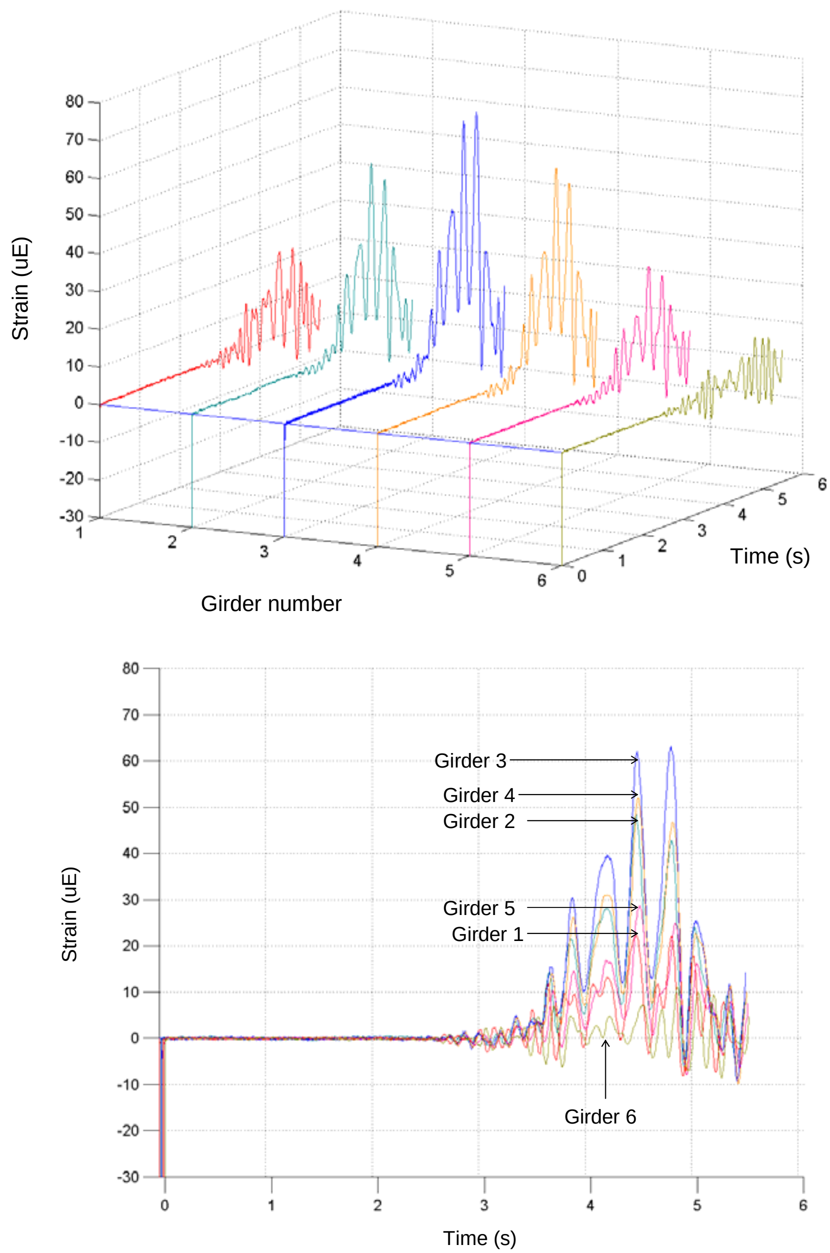

Figure A.43. Strain histories measured at bottom of girders in section #4 for case #7 (run 2).

Table A.22. The impact factor computed from strain history for the first span in the case #7.

Girder number	1			2			3			4			5			6		
	D	S	I_S	D	S	I_S	D	S	I_S	D	S	I_S	D	S	I_S	D	S	I_S
Run 1	37.9	2.2	16.23	46.8	16.3	1.87	59.5	36.6	0.63	57.3	37.8	0.52	40.0	17.6	1.27	34.3	4.8	6.15
Run 2	44.8		19.36	46.0		1.82	65.6		0.79	53.0		0.40	35.0		0.99	34.0		6.08

Table A.23. The impact factor computed from strain history for the middle span in the case # 7.

Girder number	1			2			3			4			5			6		
	D	S	I_S	D	S	I_S	D	S	I_S	D	S	I_S	D	S	I_S	D	S	I_S
Run 1	11.1	2.2	4.05	32.5	16.3	0.99	57.6	36.6	0.57	57.7	37.8	0.53	30.9	17.6	0.76	9.4	4.8	0.96
Run 2	22.4		9.18	48.4		1.97	63.2		0.73	52.1		0.38	28.6		0.63	11.2		1.33

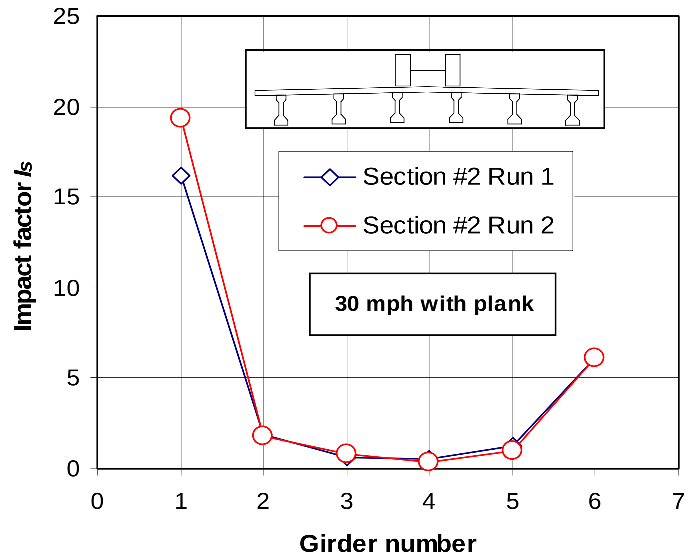

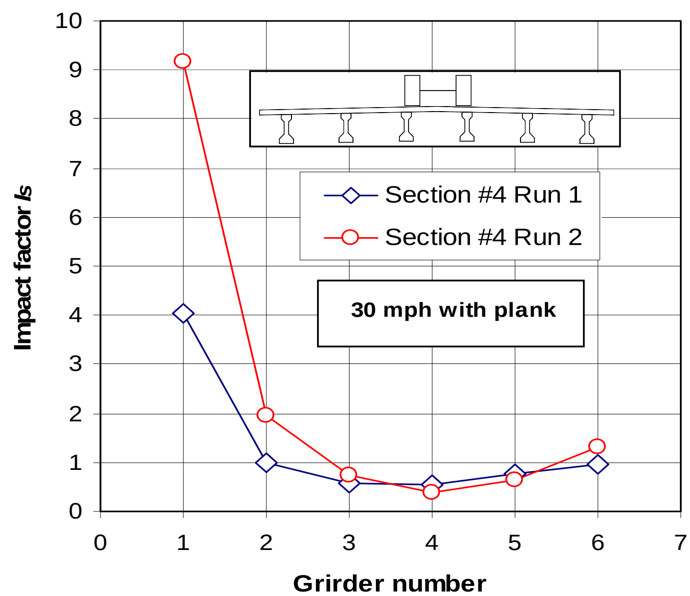

Figure A.44. Impact factor I_S for case # 7 (speed 30 mph with the plank on the bridge deck).

A.2.9. Case 8 - One truck running on the center of roadway at 50 mph with plank

In this case also, as in previous cases, a symmetrical effect of the bridge behavior was expected. Results presented below clearly show that the effect was symmetrical as expected (except for run 2 for the section #4). Comparison with the previous case shows the influence of the increased speed. For the span deflection measured, this difference is about 15-20%. This increase is significant for the strains and for the section #2 it is about 70%. This clearly demonstrates influence of additional vibrations caused by introducing wooden plank as obstacle. Computed on this basis, impact factors (I_S) reached the maximum values for the first span. For the girder #3 this value equals 1.64. In the next phase, when the truck is crossing this obstacle, these vibrations are slowly extinguished by the bridge. Therefore, for the next span the recorded strains are smaller and I_S values also decline. Especially recorded readings in the section # 2 indicate the beginning of free vibrations, when the truck is leaving the first span.

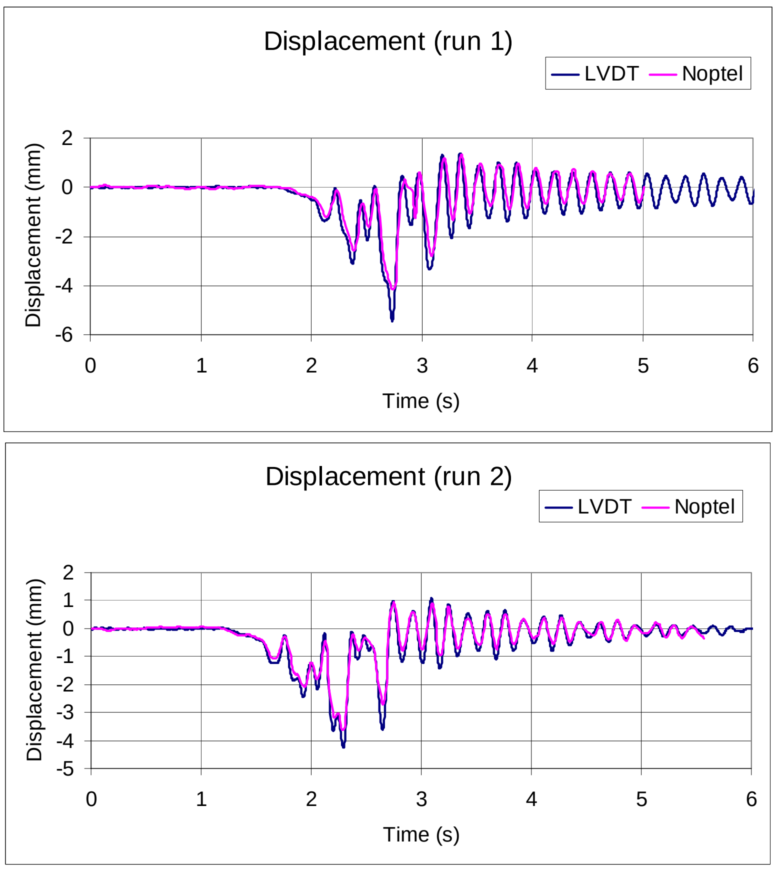

Figure A.45. The displacement of the point at the middle of girder #3 for case 8.

Table A.24. The impact factor for girder #3 from displacement history for case #8.

	LVDT (dynamic max) [mm]	LVDT (static) [mm]	Impact factor from LVDT I_D	Noptel (dynamic max) [mm]	Noptel (static) [mm]	Impact factor from Noptel I_D
Run 1	-5.47	-1.46	2.75	-4.16	-1.94	1.14
Run 2	-4.26		1.92	-3.61		0.86
Average			2.34			1.0

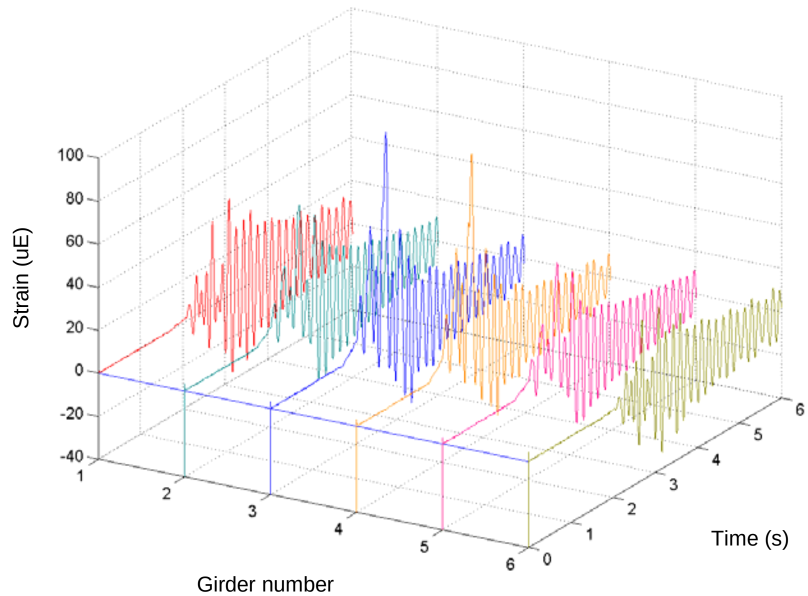

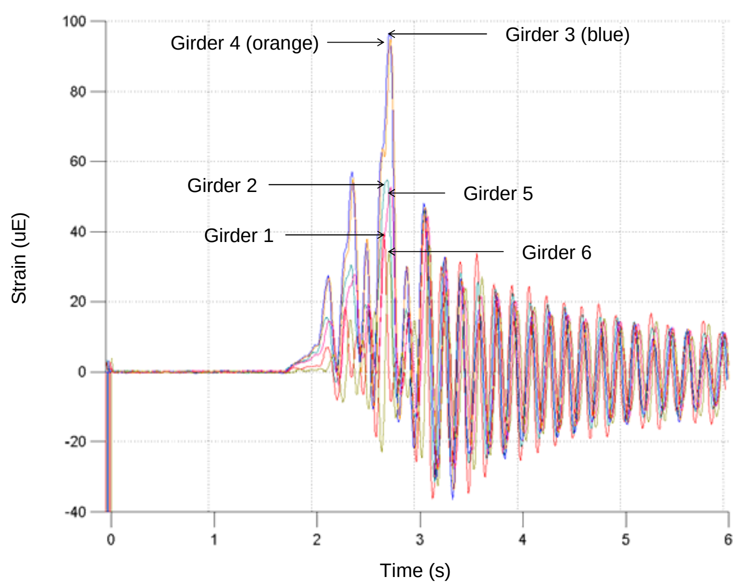

Figure A.46. Strain histories measured at bottom of girders in section #2 for case #8 (run 1).

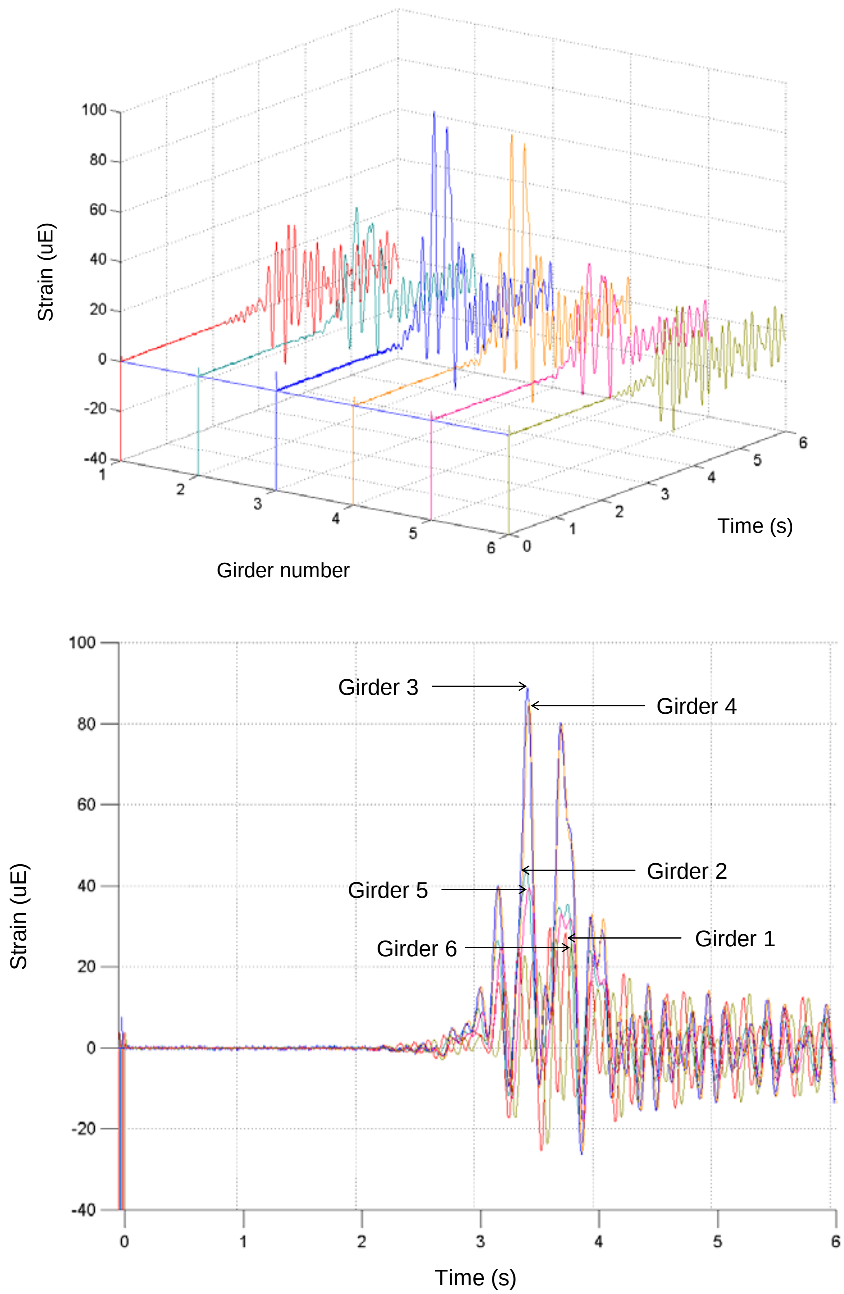

Figure A.47. Strain histories measured at bottom of girders in section #4 for case #8 (run 1).

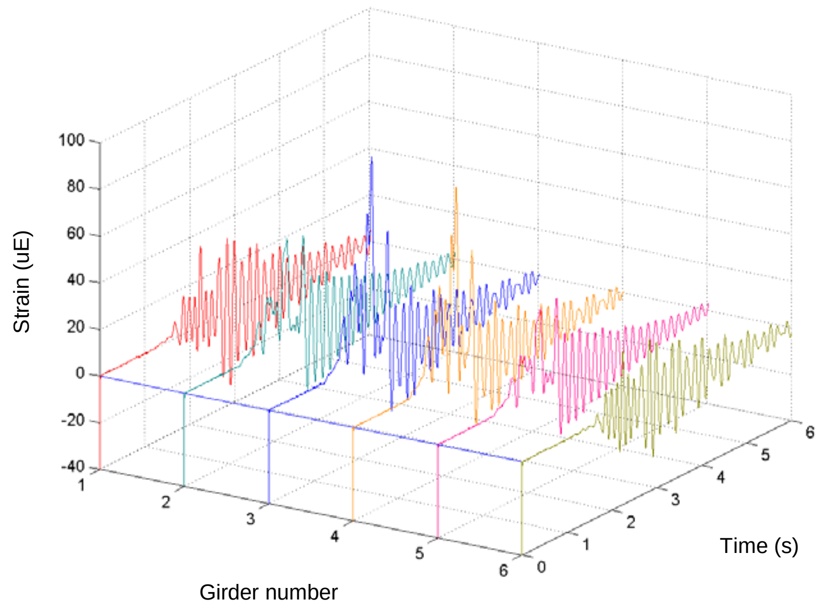

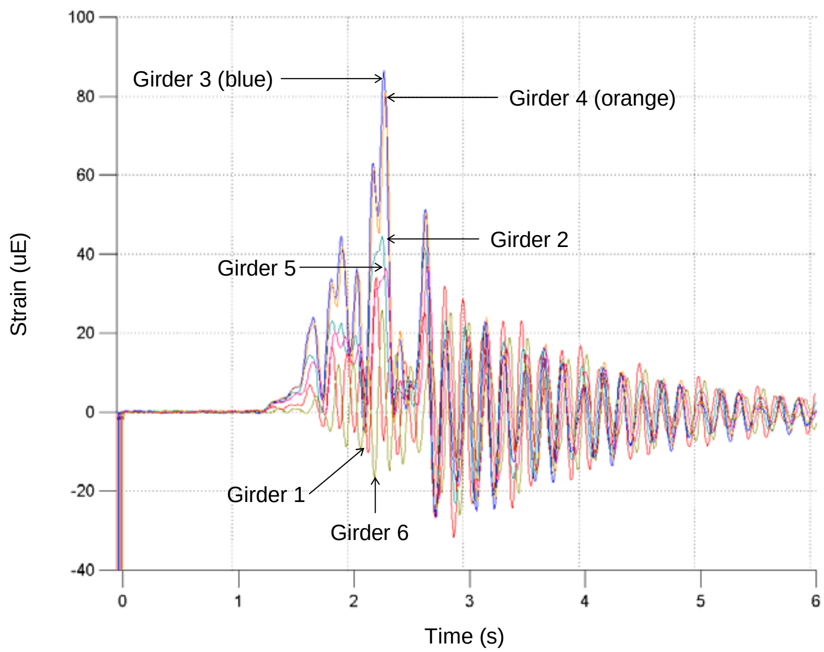

Figure A.48. Strain histories measured at bottom of girders in section #2 for case #8 (run 2).

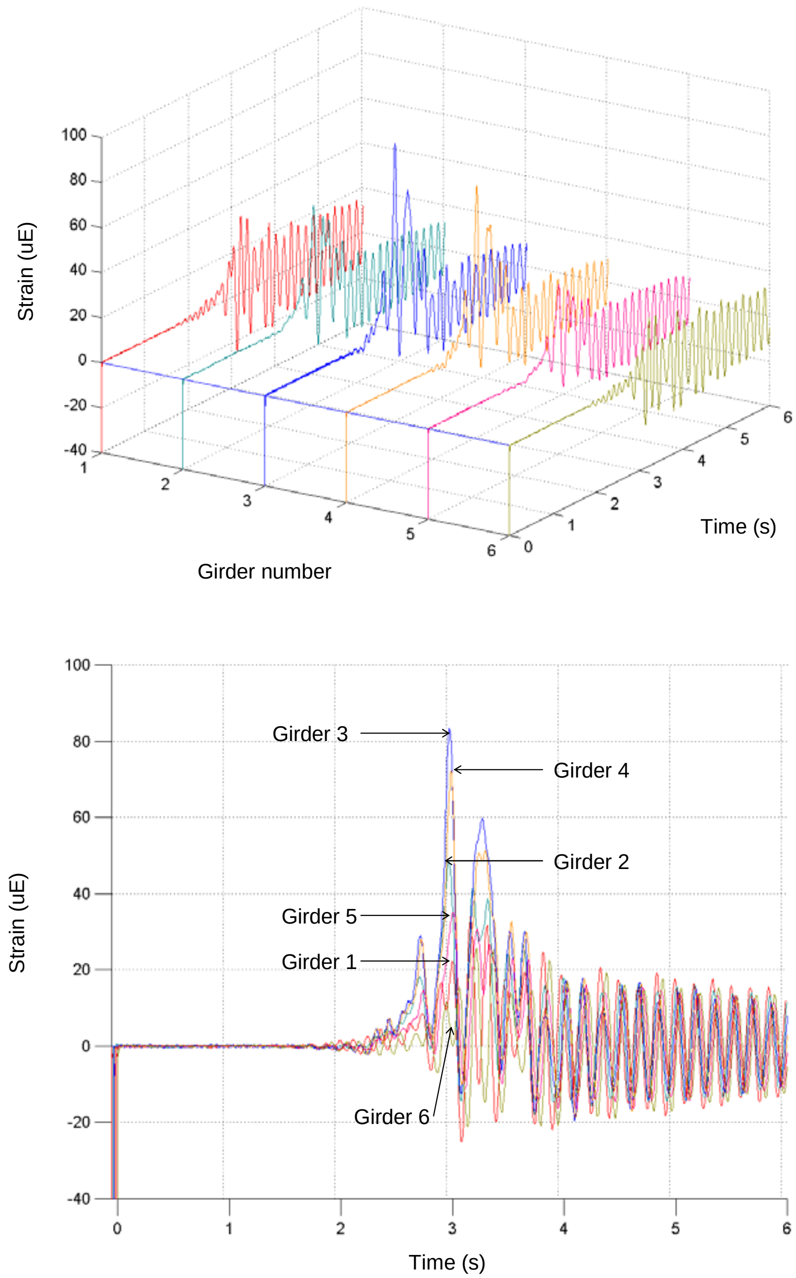

Figure A.49. Strain histories measured at bottom of girders in section #4 for case #8 (run 2).

Table A.25. The impact factor computed from strain history for the first span in the case #8.

Girder number	1			2			3			4			5			6		
	D	S	I_S	D	S	I_S	D	S	I_S	D	S	I_S	D	S	I_S	D	S	I_S
Run 1	45.0	2.2	19.45	54.7	16.3	2.36	96.7	36.6	1.64	92.9	37.8	1.46	52.8	17.6	2.00	36.7	4.8	6.65
Run 2	34.0		15.40	44.5		1.73	86.4		1.36	78.8		1.08	37.2		1.11	26.4		4.50

Table A.26. The impact factor computed from strain history for the middle span in the case #8.

Girder number	1			2			3			4			5			6		
	D	S	I_S	D	S	I_S	D	S	I_S	D	S	I_S	D	S	I_S	D	S	I_S
Run 1	29.5	2.2	12.41	44.1	16.3	1.71	88.8	36.6	1.43	85.4	37.8	1.26	39.4	17.6	1.24	26.7	4.8	4.56
Run 2	34.1		14.5	48.3		1.96	83.3		1.27	72.1		0.91	35.0		0.99	25.8		4.38

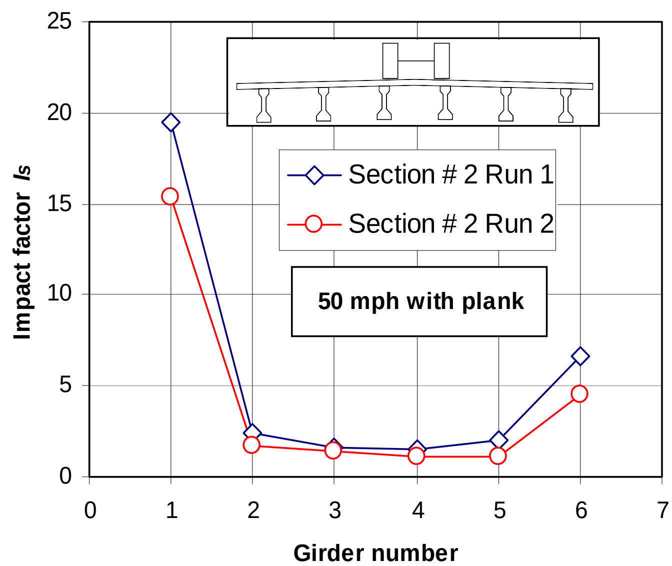

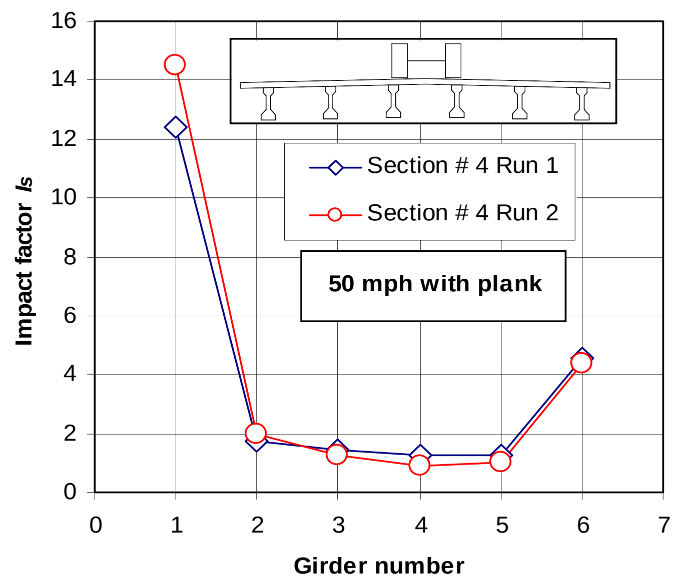

Figure A.50. Impact factor I_s for case # 8 (speed 50 mph with the plank on the bridge deck).

A.2.10. Case 9 - Two trucks running at the centers of both lanes at 30 mph without plank

The most important case, which has a big influence on the bridge behavior, is the situation with two trucks on the bridge at the same time. Such coincidence was studied in next two tests. For the first one the trucks crossed the bridge side by side at 30 mph (48 km/h). Differences in results are obvious. The displacement occurred is comparable with the case, when the truck was crossing the bridge on the center with the plank placed on the deck. However, the shape of recorded deflection curve is very smooth. Maximum dynamic factor (I_D) reached the value 0.25. The study of the strain history shows very interesting results. Figures presented below clearly demonstrate that the right side of the bridge (girder # 4) is more loaded than the symmetric girder # 3. This situation appears in the first span and increases for the second span. This behavior could be attributed to the external factors such as the bigger depression on the right lane and the threshold effect in the joint between asphalt and concrete slab just before the bridge deck. This higher dynamic effect of the truck running on the right lane is transmitted directly from the truck suspension system through wheels to the bridge slab. The maximum impact factor (I_S) computed from strain history equals 0.2 for the first span and 0.23 for the second.

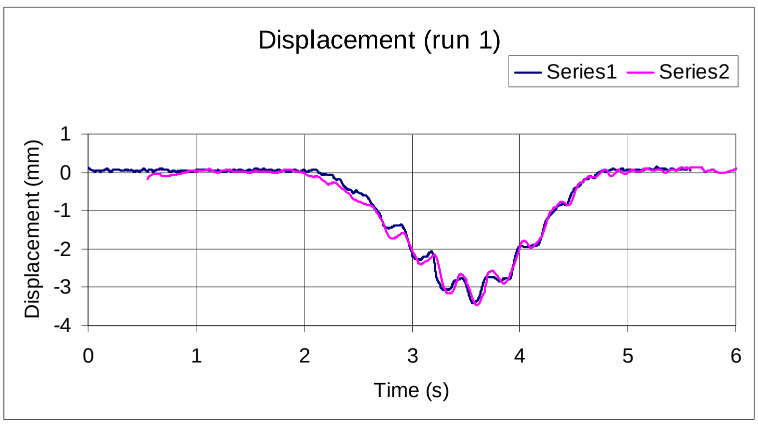

Figure A.51. The displacement of the point at the middle of girder #3 for case #9.

Table A.27. The impact factor for girder # 3 from displacement history for case #9.

	LVDT (dynamic max) [mm]	LVDT (static) [mm]	Impact factor from LVDT I_D	Noptel (dynamic max) [mm]	Noptel (static) [mm]	Impact factor from Noptel I_D
Run 1	-3.40	-2.73	0.25	-3.47	-3.15	0.10

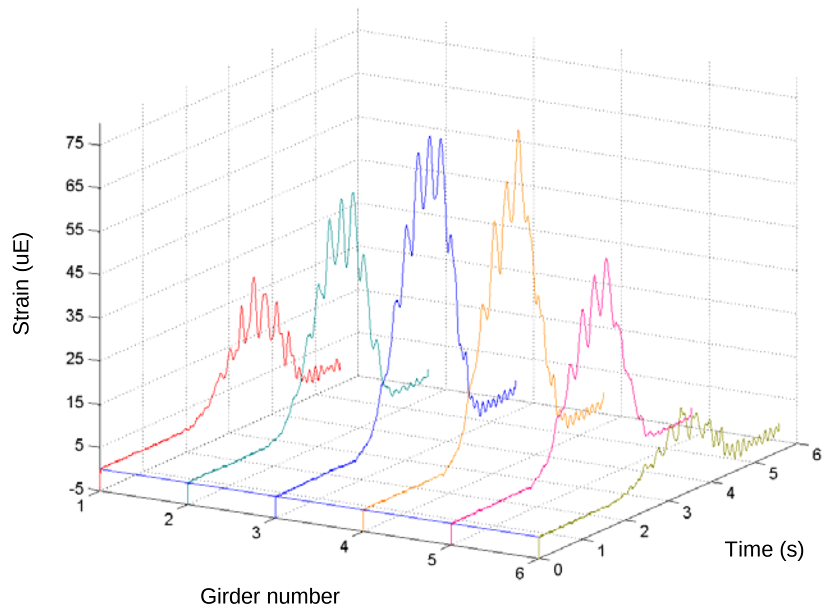

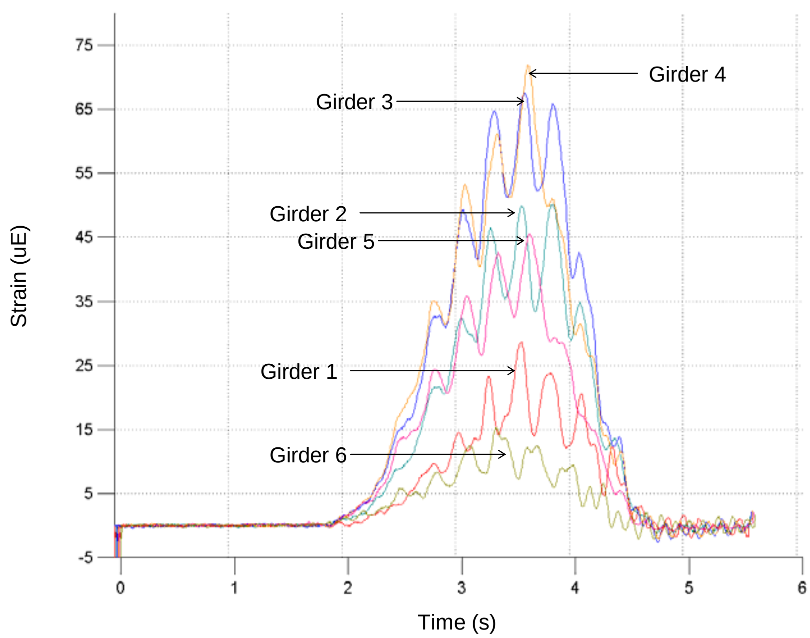

Figure A.52. Strain histories measured at bottom of girders in section #2 for case #9 (run 1).

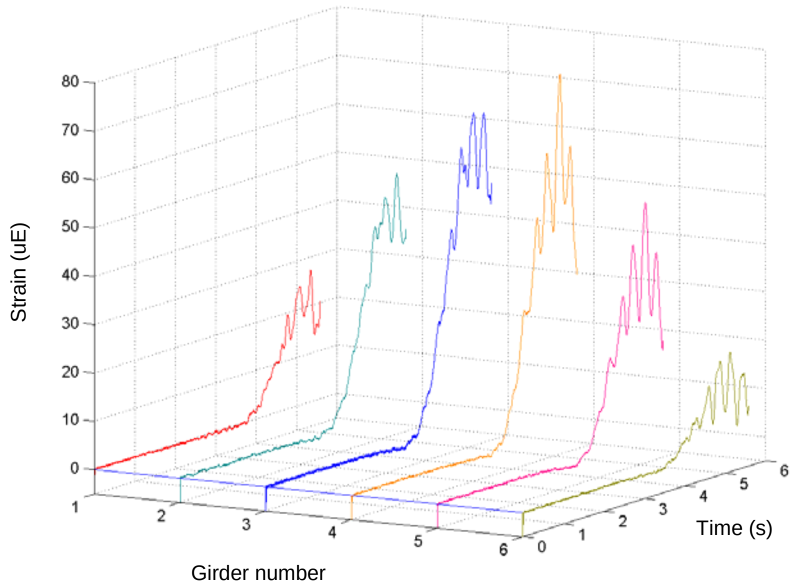

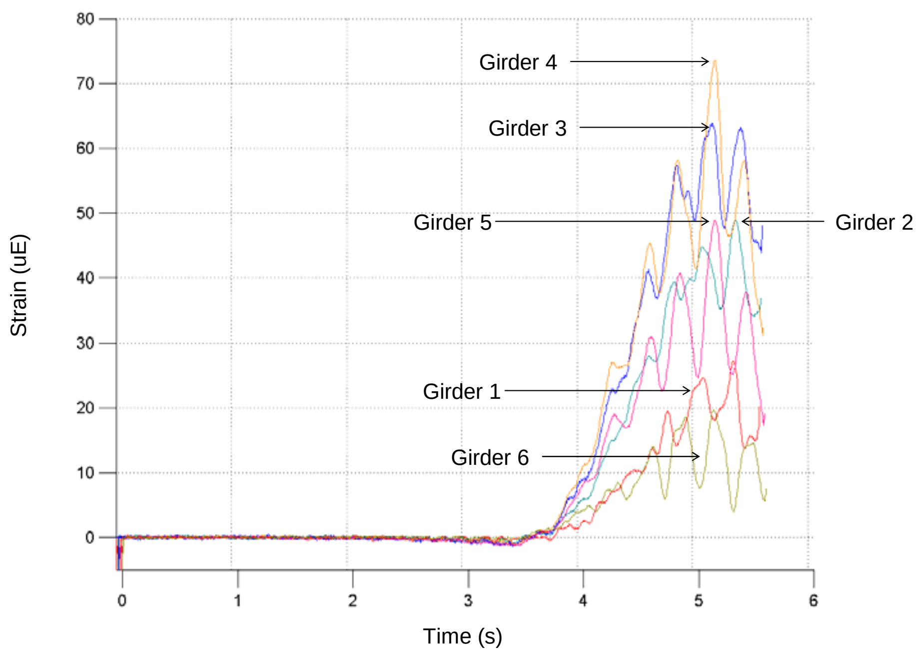

Figure A.53. Strain histories measured at bottom of girders in section #4 for case #9 (run 1).

Table A.28. The impact factor computed from strain history for the first span in the case #9.

Girder number	1			2			3			4			5			6		
	D	S	I_S	D	S	I_S	D	S	I_S	D	S	I_S	D	S	I_S	D	S	I_S
Run 1	28.7	10.6	1.71	50.1	37.7	0.33	67.5	60.5	0.12	71.5	59.6	0.20	45.5	41.0	0.11	16.7	12.1	0.38

Table A.29. The impact factor computed from strain history for the middle span in the case # 9.

Girder number	1			2			3			4			5			6		
	D	S	I_S	D	S	I_S	D	S	I_S	D	S	I_S	D	S	I_S	D	S	I_S
Run 1	27.3	10.6	1.58	49.0	37.7	0.30	64.0	60.5	0.06	73.6	59.6	0.23	49.0	41.0	0.19	19.7	12.1	0.63

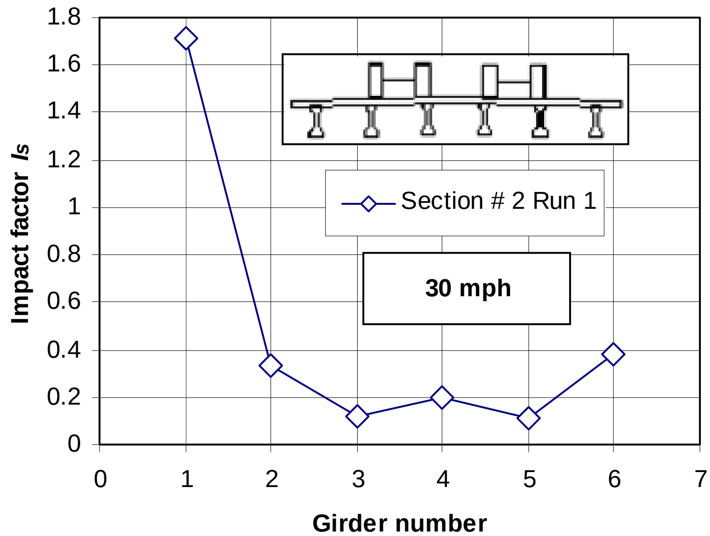

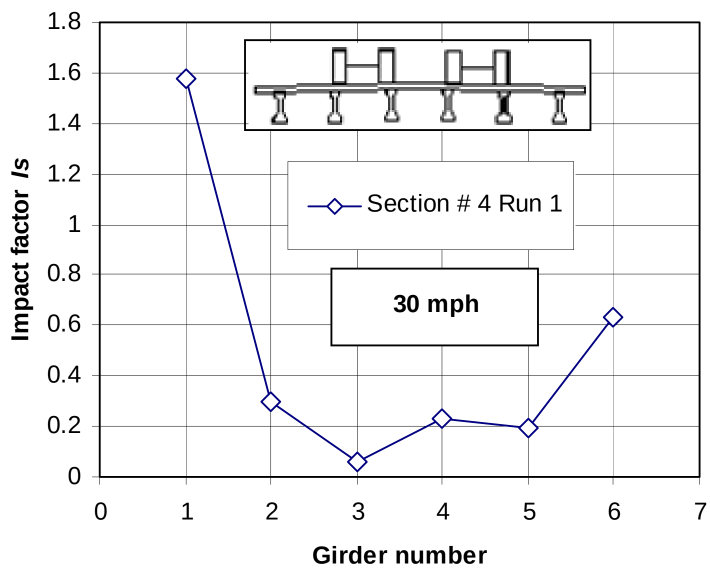

Figure A.54. Impact factor I_S for case # 9 (speed 30 mph without the plank on the bridge deck, two trucks).

A.2.11. Case 10 - Two trucks running at the centers of both lanes at 50 mph without plank

This test was performed using two trucks running side by side at 50 mph (80 km/h). The previous cases have confirmed that the truck speed influences the increase of the span deflection and recorded strains. For girder #3 the increase is about 25% for the measured displacement at the bottom. Also, the value of the calculated impact factor (I_D) is higher and equals 0.56. Strain histories presented below show unsymmetrical shape. It indicates that the external conditions like the bridge approach affect the strains for the girder #4. In this case, the impact factor (I_S) reaches the value 0.77 for the middle span. There were appreciable differences in the strain histories for girders 1 & 6 (the first span, Figure A.57). At the same time, when the truck is leaving the first span, strain amplitude for the girder # 6 decreases slowly while for the girder #1 it increases slowly. The main reason for this situation could be the small difference between the speeds of these trucks. The confirmation of this fact is demonstrated in the Figure A.57.

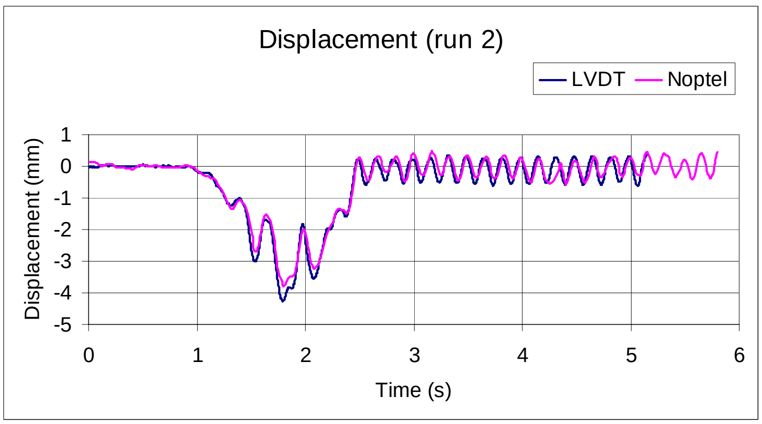

Figure A.55. The displacement of the point at the middle of girder #3 for case #10.

Table A.30. The impact factor for girder #3 from displacement history for case #10.

	LVDT (dynamic max) [mm]	LVDT (static) [mm]	Impact factor from LVDT I_D	Noptel (dynamic max) [mm]	Noptel (static) [mm]	Impact factor from Noptel I_D
Run 1	-4.27	-2.73	0.56	-3.78	-3.15	0.2

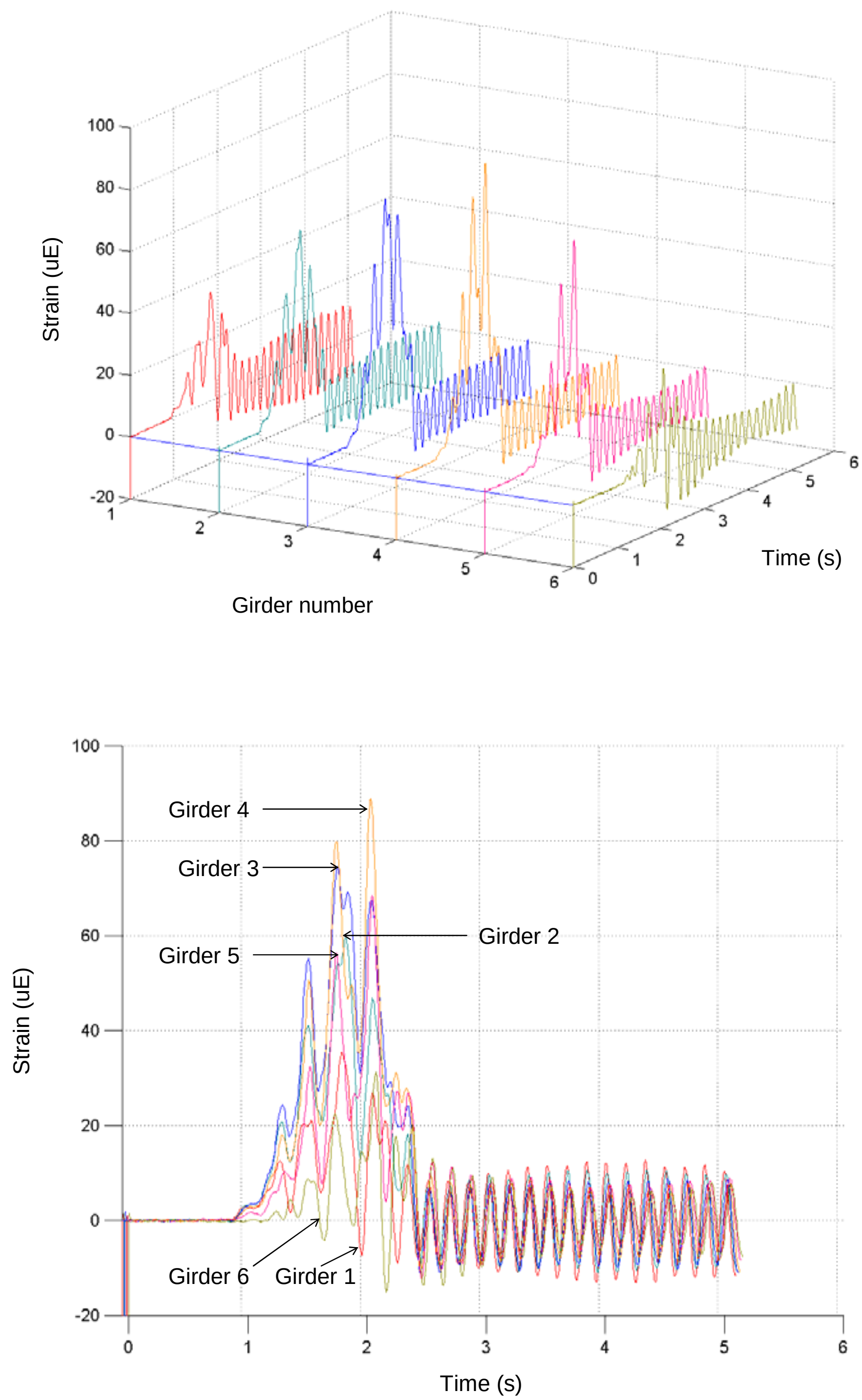

Figure A.56. Strain histories measured at bottom of girders in section #2 for case #10 (run 1).

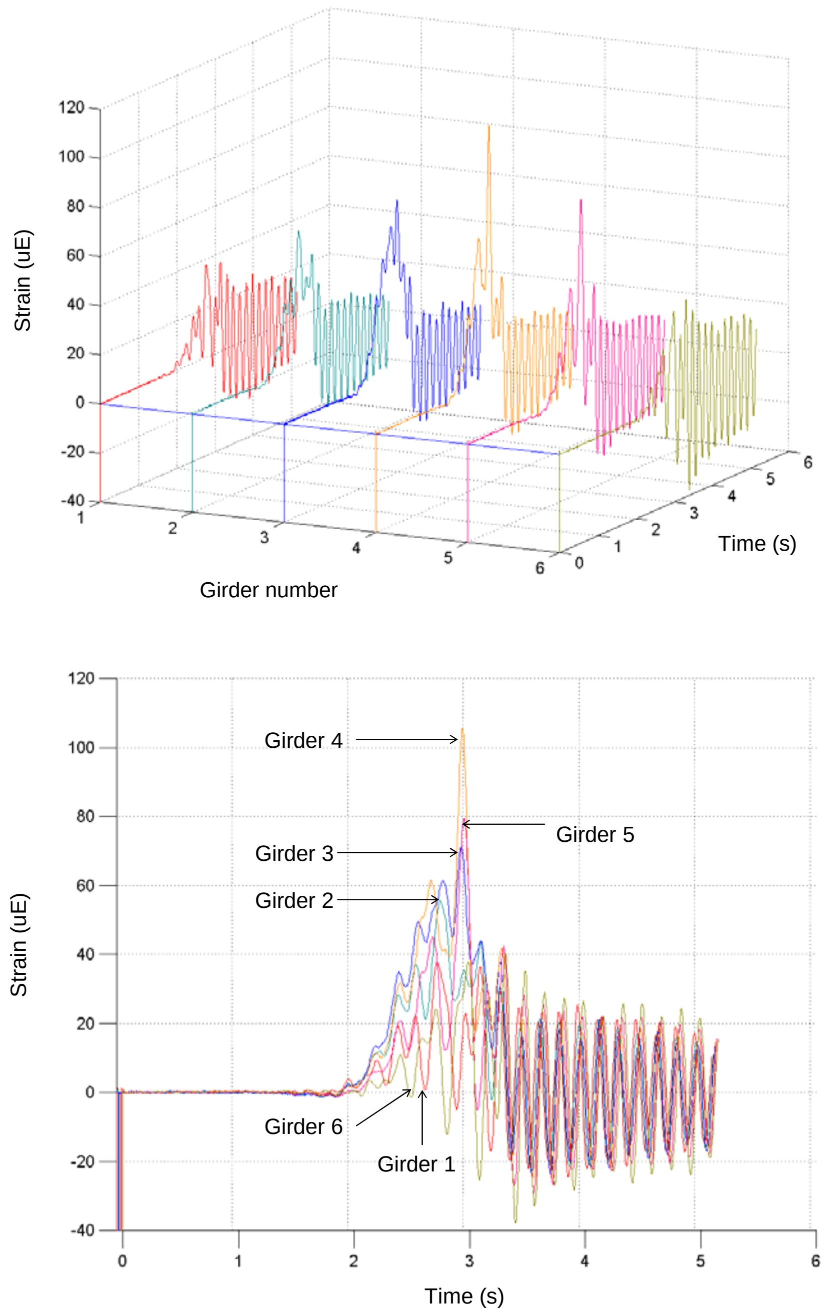

Figure A.57. Strain histories measured at bottom of girders in section #4 for case #10 (run 1).

Table A.31. The impact factor calculated from strain history for east span in case #10.

Girder number	1			2			3			4			5			6		
	D	S	I_S	D	S	I_S	D	S	I_S	D	S	I_S	D	S	I_S	D	S	I_S
Run 1	35.4	10.6	2.34	59.7	37.7	0.58	74.5	60.5	0.23	89.7	59.6	0.51	68.6	41.0	0.67	33.0	12.1	1.73

Table A.32. The impact factor computed from strain history for the middle span in the case #10.

Girder number	1			2			3			4			5			6		
	D	S	I_S	D	S	I_S	D	S	I_S	D	S	I_S	D	S	I_S	D	S	I_S
Run 1	37.8	10.6	2.57	55.5	37.7	0.47	71.0	60.5	0.17	105.6	59.6	0.77	79.3	41.0	0.93	40.2	12.1	2.32

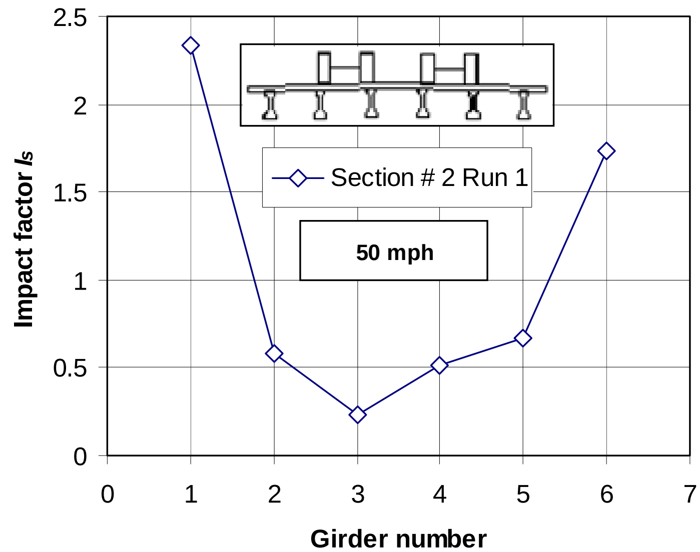

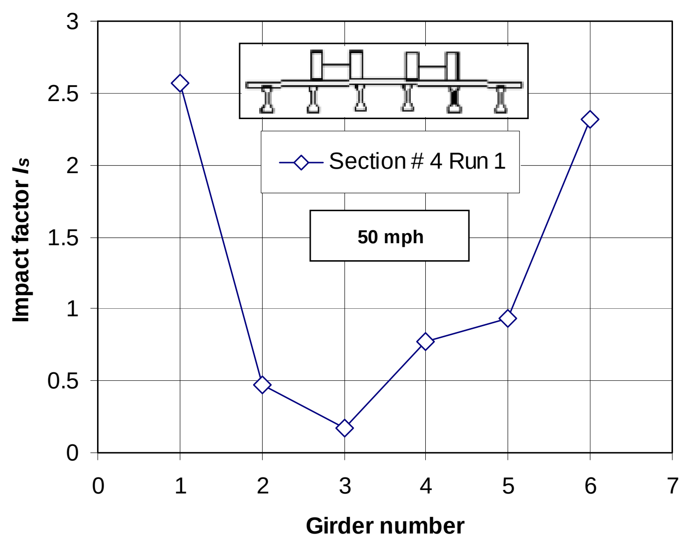

Figure A.58. Impact factor I_s for case # 10 (speed 50 mph without the plank on the bridge deck, two trucks).

A.2.12. Case 11 - One empty truck running on the west bound lane at 50 mph with plank

Additionally two cases with empty truck were analyzed. Main aim was to compare the results of these tests with similar cases with loading. Obviously small values of displacement and strains were recorded. This affected the values of calculated impact factors for both tests. For the span deflection the maximum value equals I_D =2.16 and for strains I_S = 1.42 for the girder # 4. Interestingly, higher values of strains were measured for the first span. It means that for trucks without a loading the impact effect is significant only for the first crossed span. Next spans smoothly extinguish induced vibrations. It clearly shows the effect of the mass. In this case the vibration amplitudes are smaller and are faster damped by the concrete bridge structure. The results presented below show unsymmetrical behavior of the bridge. This is due to the fact that the truck was located on the west bound lane.

Table A.33. The impact factor for girder 3 from displacement history.

	LVDT (dynamic max) [mm]	LVDT (static) [mm]	Impact factor from LVDT I_D	Noptel (dynamic max) [mm]	Noptel (static) [mm]	Impact factor from Noptel I_D
Run 1	-2.50	-0.79	2.16	-1.82	-0.67	1.72

Table A.34. The impact factor computed from strain history for the first span in the case 11.

Girder number	1			2			3			4			5			6		
	D	S	I_S	D	S	I_S	D	S	I_S	D	S	I_S	D	S	I_S	D	S	I_S
Run 1	18.0	1.3	12.8	22.6	6.5	2.38	45.5	14.4	2.16	60.5	25.0	1.42	51.5	22.4	1.30	35.6	10.9	2.27

Table A.35. The impact factor computed from strain history for the middle span in the case 11.

Girder number	1			2			3			4			5			6		
	D	S	I_S	D	S	I_S	D	S	I_S	D	S	I_S	D	S	I_S	D	S	I_S
Run 1	14.1	1.3	9.85	17.4	6.5	1.68	36.9	14.4	1.56	57.1	25.0	1.28	45.9	22.4	1.05	29.1	10.9	1.67

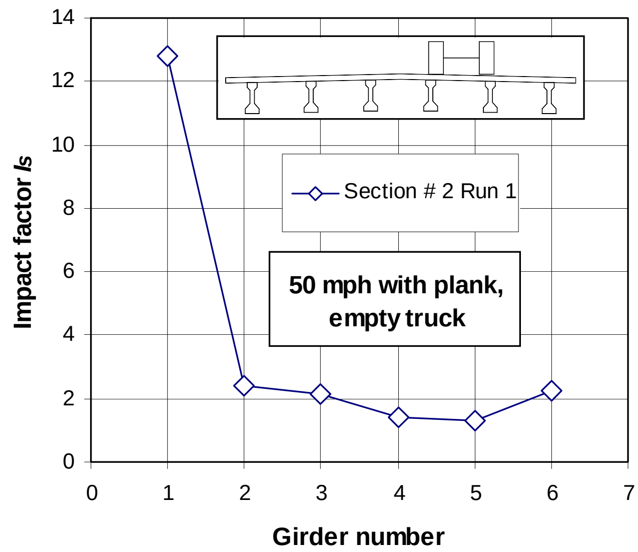

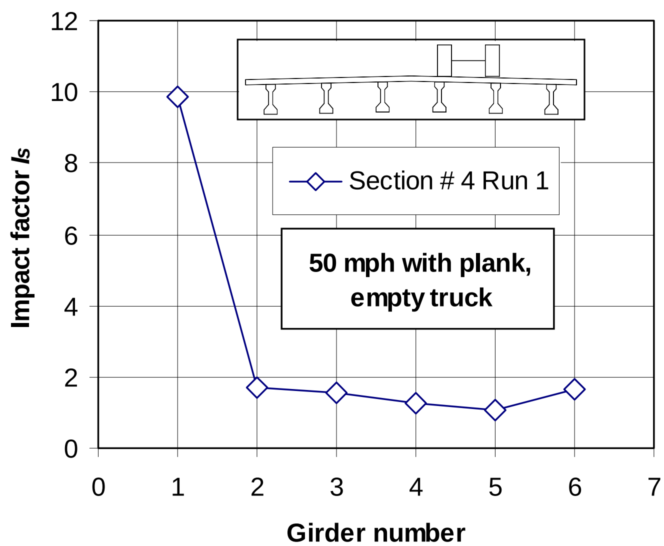

Figure A.59. Impact factor I_s for case # 11 (speed 50 mph with the plank on the bridge deck, truck without the loading).

A.2.13. Case 12 - One empty truck running at the center at 50 mph with plank

This case was similar to the previous one except that the empty truck crossed the bridge on the center of the road. Recorded strains show very good symmetry unlike the cases with the loading. It means that the inertial forces developed in the cases with loading can cause some effects, which produce unsymmetrical bridge behavior. Calculated impact factors are 1.41 for displacements and 1.38 for strains recorded in the middle span. Interestingly, in this case the higher impact factor is in the middle span, unlike the previous case. This effect could be attributed to the change in the position of the empty truck and the influence of the approach depression and the condition of the joint between the asphalt and the concrete slab.

Table A.36. The impact factor for girder # 3 from displacement history.

	LVDT (dynamic max) [mm]	LVDT (static) [mm]	Impact factor from LVDT I_D	Noptel (dynamic max) [mm]	Noptel (static) [mm]	Impact factor from Noptel I_D
Run 1	-2.72	-1.13	1.41	-2.04	-0.88	1.32

Table A.37. The impact factor computed from strain history for the first span in the case # 12.

Girder number	1			2			3			4			5			6		
	D	S	I_S	D	S	I_S	D	S	I_S	D	S	I_S	D	S	I_S	D	S	I_S
Run 1	25.2	2.1	11.0	29.4	10.5	1.8	48.8	21.5	1.27	50.1	22.8	1.20	27.9	13.0	1.15	25.5	4.8	4.31

Table A.38. The impact factor computed from strain history for the middle span in the case #12.

Girder number	1			2			3			4			5			6		
	D	S	I_S	D	S	I_S	D	S	I_S	D	S	I_S	D	S	I_S	D	S	I_S
Run 1	34.5	2.1	15.43	34.5	10.5	3.27	51.2	21.5	1.38	53.2	22.8	1.33	33.5	13.0	1.58	31.6	4.8	5.58

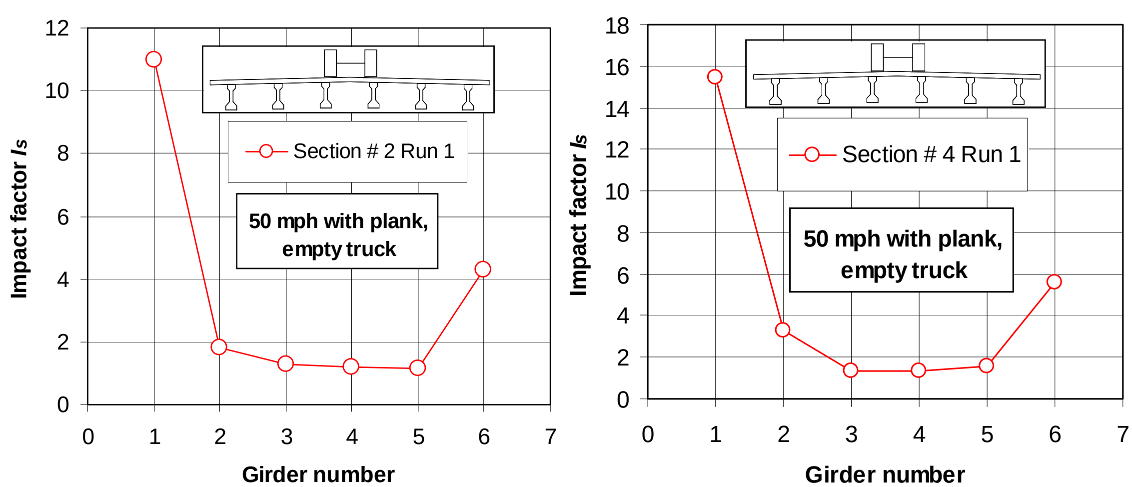

Figure A.60. Impact factor I_s for case # 12 (speed 50 mph with the plank on the bridge deck, truck without the loading).

A.3. Conclusions from performed analysis

The focus of this study was to analyze the behavior of girders #3 and #4 as these two girders were mainly loaded and tensioned. Impact factors for external girders increase very fast compared to the internal girders. This situation takes place because these beams are not directly loaded by truck wheels and the static strains are very small compared to the strains for internal girders, mainly girders # 3 and 4. Obtained results are presented in Tables A.39, A.40, A.41 and A.42. Outcomes of the tests were investigated from many points of view. Various factors such as truck position, truck speed, number of trucks, truck weight and, plank influence were taken into account for analysis. Each of these effects is discussed and concluded separately.

Effect of truck position

For each case the change of truck position from the west bound lane to the center of the roadway caused the deflection increase, which was measured at the bottom of girder # 3 in the first span. This causes the impact factors calculated from displacement results to decrease. Thus, the span deflection and impact factor I_D are inversely proportional. Furthermore, this situation took place for both, loaded and unloaded, trucks in all considered cases. The impact factors calculated based on the strains histories (I_S) are much more complicated. For all cases without the plank the computed I_S for girders #3 and #4 located at the center of the road have higher values when the truck is crossing the bridge over the center of the roadway. This phenomenon appears for both spans tested. Obviously, the higher values were obtained for the second span. It confirms that some vibrations are transferred from the first span to the second one and are amplified.

Effect of truck speed

From mechanical point of view, the increase in the truck speed means the higher dynamic effect. This theory was confirmed for all analyzed cases. In general, higher values of recorded displacements and strain histories were observed for the tests with higher truck speed. Generally, truck at higher speed generates higher values of inertial forces, which strongly depend on velocity and its action on the bridge deck is more noticeable. This influence is noticeable for the first and the second span, where the I_S values are higher with the exception of one case with the plank when truck is crossing the bridge at 50 mph. For this velocity, generated impact forces are higher at the first phase of driving. Main reason for this situation is related to the higher induced vibrations after crossing the plank. In the second phase this artificial vibrations are extinguished by the bridge structure.

Effect of number of trucks (number of loaded lanes)

The increased number of trucks directly causes increase in the loading. The most critical case for investigated bridge was the situation when two trucks were running on the bridge deck at the same time. In this case the computed impact factor (I_S) is smaller than for the cases with one truck. However, during this test both the girders were the most loaded and tensioned. Additionally, as in previous one-truck runs, the speed increase resulted in higher values of (I_S). In this case, the symmetrical effect for analyzed girders was expected. However, this situation was not observed. External factors such as higher bridge depression and higher threshold on the right lane disturbed this symmetry. In addition, these parameters caused higher strain at this part of the bridge and an appreciable increase in the I_S was observed for increase speed, especially for the second span.

Effect of truck weight

Two tests were conducted with empty trucks at 50 mph, which started to cross the bridge from two different positions. In the first run at right lane and in the second run at the center of roadway. Recorded results show that, this weight decrease causes the increase in the impact factor value. Furthermore the condition of the bridge approach gives the higher values of I_S for the first span when the truck is located on the westbound lane. Similar situation was not observed during the test when the empty truck crossed the bridge with plank on the deck. Therefore, this effect can be exaggerated in this case. However, this still confirms the bridge approach effect and its negative influence.

Effect of plank

In general, increase in the impact factor was observed for all analyzed cases with plank. It means that artificially induced vibrations in the truck are transferred to the bridge deck and it causes higher strains in girders. Additionally the computed impact factors for the first span have higher values than for the second one. It confirms that in the second phase the structural damping effect takes place and induced vibrations disappear. However, many other aspects are related to the artificial disturbance. One of them is the fact that the impact factor in the girder #3 has higher values than for girder #4; even when the truck was on the right lane. This phenomenon clearly is related to the bridge depression and the existence of threshold between the asphalt and the concrete deck.

Table A.39. The impact factor (I_D) and deflections of the girder # 3 in the first span for all analyzed cases (run 1).

Cases		**1 WB**	**2 WB**	**3 WB**	**4 WB**	**5 CB**	**6 CB**	**7 CB**	**8 CB**	**9 2TR**	**10 2TR**	**11 ETR,WB**	**12 ETR,CB**
Deflection from two devices [mm]	LVDT	1.33	1.31	**2.41**	**3.24**	1.99	3.08	**3.62**	**5.47**	3.40	4.27	**2.50**	**2.72**
	Neoptel	1.62	0.7	**-**	**2.82**	2.22	2.95	**2.88**	**4.16**	3.47	3.78	**1.82**	**2.04**
Impact factor I_D		0.55	1.56	**2.8**	**2.77**	0.36	1.12	**1.48**	**2.75**	0.25	0.56	**2.16**	**1.41**
		0.15	0.7	**-**	**1.0**	0.14	0.52	**0.48**	**1.14**	0.10	0.2	**1.72**	**1.32**

LEGEND:

- truck speed 30 mph (48 km/h)
- truck speed 50 mph (80 km/h)

1.37 - impact factor for cases without the plank (e.g.)

2.50 - impact factor for cases with the plank (e.g.)

WB - truck located on the west bound

CB - truck located on the center of roadway

2TR - two trucks side by side

ETR - empty truck

Table A.40 The impact factor (I_D) and deflections of the girder # 3 in the first span for all analyzed cases (run 2).

Cases		**1 WB**	**2 WB**	**3 WB**	**4 WB**	**5 CB**	**6 CB**	**7 CB**	**8 CB**	**9 2TR**	**10 2TR**	**11 ETR,WB**	**12 ETR,CB**
Deflection from two devices [mm]	LVDT	1.37	2.42	**2.50**	**3.44**	1.91	3.86	**3.83**	**4.26**	-	-	-	-
	Neoptel	1.55	2.66	**2.13**	**2.92**	2.02	3.39	**3.1**	**3.61**	-	-	-	-
Impact factor I_D	LVDT	0.59	1.81	**2.91**	**2.0**	0.31	1.65	**1.63**	**1.92**	-	-	-	-
	Neoptel	0.1	0.89	**1.51**	**1.07**	0.04	0.75	**0.62**	**0.86**	-	-	-	-

Table A.41. The impact factor computed from strain histories for the girder # 3.

Cases		**1 WB**	**2 WB**	**3 WB**	**4 WB**	**5 CB**	**6 CB**	**7 CB**	**8 CB**	**9 2TR**	**10 2TR**	**11 ETR,WB**	**12 ETR,CB**
Section #2	Run1	0.23	0.77	**0.72**	**1.4**	0.19	0.75	**0.63**	**1.64**	0.12	0.23	**2.16**	**1.27**
	Run2	0.23	0.98	**0.85**	**1.5**	0.06	1.04	**0.79**	**1.36**	-	-	-	-
Section # 4	Run1	0.30	1.05	-	**1.7**	0.3	1.08	**0.57**	**1.43**	0.06	0.17	**1.56**	**1.38**
	Run2	-	1.57	**0.52**	**1.6**	0.18	1.6	**0.73**	**1.27**	-	-	-	-

Table A.42. The impact factor computed from strain histories for the girder # 4.

Cases		**1 WB**	**2 WB**	**3 WB**	**4 WB**	**5 CB**	**6 CB**	**7 CB**	**8 CB**	**9 2TR**	**10 2TR**	**11 ETR,WB**	**12 ETR,CB**
Section #2	Run1	0.03	0.46	**0.36**	**1.02**	0.11	0.83	**0.52**	**1.46**	0.20	0.51	**1.42**	**1.20**
	Run2	-0.04	0.71	**0.29**	**0.92**	0.15	0.66	**0.40**	**1.08**	-	-	-	-
Section #4	Run1	0.18	0.66	-	**1.2**	0.23	1.21	**0.53**	**1.26**	0.23	0.77	**1.28**	**1.33**
	Run2	-	1.18	**0.23**	**0.95**	0.33	1.05	**0.38**	**0.91**	-	-	-	-

APPENDIX B

NUMERICAL RESULTS

B.1. Case #1 – V=35mph, bridge#1, truck#1

The case #1 was defined for the truck #1 running through the bridge #1 with speed V=35mph. Figure B.1 presents the time histories of strains calculated in the middle of the span for each girder. Figure B.2 shows corresponding stresses caused by the crossing vehicle. In Figure B.3 maximum dynamitic strains are compared for each girder with the static strains. Impact factor was calculated for girder #4 with the maximum dynamic strain ε^D= 57.46 micro strains (σ^D= 2.16MPa). The representative value of the impact factor for case #1 is:

$$IM_{case\#1} = 23.65\%$$

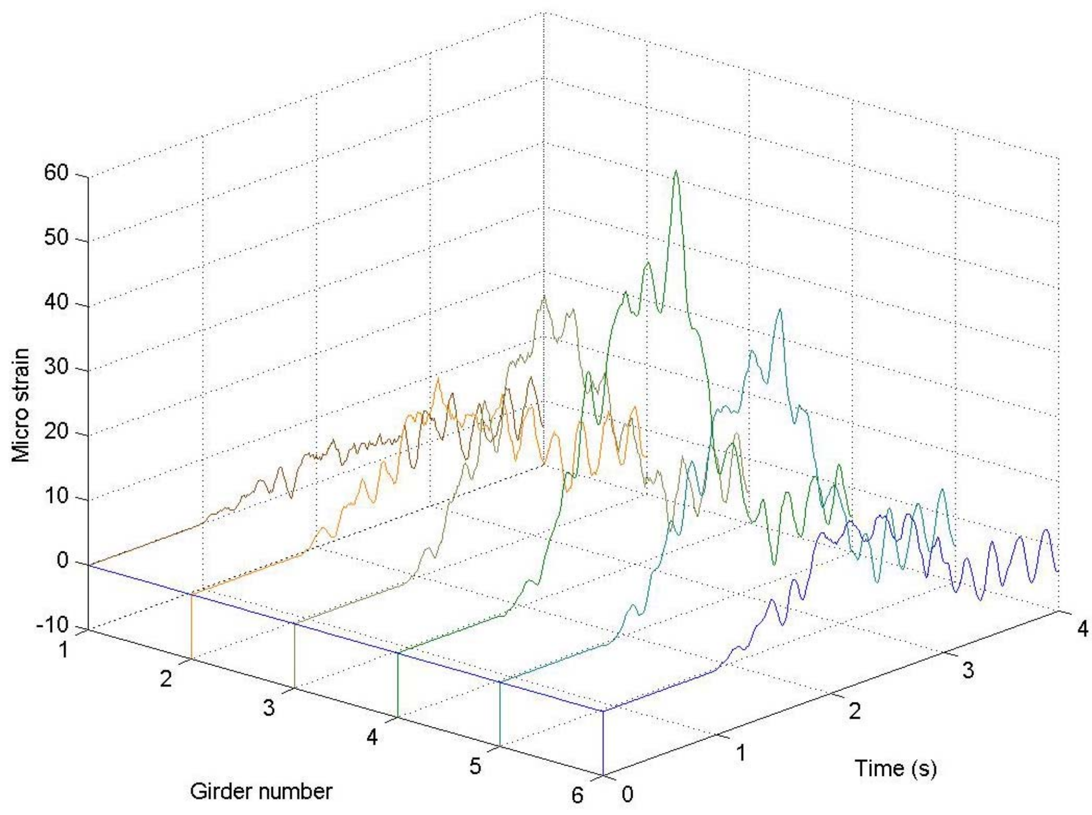

Figure B.1. Time histories of micro strains in girders for Case #1.

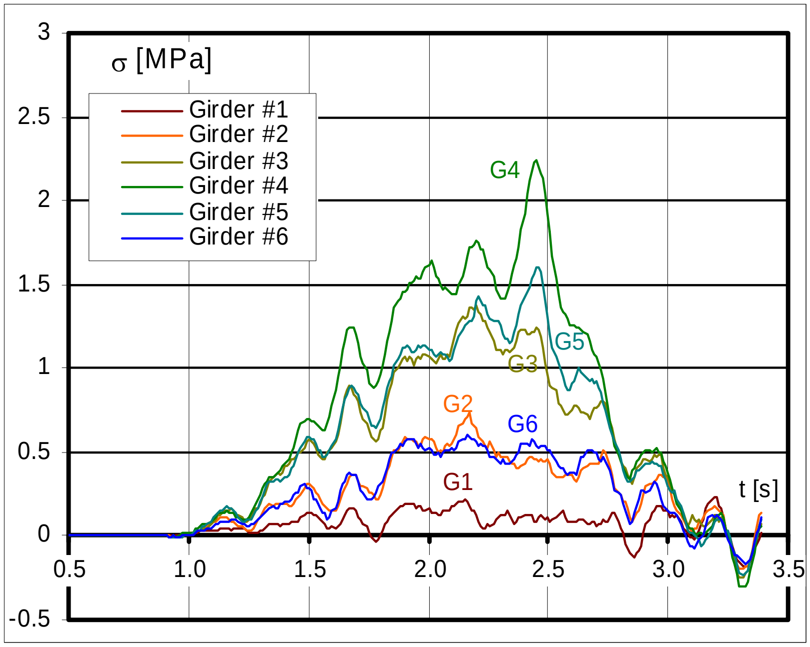

Figure B.2. Time histories of stresses in girders for Case #1.

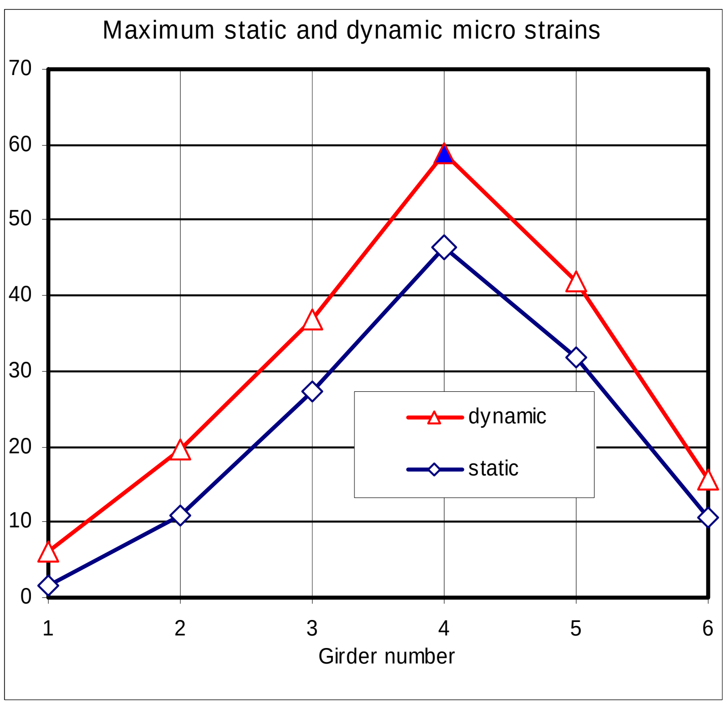

Figure B.3 Comparison of maximum static and dynamic strains for Case #1.

B.2. Case #2 – V=35mph, bridge#1, truck#2

The case #2 was defined for the truck #2 running through the bridge #1 with speed V=35mph. Figure B.4 presents the time histories of strains calculated for each girder in the middle of the span. Figure B.5 shows corresponding stresses caused by passing vehicle. In Figure B.6 maximum dynamitic strains are compared for each girder with the static strains. Impact factor was calculated for girder #4 with the maximum dynamic strain ε^D=65.95 micro strains (σ^D=2.48 MPa). The representative value of the impact factor for case #2 is:

$$IM_{case\#2} = 10.6\ \%$$

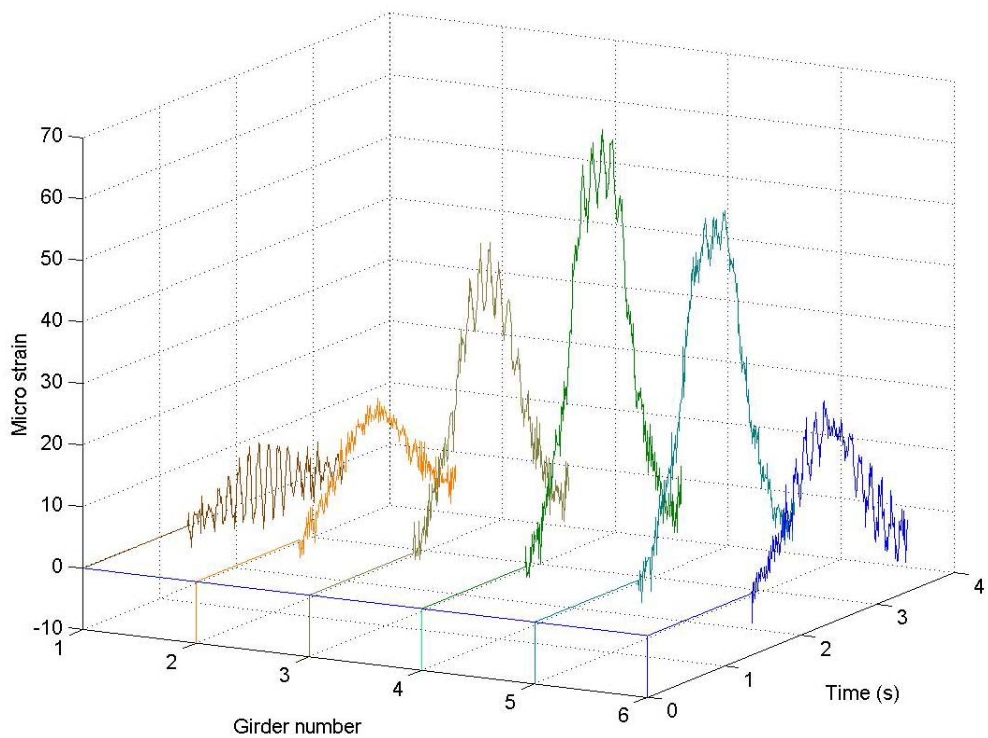

Figure B.4 Time histories of micro strains in girders for Case #2.

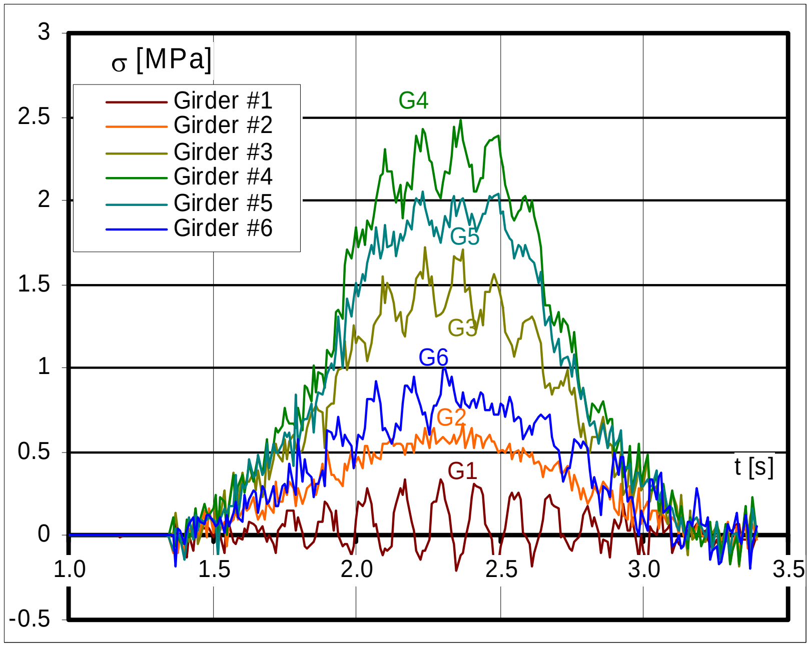

Figure B.5. Time histories of stresses in girders for Case #2.

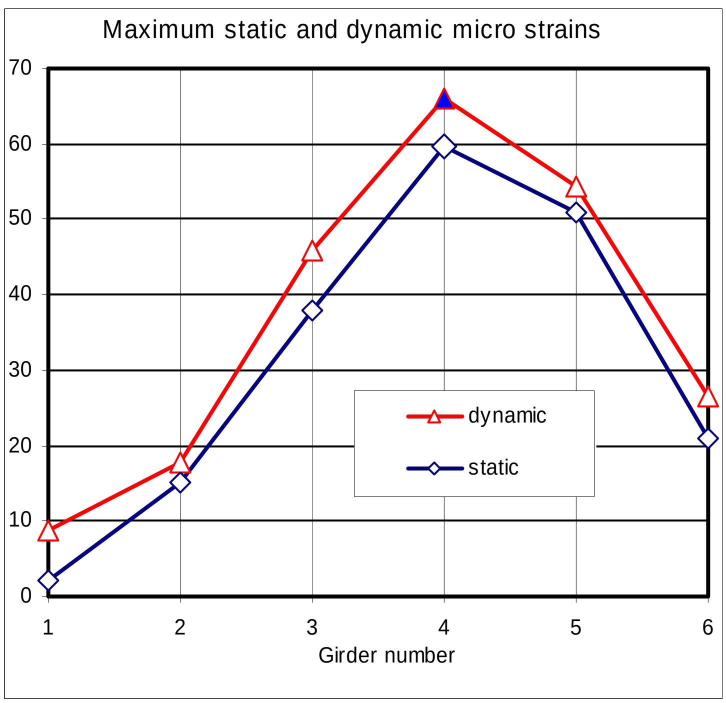

Figure B.6. Comparison of maximum static and dynamic strains for Case #2.

B.3. Case #3 – V=35mph, bridge#1, truck#3

The case #3 was defined for the truck #3 running through the bridge #1 with speed V=35mph. Figure B.7 presents the time histories of strains calculated for each girder in the middle of the span. Figure B.8 shows corresponding stresses caused by passing vehicle. In Figure B.9 maximum dynamitic strains are compared for each girder with the static strains. Impact factor was calculated for girder #4 with the maximum dynamic strain ε^D= 69.48 micro strains (σ^D= 2.63 MPa). The representative value of the impact factor for case #3 is:

$$IM_{case\#3} = 7.02\%$$

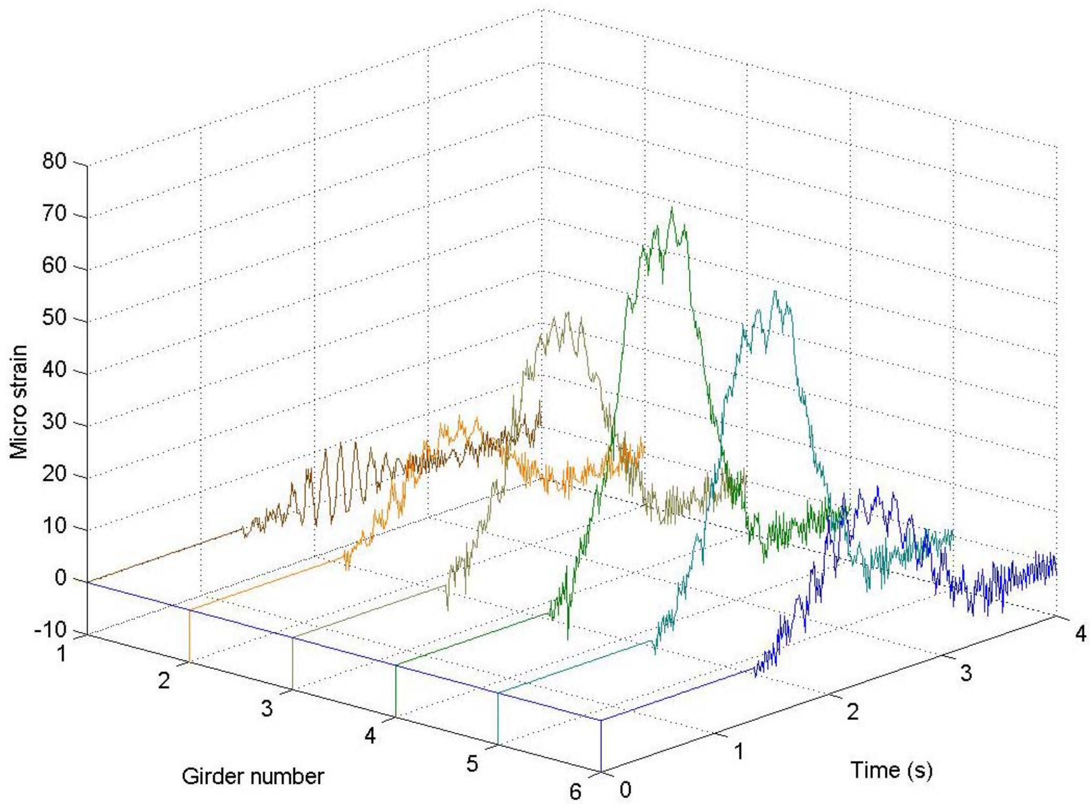

Figure B.7 Time histories of micro strains in girders for Case #3.

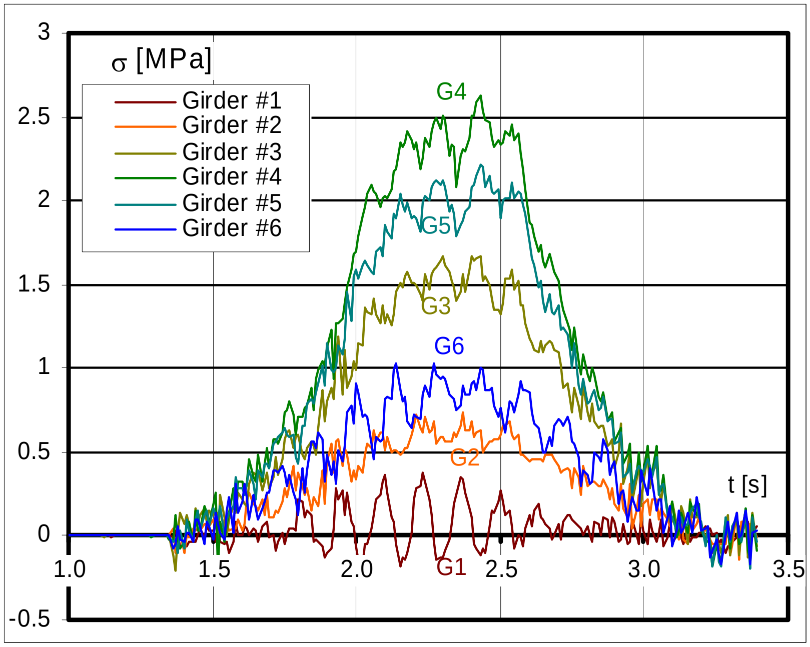

Figure B.8. Time histories of stresses in girders for Case #3.

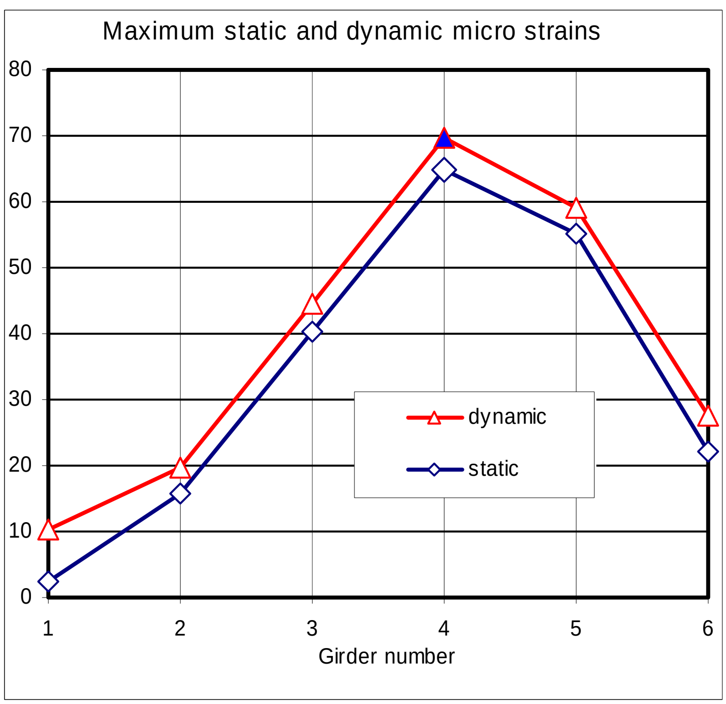

Figure B.9. Comparison of maximum static and dynamic strains for Case #3.

B.4. Case #4 – V=35mph, bridge#1, truck#4

The case #4 was defined for the truck #4 running through the bridge #1 with speed V=35mph. Figure B.10 presents the time histories of strains calculated for each girder in the middle of the span. Figure B.11 shows corresponding stresses caused by passing vehicle. In Figure B.12 maximum dynamitic strains are compared for each girder with the static strains. Impact factor was calculated for girder #4 with the maximum dynamic strain ε^D= 71.39 micro strains (σ^D= 2.68 MPa). The representative value of the impact factor for case #4 is:

$$IM_{case\#4} = 2.74\ \%$$

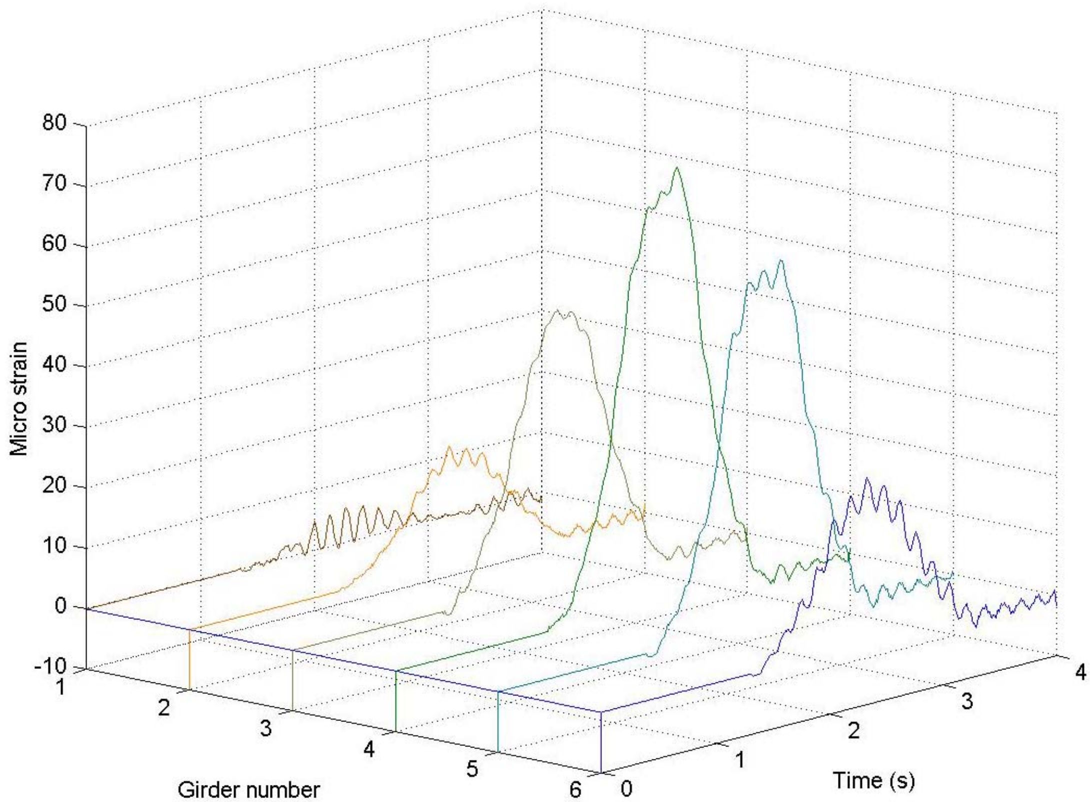

Figure B.10. Time histories of micro strains in girders for Case #4.

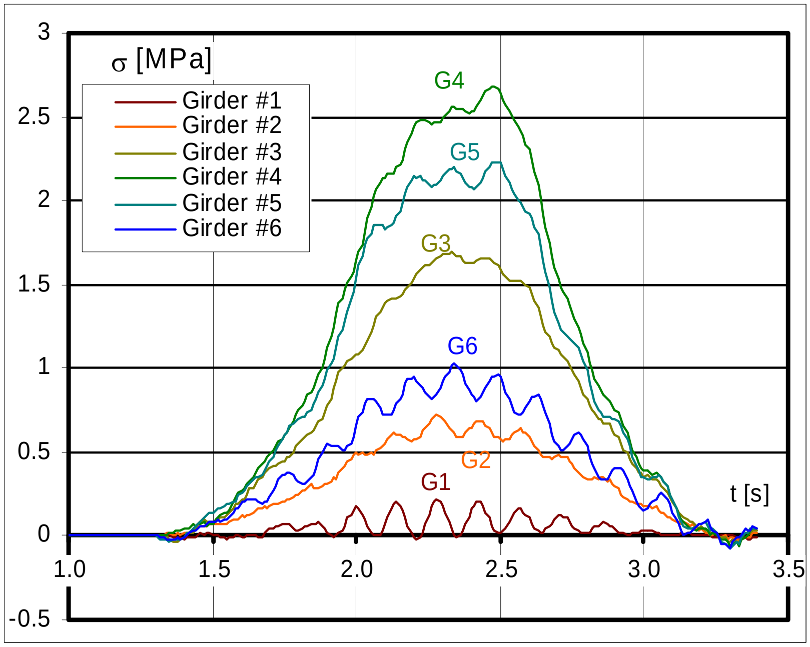

Figure B.11. Time histories of stresses in girders for Case #4.

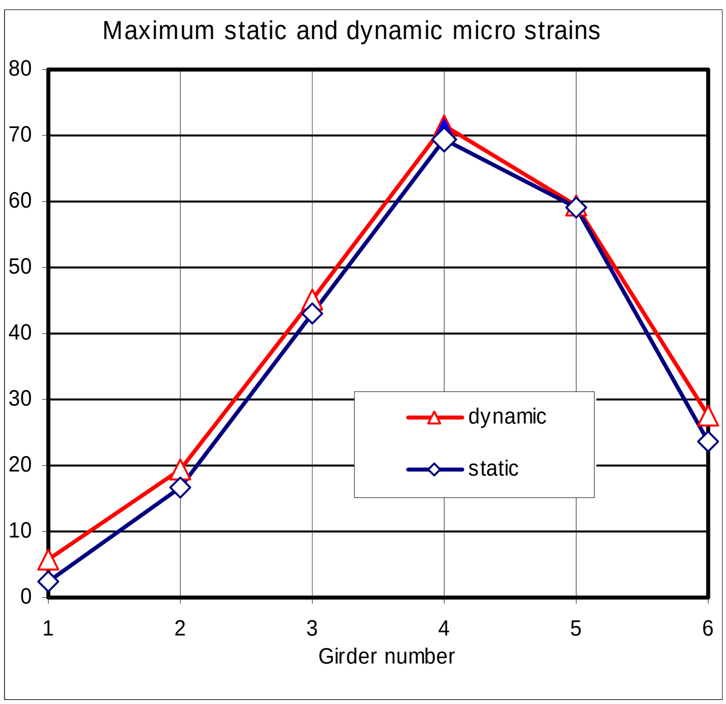

Figure B.12. Comparison of maximum static and dynamic strains for Case #4.

B.5. Case #5 – V=35mph, bridge#3, truck#1

The case #5 was defined for the truck #1 running through the bridge #3 with speed V=35mph. Figure B.13 presents the time histories of strains calculated for each girder in the middle of the span. Figure B.14 shows corresponding stresses caused by passing vehicle. In Figure B.15 maximum dynamitic strains are compared for each girder with the static strains. Impact factor was calculated for girder #4 with the maximum dynamic strain ε^D= 54.89 micro strains (σ^D= 1.63 MPa). The representative value of the impact factor for case #5 is:

$$IM_{case\#5} = 25.95\ \%$$

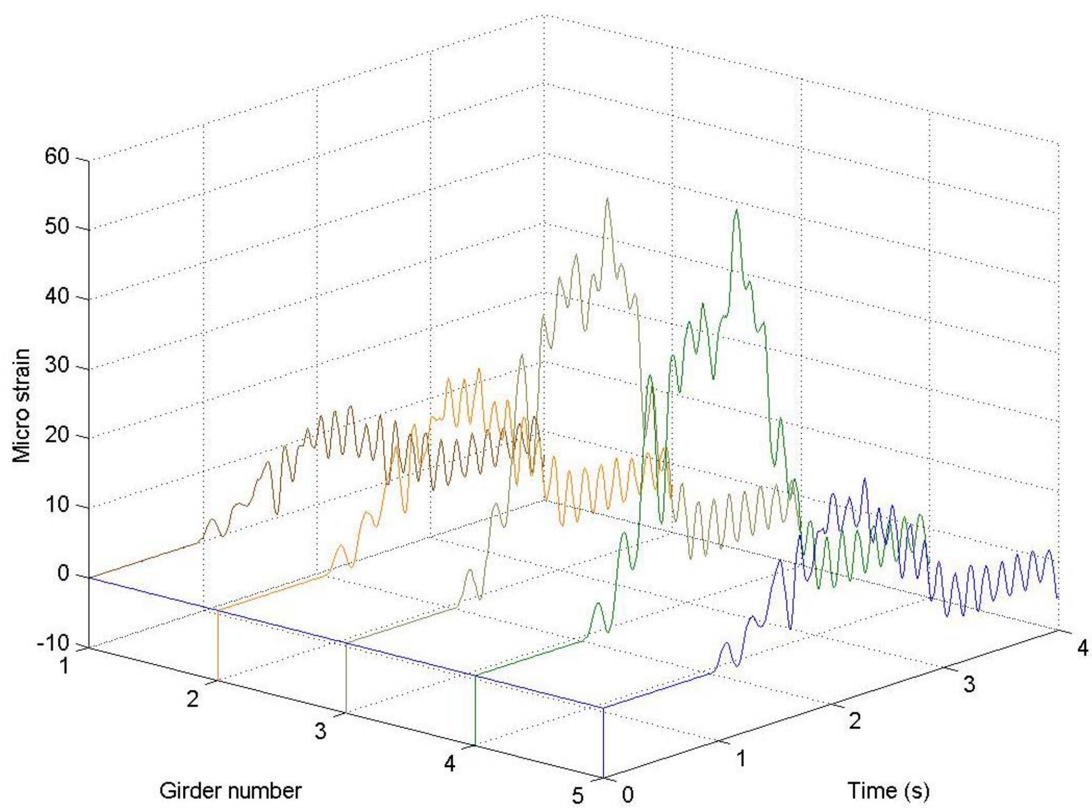

Figure B.13. Time histories of micro strains in girders for Case #5.

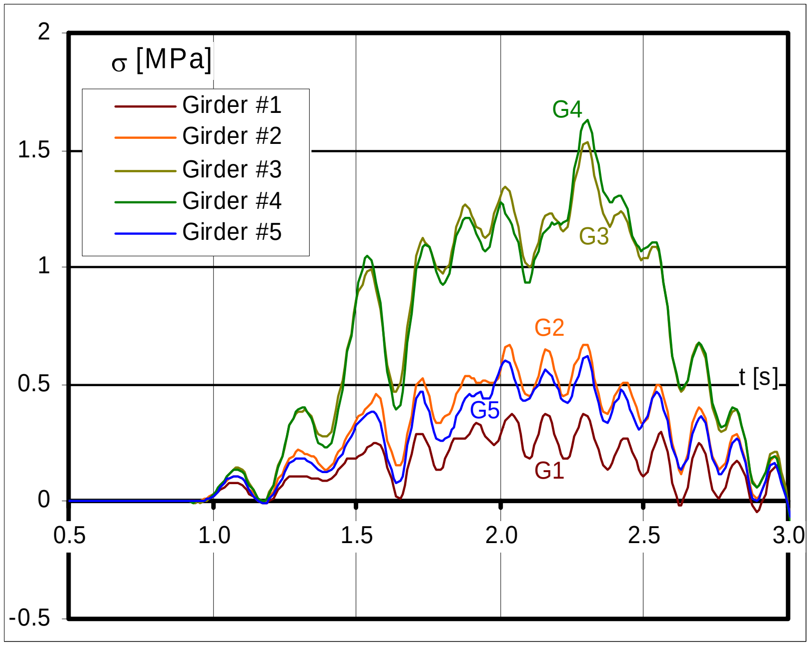

Figure B.14. Time histories of stresses in girders for Case #5.

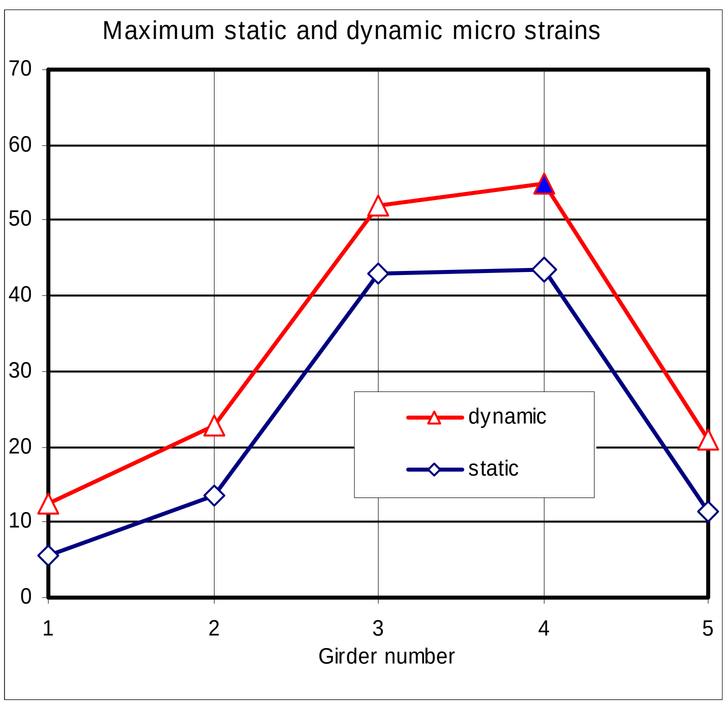

Figure B.15. Comparison of maximum static and dynamic strains for Case #5.

B.6. Case #6 – V=35mph, bridge#3, truck#2

The case #6 was defined for the truck #2 running through the bridge #3 with speed V=35mph. Figure B.16 presents the time histories of strains calculated for each girder in the middle of the span. Figure B.17 shows corresponding stresses caused by passing vehicle. In Figure B.18 maximum dynamitic strains are compared for each girder with the static strains. Impact factor was calculated for girder #4 with the maximum dynamic strain ε^D= 70.92 micro strains (σ^D= 2.11 MPa). The representative value of the impact factor for case #6 is:

$$IM_{case\#6} = 11.01\ \%$$

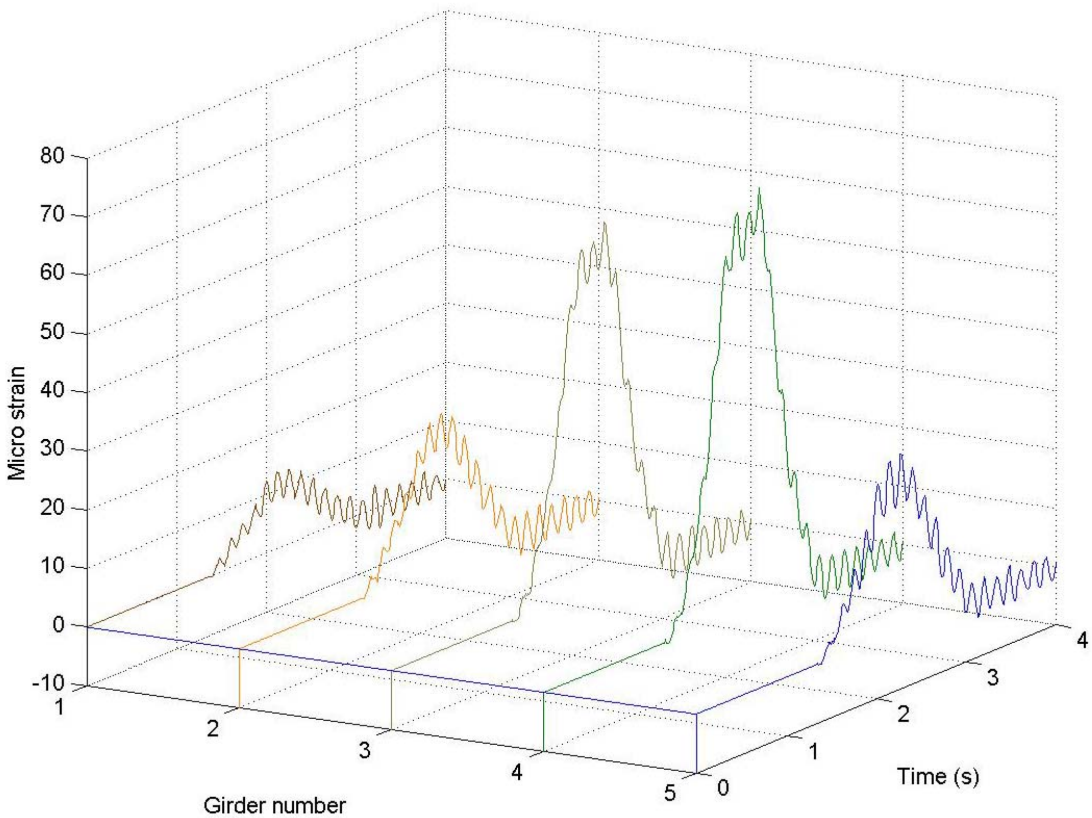

Figure B.16. Time histories of micro strains in girders for Case #6.

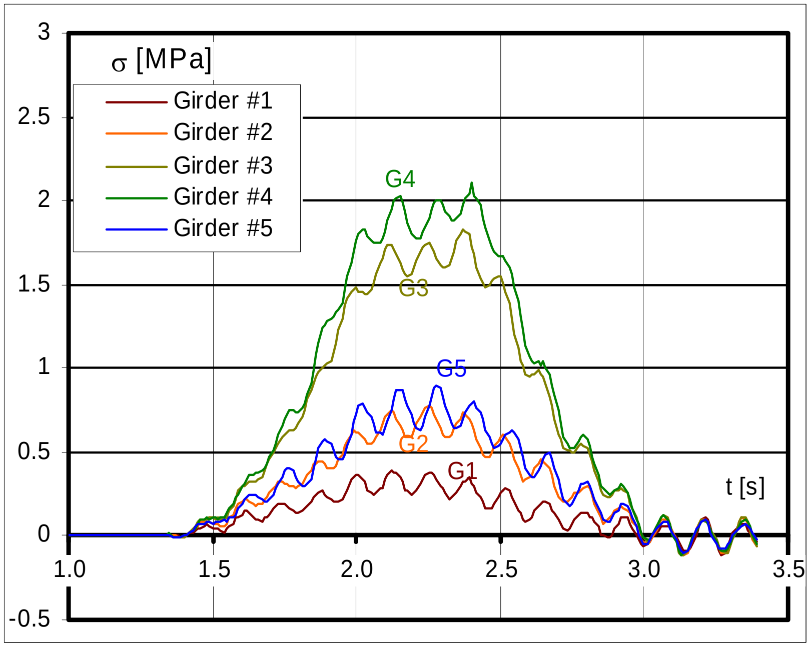

Figure B.17. Time histories of stresses in girders for Case #6.

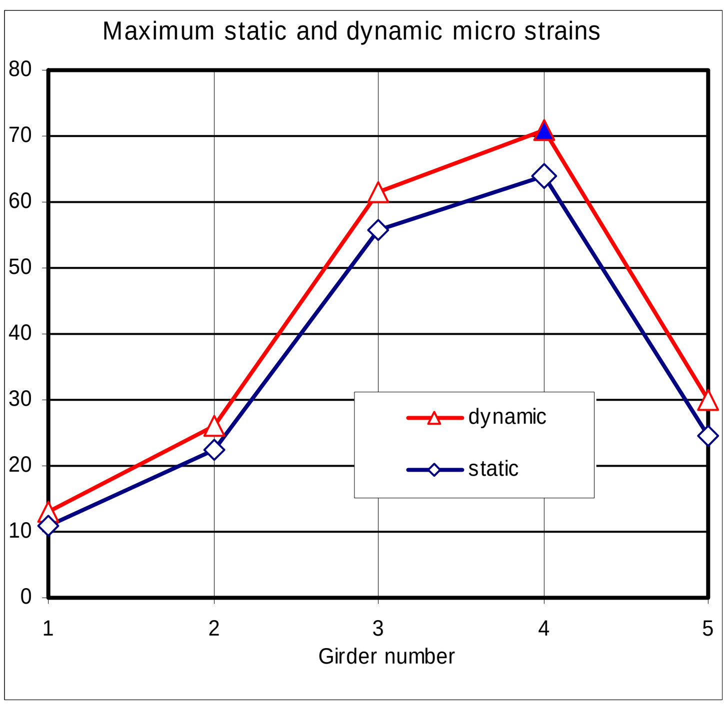

Figure B.18. Comparison of maximum static and dynamic strains for Case #6.

B.7. Case #7 – V=35mph, bridge#3, truck#3

The case #7 was defined for the truck #3 running through the bridge #3 with speed V=35mph. Figure B.19 presents the time histories of strains calculated for each girder in the middle of the span. Figure B.20 shows corresponding stresses caused by passing vehicle. In Figure B.21 maximum dynamitic strains are compared for each girder with the static strains. Impact factor was calculated for girder #4 with the maximum dynamic strain ε^D= 72.31 micro strains (σ^D= 2.14 MPa). The representative value of the impact factor for case #7 is:

$$IM_{case\#7} = 7.21\ \%$$

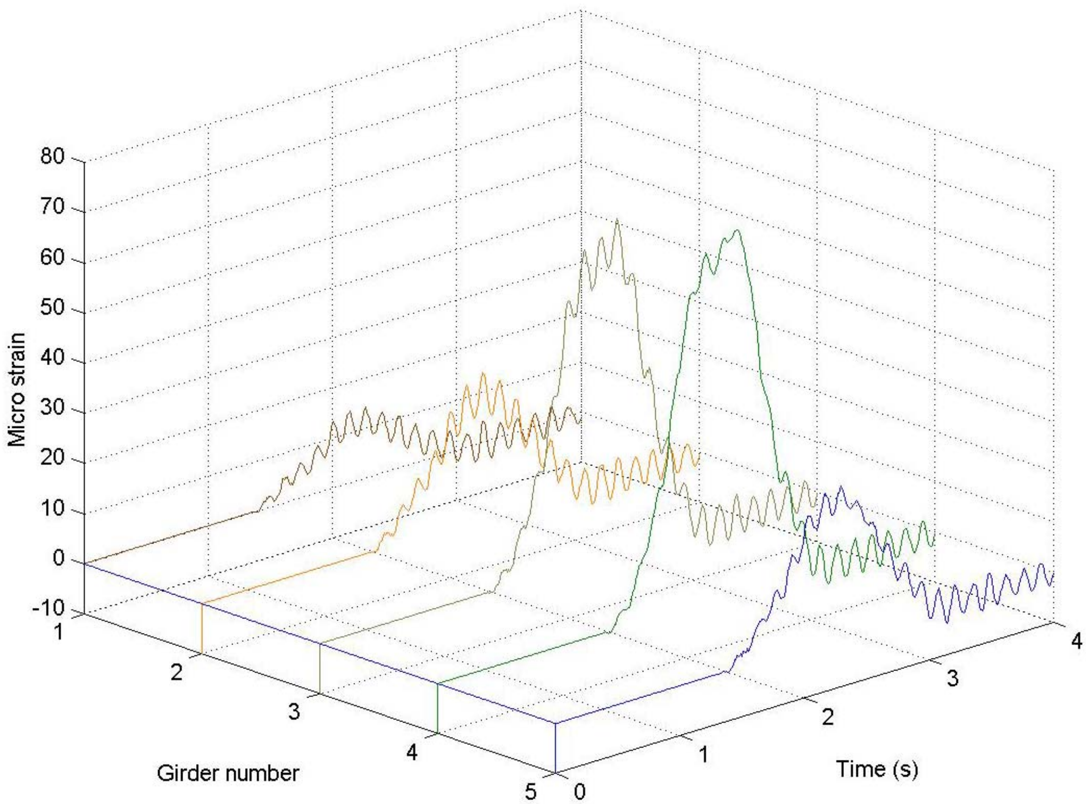

Figure B.19. Time histories of micro strains in girders for Case #7.

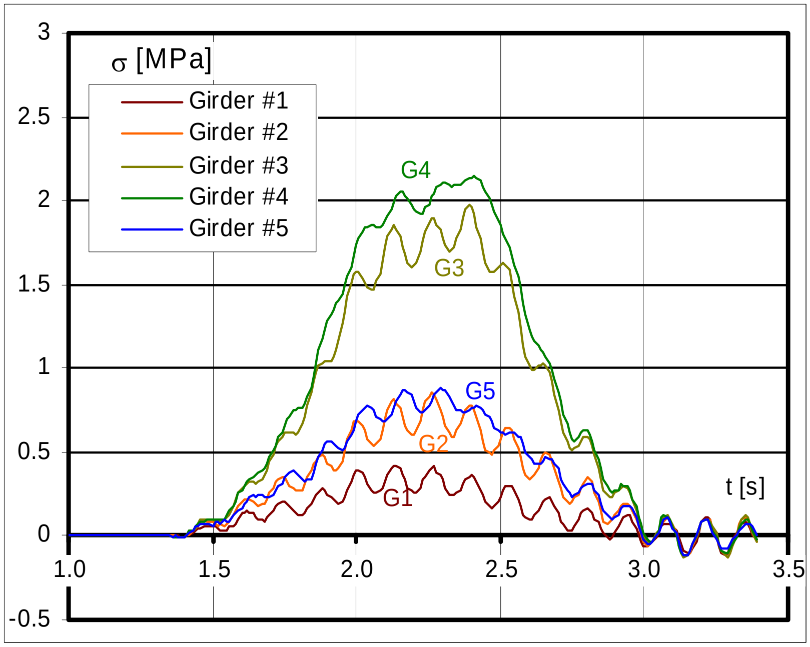

Figure B.20. Time histories of micro strains in girders for Case #7.

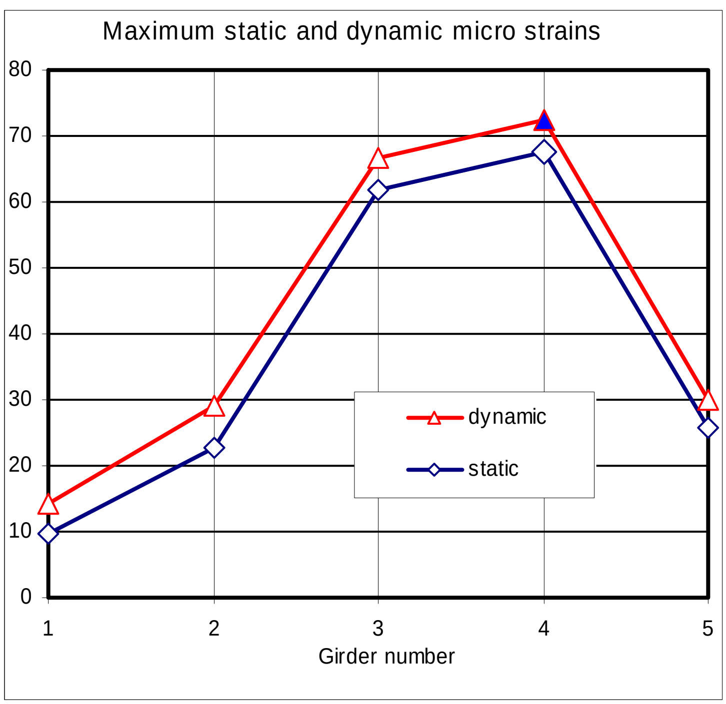

Figure B.21. Comparison of maximum static and dynamic strains for Case #7.

B.8. Case #8 – V=35mph, bridge#3, truck#4

The case #8 was defined for the truck #4 running through the bridge #3 with speed V=35mph. Figure B.22 presents the time histories of strains calculated for each girder in the middle of the span. Figure B.23 shows corresponding stresses caused by passing vehicle. In Figure B.24 maximum dynamitic strains are compared for each girder with the static strains. Impact factor was calculated for girder #4 with the maximum dynamic strain ε^D= 80.91 micro strains (σ^D= 2.40 MPa). The representative value of the impact factor for case #8 is:

$$IM_{case\#8} = 3.67\%$$

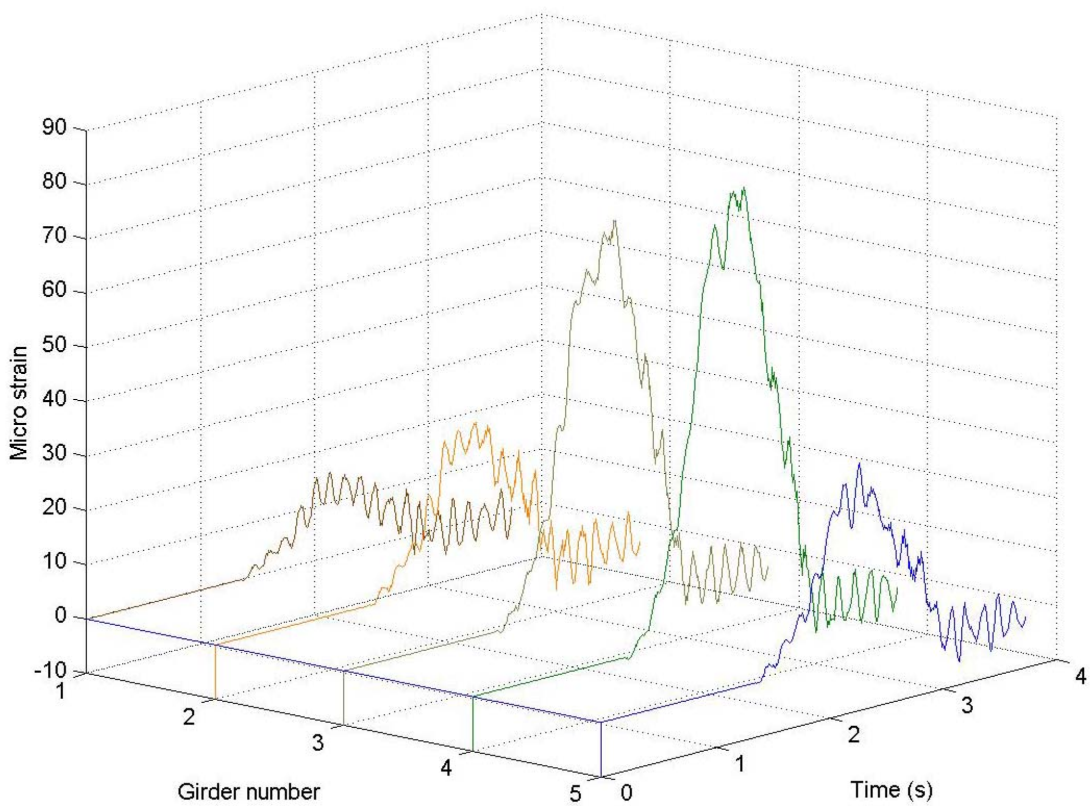

Figure B.22. Time histories of micro strains in girders for Case #8.

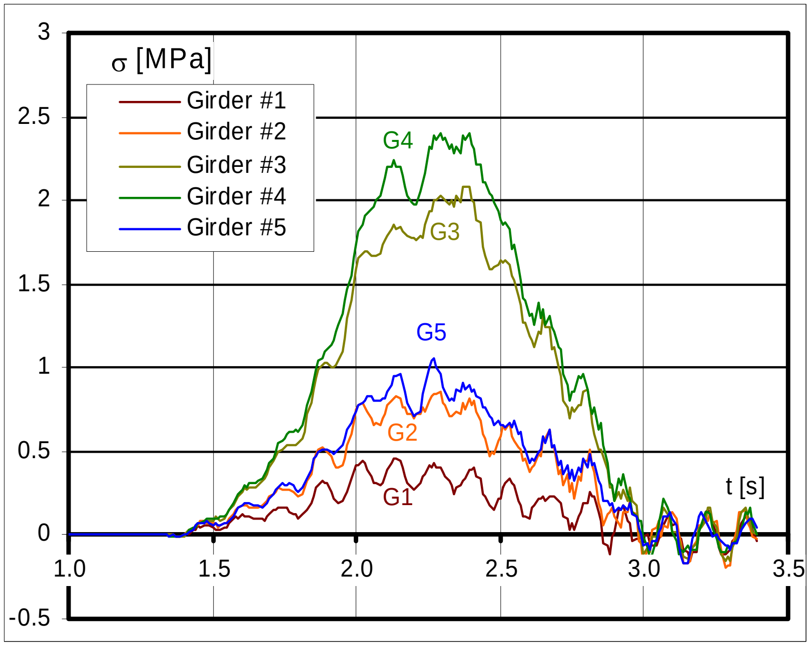

Figure B.23. Time histories of micro strains in girders for Case #8.

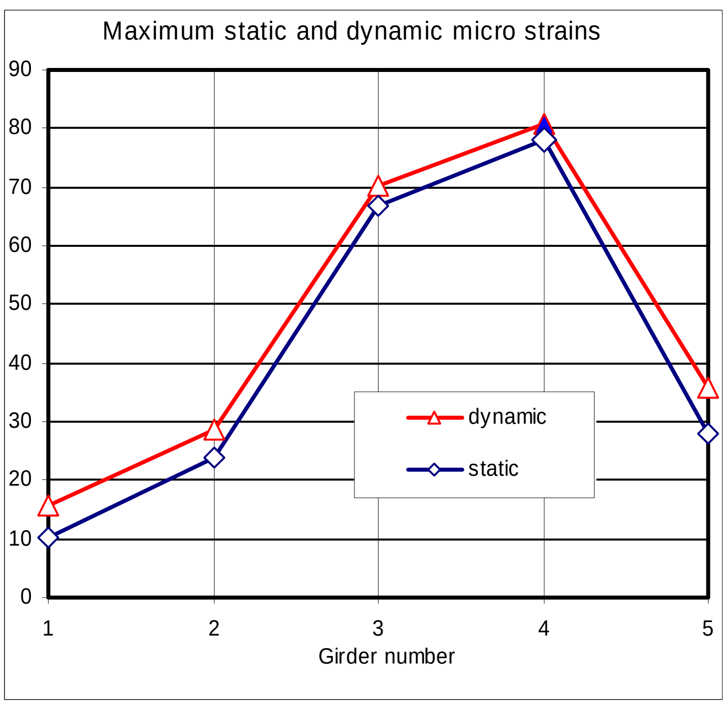

Figure B.24. Comparison of maximum static and dynamic strains for Case #8.

B.9. Case #9 – V=45mph, bridge#1, truck#1

The case #9 was defined for the truck #1 running through the bridge #1 with speed V=45mph. Figure B.25 presents the time histories of strains calculated for each girder in the middle of the span. Figure B.26 shows corresponding stresses caused by passing vehicle. In Figure B.27 maximum dynamitic strains are compared for each girder with the static strains. Impact factor was calculated for girder #4 with the maximum dynamic strain ε^D= 62.62 micro strains (σ^D= 2.35 MPa). The representative value of the impact factor for case #9 is:

$$IM_{case\#9} = 34.75\ \%$$

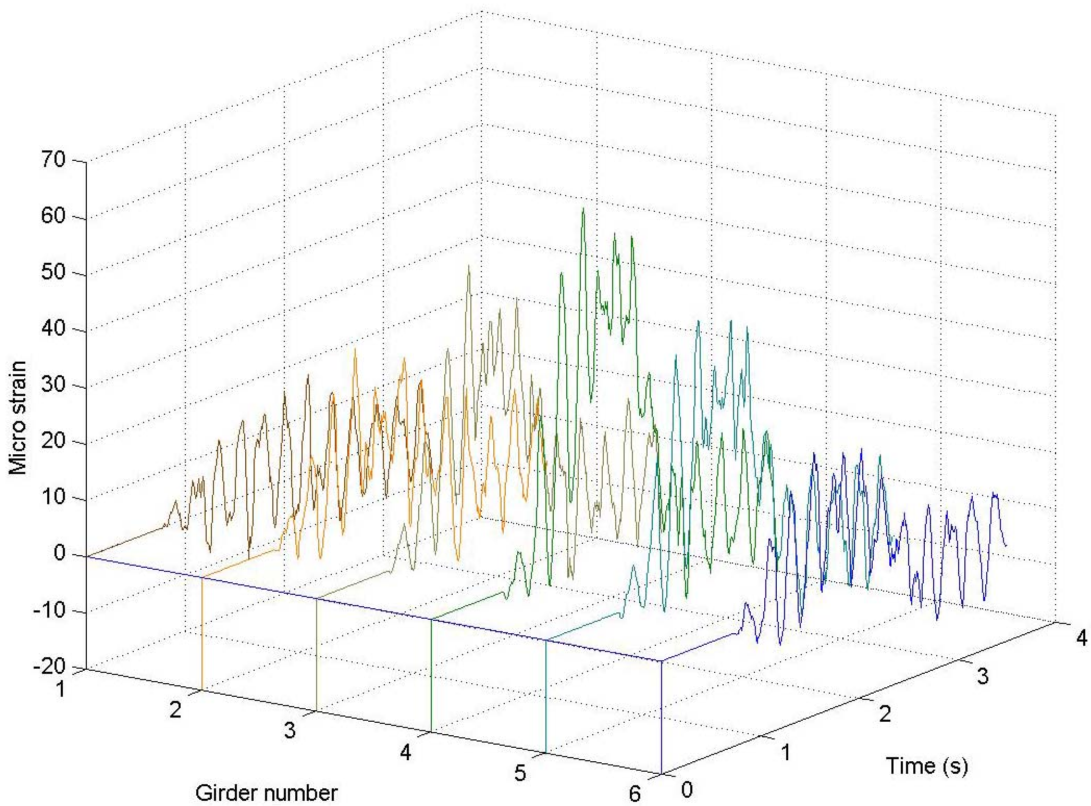

Figure B.25. Time histories of micro strains in girders for Case #9.

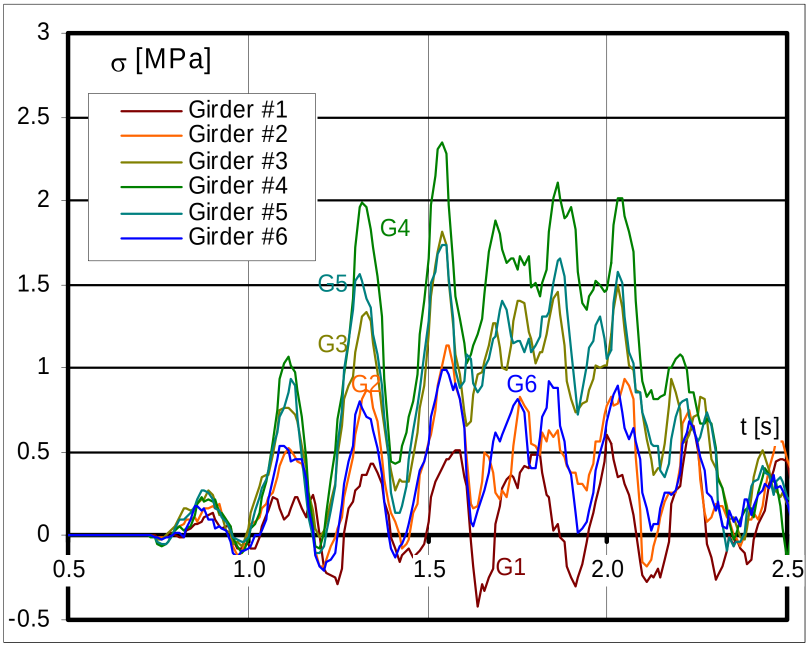

Figure B.26. Time histories of micro strains in girders for Case #9.

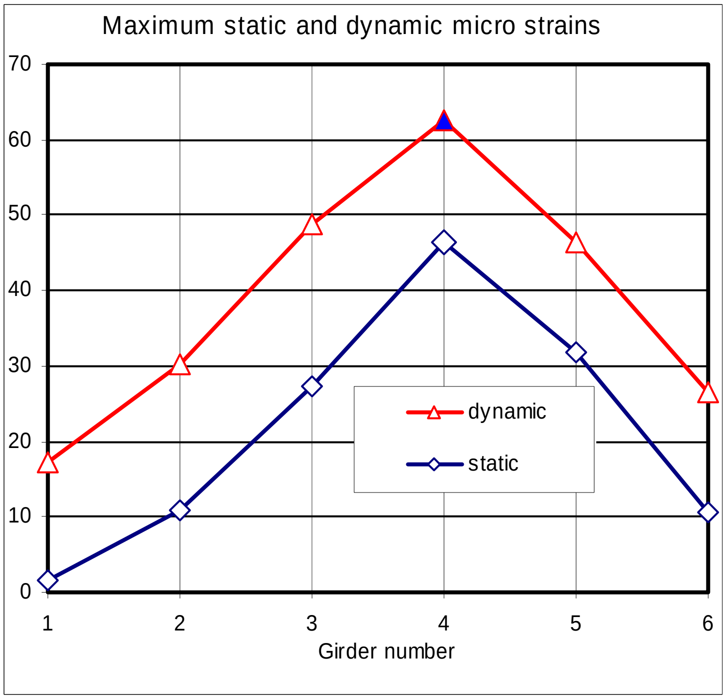

Figure B.27. Comparison of maximum static and dynamic strains for Case #9.

B.10. Case #10 – V=45mph, bridge#1, truck#2

The case #10 was defined for the truck #2 running through the bridge #1 with speed V=45mph. Figure B.28 presents the time histories of strains calculated for each girder in the middle of the span. Figure B.29 shows corresponding stresses caused by passing vehicle. In Figure B.30 maximum dynamitic strains are compared for each girder with the static strains. Impact factor was calculated for girder #4 with the maximum dynamic strain ε^D= 66.36 micro strains (σ^D= 2.49 MPa). The representative value of the impact factor for case #10 is:

$$IM_{case\#10} = 11.26\%$$

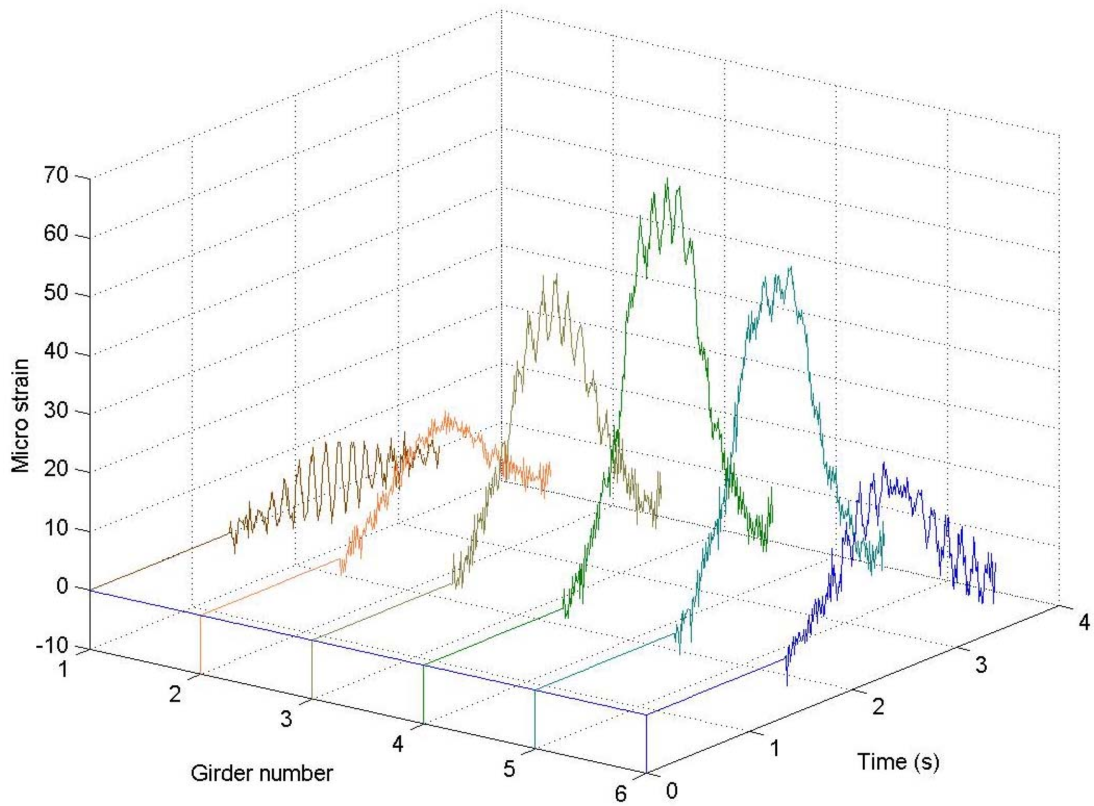

Figure B.28. Time histories of micro strains in girders for Case #10.

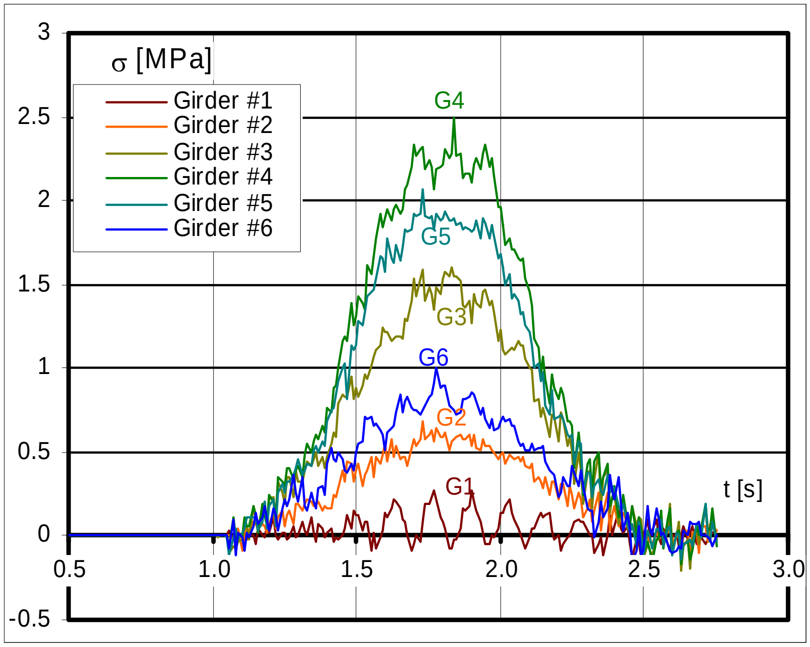

Figure B.29. Time histories of stresses in girders for Case #10.

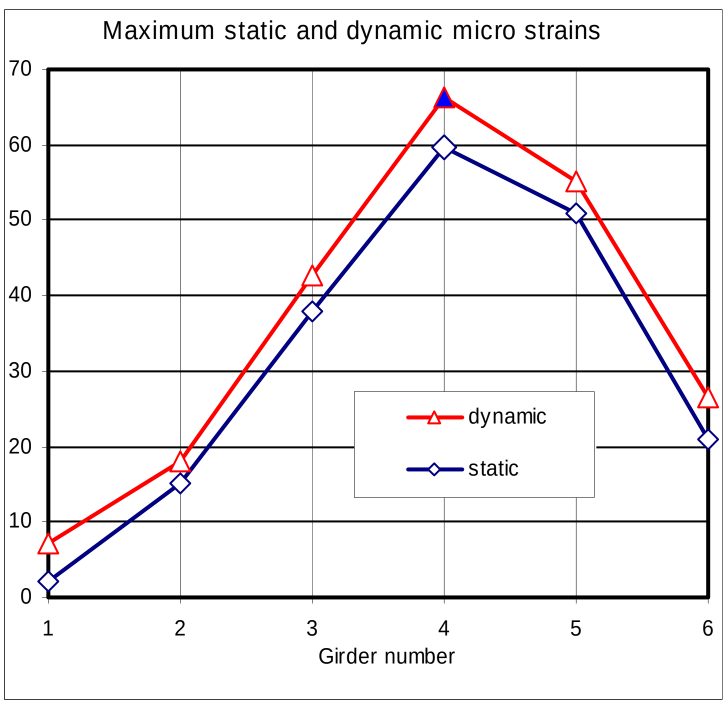

Figure B.30. Comparison of maximum static and dynamic strains for Case #10.

B.11. Case #11 – V=45mph, bridge#1, truck#3

The case #11 was defined for the truck #3 running through the bridge #1 with speed V=45mph. Figure B.31 presents the time histories of strains calculated for each girder in the middle of the span. Figure B.32 shows corresponding stresses caused by passing vehicle. In Figure B.33 maximum dynamitic strains are compared for each girder with the static strains. Impact factor was calculated for girder #4 with the maximum dynamic strain ε^D= 70.32 micro strains (σ^D= 2.65 MPa). The representative value of the impact factor for case #11 is:

$$IM_{case\#11} = 8.32\%$$

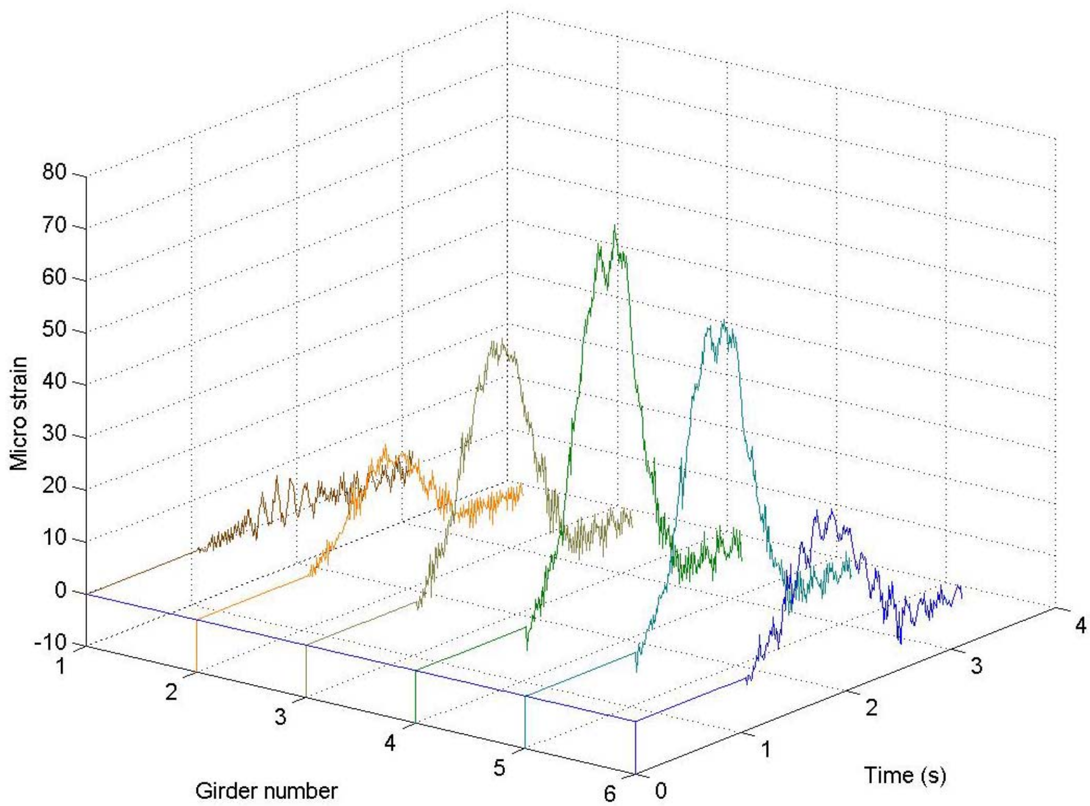

Figure B.31. Time histories of micro strains in girders for Case #11.

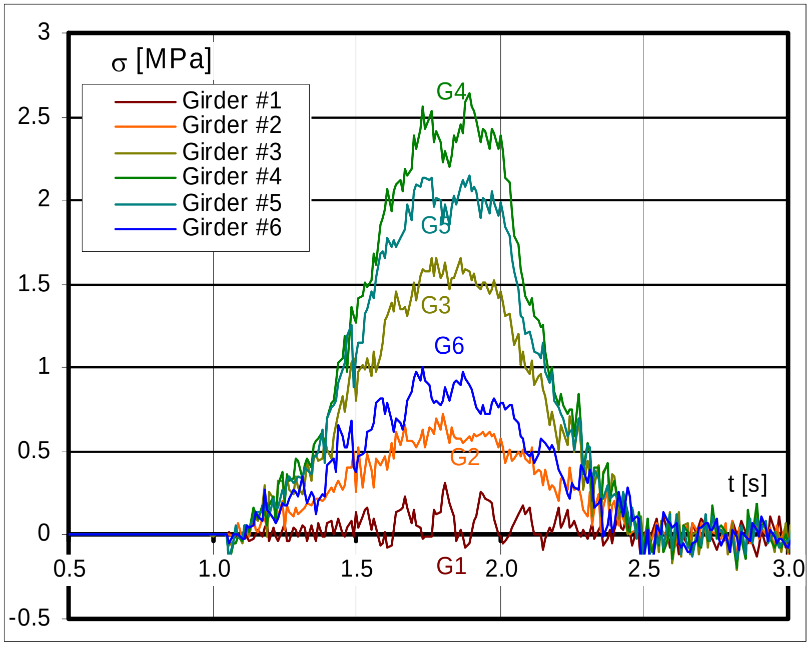

Figure B.32.Time histories of stresses in girders for Case #11.

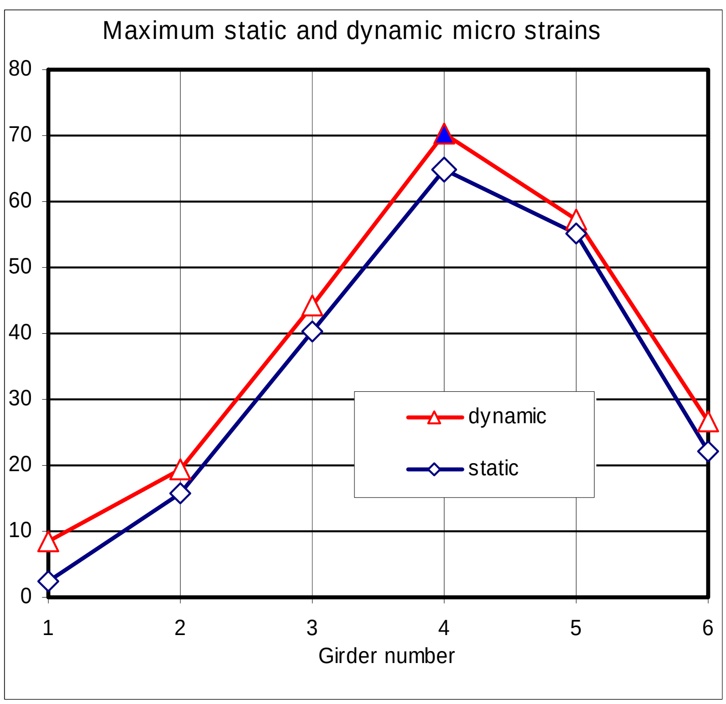

Figure B.33. Comparison of maximum static and dynamic strains for Case #11.

B.12. Case #12 – V=45mph, bridge#1, truck#4

The case #12 was defined for the truck #4 running through the bridge #1 with speed V=45mph. Figure B.34 presents the time histories of strains calculated for each girder in the middle of the span. Figure B.35 shows corresponding stresses caused by passing vehicle. In Figure B.36 maximum dynamitic strains are compared for each girder with the static strains. Impact factor was calculated for girder #4 with the maximum dynamic strain ε^D= 71.47 micro strains (σ^D= 2.69 MPa). The representative value of the impact factor for case #12 is:

$$IM_{case\#12} = 2.85\%$$

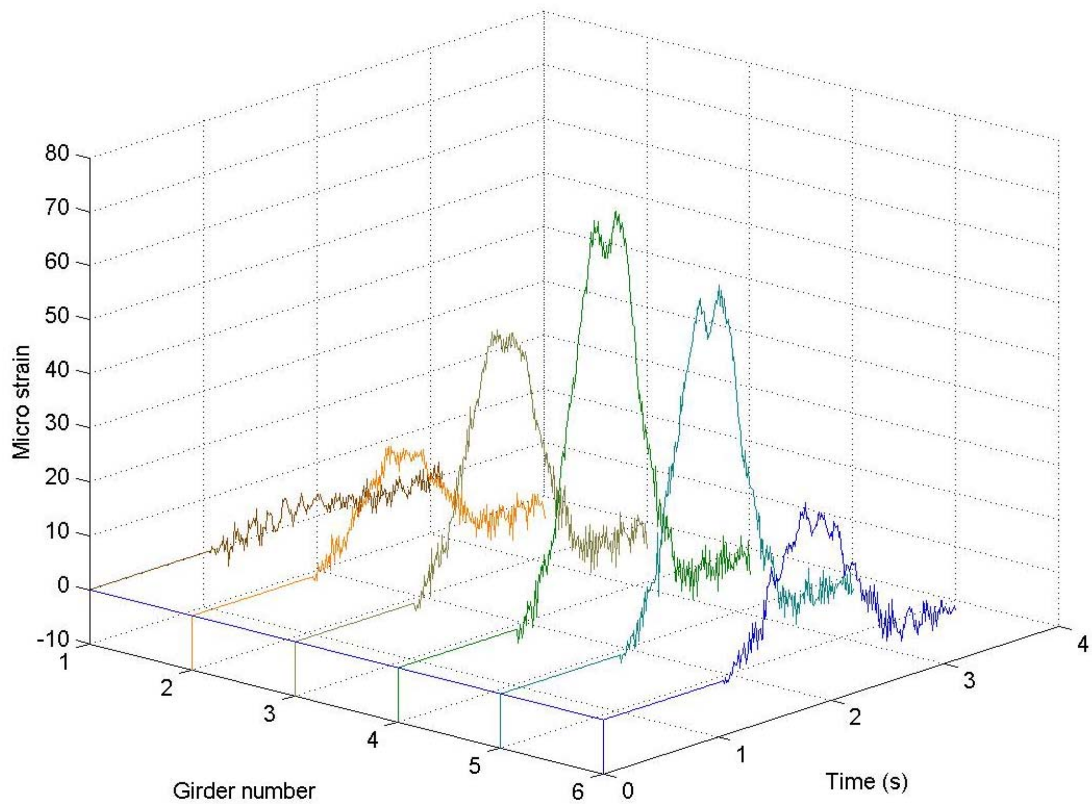

Figure B.34. Time histories of micro strains in girders for Case #12.

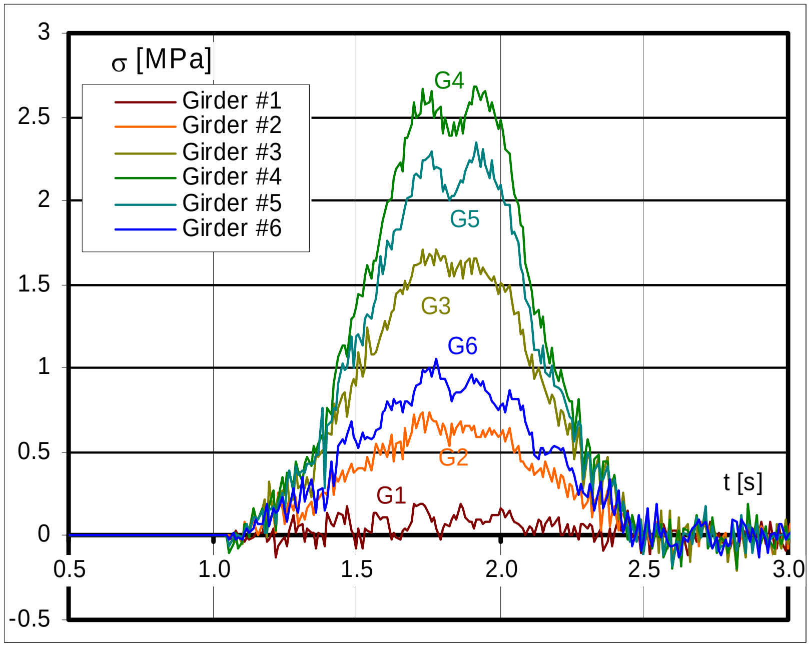

Figure B.35.Time histories of stresses in girders for Case #12.

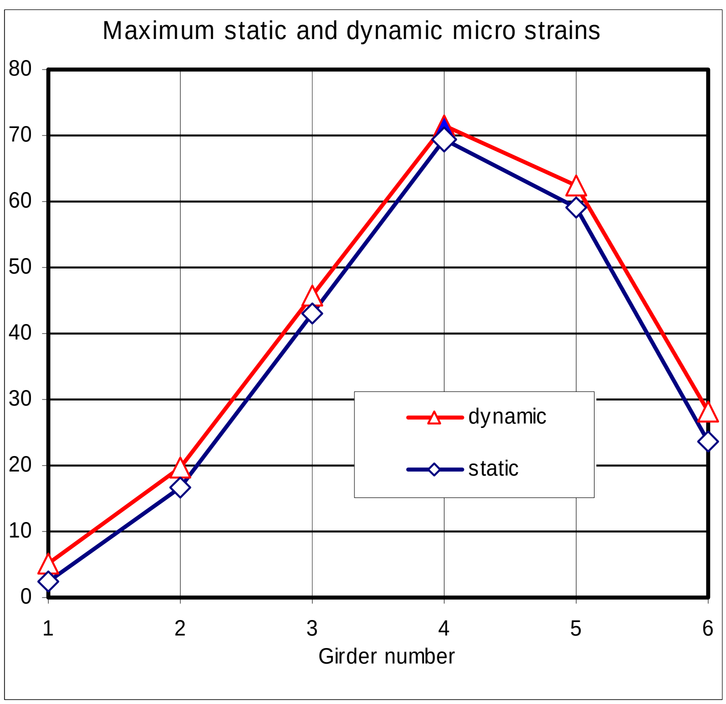

Figure B.36. Comparison of maximum static and dynamic strains for Case #12.

B.13. Case #13 – V=45mph, bridge#1, truck#5

The case #13 was defined for the truck #5 running through the bridge #1 with speed V=45mph. Figure B.37 presents the time histories of strains calculated for each girder in the middle of the span. Figure B.38 shows corresponding stresses caused by passing vehicle. In Figure B.39 maximum dynamitic strains are compared for each girder with the static strains. Impact factor was calculated for girder #4 with the maximum dynamic strain ε^D= 66.77micro strains (σ^D= 2.53MPa). The representative value of the impact factor for case #13 is:

$$IM_{case\#13} = 11.95\%$$

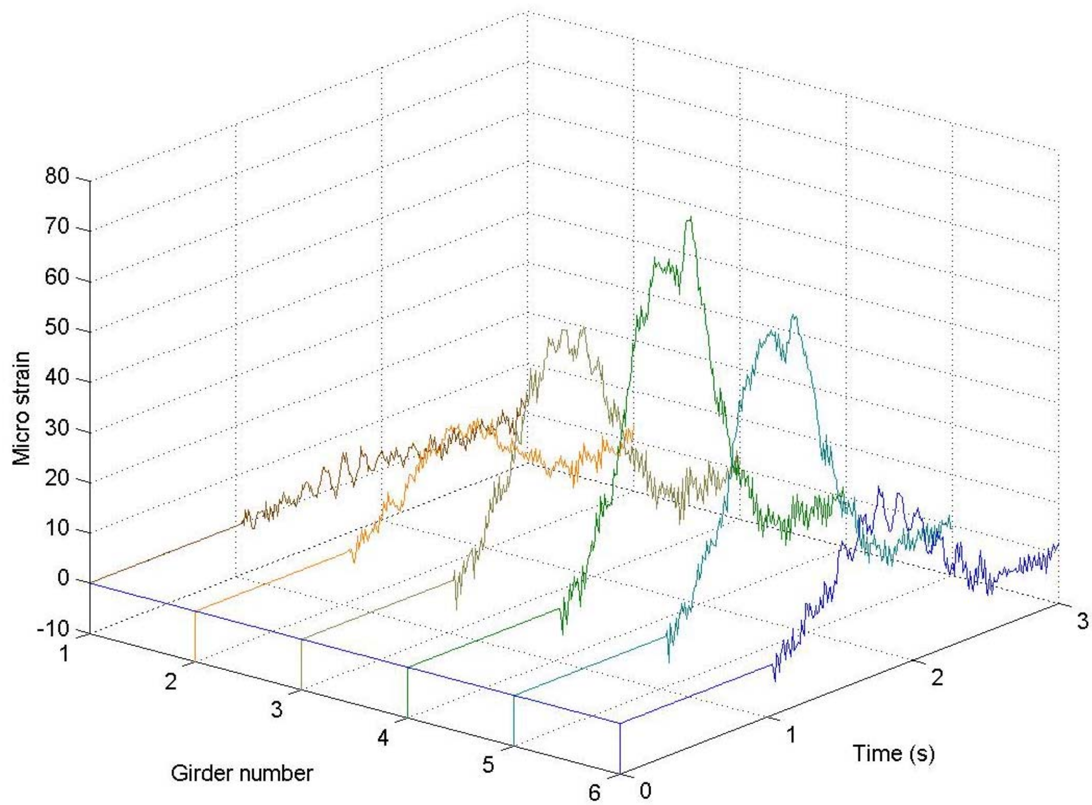

Figure B.37. Time histories of micro strains in girders for Case #13.

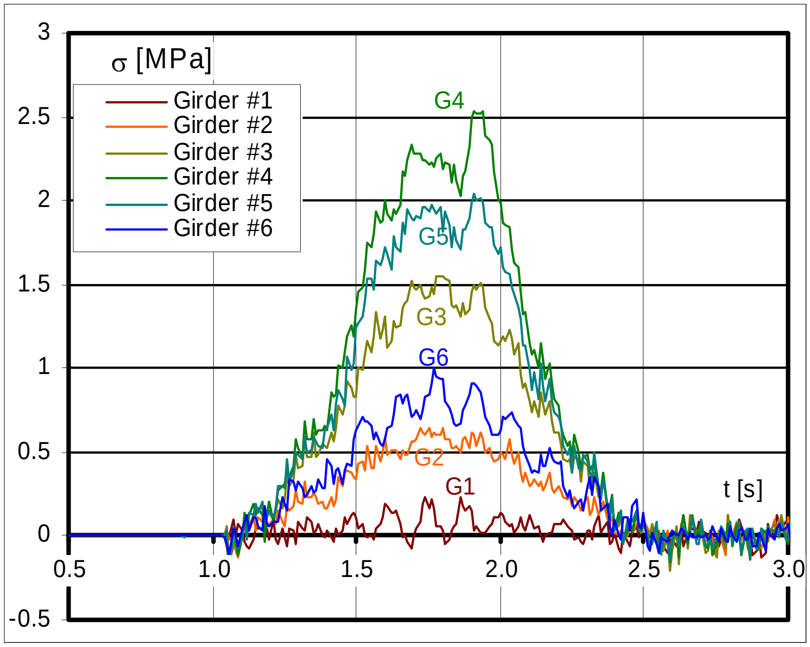

Figure B.38.Time histories of stresses in girders for Case #13.

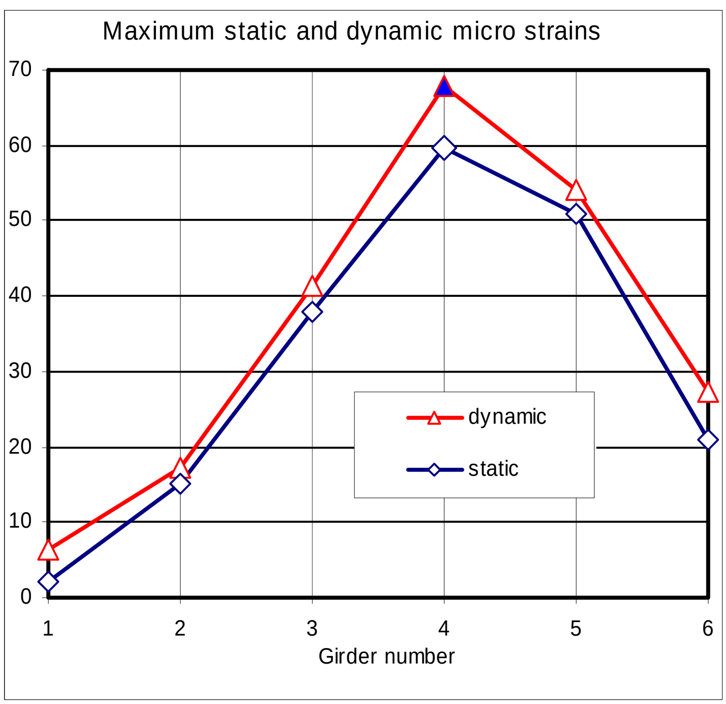

Figure B.39. Comparison of maximum static and dynamic strains for Case #13.

B.14. Case #14 – V=45mph, bridge#1, truck#6

The case #14 was defined for the truck #6 running through the bridge #1 with speed V=45mph. Figure B.40 presents the time histories of strains calculated for each girder in the middle of the span. Figure B.41 shows corresponding stresses caused by passing vehicle. In Figure B.42 maximum dynamitic strains are compared for each girder with the static strains. Impact factor was calculated for girder #4 with the maximum dynamic strain ε^D= 64.2 micro strains (σ^D= 2.41MPa). The representative value of the impact factor for case #14 is:

$$IM_{case\#14} = 7.63\ \%$$

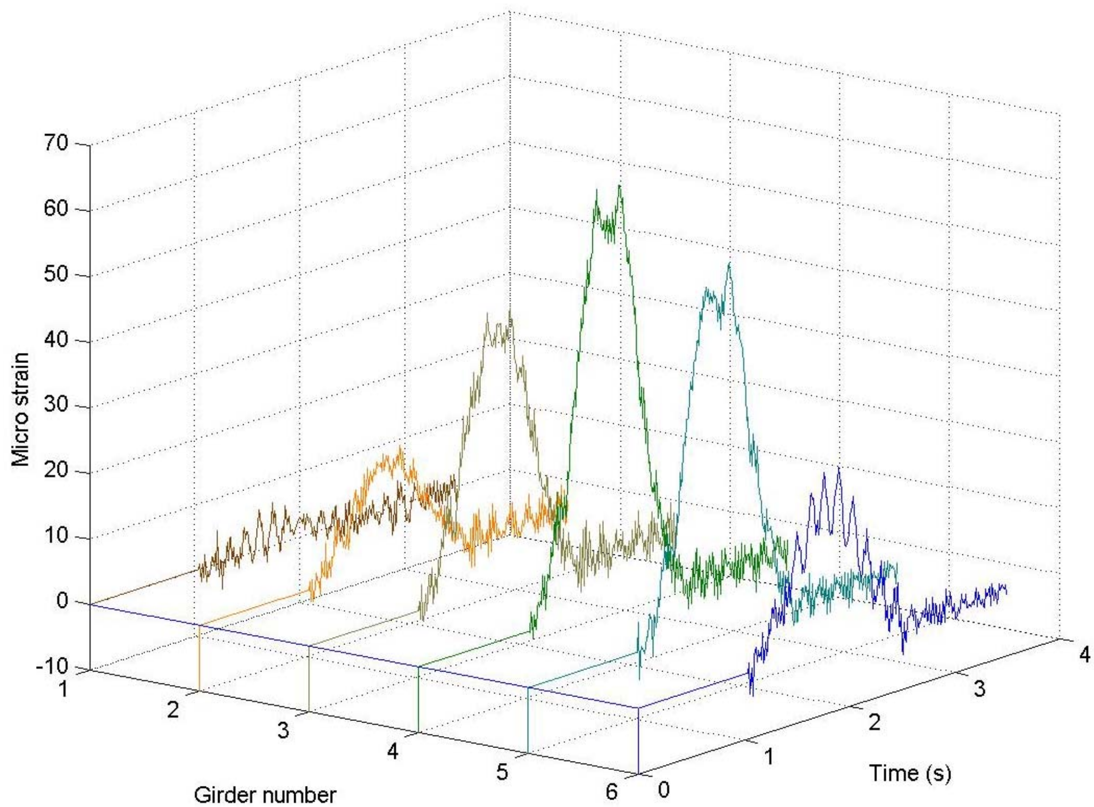

Figure B.40. Time histories of micro strains in girders for Case #14.

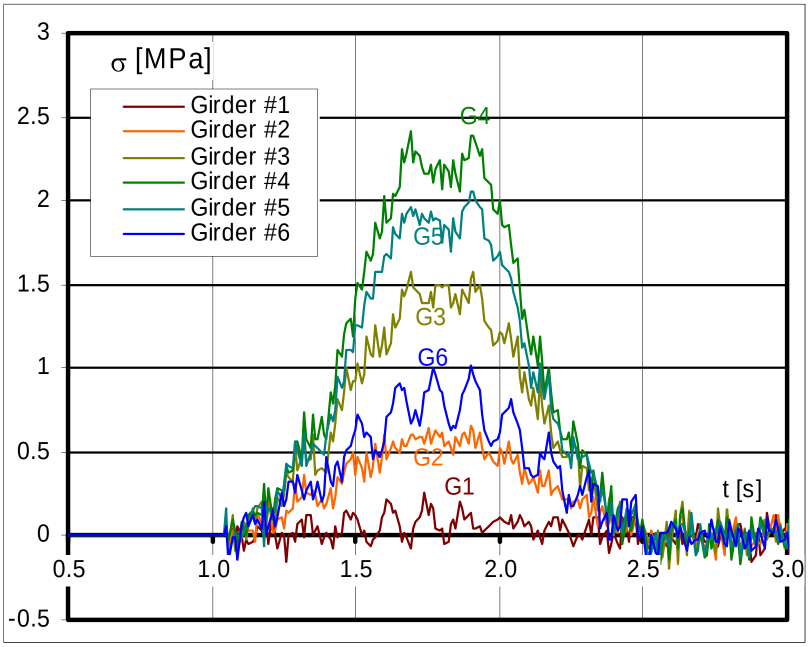

Figure B.41.Time histories of stresses in girders for Case #14.

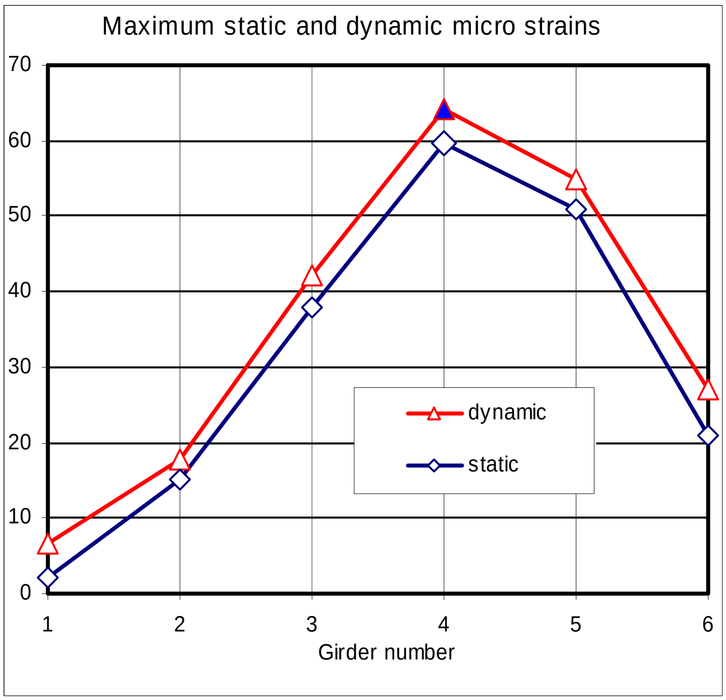

Figure B.42. Comparison of maximum static and dynamic strains for Case #14.

B.15. Case #15 – V=55mph, bridge#1, truck#1

The case #15 was defined for the truck #5 running through the bridge #1 with speed V=55mph. Figure B.43 presents the time histories of strains calculated for each girder in the middle of the span. Figure B.44 shows corresponding stresses caused by passing vehicle. In Figure B.45 maximum dynamitic strains are compared for each girder with the static strains. Impact factor was calculated for girder #4 with the maximum dynamic strain ε^D= 74.44 micro strains (σ^D= 2.78 MPa). The representative value of the impact factor for case #15 is:

$$IM_{case\#15} = 60.19\ \%$$

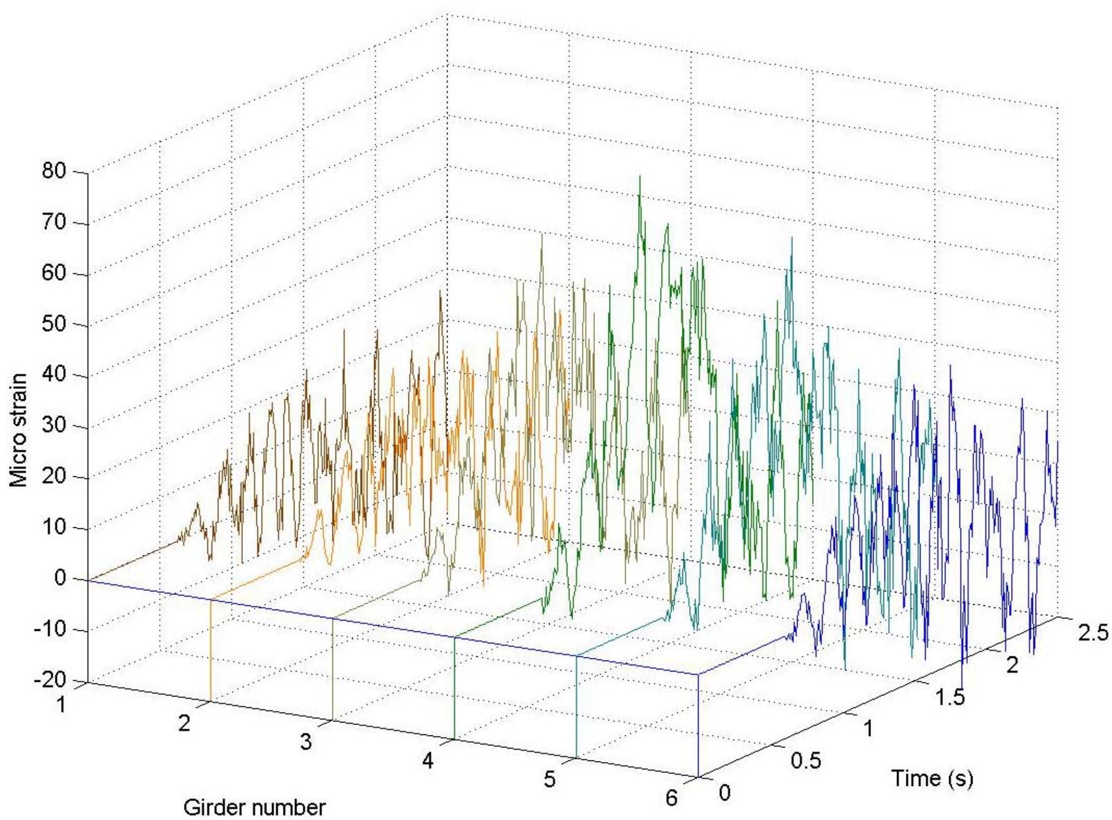

Figure B.43. Time histories of micro strains in girders for Case #15.

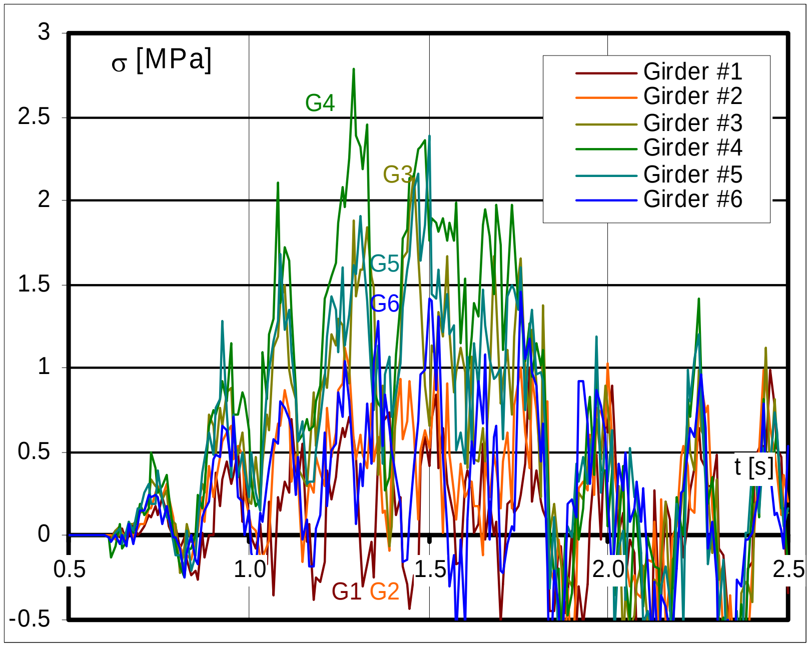

Figure B.44.Time histories of stresses in girders for Case #15.

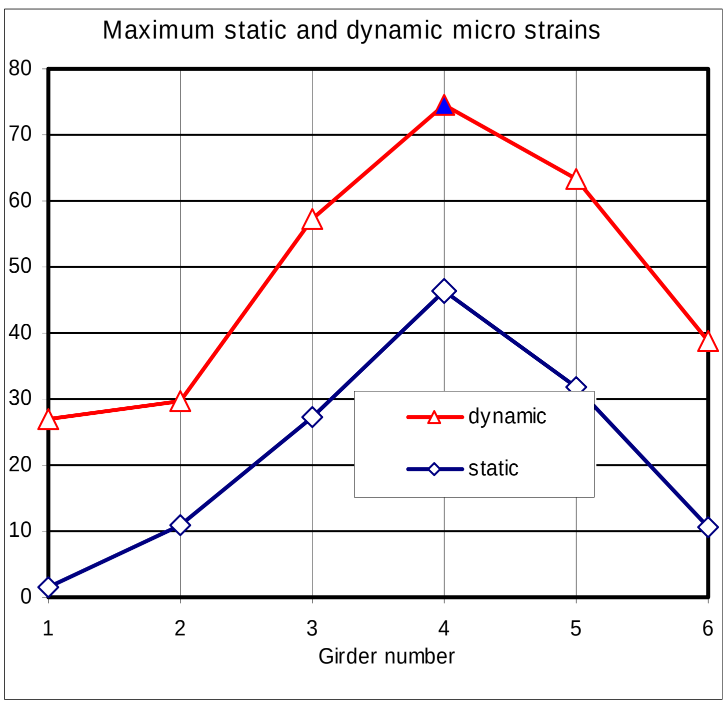

Figure B.45. Comparison of maximum static and dynamic strains for Case #15.

B.16. Case #16 – V=55mph, bridge#1, truck#2

The case #16 was defined for the truck #2 running through the bridge #1 with speed V=55mph. Figure B.46 presents the time histories of strains calculated for each girder in the middle of the span. Figure B.47 shows corresponding stresses caused by passing vehicle. In Figure B.48 maximum dynamitic strains are compared for each girder with the static strains. Impact factor was calculated for girder #4 with the maximum dynamic strain ε^D= 67.23 micro strains (σ^D= 2.52 MPa). The representative value of the impact factor for case #16 is:

$$IM_{case\#16} = 12.7\ \%$$

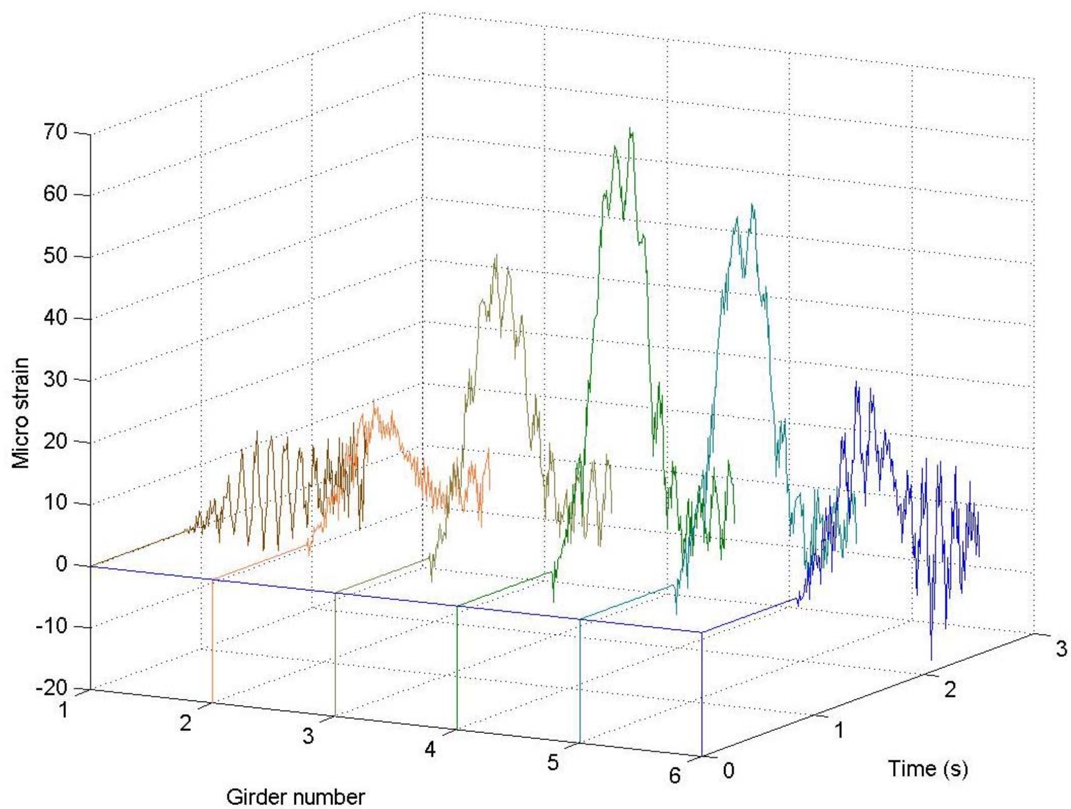

Figure B.46. Time histories of micro strains in girders for Case #16.

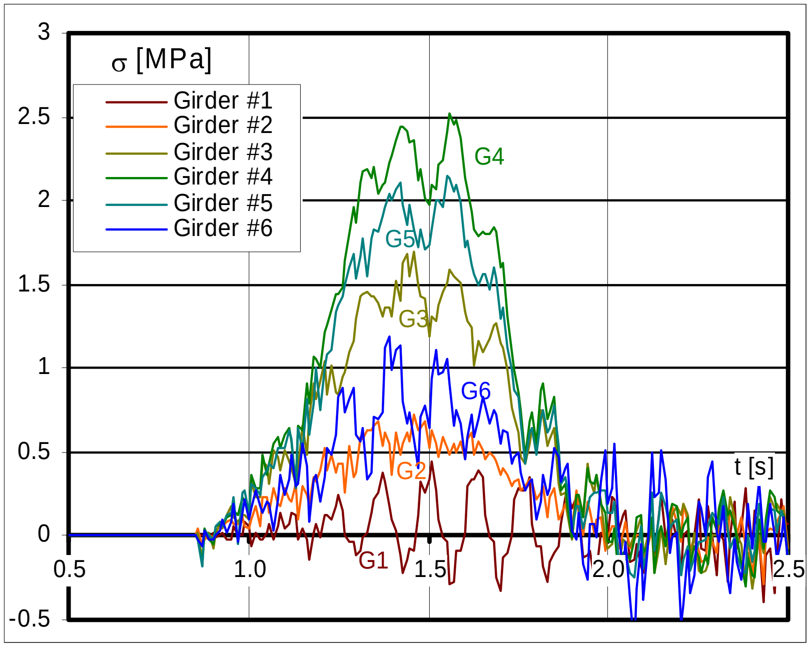

Figure B.47. Time histories of stresses in girders for Case #16.

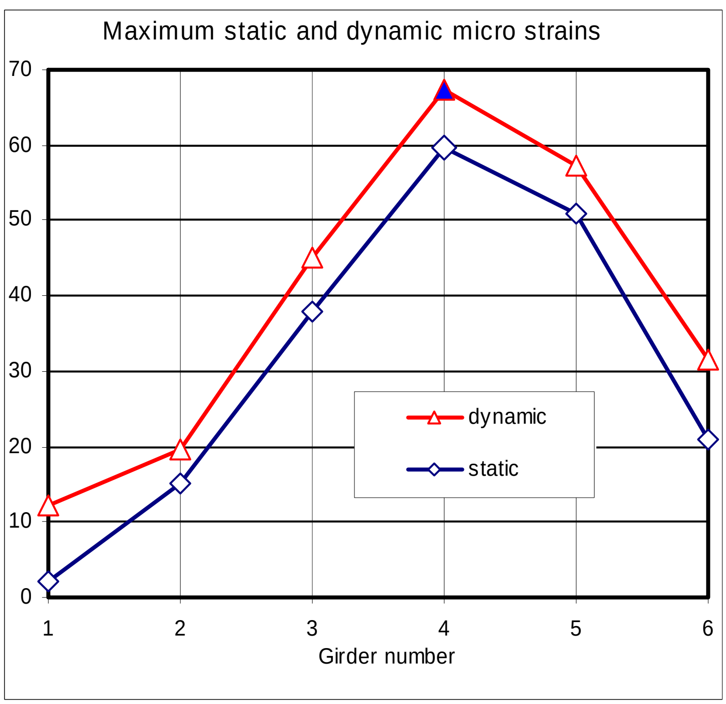

Figure B.48. Comparison of maximum static and dynamic strains for Case #16.

B.17. Case #17 – V=55mph, bridge#1, truck#3

The case #17 was defined for the truck #3 running through the bridge #1 with speed V=55mph. Figure B.49 presents the time histories of strains calculated for each girder in the middle of the span. Figure B.50 shows corresponding stresses caused by passing vehicle. In Figure B.51 maximum dynamitic strains are compared for each girder with the static strains. Impact factor was calculated for girder #4 with the maximum dynamic strain ε^D= 71.51 micro strains (σ^D= 2.67 MPa). The representative value of the impact factor for case #17 is:

$$IM_{case\#17} = 10.14\%$$

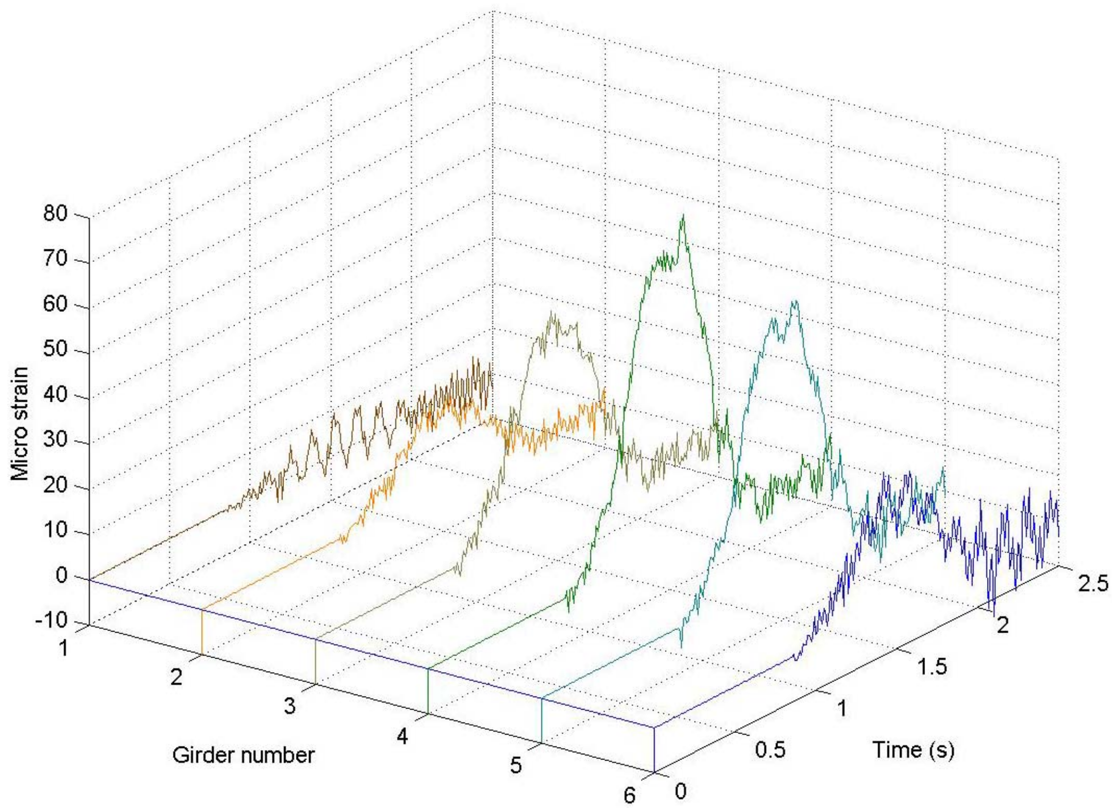

Figure B.49. Time histories of micro strains in girders for Case #17.

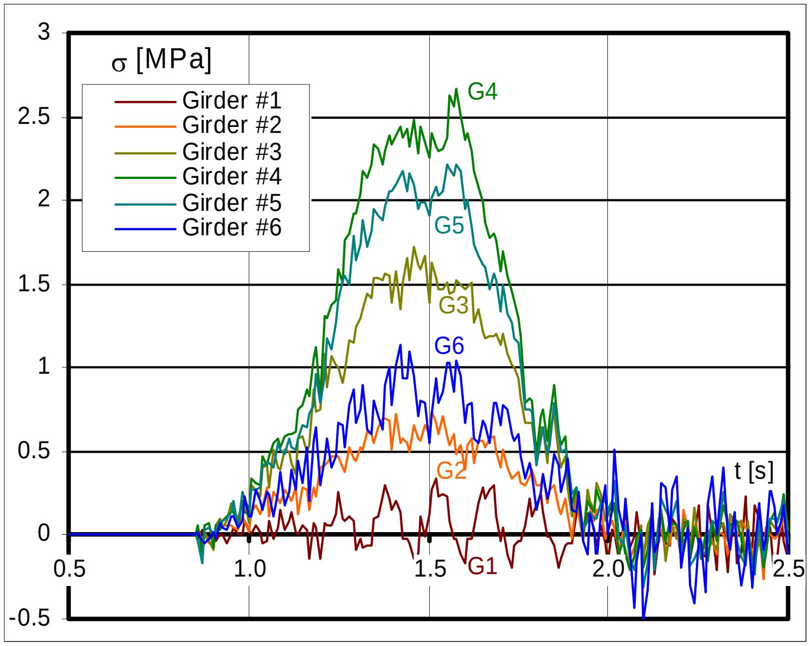

Figure B.50. Time histories of stresses in girders for Case #17.

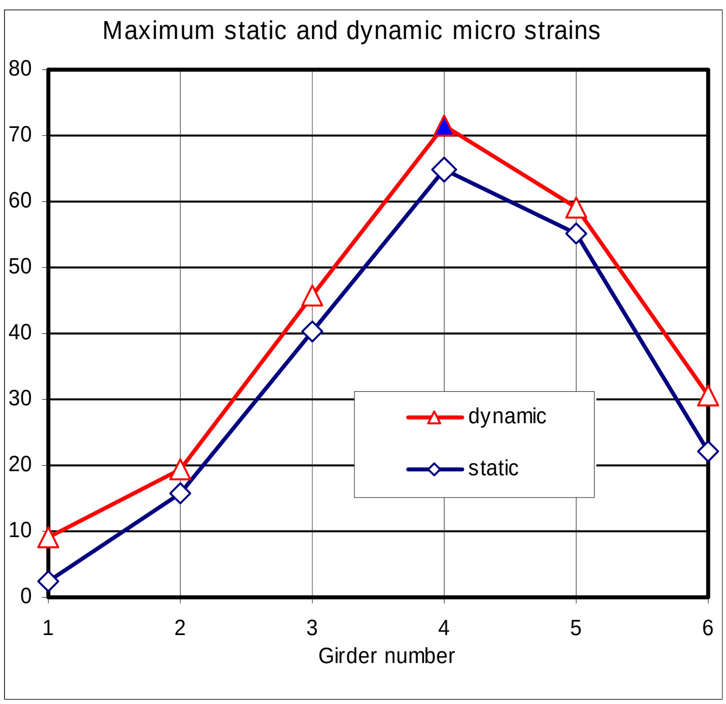

Figure B.51. Comparison of maximum static and dynamic strains for Case #17.

B.18. Case #18 – V=55mph, bridge#1, truck#4

The case #18 was defined for the truck #4 running through the bridge #1 with speed V=55mph. Figure B.52 presents the time histories of strains calculated for each girder in the middle of the span. Figure B.53 shows corresponding stresses caused by passing vehicle. In Figure B.54 maximum dynamitic strains are compared for each girder with the static strains. Impact factor was calculated for girder #4 with the maximum dynamic strain ε^D= 71.95 micro strains (σ^D= 2.7 MPa). The representative value of the impact factor for case #18 is:

$$IM_{case\#18} = 3.54\ \%$$

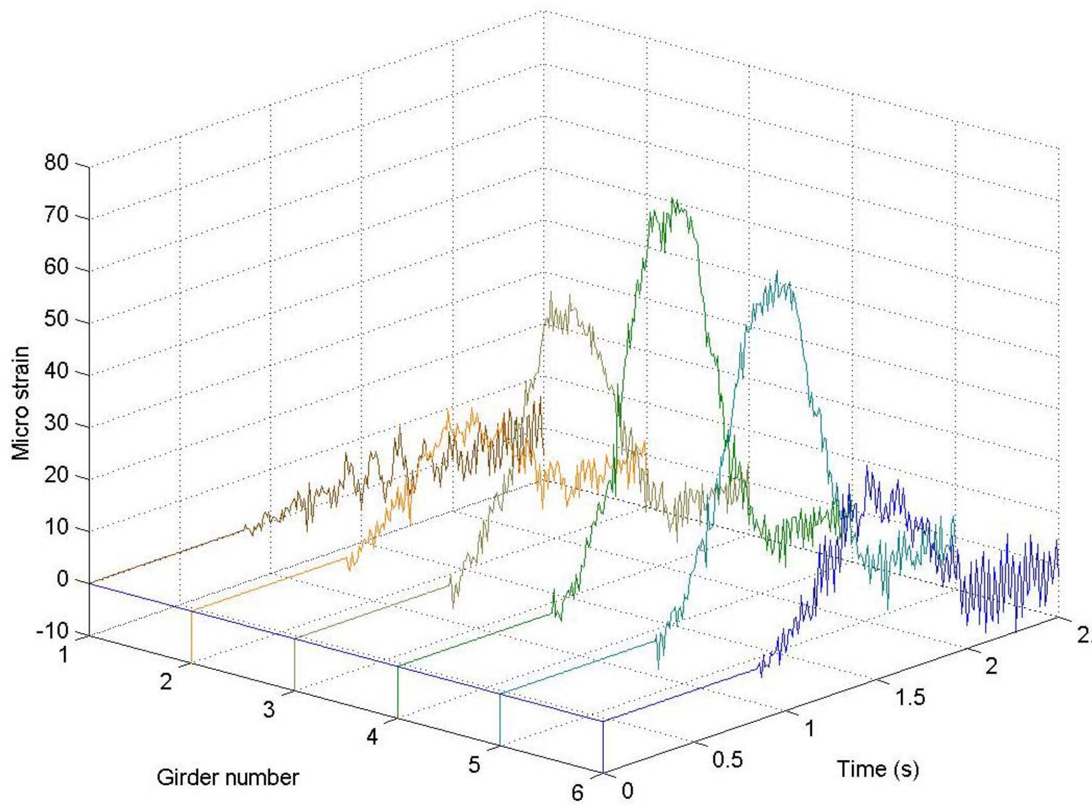

Figure B.52. Time histories of micro strains in girders for Case #18.

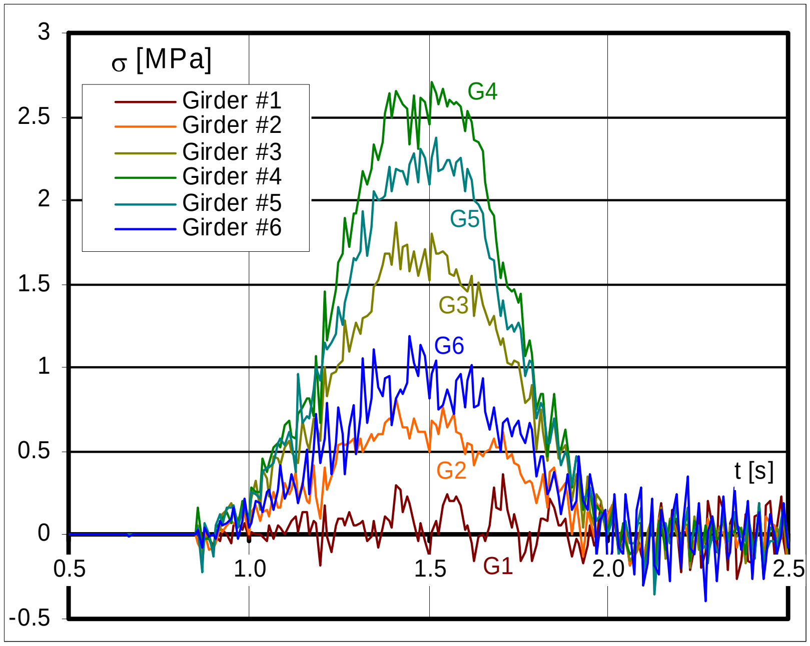

Figure B.53. Time histories of stresses in girders for Case #18.

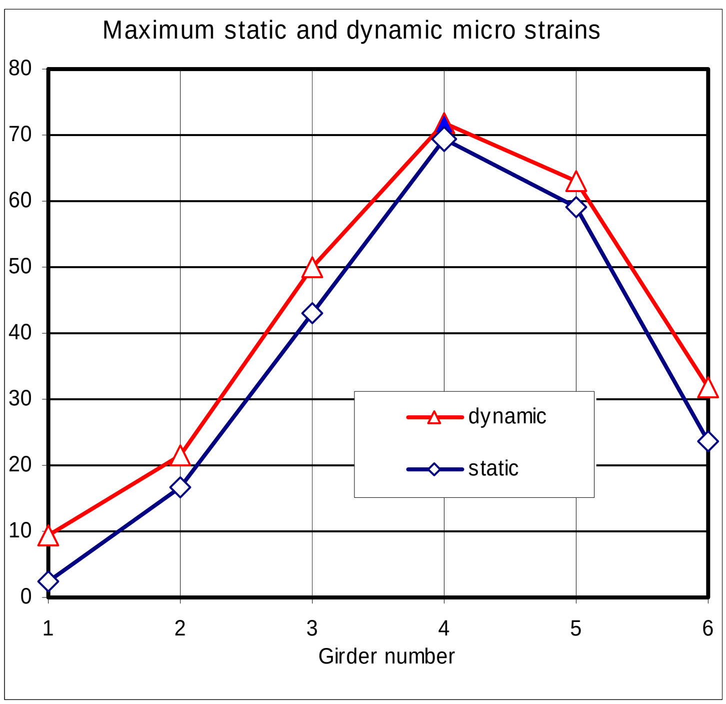

Figure B.54. Comparison of maximum static and dynamic strains for Case #18.

B.19. Case #19 – V=55mph, bridge#1, truck#5

The case #19 was defined for the truck #5 running through the bridge #1 with speed V=55mph. Figure B.55 presents the time histories of strains calculated for each girder in the middle of the span. Figure B.56 shows corresponding stresses caused by passing vehicle. In Figure B.57 maximum dynamitic strains are compared for each girder with the static strains. Impact factor was calculated for girder #4 with the maximum dynamic strain ε^D= 66.27micro strains (σ^D= 2.49MPa). The representative value of the impact factor for case #19 is:

$$IM_{case\#19} = 11.1\%$$

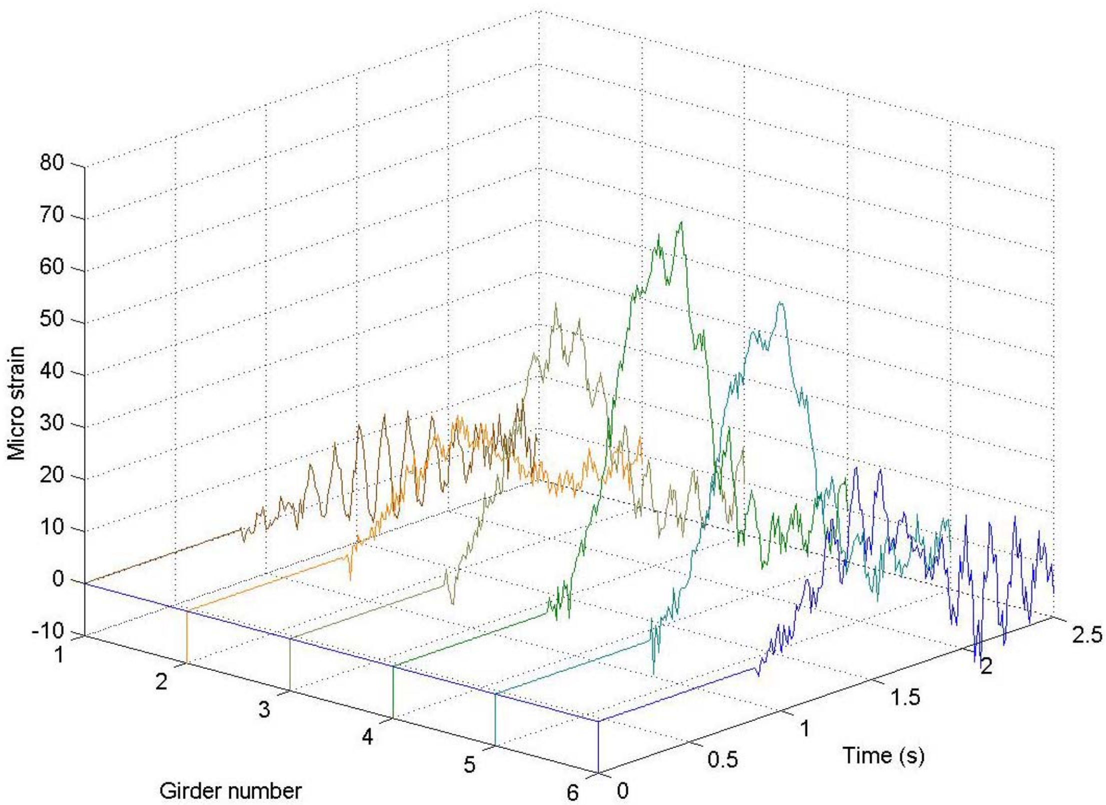

Figure B.55. Time histories of micro strains in girders for Case #19.

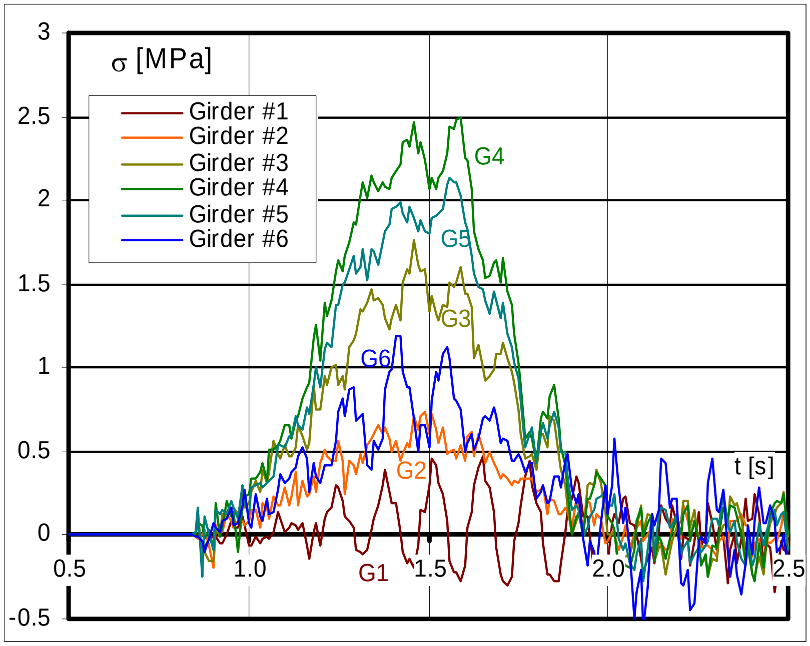

Figure B.56. Time histories of stresses in girders for Case #19.

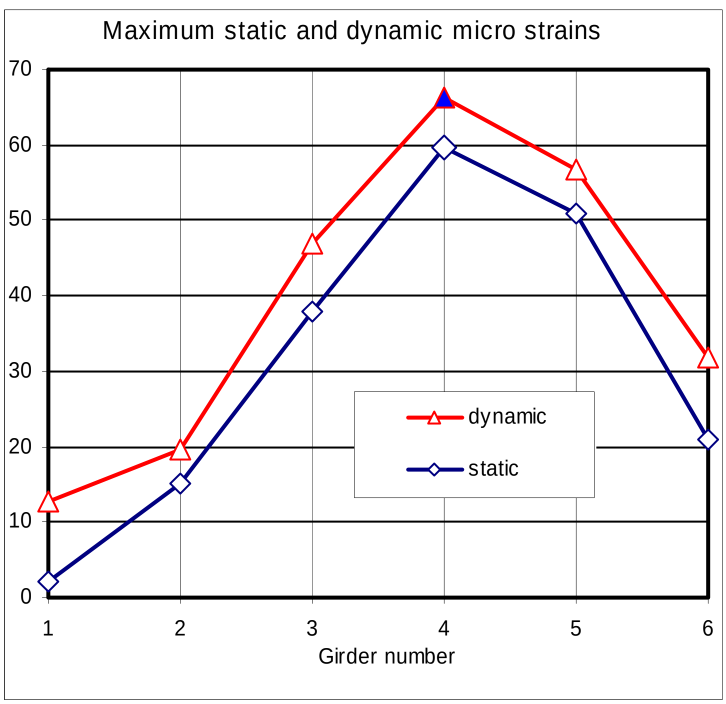

Figure B.57. Comparison of maximum static and dynamic strains for Case #19.

B.20. Case #20 – V=55mph, bridge#1, truck#6

The case #20 was defined for the truck #6 running through the bridge #1 with speed V=55mph. Figure B.58 presents the time histories of strains calculated for each girder in the middle of the span. Figure B.59 shows corresponding stresses caused by passing vehicle. In Figure B.60 maximum dynamitic strains are compared for each girder with the static strains. Impact factor was calculated for girder #4 with the maximum dynamic strain ε^D= 64.94 micro strains (σ^D= 2.44 MPa). The representative value of the impact factor for case #20 is:

$$IM_{case\#20} = 8.88\%$$

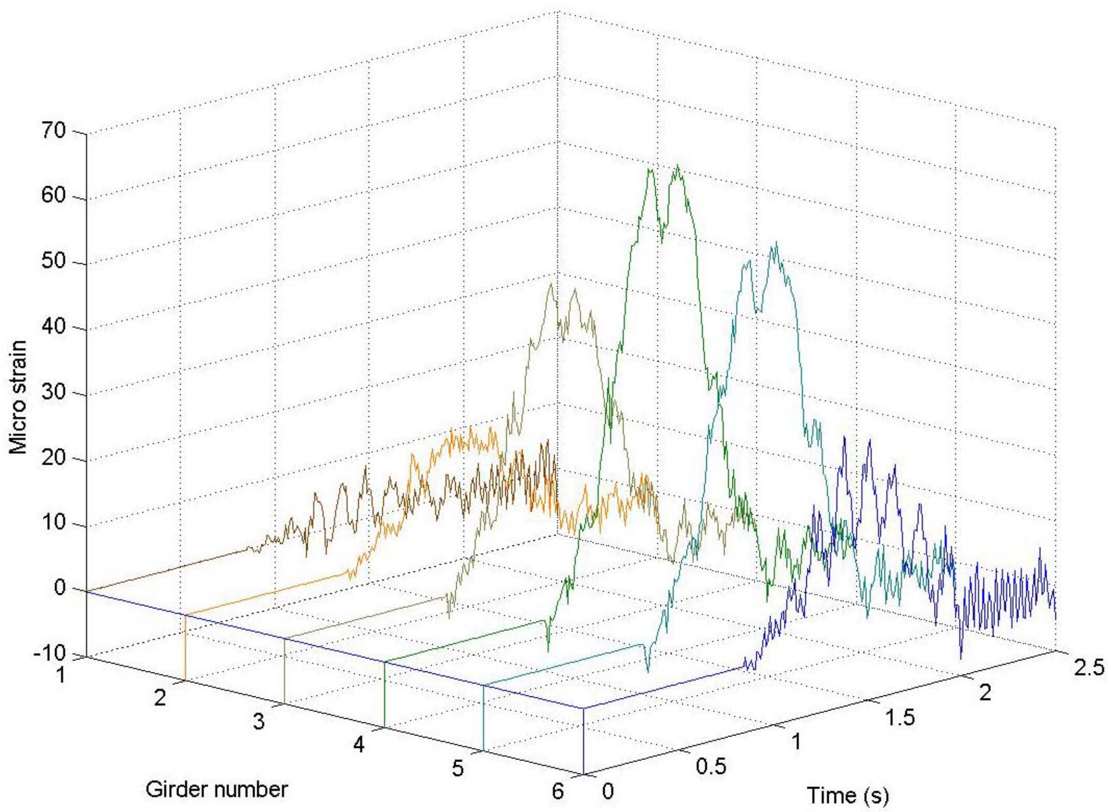

Figure B.58. Time histories of micro strains in girders for Case #20.

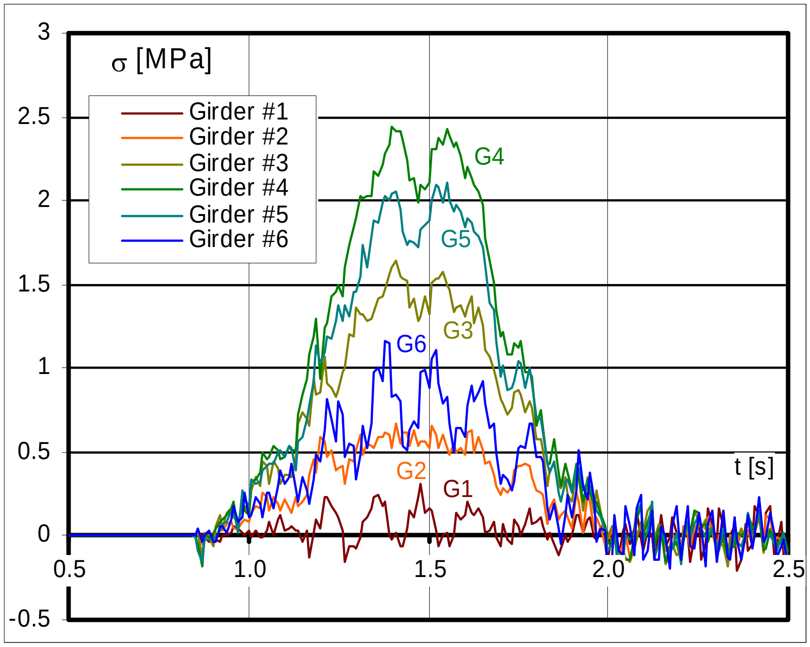

Figure B.59. Time histories of stresses in girders for Case #20.

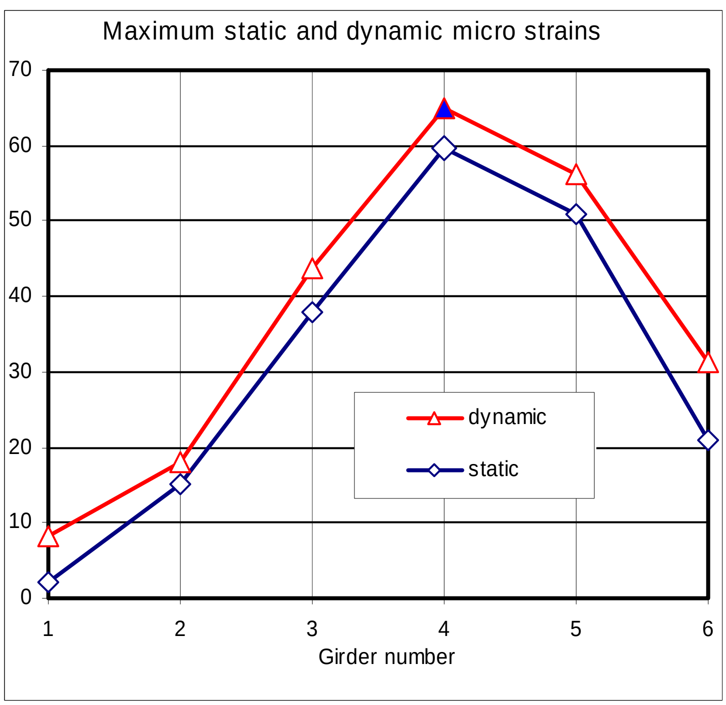

Figure B.60. Comparison of maximum static and dynamic strains for Case #20

B.21. Case #21 – V=55mph, bridge#2, truck#1

The case #21 was defined for the truck #1 running through the bridge #2 with speed V=55mph. Figure B.61 presents the time histories of strains calculated for each girder in the middle of the span. Figure B.62 shows corresponding stresses caused by passing vehicle. In Figure B.63 maximum dynamitic strains are compared for each girder with the static strains. Impact factor was calculated for girder #4 with the maximum dynamic strain ε^D= 79.11 micro strains (σ^D= 3.01 MPa). The representative value of the impact factor for case #21 is:

$$IM_{case\#21} = 51.37\%$$

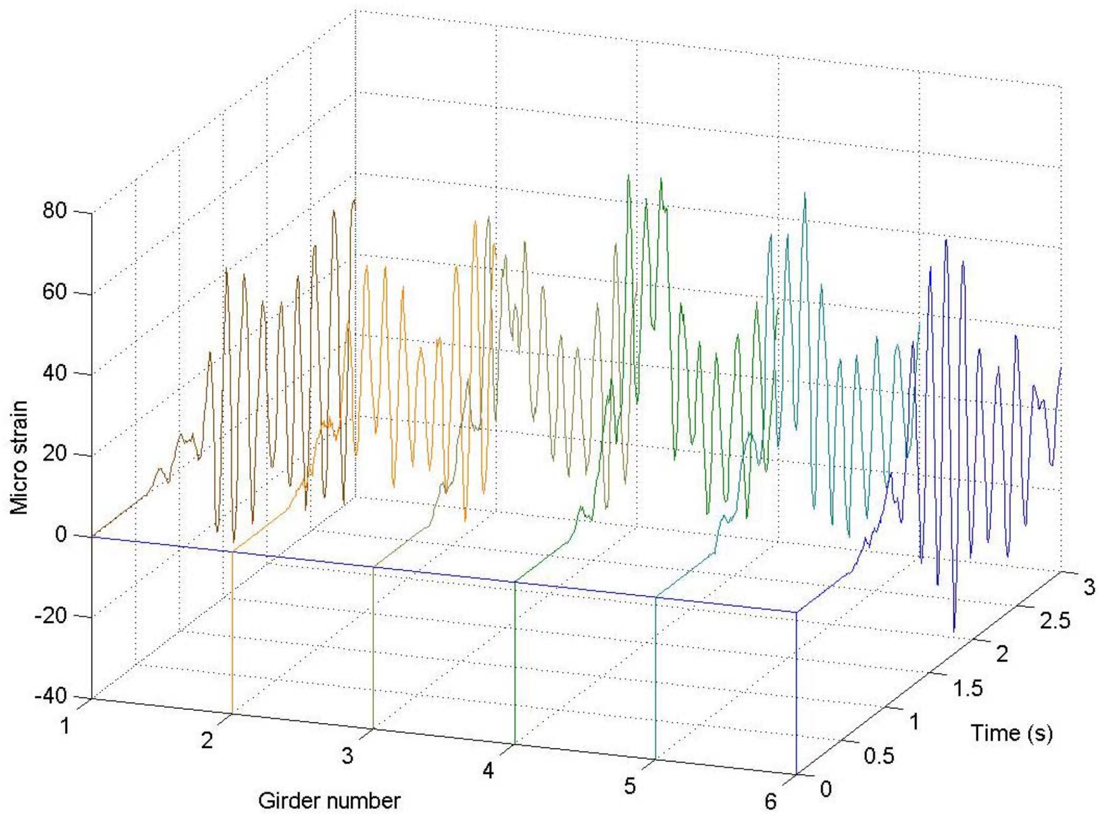

Figure B.61. Time histories of micro strains in girders for Case #21.

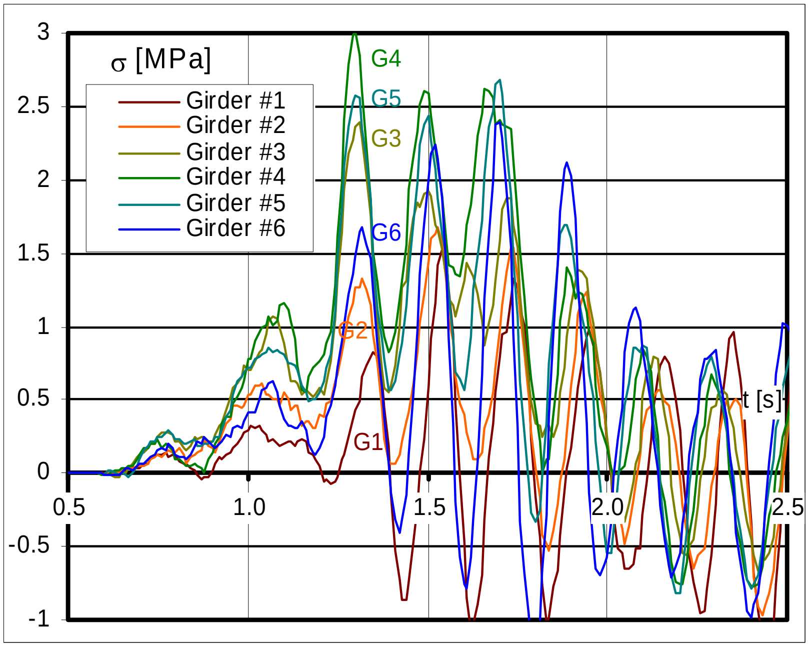

Figure B.62. Time histories of stresses in girders for Case #21.

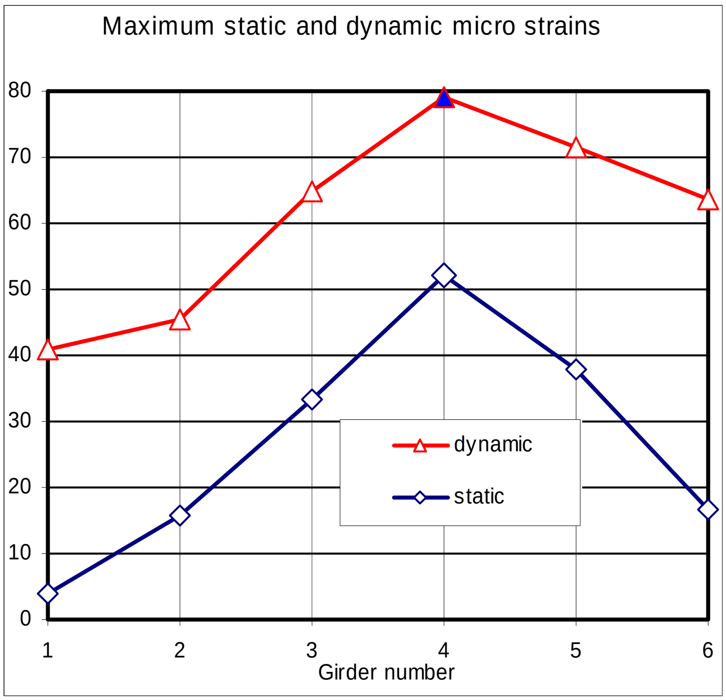

Figure B.63. Comparison of maximum static and dynamic strains for Case #21.

B.22. Case #22 – V=55mph, bridge#2, truck#2

The case #22 was defined for the truck #2 running through the bridge #2 with speed V=55mph. Figure B.64 presents the time histories of strains calculated for each girder in the middle of the span. Figure B.65 shows corresponding stresses caused by passing vehicle. In Figure B.66 maximum dynamitic strains are compared for each girder with the static strains. Impact factor was calculated for girder #4 with the maximum dynamic strain ε^D= 72.95 micro strains (σ^D= 2.74 MPa). The representative value of the impact factor for case #22 is:

$$IM_{case\#22} = 7.89\%$$

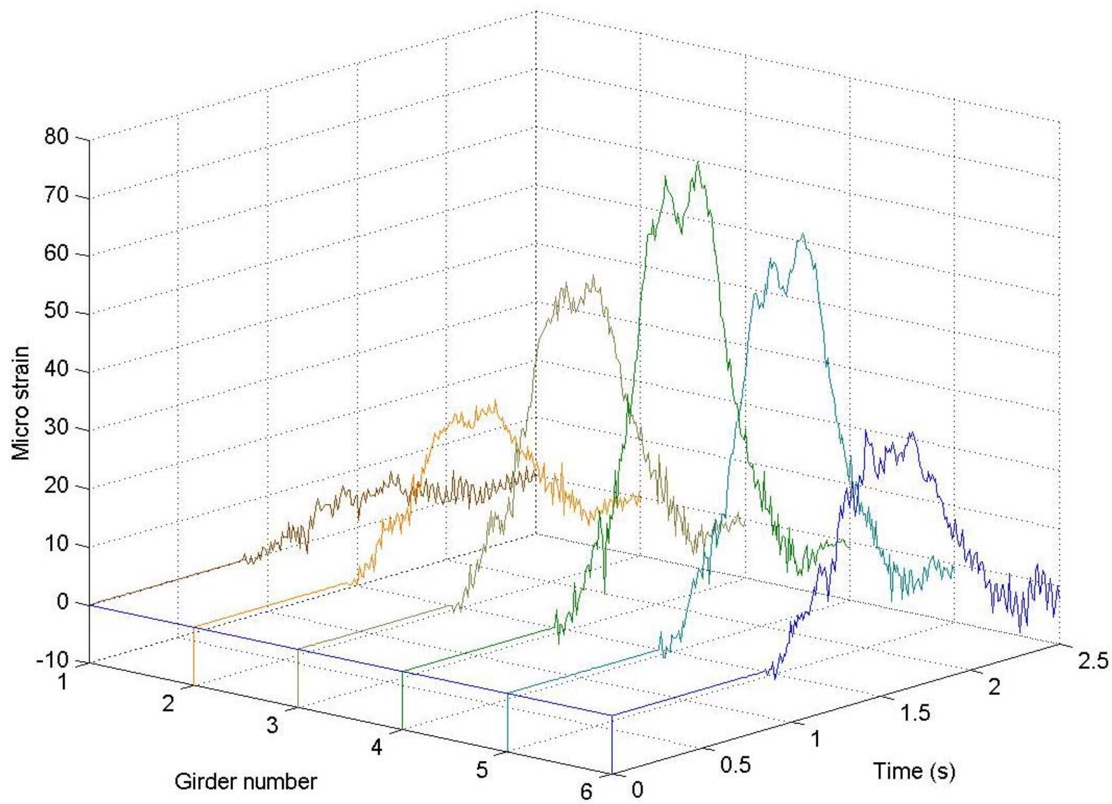

Figure B.64. Time histories of micro strains in girders for Case #22.

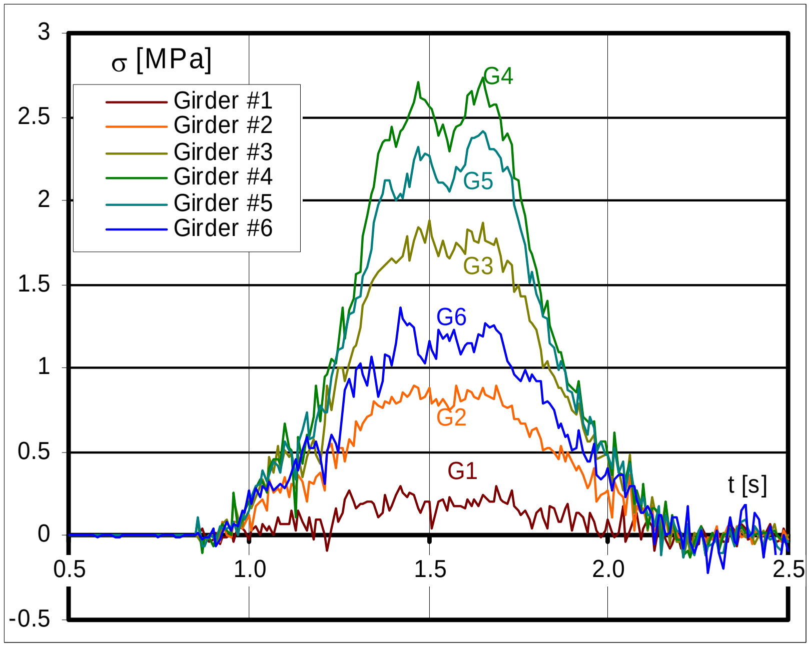

Figure B.65. Time histories of stresses in girders for Case #22.

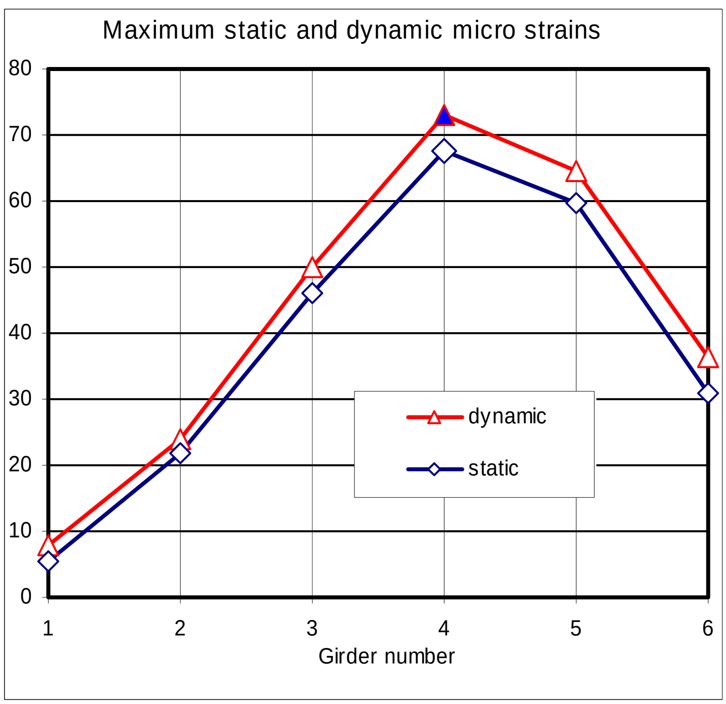

Figure B.66. Comparison of maximum static and dynamic strains for Case #22.

B.23. Case #23 – V=55mph, bridge#2, truck#3

The case #23 was defined for the truck #3 running through the bridge #2 with speed V=55mph. Figure B.67 presents the time histories of strains calculated for each girder in the middle of the span. Figure B.68 shows corresponding stresses caused by passing vehicle. In Figure B.69 maximum dynamitic strains are compared for each girder with the static strains. Impact factor was calculated for girder #4 with the maximum dynamic strain ε^D= 77.84 micro strains (σ^D= 2.93 MPa). The representative value of the impact factor for case #23 is:

$$IM_{case\#23} = 6.24\%$$

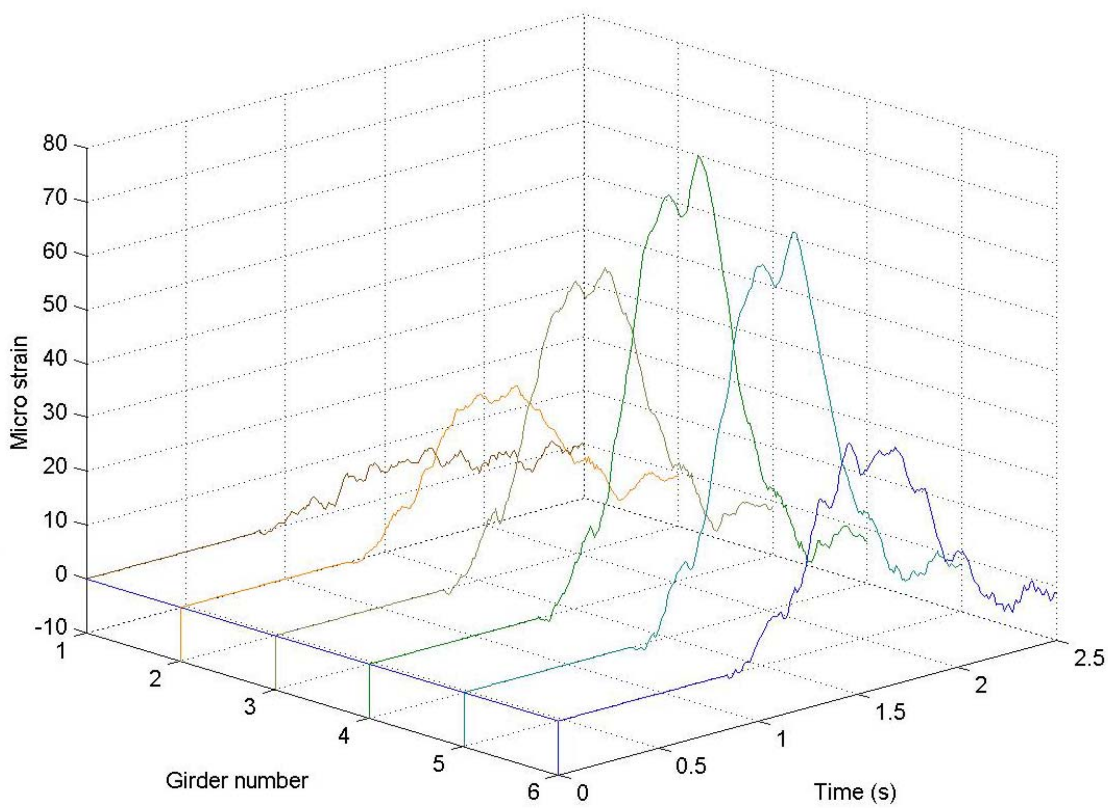

Figure B.67. Time histories of micro strains in girders for Case #23.

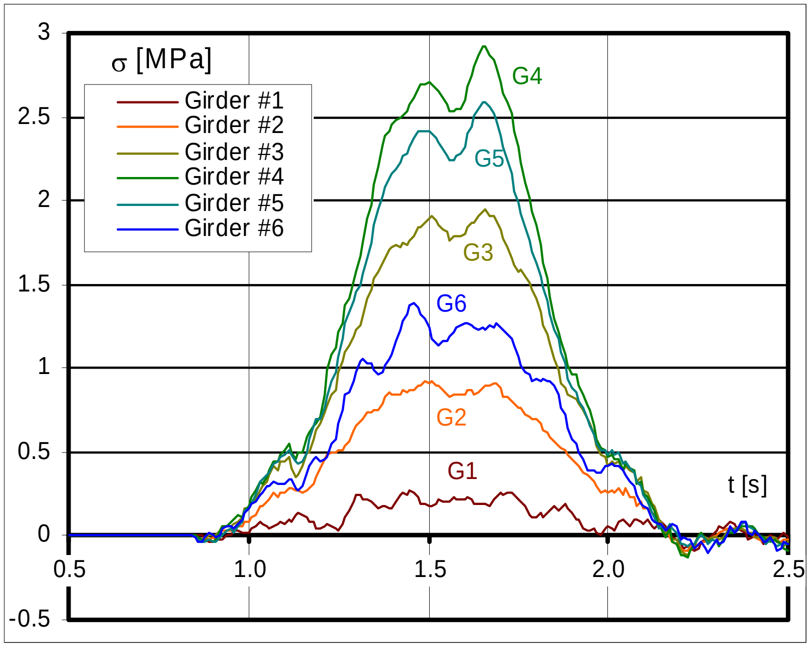

Figure B.68. Time histories of stresses in girders for Case #23.

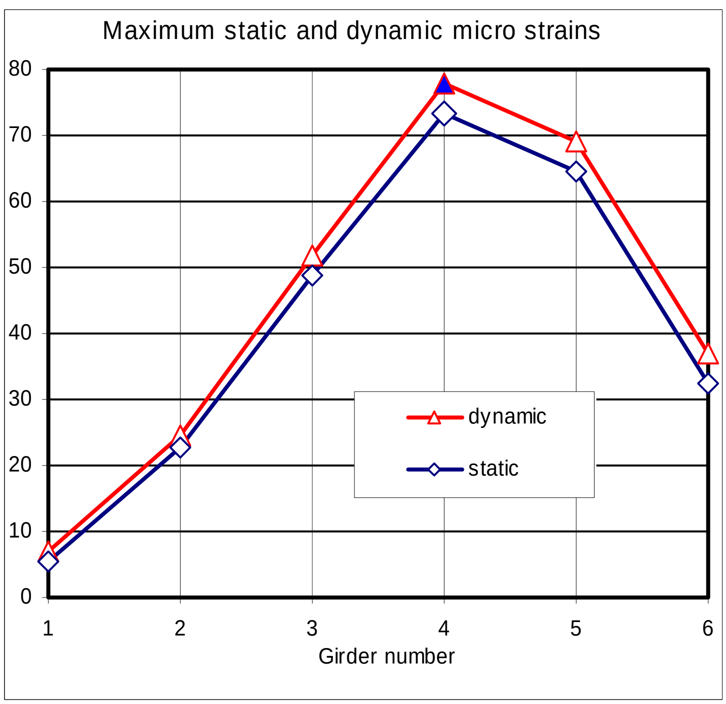

Figure B.69. Time histories of stresses in girders for Case #23.

B.24. Case #24 – V=55mph, bridge#2, truck#4

The case #24 was defined for the truck #4 running through the bridge #2 with speed V=55mph. Figure B.70 presents the time histories of strains calculated for each girder in the middle of the span. Figure B.71 shows corresponding stresses caused by passing vehicle. In Figure B.72 maximum dynamitic strains are compared for each girder with the static strains. Impact factor was calculated for girder #4 with the maximum dynamic strain ε^D= 80.75 micro strains (σ^D= 3.05 MPa). The representative value of the impact factor for case #24 is:

$$IM_{case\#24} = 2.96\%$$

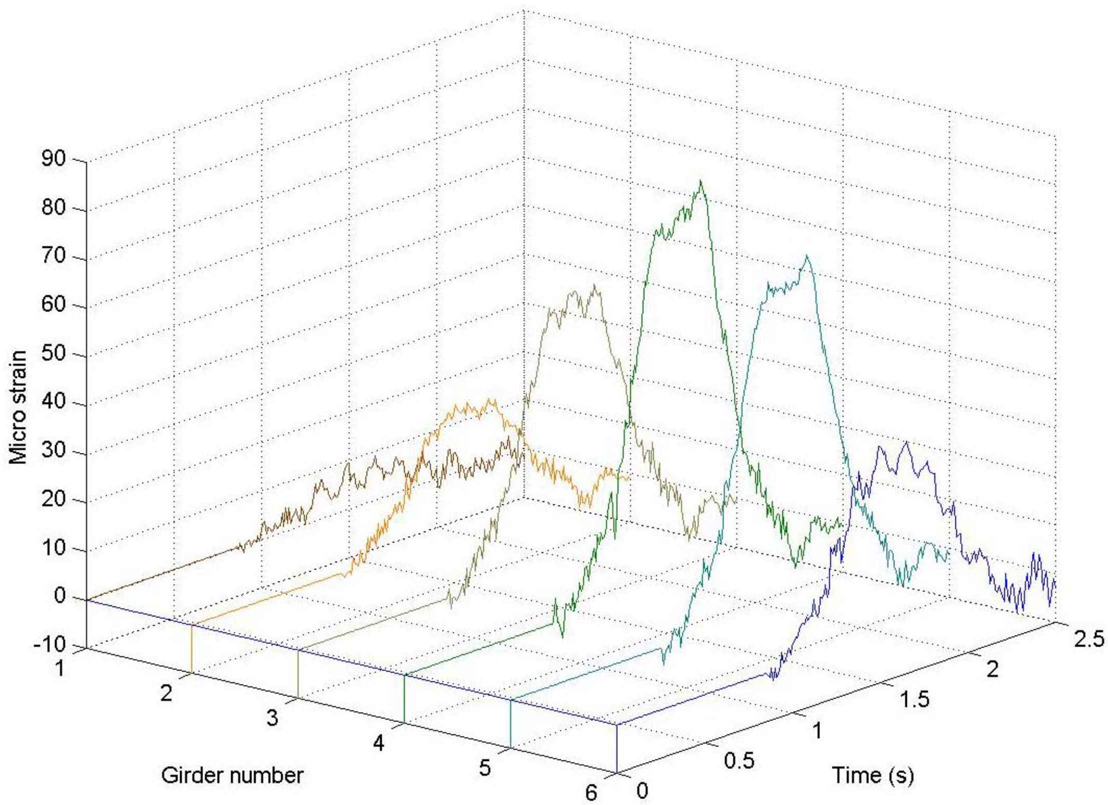

B.70. Time histories of micro strains in girders for Case #24.

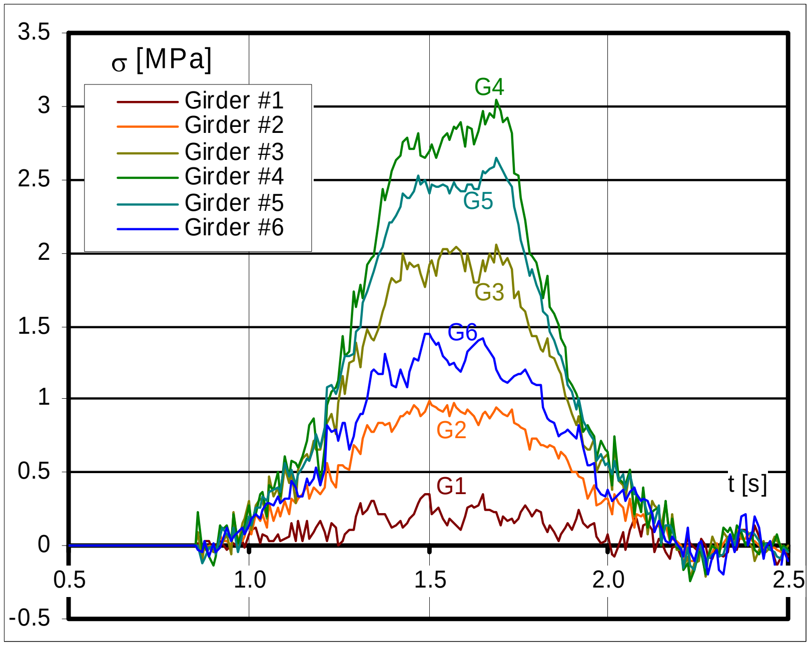

Figure B.71. Time histories of stresses in girders for Case #24.

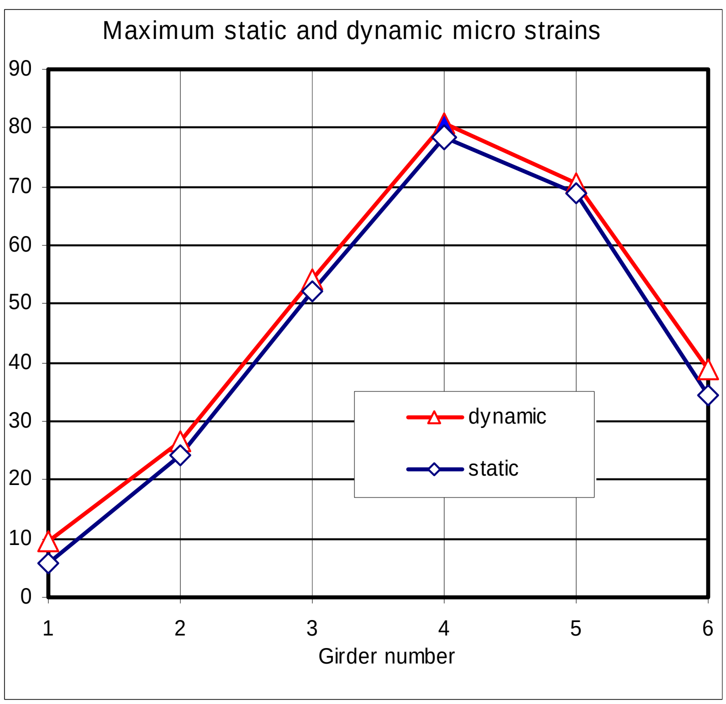

Figure B.72. Time histories of stresses in girders for Case #24.

B.25. Case #25 – V=55mph, bridge#2, truck#5

The case #25 was defined for the truck #5 running through the bridge #2 with speed V=55mph. Figure B.73 presents the time histories of strains calculated for each girder in the middle of the span. Figure B.74 shows corresponding stresses caused by passing vehicle. In Figure B.75 maximum dynamitic strains are compared for each girder with the static strains. Impact factor was calculated for girder #4 with the maximum dynamic strain ε^D= 72.03 micro strains (σ^D= 2.71 MPa). The representative value of the impact factor for case #25 is:

$$IM_{case\#25} = 6.53\%$$

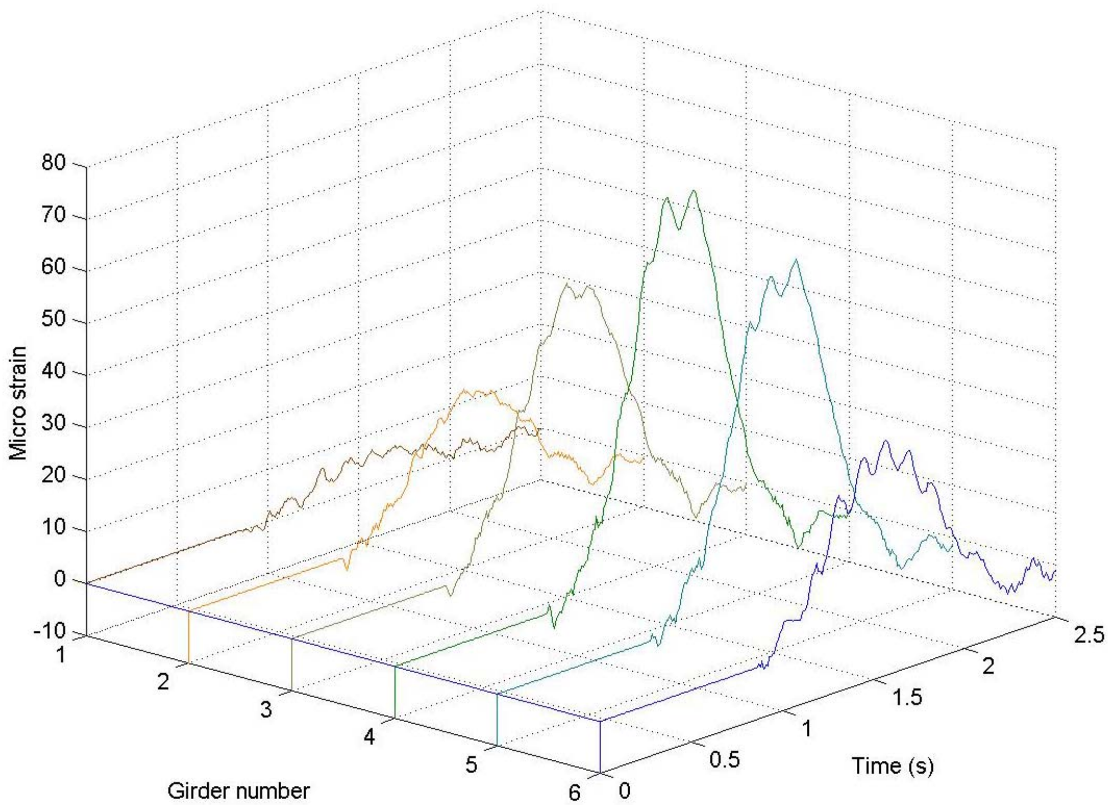

B.73. Time histories of micro strains in girders for Case #25.

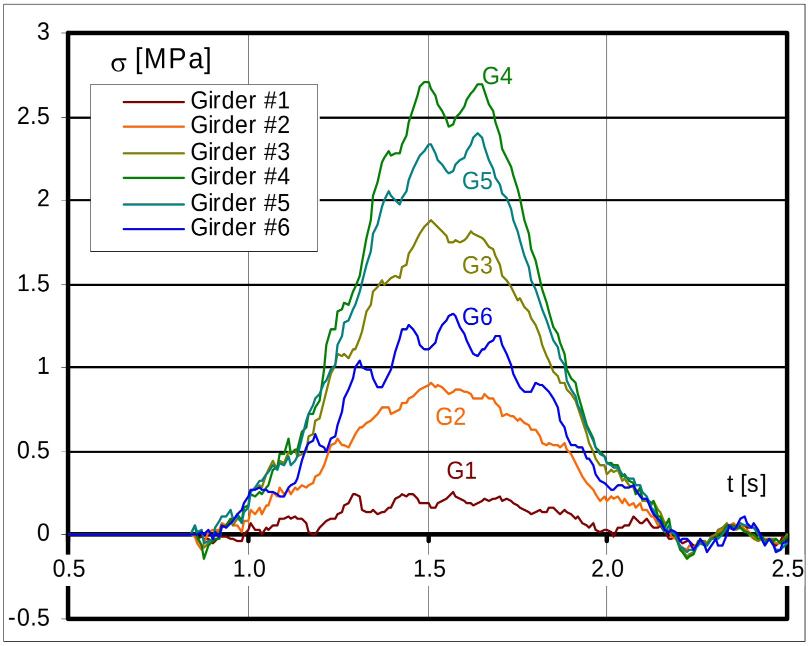

Figure B.74. Time histories of stresses in girders for Case #25.

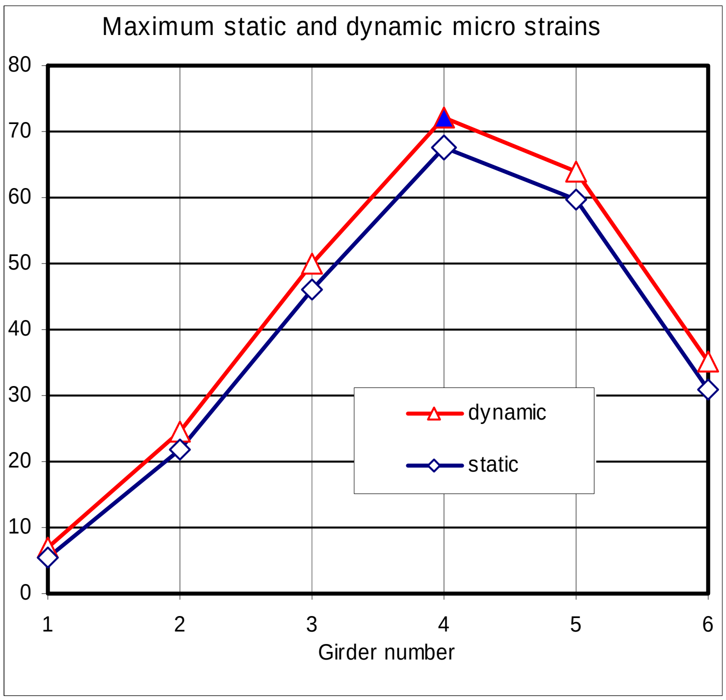

Figure B.75. Time histories of stresses in girders for Case #25.

B.26. Case #26 – V=55mph, bridge#2, truck#6

The case #26 was defined for the truck #6 running through the bridge #2 with speed V=55mph. Figure B.76 presents the time histories of strains calculated for each girder in the middle of the span. Figure B.77 shows corresponding stresses caused by passing vehicle. In Figure B.78 maximum dynamitic strains are compared for each girder with the static strains. Impact factor was calculated for girder #4 with the maximum dynamic strain ε^D= 71.87micro strains (σ^D= 2.70MPa). The representative value of the impact factor for case #26 is:

$$IM_{case\#26} = 6.29\%$$

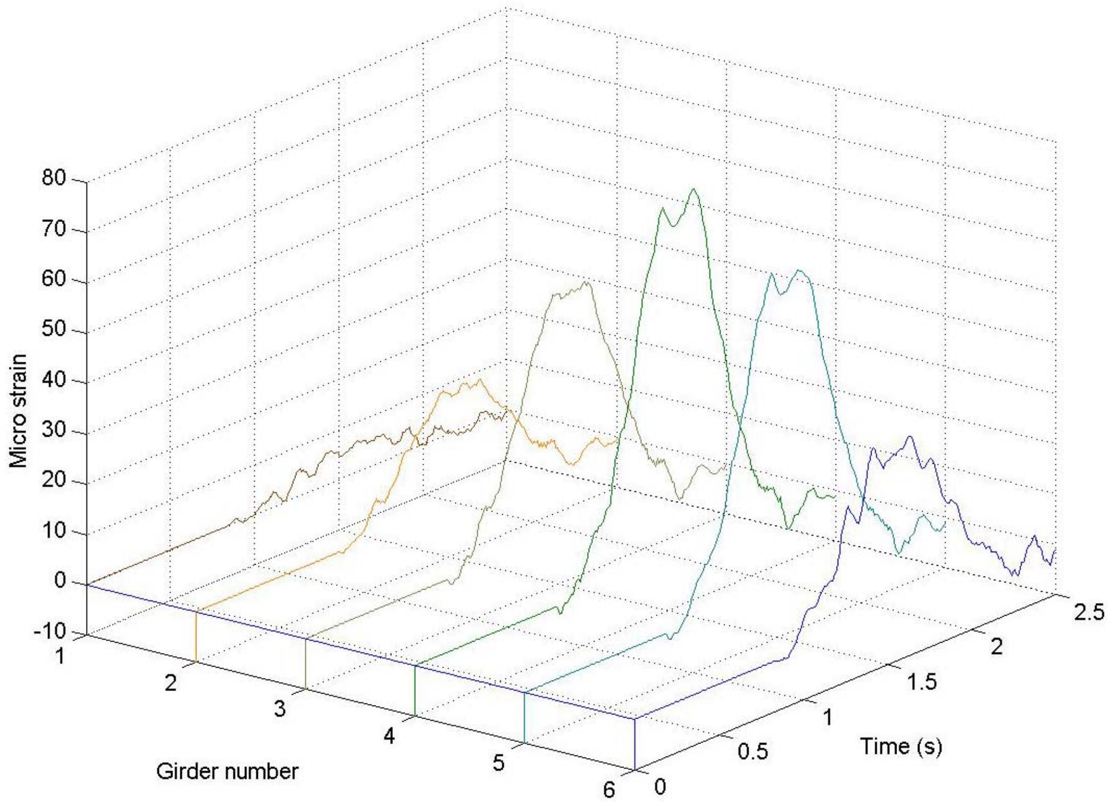

B.76. Time histories of micro strains in girders for Case #26.

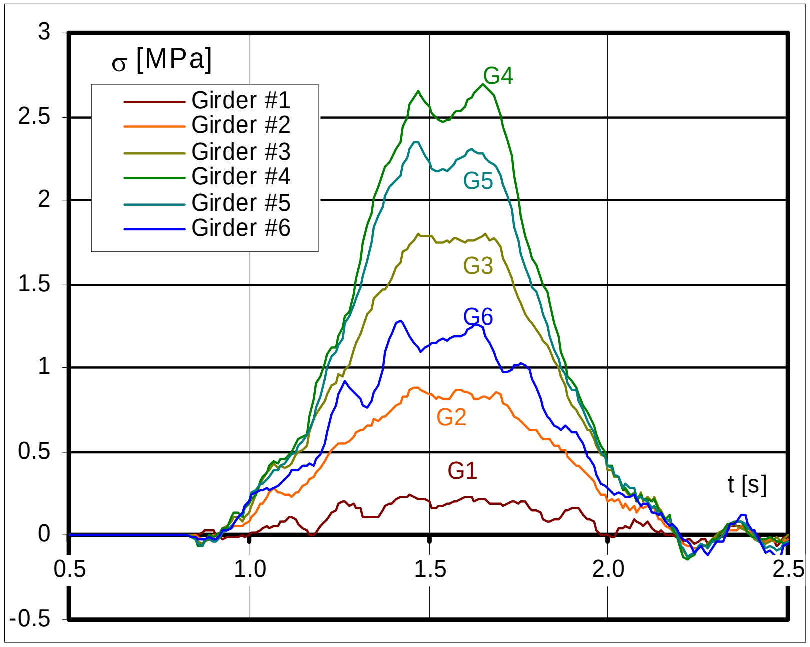

Figure B.77. Time histories of stresses in girders for Case #26.

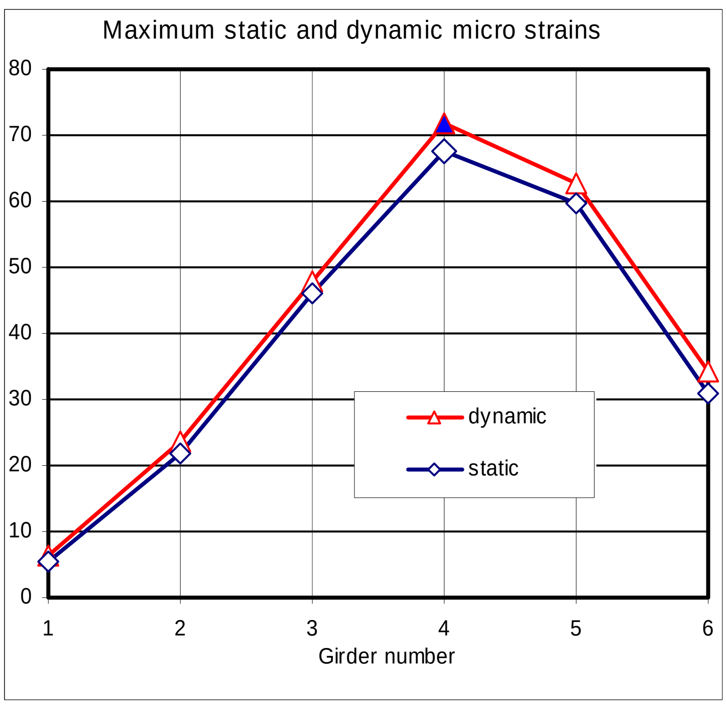

Figure B.78. Time histories of stresses in girders for Case #26.

B.27. Case #27 – V=55mph, bridge#3, truck#1

The case #27 was defined for the truck #1 running through the bridge #3 with speed V=55mph. Figure B.79 presents the time histories of strains calculated for each girder in the middle of the span. Figure B.80 shows corresponding stresses caused by passing vehicle. In Figure B.81 maximum dynamitic strains are compared for each girder with the static strains. Impact factor was calculated for girder #4 with the maximum dynamic strain ε^D= 80.63 micro strains (σ^D= 2.42 MPa). The representative value of the impact factor for case #27 is:

$$IM_{case\#27} = 85.00\ \%$$

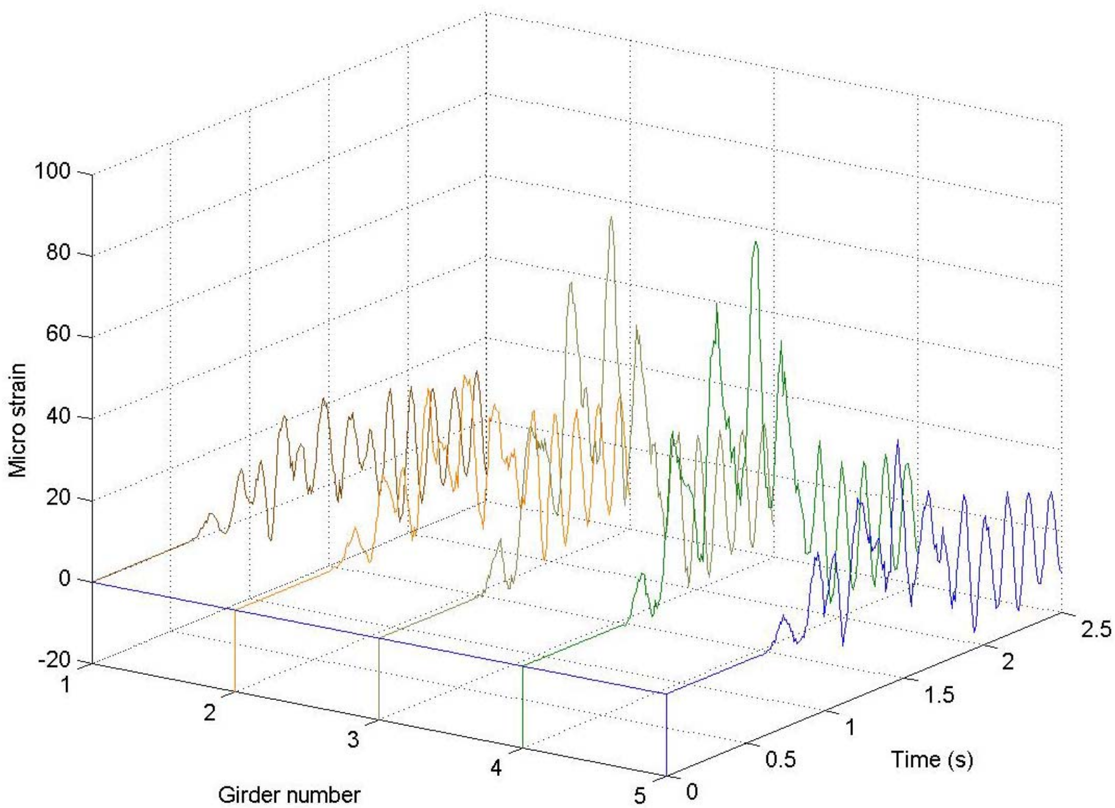

B.79. Time histories of micro strains in girders for Case #27.

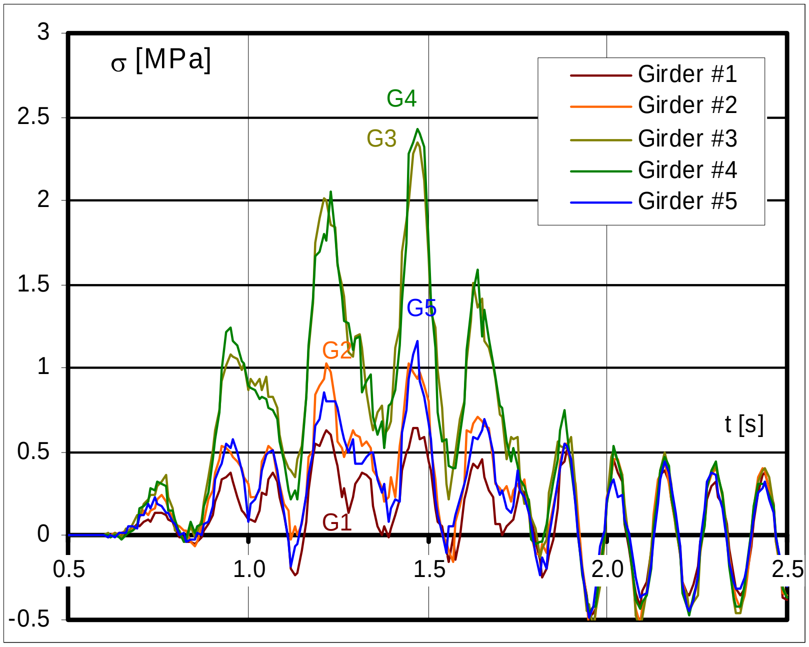

Figure B.80. Time histories of stresses in girders for Case #27.

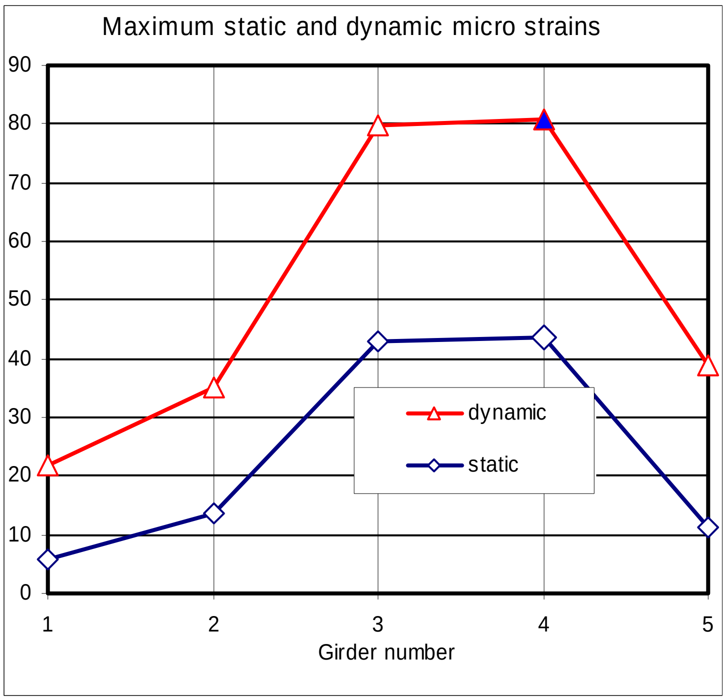

Figure B.81. Time histories of stresses in girders for Case #27.

B.28. Case #28 – V=55mph, bridge#3, truck#2

The case #28 was defined for the truck #2 running through the bridge #3 with speed V=55mph. Figure B.82 presents the time histories of strains calculated for each girder in the middle of the span. Figure B.83 shows corresponding stresses caused by passing vehicle. In Figure B.84 maximum dynamitic strains are compared for each girder with the static strains. Impact factor was calculated for girder #4 with the maximum dynamic strain ε^D= 73.64 micro strains (σ^D= 2.18 MPa). The representative value of the impact factor for case #28 is:

$$IM_{case\#28} = 15.26\%$$

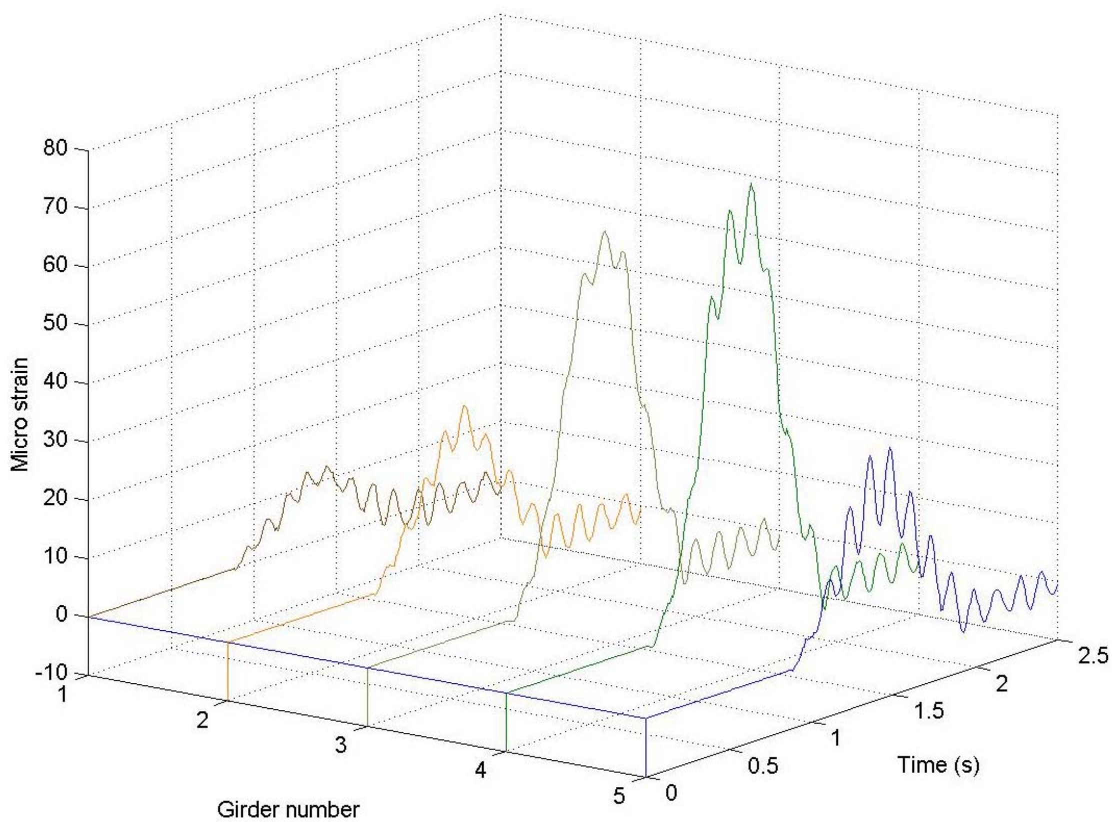

Figure B.82. Time histories of micro strains in girders for Case #28.

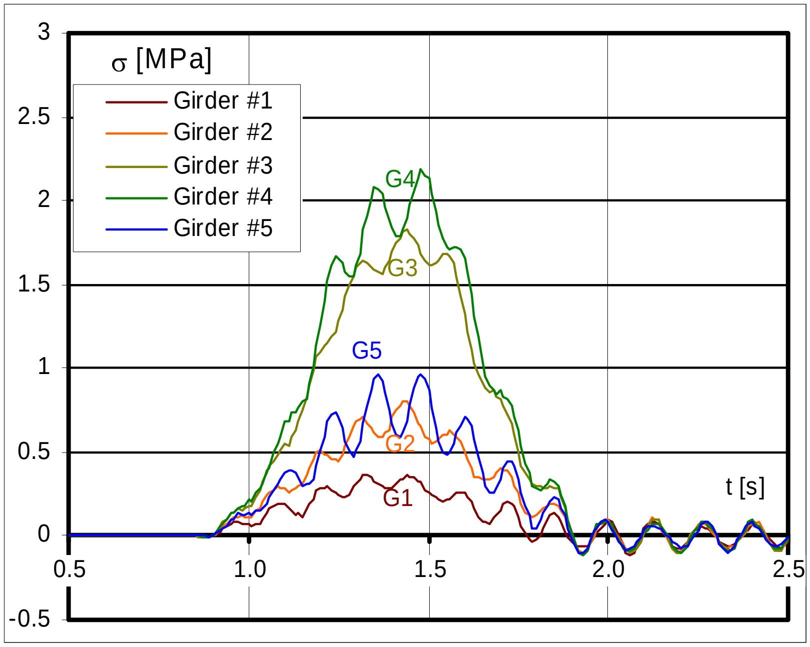

Figure B.83. Time histories of stresses in girders for Case #28.

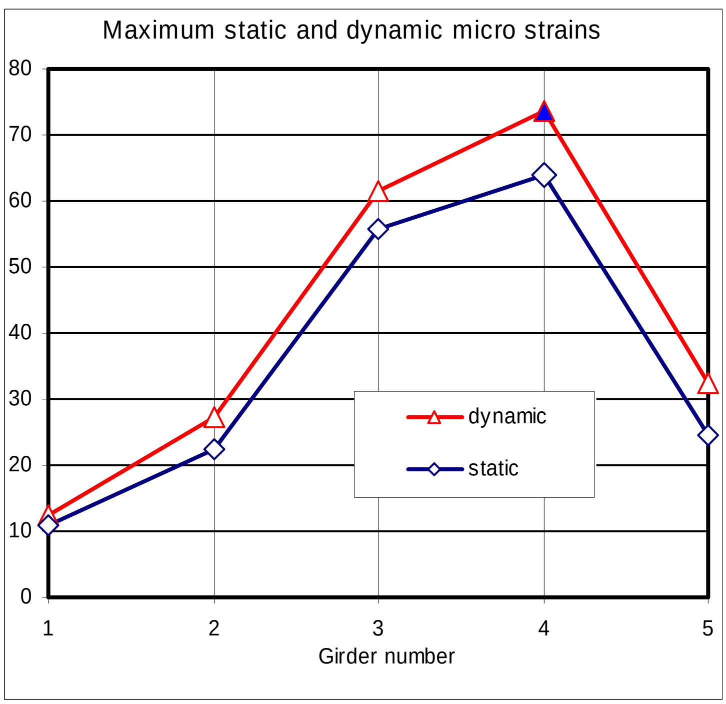

Figure B.84. Comparison of maximum static and dynamic strains for Case #28.

B.29. Case #29 – V=55mph, bridge#3, truck#3

The case #29 was defined for the truck #3 running through the bridge #3 with speed V=55mph. Figure B.85 presents the time histories of strains calculated for each girder in the middle of the span. Figure B.86 shows corresponding stresses caused by passing vehicle. In Figure B.87 maximum dynamitic strains are compared for each girder with the static strains. Impact factor was calculated for girder #4 with the maximum dynamic strain ε^D= 75.22 micro strains (σ^D= 2.23 MPa). The representative value of the impact factor for case #29 is:

$$IM_{case\#29} = 11.53\ \%$$

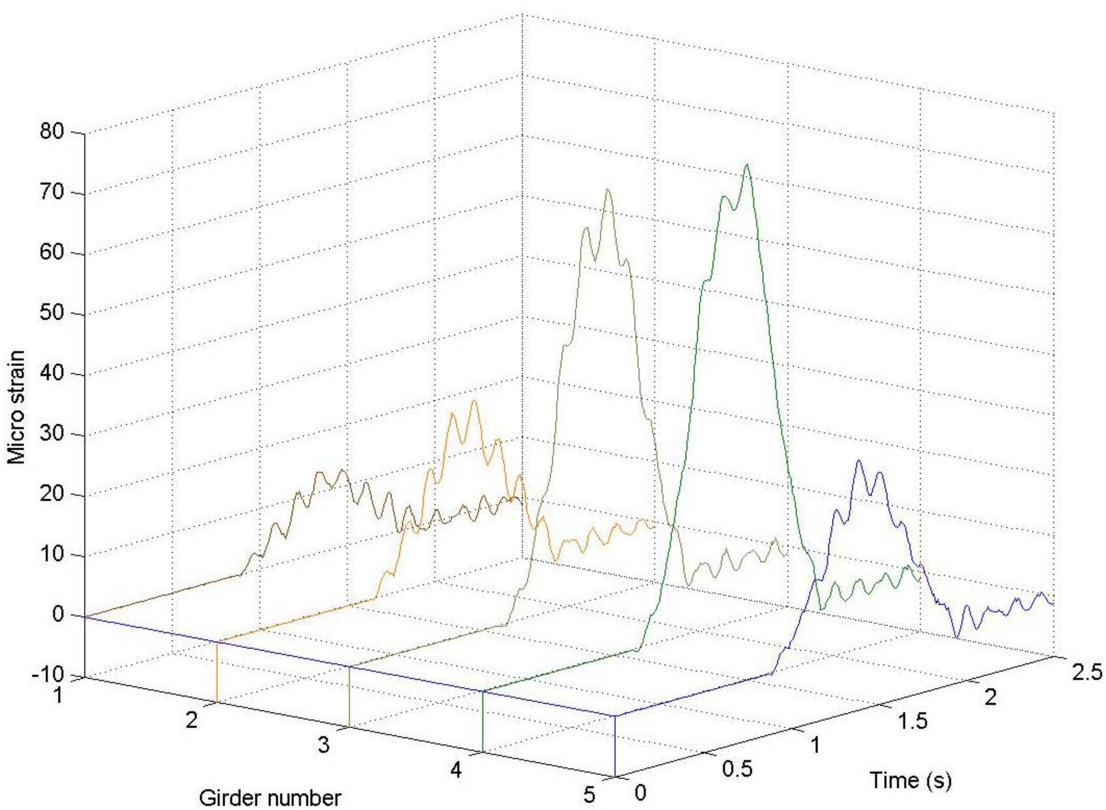

Figure B.85. Time histories of micro strains in girders for Case #29.

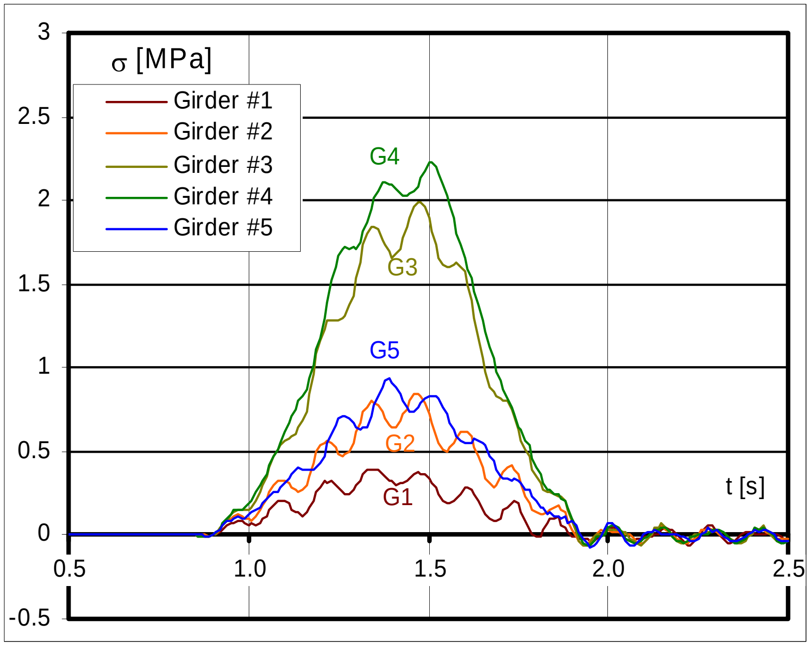

Figure B.86. Time histories of stresses in girders for Case #29.

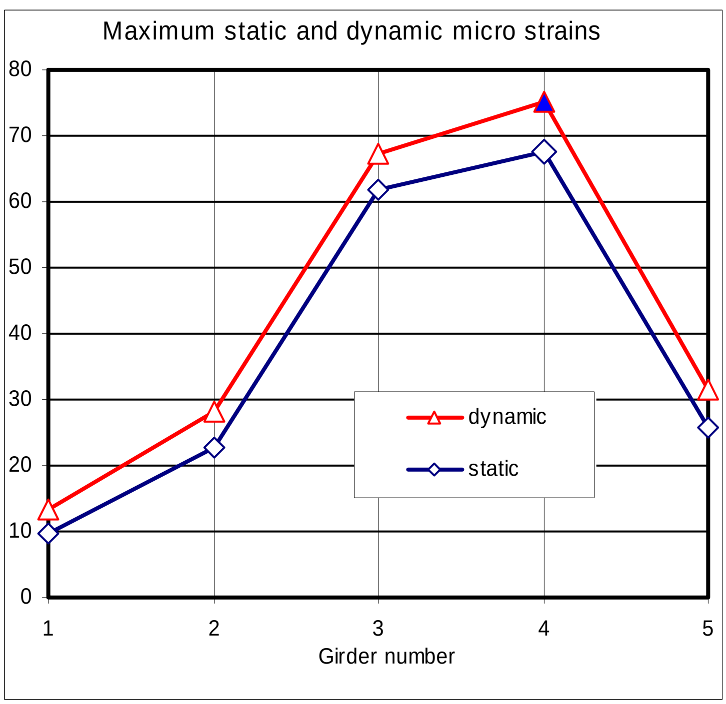

Figure B.87. Comparison of maximum static and dynamic strains for Case #29.

B.30. Case #30 – V=55mph, bridge#3, truck#4

The case #30 was defined for the truck #4 running through the bridge #3 with speed V=55mph. Figure B.88 presents the time histories of strains calculated for each girder in the middle of the span. Figure B.89 shows corresponding stresses caused by passing vehicle. In Figure B.90 maximum dynamitic strains are compared for each girder with the static strains. Impact factor was calculated for girder #4 with the maximum dynamic strain ε^D= 81.30 micro strains (σ^D= 2.41 MPa). The representative value of the impact factor for case #30 is:

$$IM_{case\#30} = 4.17\%$$

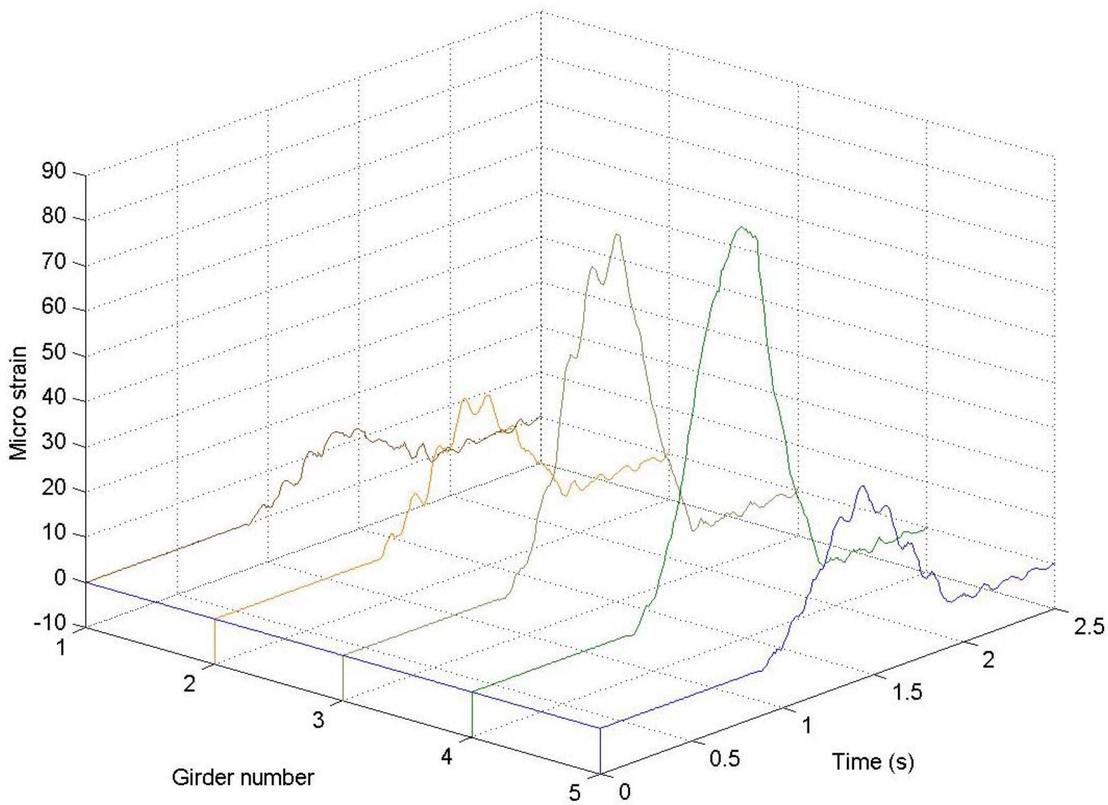

Figure B.88. Time histories of micro strains in girders for Case #30.

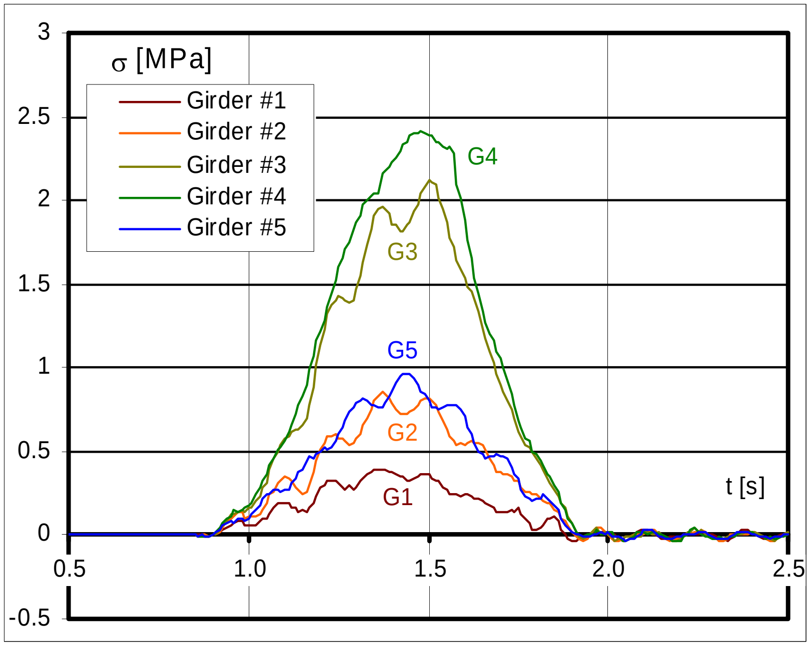

Figure B.89. Time histories of stresses in girders for Case #30.

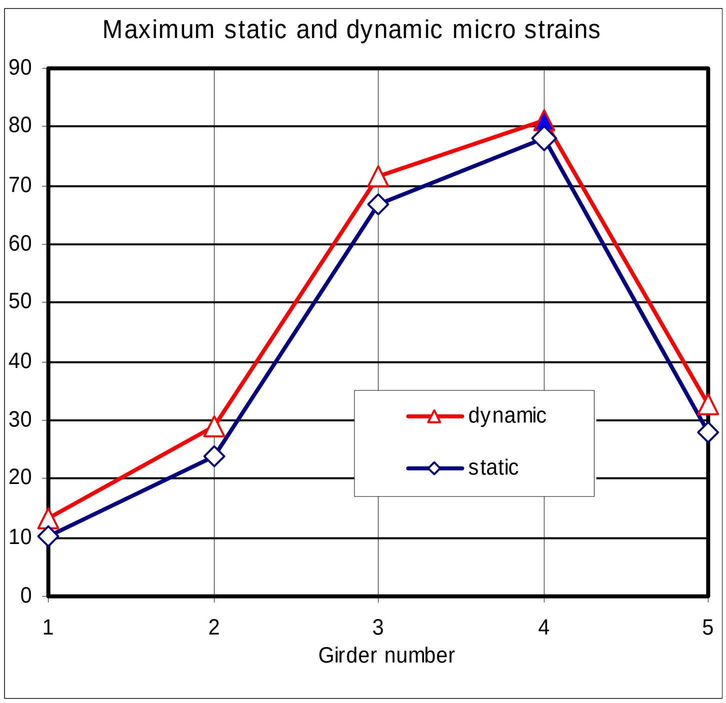

Figure B.90. Comparison of maximum static and dynamic strains for Case #30.

B.31. Case #31 – V=55mph, bridge#3, truck#5

The case #31 was defined for the truck #5 running through the bridge #3 with speed V=55mph. Figure B.91 presents the time histories of strains calculated for each girder in the middle of the span. Figure B.92 shows corresponding stresses caused by passing vehicle. In Figure B.93 maximum dynamitic strains are compared for each girder with the static strains. Impact factor was calculated for girder #4 with the maximum dynamic strain ε^D= 72.55micro strains (σ^D= 2.15MPa). The representative value of the impact factor for case #31 is:

$$IM_{case\#31} = 13.57\%$$

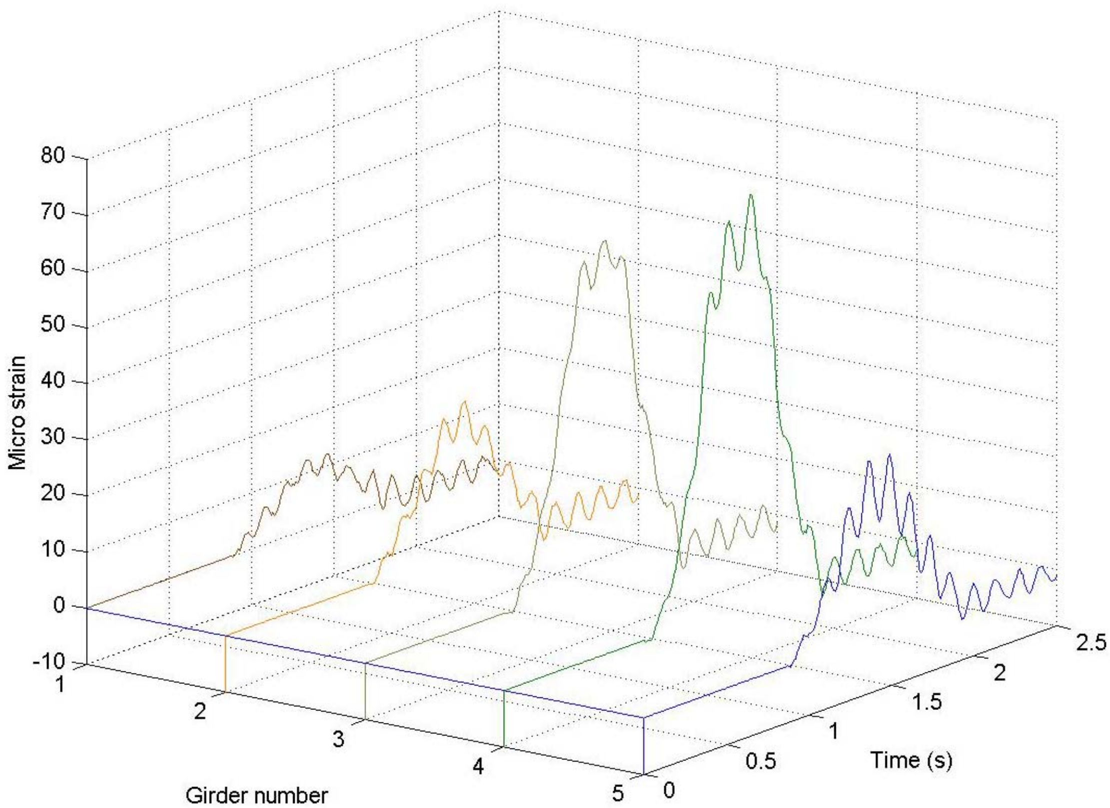

Figure B.91. Time histories of micro strains in girders for Case #31.

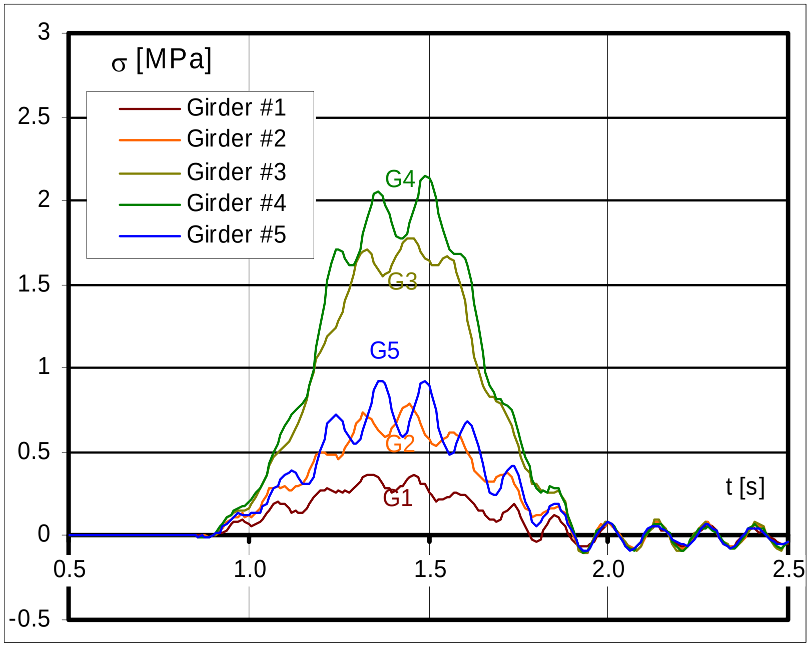

Figure B.92. Time histories of stresses in girders for Case #31.

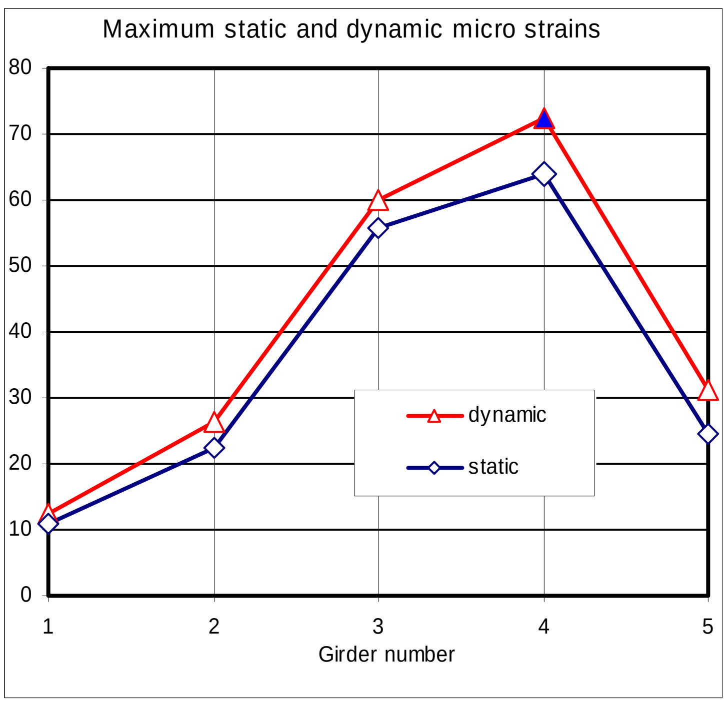

Figure B.93. Comparison of maximum static and dynamic strains for Case #31.

B.32. Case #32 – V=55mph, bridge#3, truck#6

The case #32 was defined for the truck #6 running through the bridge #3 with speed V=55mph. Figure B.94 presents the time histories of strains calculated for each girder in the middle of the span. Figure B.95 shows corresponding stresses caused by passing vehicle. In Figure B.96 maximum dynamitic strains are compared for each girder with the static strains. Impact factor was calculated for girder #4 with the maximum dynamic strain ε^D= 72.11micro strains (σ^D= 2.14MPa). The representative value of the impact factor for case #32 is:

$$IM_{case\#32} = 12.88\%$$

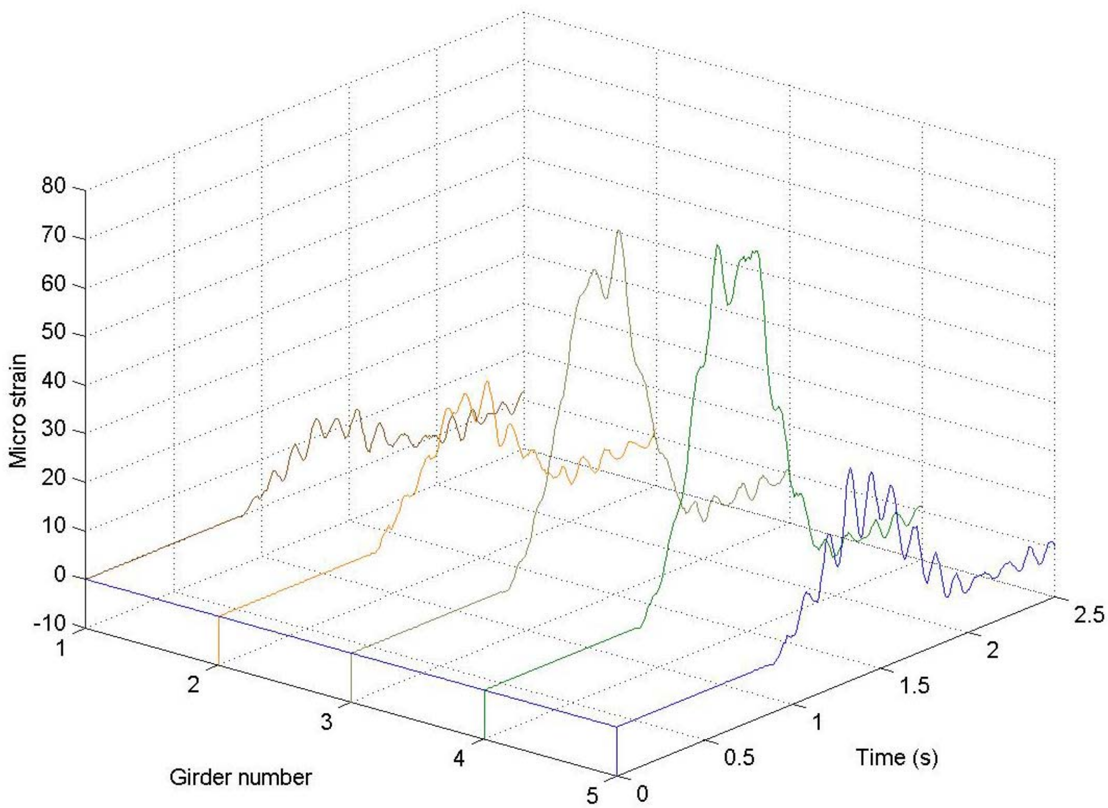

Figure B.94. Time histories of micro strains in girders for Case #32.

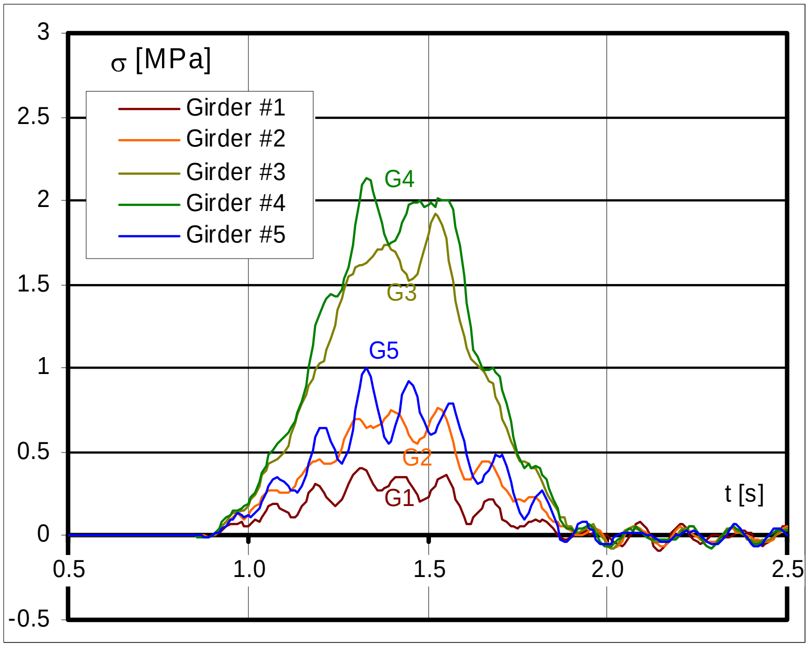

Figure B.95. Time histories of micro strains in girders for Case #32.

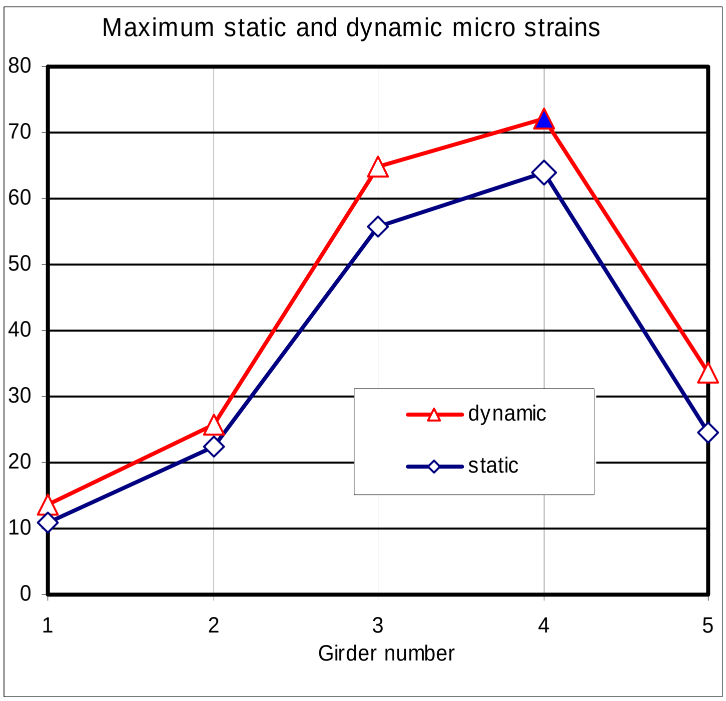

Figure B.96. Comparison of maximum static and dynamic strains for Case #32.